Sveučilište u Zagrebu

FACULTY OF MECHANICAL ENGINEERING AND NAVAL ARCHITECTURE

GORAN STUNJEK

MODELING THE OPTIMAL WATER-ENERGY NEXUS TO MAXIMIZE SOCIAL WELFARE UNDER UNCERTAINTY OF CLIMATE CHANGE FORECASTING AND MARKET PRICES

DOCTORAL THESIS

Zagreb, 2025

Sveučilište u Zagrebu

FAKULTET STROJARSTVA I BRODOGRADNJE

GORAN STUNJEK

MODELIRANJE OPTIMALNE SPONE VODNIH I ENERGETSKIH SUSTAVA ZA MAKSIMIZACIJU DRUŠTVENE DOBROBITI U UVJETIMA NESIGURNOSTI PROGNOZE KLIMATSKIH PROMJENA I TRŽIŠNIH CIJENA

DOKTORSKI RAD

Zagreb, 2025.

Sveučilište u Zagrebu

FACULTY OF MECHANICAL ENGINEERING AND NAVAL ARCHITECTURE

GORAN STUNJEK

MODELING THE OPTIMAL WATER-ENERGY NEXUS TO MAXIMIZE SOCIAL WELFARE UNDER UNCERTAINTY OF CLIMATE CHANGE FORECASTING AND MARKET PRICES

DOCTORAL THESIS

SUPERVISOR:

Prof.dr.sc. GORAN KRAJAČIĆ

Zagreb, 2025

Sveučilište u Zagrebu

FAKULTET STROJARSTVA I BRODOGRADNJE

GORAN STUNJEK

MODELIRANJE OPTIMALNE SPONE VODNIH I ENERGETSKIH SUSTAVA ZA MAKSIMIZACIJU DRUŠTVENE DOBROBITI U UVJETIMA NESIGURNOSTI PROGNOZE KLIMATSKIH PROMJENA I TRŽIŠNIH CIJENA

DOKTORSKI RAD

Mentor:

Prof.dr.sc. Goran Krajačić

Zagreb, 2025.

BIBLIOGRAPHY DATA

UDC: **620.9**
681.52
621.039.534

Keywords: holistic energy system planning, district heating, water-energy-food-ecosystem nexus, optimisation, uncertainty modelling

Scientific area: TECHNICAL SCIENCES

Scientific field: Mechanical engineering

Institution: Faculty of Mechanical Engineering and Naval Architecture

Thesis supervisor: Prof. Goran Krajačić, PhD

Number of pages: 203

Number of figures: 28

Number of tables: 3

Number of references: 142

Date of examination: 18th of February, 2026

Thesis defence commission:

1. *Prof. Andrej Jokić, PhD – Chairman of defence commission*
2. *Prof. Nataša Markovska, PhD – Member*
3. *Asst. prof. Marko Mimica – Member*

Archive: Faculty of Mechanical Engineering and Naval Architecture

TABLE OF CONTENTS

ACKNOWLEDGEMENT

The work presented in this thesis was carried out at the Department of Energy, Power and Environmental Engineering of the Faculty of Mechanical Engineering and Naval Architecture, University of Zagreb.

First and foremost, I would like to express my deepest gratitude to my friend and supervisor Goran Krajačić. From the late graduation days throughout the PhD itself, he was my *Virgil*. He guided me when I was lost and helped me achieve the final goal. His support and friendship were the cornerstone of this thesis.

My greatest thanks go to the whole *Powerlab* research group. From the early days of my research, and best company of friends: Hrvoje Dorotić, Ana Kodba, Borna Doračić, Marko Mimica, Nikola Matak, Vladimir Vidović, Marijan Marković, Hrvoje Stančin, Filip Jurić, Tibor Bešenić, Ivan Pađen, Marko Ban, Stanislav Boldyryev, Antun Pfeifer, Duško Stajić, to the new friendships gathered along the PhD path: Josip Miškić, Doris Beljan, Luka Herc, Petar Lonić, Luka Simić, Marko Starčević, Stela Perković, Katarina Mišić, Ana Glavina, Ana Ređep, Alina Al-Garby, Ana-Daria Bokan, Mario Mihetec, Katarina Juričev-Martinčev, Sunčan Vojvodić, Roko Bračić, Stjepan Družinec. Huge thanks go to my *Termići* crew, Ivan Matas, Petar Filipović, Juraj Čukelj, Stjepan Herceg, Dino Miše, for their friendship and countless discussions on research and non-research related topics. Big respect and many thanks to all professors and colleagues from 8th floor. They were always ready to give their unconditional help. In addition, I would like to thank employees of the SDEWES Centre for all their support. You ALL are the most important thing that came out of my PhD journey, and I am immensely grateful for your support.

I would like to express my deepest gratitude to my parents and my whole family. Even though they never really understood what I was doing all those research years, they gave their unconditional love and support not only during my studies, but throughout my entire life.

Finally, I reserve my warmest thanks for my Katarina. She was my *Beatrice*, appearing at the end to guide me through the brightest reaches of these final chapters, drawing me ever upward toward greatness and calmness.

PREFACE

"Push the envelope, watch it bend."

Lateralus, Tool

0, 1, 1, 2, 3, 5, 8, 13, 21, 34, 55, 89, 144, 233, 377, 610, 987, 1597... Spiral out, keep going!

SUMMARY

Climate variability, rising resource demands, and evolving socio-economic pressures increasingly expose the limits of treating water, energy, food, and ecosystems (WEFE) as separate systems. This research addresses these interdependencies through the WEFE nexus and develops optimisation models that quantify how cross-sectoral linkages influence investment and operation under uncertainty. The central premise is that integrated and uncertainty-aware planning yields greater resilience, efficiency, and social welfare than traditional sectoral approaches.

The motivation stems from the need to design sustainable resource systems aligned with the European Green Deal and global decarbonisation goals. The research aims to validate an integrated model of the water–energy (WE) nexus that supports cost-efficient infrastructure planning, optimal resource management, and adaptation to climate variability. The working hypothesis assumes that embedding detailed WE interactions and climate-informed scenarios in an optimisation framework enables decisions that reduce resource use, strengthen supply security, and facilitate renewable energy integration.

The methodological framework evolves in three stages. First, a mixed-integer linear programming (MILP) model for district heating in urban agglomerations optimises investments, interconnection, and operational flexibility while minimising total socio-economic cost. The second stage expands the model to the WE domain by coupling renewable (RES) generation and storage with desalination systems, revealing the role of flexibility and storage in balancing hourly variations in water and energy demand. The third stage introduces a two-stage stochastic optimisation that captures climate and market uncertainty within a comprehensive WEFE formulation. This unified environment integrates technical, economic, and environmental criteria and evaluates how decisions in one domain affect others.

Applications across multiple contexts confirm the model's versatility. In the Zagreb DH case, coordinated optimisation of distribution networks and storage reduces total annualised cost and emissions while increasing RES shares. For the island WE system of Unije, the analysis identifies cost thresholds for RES generation and storage and highlights their interaction in ensuring reliable water supply. The most comprehensive case, the hybrid solar-hydro system at PSH Velebit, extends the stochastic framework to include floating photovoltaic (FPV) technology. FPV improves the utilisation of water surfaces, increases power generation, and reduces evaporation, producing clear benefits for both the energy and water dimensions of the

nexus. The optimisation results confirm that combined solar-hydro operation enhances system flexibility, mitigates output variability, and supports sustainable long-term operation of hydropower assets.

Overall, the research demonstrates that integrated optimisation under uncertainty consistently outperforms sector-specific planning. By coupling multiple resource systems within a stochastic, multi-objective decision framework, the thesis provides a robust tool for evaluating investments and operations that remain resilient across climate and market variability. The findings emphasise the importance of nexus-based modelling as a foundation for sustainable infrastructure planning, offering a transparent and adaptable approach to balance economic performance, resource security, and environmental protection.

SAŽETAK

Klimatska promijene, rastuće potrebe za resursima i promjenjivi socioekonomski uvjeti sve više ukazuju na ograničenja planiranja koje zasebno promatra vodne i energetske sustave, poljoprivredu i utjecaj na okoliš. Ovo istraživanje pristupa tim međuovisnostima kroz koncept WEFE (eng. Water-Energy-Food-Ecosystem - WEFE) i razvija optimizacijske modele koji kvantificiraju utjecaj međusektorskih veza na investicije i vođenje sustava u uvjetima nesigurnosti. Središnja pretpostavka istraživanja jest da integrirano planiranje dovodi do veće otpornosti i učinkovitosti sustava te veće društvene dobrobiti u odnosu na tradicionalne sektorske pristupe.

Polazišna motivacija proizlazi iz potrebe za oblikovanjem održivih sustava upravljanja resursima u skladu s ciljevima Europskog zelenog plana i globalnog cilja dekarbonizacije. Cilj istraživanja je potvrditi integrirani model kompleksne veze vodnih i energetskih sustava koji omogućuje troškovno učinkovito planiranje infrastrukture, optimalno upravljanje resursima i prilagodbu klimatskim promjenama. Polazna hipoteza pretpostavlja da uključivanje detaljnih interakcija između vodnih i energetskih sustava te klimatskih scenarija u optimizacijski okvir omogućuje donošenje odluka koje smanjuju potrošnju resursa, povećavaju sigurnost opskrbe i potiču dublju integraciju obnovljivih izvora energije.

Metodološki okvir razvija se u tri faze. U prvoj je izrađen model u obliku mješovitog cjelobrojnog linearnog programiranja za optimizaciju centraliziranih toplinskih sustava u urbanim aglomeracijama, kojim se istodobno odlučuje o investicijama, povezivanju mreža i fleksibilnosti pogona uz minimizaciju ukupnih društveno-ekonomskih troškova. U drugoj fazi model se proširuje na vodno-energetski sustav integracijom obnovljivih izvora i spremnika energije s desalinizacijskim postrojenjima, čime se opisuje međudjelovanje opskrbe električnom energijom, proizvodnje vode i skladištenja u vremenski promjenjivim uvjetima. Treća faza uvodi dvo-stupanjski stohastički optimizacijski model koji obuhvaća klimatsku i tržišnu nesigurnost u okviru cjelovitog WEFE koncepta te povezuje tehničke, ekonomske i okolišne pokazatelje u jedinstveno okruženje za donošenje odluka.

Primjena modela na više prostornih i sektorskih razina potvrđuje njegovu svestranost. U slučaju sustava centraliziranog toplinskog sustava grada Zagreba optimizacija povezanih mreža i spremnika smanjuje ukupne troškove i emisije uz povećanje udjela obnovljivih izvora. U vodno-energetskom sustavu otoka Unije model određuje granične uvjete isplativosti fotonaponskih sustava i spremnika energije te pokazuje njihovu međusobnu ulogu u

osiguravanju pouzdane opskrbe vodom. Najsloženiji primjer, hibridni sustav fotonaponske elektrane i reverzibilne hidroelektrane (RH) Velebit, proširuje stohastički okvir uključivanjem plutajuće fotonaponske (eng. Floating photovoltaic - FPV) tehnologije. FPV omogućuje učinkovitije korištenje vodnih površina, povećava proizvodnju električne energije i smanjuje ishlapljivanje, čime se ostvaruju prednosti za energetski i vodni sektor, ali i generalni utjecaj na cjelokupni WEFE sektor. Rezultati optimizacije potvrđuju da hibridno pogon FPV i RH povećava fleksibilnost sustava, ublažava varijabilnost proizvodnje te doprinosi održivom dugoročnom radu hidroenergetskih objekata.

Provedena istraživanja pokazuju da integrirana optimizacija u uvjetima nesigurnosti dosljedno daje bolje rezultate od sektorskog planiranja. Povezivanjem više resursnih sustava u stohastički, višekriterijski okvir odlučivanja, rad pruža robustan alat za procjenu ulaganja i strategija vođenja sustava koje ostaju učinkovite unatoč klimatskim i tržišnim promjenama. Dobiveni rezultati potvrđuju važnost WEFE koncepta kao temeljne smjernice za održivo planiranje infrastrukture te nude transparentan i prilagodljiv pristup uravnoteženju gospodarske učinkovitosti, sigurnosti resursa i zaštite okoliša.

PROŠIRENI SAŽETAK

Klimatske promjene, rastuće potrebe za resursima i promjenjivi socioekonomski uvjeti sve više ukazuju na ograničenja planiranja koje zasebno promatra vodne i energetske sustave, poljoprivredu i ekosustave. Ovo istraživanje pristupa tim međuovisnostima kroz koncept WEFE (eng. Water-Energy-Food-Ecosystem – WEFE) i razvija optimizacijske modele koji kvantificiraju kako međusektorske veze oblikuju investicije i vođenje sustava u stvarnim uvjetima nesigurnosti. Središnja pretpostavka istraživanja jest da odluke koje zajednički razmatraju te međusobne ovisnosti mogu osigurati veću društvenu dobrobit, otpornost sustava i povoljnije okolišne ishode u odnosu na sektorsko planiranje. Na temelju te motivacije, istraživanje ima za cilj potvrditi integrirani model kompleksne povezanosti vodnih i energetskih sustava (eng. Water-Energy nexus - WE), unaprijediti planiranje infrastrukture i troškovnu učinkovitost, omogućiti potpuniju integraciju raspoloživih vodnih resursa i obnovljivih izvora energije te ispitati mogućnosti prilagodbe klimatskim promjenama i povezanim ekstremnim pojavama. Radna hipoteza polazi od pretpostavke da uključivanje detaljnih prikaza vodno-energetskih veza i klimatskih scenarija u optimizacijski okvir omogućuje planiranje pogona koje smanjuje potrošnju resursa, povećava sigurnost opskrbe, jača učinkovitost i omogućuje dublju integraciju varijabilnih obnovljivih izvora.

Metodološki okvir rada razvija se u fazama koje odražavaju postupno proširenje obuhvata WEFE koncepta. U prvoj fazi formuliran je model mješovitog cjelobrojnog linearnog programiranja za optimizaciju centraliziranih toplinskih sustava u urbanim aglomeracijama, u kojem se o međupovezanosti mreža, spremnicima toplinske energije i opcijama elektrifikacije odlučuje endogeno s ciljem minimizacije ukupnog društveno-ekonomskog troška uz poštivanje pogonskih i okolišnih ograničenja. Fokus se zatim prebacuje na vodno-energetske sustave na otocima, gdje se istodobno optimiziraju proizvodnja iz obnovljivih izvora i spremanje energije uz desalinizaciju vode. Ovaj pristup opisuje satnu povezanost između opskrbe električnom energijom, proizvodnje vode, skladištenja i potražnje, pokazujući operativnu vrijednost fleksibilnosti u sezonski promjenjivim uvjetima. Završna faza uvodi nesigurnost i proširuje okvir na cjeloviti WEFE koncept kroz dvo-stupanjski stohastički optimizacijski model koji procjenjuje veličinu kapaciteta i vođenje sustava uzimajući u obzir klimatske i tržišne nesigurnosti. U takvom stohastičkom okruženju model razlikuje četiri optimizacijska pristupa, energetski, WE, WEF (eng. Water-Energy-Food - WEF) i WEFE, koji dijele istu investicijsku strukturu, ali uključuju različite financijske i ekonomske tokove u funkciji cilja. Od prihoda od električne energije do novčane vrijednosti uštede isparavanja, potrebe za navodnjavanjem,

uštede zbog ne korištenja zemljišta, izbjegnutih emisija i troškova ekosustava. Cjeloviti skup ograničenja osigurava fizičku izvedivost kroz kreirane hidrološke scenarije, uključujući vodne bilance gornjeg i donjeg akumulacijskog bazena s dotocima, padalinama, protokom kroz hidroelektranu, isparavanjem, preljevom i sektorskom potrošnjom.

Tri provedene studije slučaja prikazuju primjenjivost metodologije u različitim prostornim i sektorskim kontekstima. U urbanom slučaju model analizira zagrebački centralizirani toplinski sustava i okolne mreže, ispitujući vrijednost međupovezanosti, spremnika energije i opcija proizvodnih kapaciteta. Rezultati pokazuju da koordinirana ulaganja i vođenje sustava mogu znatno smanjiti ukupne troškove i emisije te povećati udio obnovljivih izvora, potvrđujući društveno-ekonomsku opravdanost povezivanja mreža i povećanja fleksibilnosti. U vodno-energetskom sustavu otoka Unije, istodobna optimizacija fotonaponske (eng. Photovoltaic - PV) proizvodnje, spremnika energije i vode te postrojenja reverzne osmoze pokazuje kako relativni troškovi PV sustava i spremnika određuju optimalne kapacitete i pogonske obrasce. Kada su investicijski troškovi PV sustava niski, potreba za spremnicima energije je manja, dok veći investicijski troškovi povećavaju važnost spremnika jer čuvaju vrijednost svake proizvedene jedinice električne energije. Analiza određuje granične uvjete ekonomske isplativosti i pokazuje kako sezonske varijacije potražnje za vodom i električnom energijom omogućuju preusmjeravanje proizvodnje u razdoblja viška obnovljive energije.

Najveća razina integracije ostvarena je u istraživanju hibridnog solarno-hidroenergetskog sustava na reverzibilnoj hidroelektrani (RH) RH Velebit. U ovom slučaju stohastički WEFE okvir istodobno optimizira vođenje sustava RH i raspored plutajućih fotonaponskih (FPV) panela na gornjem akumulacijskom jezeru, uzimajući u obzir hidrološku varijabilnost i međusektorske interakcije. Model identificira optimalni FPV-RH sustav koji uravnotežuje proizvodnju električne energije i zadržavanje vode, povećavaju pogonsku fleksibilnost i osiguravaju stabilniju opskrbu električnom energijom. Osim energetskih pokazatelja, model obuhvaća i vodni aspekt kroz smanjenje isparavanja te utjecaj poljoprivrede kroz planiranje navodnjavanja, dok se ekosustavni aspekt uključuje kroz uštede zbog ne korištenja zemljišta, izbjegnute emisije i utjecaje pogona sustava hidroelektrane na ekosustav. Dobiveni hibridni sustavi ublažavaju varijabilnost hidroelektrane i omogućuju strateško korištenje spremnika, što dugoročno može smanjiti mehanička naprezanja te povećati pouzdanost i ekonomičnost rada postrojenja.

Sveukupno, rezultati pokazuju da integrirana optimizacija u uvjetima nesigurnosti sustavno daje bolje ishode od sektorskog planiranja, u pogledu troškova, otpornosti i utjecaja na okoliš. Prijelaz s determinističkih, sektorski ograničenih modela na stohastičko, međusektorsko okruženje odlučivanja omogućuje transparentnu usporedbu investicijskih scenarija i strategija vođenja sustava koje ostaju učinkovite unatoč klimatskim i tržišnim promjenama. Ovim radom razvijen je jedinstveni optimizacijski okvir koji povezuje detaljna fizička ograničenja s višekriterijskom i scenarijskom analizom, omogućujući donositeljima odluka da kvantificiraju sinergije, prepoznaju ograničenja te razumiju kako politike i tržišni signali utječu na povezane resursne sustave. Time se nudi praktičan i prilagodljiv alat za usklađivanje razvoja infrastrukture s ciljevima održivosti i istodobnog upravljanja nesigurnostima čime se potvrđuje vrijednost WEFE koncepta u oblikovanju otpornih, učinkovitih i društveno korisnih resursnih sustava.

CILJ I HIPOTEZA

Ciljevi ovoga istraživanja su sljedeći:

1. Validirati modele kompleksne veze vodnih i energetskih sustava,
2. Unaprijediti planiranje i smanjenje troška izgradnje infrastrukture,
3. Osigurati cjelovitiju integraciju dostupnih vodnih resursa i obnovljivih izvora energije kroz optimalno planiranje i vođenje sustava,
4. Analizirati scenarije prilagodbe energetskih i vodnih sustava klimatskim promjenama i ekstremnim vremenskim uvjetima koji nastaju kao posljedica klimatskih promjena.

Hipoteza ovog istraživanja jest da se pomoću detaljne analize vodnih i energetskih sustava, uz primjenu dubinske analize podataka kompleksne veze dvaju sektora i raspoloživih prognoza klimatskih modela, mogu kreirati modeli za planiranje optimalnog rada vodnih i energetskih sustava, što će rezultirati minimalnom potrošnjom vode i energije, većom sigurnošću dobave od trenutno postojeće, maksimalnom učinkovitosti spone sustava te maksimalnom integracijom varijabilnih obnovljivih izvora energije.

ZNANSTVENI DOPRINOS

Očekivani znanstveni doprinosi ovog istraživanja su unaprijeđeni i razvijeni modeli za optimiranje rada vodnih i energetskih sustava pod različitim tržišnim i klimatskim okolnostima,

u uvjetima ekstremnih klimatskih promjena te u slučajevima različite potražnje za vodom i energijom u sektorima poljoprivrede, turizma, industrije te urbanim i ruralnim naseljima.

METODE I POSTUPCI

Metodološki okvir razvijen u ovom istraživanju slijedi strukturirani, postupni pristup koji se nadovezuje od optimizacije pojedinačnih sektora prema potpuno integriranom stohastičkom okviru WEFE koncepta. Svaka faza uvodi novu razinu složenosti, prostornog obuhvata i međusektorske povezanosti, uz zadržavanje jedinstvene optimizacijske filozofije temeljene na mješovitom cjelobrojnom linearnom programiranju (MILP) i načelima stohastičkog modeliranja.

U prvoj fazi uspostavljen je tehno-ekonomski i okolišni optimizacijski model za centralizirane toplinske sustave u urbanim aglomeracijama. Formulacija minimizira ukupne društveno-ekonomske troškove, uključujući investicijske, pogonske i troškove održavanja te troškove emisija, uz određivanje optimalne konfiguracije proizvodnih jedinica, spojnih cjevovoda i spremnika toplinske energije. Endogeno definirane varijable određuju i veličinu infrastrukture i satni pogon sustava, što omogućuje modelu da uravnoteži proizvodnju električne i toplinske energije, integraciju obnovljivih izvora te fleksibilnost mreže. Ovim pristupom kvantificiraju se koristi od prostorne međupovezanosti, učinkovitijeg korištenja spremnika energije i strateškog povezivanja elektroenergetskog i toplinskog sektora.

Druga faza metodološkog razvoja proširuje okvir na vodno-energetski sustav integracijom obnovljivih izvora energije i spremnika s desalinizacijskim postrojenjima. Model provodi satnu optimizaciju proizvodnje električne energije, vode i korištenja spremnika s ciljem minimizacije troškova sustava uz zadovoljavanje promjenjivih profila potražnje i pogonskih ograničenja. Takav pristup omogućuje detaljan prikaz međudjelovanja varijabilne obnovljive proizvodnje i potreba za vodom te analizu fleksibilnosti, potrebnih kapaciteta spremnika i graničnih troškova koji definiraju ekonomsku isplativost.

Treća, završna faza uvodi nesigurnost i proširuje obuhvat na cjeloviti WEFE koncept. Razvijeni dvo-stupanjski stohastički optimizacijski model procjenjuje investicijske i pogonske odluke u uvjetima klimatske i tržišne nesigurnosti. U prvom stupnju određuju se kapaciteti i ulaganja u infrastrukturu, dok se u drugom stupnju optimizira vođenje sustava kroz više scenarija koji predstavljaju moguće hidrološke i ekonomske uvjete. Formulacija razlikuje nekoliko optimizacijskih pristupa – energetski, WE, WEF i WEFE, koji uključuju dodatne dimenzije

financijske i ekonomske dimenzije poput troška vođenja energetskog i vodnog sustava, utjecaja potrebe za navodnjavanjem, smanjenja isparavanja, uštede zbog ne korištenja zemljišta i dodatnih troškova zbog utjecaja rada na cjelokupni ekosustav. Model obuhvaća cjelovit skup fizičkih i okolišnih ograničenja koja osiguravaju vodnu bilancu i energetsku ravnotežu u svim sektorima.

Kroz ovakav postupni razvoj metodološki okvir prerasta u jedinstveno okruženje za donošenje odluka koje omogućuje kvantificiranje kompromisa između suprotstavljenih ciljeva i identificiranje optimalnih strategija projektiranja i vođenja sustava. Integracijom determinističkih i stohastičkih pristupa u jedinstvenu strukturu, okvir pruža robustan analitički temelj za planiranje i upravljanje međusobno povezanim resursnim sustavima u uvjetima nesigurnosti.

KEYWORDS

Holistic energy system modeling

District heating

Water-energy-food-ecosystem nexus

Optimisation

Uncertainty modelling

KLJUČNE RIJEČI

Holističko modeliranje energetskih sustava

Centralizirani toplinski sustavi

Spona vodnog-energetskog-prehrambenog-okolišnog sustava

Optimizacija

Modeliranje nesigurnosti

LIST OF ABBREVIATIONS

EU	European Union
WEFE	Water-Energy-Food-Ecosystem
UN	United Nations
SDG	Sustainable development goals
UNESCO	United Nations Educational, Scientific and Cultural Organization
FAO	Food and Agriculture Organization
UNECE	United Nations Economic Commission for Europe
IPCC	Intergovernmental Panel on Climate Change
RES	Renewable energy systems
DH	District heating
MILP	Mixed-integer-linear programming
TES	Thermal energy storage
CHP	Combined heat and power
PV	Photovoltaic
RO	Reverse osmosis
BES	Battery energy storage
PVT	Photovoltaic-thermal
PSO	Particle Swarm Optimization
EA	Evolutionary Algorithms
SA	Simulated Annealing
WE	Water-Energy
DSM	Demand side management
FPV	Floating photovoltaic
PSH	Pumped storage hydropower
O&M	Operating and maintenance
PtW	Power to water
EWP	Equivalent water price
MC	Monte Carlo
USDA	Natural Resources Conservation Service

WEF	Water-energy-food
EB	Electric boilers
HP	Heat pumps
CCGT	Combined-cycle gas turbines
NREL	National Renewable Energy Laboratory
FPVC	Floating photovoltaic investment cost
LHS	Left-hand side
RHS	Right-hand side
LDC	Load duration curve

NOMENCLATURE

Chemical formulas

CO_2	carbon dioxide

Variables and parameters

$q_{conPipe,l}^{cap,maximum}$	The upper bound of the connecting pipe capacity at location l [MW]
a_l	Binary variable (do invest, don't invest) {1,0}
$q_{conPipe,l}^{cap}$	The connecting pipe capacity at location l [MW]
$q_{conPipe,l}^{cap,minimum}$	The lower bound of the connecting pipe capacity at location l [MW]
$C_{l,n,t}^{VO\&M}$	Variable operating and maintenance (O&M) cost of plant n in hour t at location l [EUR/MWh_{heat}]
$C_{l,n,t}^{fuel}$	The cost of fuel for plant n in hour t at location l [EUR/MWh_{fuel}]
C_t^{CO2}	The cost of CO_2 emission in hour t [EUR/t_{CO2}]
$K_{l,n}$	The CO2 intensity of the plant n at location l [tCO_2/MWh_{heat}]
$R_{l,n,t}^{ele}$	Revenues from electricity sales of plant n in hour t at location l [EUR/MWh_{ele}]
L_n	Electricity-to-heat generation ratio of plant n [MWh_{ele}/MWh_{heat}]
$c_{l,n,t}$	Start-up cost activation binary variable {1,0}
$C_{l,n}^{startup}$	Start-up cost of plant n at location l [EUR]
$q_{l,n,t}$	Heat power of plant n in hour t at location l [MW_{heat}]
H	One hour (used for relating the energy generated in MWh)
$C_{l,n}^{cap}$	Annualized capacity cost of plant n at location l [EUR/MW]
$C_{l,n}^{FO\&M}$	Fixed O&M cost of plant n at location l [EUR/MW]
$q_{l,n}^{cap}$	The capacity of plant n at location l [MW]
S_l	Annualized sunk investment cost in the case of piping investment decision at location l [EUR]
$E_{l,t}$	District heating energy demand in hour t at location l [MWh_{heat}]
$s_{l,t}^{ch}$	Heat charge of heat accumulator in hour t at location l [MWh_{heat}]
$s_{l,t}^{dis}$	Heat discharge of heat accumulator in hour t at location l [MWh_{heat}]
$B^{DC}_{pvc,\,bc,\,t}$	Battery discharging [kWh]
$B^{CH,G}_{pvc,\,bc,\,t}$	Battery charging from the grid [kWh]
$B^{CH,PV}_{pvc,\,bc,\,t}$	Battery charging from available PV generation [kWh]
$B^{SOC}_{pvc,\,bc,\,t}$	Battery state of charge [kWh]
$B^{P}_{pvc,\,bc,\,t}$	Battery power output [kW]
$PV^{D}_{pvc,\,bc,\,t}$	PV power used for the desalination electricity demand [kWh]

$PV^{G}_{pvc, bc, t}$	PV power transferred to the grid [kWh]
$PV^{E}_{pvc, bc, t}$	PV generation [kWh]
$X^{PV}_{pvc, bc, t}$	Binary variable allowing PV battery charging {1,0}
$X^{G}_{pvc, bc, t}$	Binary variable allowing grid battery charging {1,0}
$X^{DC}_{pvc, bc, t}$	Binary variable allowing battery discharging {1,0}
$E^{D}_{pvc, bc, t}$	Electricity demand [kWh]
$B^{NP}_{pvc, bc}$	Optimal battery power [kW]
$B^{C}_{pvc, bc}$	Optimal battery capacity [kWh]
$PV^{P}_{pvc, bc}$	Optimal PV power [kW]
$W^{B}_{pvc, bc, t}$	Water boat carriers for water demand [m^3]
e^{P}_{t}	Grid electricity price profile [EUR/kWh]
w^{BC}	Water boat carrier cost [EUR/m3]
ll^{c}	Lost load cost [EUR/kWh]
pv^{var}	Variable PV cost [EUR/kWh]
b^{MCC}	Battery storage capacity maintenance cost [EUR/kWh/a]
b^{MPC}	Battery storage power maintenance cost [EUR/kW/a]
e^{S}_{t}	Selling electricity price profile [EUR/kWh]
$b^{CC}{}_{bc}$	Battery storage capacity investment cost [EUR/kWh]
ζ	Weighting factor for the two investment battery storage costs
cr	Capital recovery factor
$b^{PC}{}_{bc}$	Battery storage power investment cost [EUR/kW]
$pv^{C}{}_{pvc}$	PV power investment cost [EUR/kW]
$icdf$	Battery storage investment cost decrease factor
pvf	Present value factor
Δ	Saturation slope vapour pressure curve at T_{hr} [kPa/°C]
R_n	Net solar radiation [MJ/m^2h]
G	Soil/water body heat flux density [MJ/m^2h]
γ	Psychrometric constant [kPa/°C]
T_{hr}	Mean hourly air temperature [°C]
$e^{0}[T_{hr}]$	Saturation vapour pressure at T_{hr} [kPa]
e_a	Average actual vapour pressure [kPa]
u_2	Average hourly wind speed at 2 m [m/s]
$w^{agri}_{s,t}$	Agriculture irrigation needs per m^2 [m^3/m^2]

p_s	Scenario s probability [%]
FPV^p	FPV nominal power [MW]
$E_{s,t}^{FPV_P}$	Electricity flow – FPV to pump [MWh]
$E_{s,t}^{P_g}$	Electricity flow – grid to pump [MWh]
$E_{s,t}^{P}$	Electricity flow – total electricity to pump [MWh]
$E_{s,t}^{T}$	Electricity flow – hydro electricity generation [MWh]
$E_{s,t}^{FPV_g}$	Electricity flow – total FPV to grid [MWh]
$W_{s,t}^{eva_{save}}$	Water flow – evaporation savings [m^3/h]
$W_{s,t}^{spill}$	Water flow – total water spillage [m^3/h]
$W_{s,t}^{ll}$	Water flow – lost load [m^3/h]
$W_{s,t}^{agri}$	Water flow – total agriculture irrigation needs [m^3/h]
$E_{s,t}^{FPV}$	Total upper storage FPV electricity generation [MWh]
$Z_{s,t}^{E}$	Energy focused sum of revenues and costs [EUR]
$Z_{s,t}^{WE}$	Water-Energy focused sum of revenues and costs [EUR]
$Z_{s,t}^{WEF}$	Water-Energy-Food focused sum of revenues and costs [EUR]
$Z_{s,t}^{WEFE}$	Water-Energy-Food-Ecosystem focused sum of revenues and costs [EUR]
ic^{FPV}	FPV investment cost [EUR/MW]
cr	Capital recovery factor
p_s	Scenario s probability [%]
isc	Inverter share cost in total RES CAPEX cost [%]
pvf_r	Present value factor for replacement r
lsr	Land sparing ratio (PV to FPV area ratio)
lus	Land use savings [EUR/m^2]
λ_t^{emp}	Electricity market price [EUR/MWh]
bb	Electricity buy-back factor [%]
hyd^{omc}	Hydropower operation and maintenance cost [EUR/MWh]
fpv^{omc}	FPV operation and maintenance cost [EUR/MWh]
λ^{ewp}	Equivalent water price [EUR/m^3]
λ^{spill}	Water spillage cost [EUR/m^3]
λ^{wll}	Water lost load cost [EUR/m^3]
λ^{eco}	Ecological external cost on hydropower generation [EUR/MWh]
sn	Small number cost value
co_2^{geq}	Grid equivalent CO_2 emissions [tCO2/MWh]

co_2^{FPV}	FPV CO_2 emissions [tCO2/MWh]
co_2^{hyd}	Hydropower CO_2 emissions [tCO2/MWh]
$co_{2_{cp}}^{c}$	CO_2 price [EUR/tCO2]
ET_0	Reference evapotranspiration [mm/h]
ET_c	Crop evapotranspiration under standard conditions [mm/h]
K_c	Crop coefficient
P_{eff}	Effective precipitation [mm/h]
P_{tot}	Total precipitation [mm/h]

Sets

$l \in L$	Location set
$n \in N$	Technology set
$t \in T$	Time step set
$pc \in PC$	Parameter change set
$pvc \in PVC$	PV power investment cost set
bc ∈ BC	Battery storage capacity investment cost set
s ∈ S	Set of scenarios

LIST OF FIGURES

LIST OF TABLES

1 INTRODUCTION

The interdependence of water, energy, food, and ecosystems has become a defining challenge in achieving sustainable and climate-resilient development. Understanding and optimising these cross-sectoral linkages is essential for efficient resource use, renewable energy integration, and social welfare under uncertain climatic and economic conditions. The chapter introduces this context, outlining the evolution of integrated resource-system thinking, key motivations, methodological approaches, and the scientific contributions that shape the scope of the thesis

1.1 Background

The European Union (EU) has taken a global leadership role in advancing climate action, sustainable development, and systemic resource efficiency. Through its flagship policy, the European Green Deal and complementary frameworks like Fit for 55, the EU has committed to achieving climate neutrality by 2050, aiming to transform its economy and society to meet environmental challenges while ensuring prosperity and equity [1]. Key objectives include a 55% reduction in greenhouse gas emissions by 2030, a significant scale-up of renewable energy, and improvements in energy efficiency across sectors.

Achieving these goals, however, requires more than just decarbonizing the power sector. It demands the holistic integration of multiple sectors, including water, heating and cooling, food production, and ecosystem management. This systemic approach is encapsulated in concepts such as sector coupling and nexus thinking. The Water-Energy-Food-Ecosystem (WEFE) nexus offers a framework to assess and govern the interdependencies between these critical systems, while explicitly incorporating ecosystem services as both enablers and constraints [2].

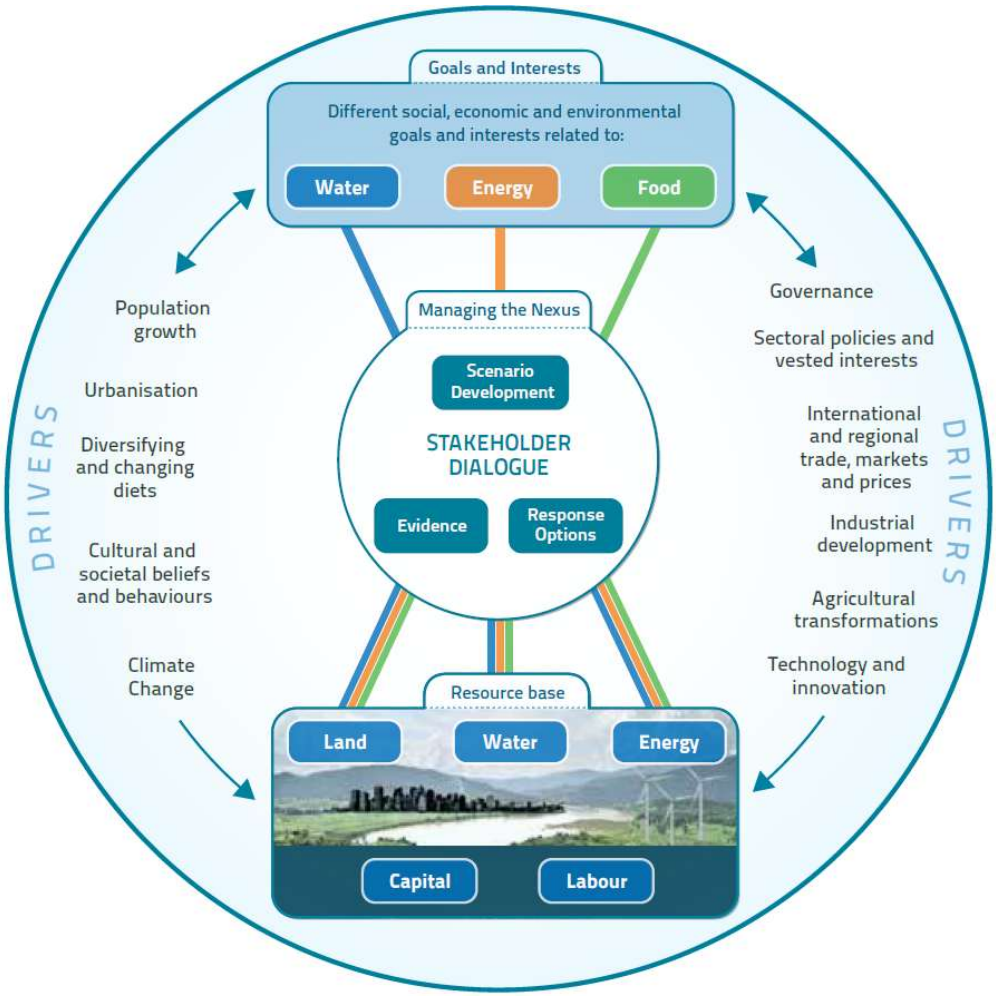

Figure 1. WEFE nexus approach schematics [3]

The concept of the WEFE nexus has evolved as a strategic framework for managing critical resources under interconnected stressors such as climate change, demographic growth, and economic development (Figure 1). While early uses of the "nexus" terminology trace back to the 1980s, a major turning point occurred in 2011, when the World Economic Forum identified the water-energy-food-climate nexus as a global risk and emphasized the urgent need to assess interconnections between these critical systems [4]. This landmark moment helped elevate the nexus from an academic construct to a recognized global policy priority, catalysing interdisciplinary dialogue and funding efforts focused on integrated resource management [5]. Following this, the WEFE nexus gained further visibility through UN-led climate and development conferences which introduced the concept into formal negotiations [6], [7]. Efforts like the Future Earth platform contributed to international research on system interdependencies and resilience [8]. Institutions such as the International Water Resources Association and World Water Council subsequently adopted the nexus framework to guide long-term planning and Sustainable Development Goals (SDG) implementation strategies, especially at the interface of

water, energy, agriculture, and ecosystems [9], [10]. From 2015 onward, significant investments and political initiatives further institutionalized the nexus approach. For instance, the National Science Foundation's "*Innovations at the Nexus of Food, Energy and Water Systems*" program in the U.S. and the EU-funded PRIMA program in the Mediterranean helped structure funding calls explicitly targeting WEFE nexus projects and communities of practice [11], [12], [13].

The direct inclusion of ecosystems as a fourth nexus dimension was a critical milestone. As described by UNESCO in 2021, this shift acknowledged the essential role ecosystems play in sustaining water, food, and energy flows, particularly through services like flood protection, land-use, emission savings, and climate regulation [14]. Today, the WEFE Nexus is recognized not only for its conceptual clarity but for its operational potential to support SDG integration, climate adaptation, and transboundary resource governance [3], [15], [16].

The interdependence between the four sectors is both functional and systemic. Water is indispensable for energy generation, whether in hydropower generation, thermal cooling, and equally vital for agricultural irrigation and food processing. In turn, energy is essential for water treatment, pumping, and distribution, as well as for agricultural activities such as pump operation and food storage. Food production depends on both water and energy availability and has direct implications for land use, emissions, and biodiversity [17]. Heating and cooling systems are also tightly coupled with water availability, land-use patterns, and ecosystem capacity, particularly in urban and industrial contexts [3], [18]. Ecosystems, meanwhile, support all other sectors by regulating hydrological cycles, maintaining soil fertility, and absorbing pollution and greenhouse gases. Disruption in one system, such as drought affecting water supply or change in market conditions, can cascade into energy shortages, reduced agricultural yields, and ecosystem degradation, highlighting the need for coordinated responses across the nexus [19]. Climate change amplifies the complexity and urgency of managing these interactions. Shifts in temperature, precipitation variability, and the frequency of extreme weather events are directly influencing water availability, agricultural productivity, and energy reliability. Moreover, the uncertainty embedded in long-term climate models complicates infrastructure planning, resource allocation, and operational decision-making [20].

In this context, the WEFE nexus does more than guide policy coordination. It serves as a conceptual and operational tool that emphasizes the need for holistic modelling and integrated analysis. By accounting for the cross-sectoral linkages among energy, heating, cooling, water, food, and ecosystem services, the WEFE framework encourages planners, modelers, and

policymakers to shift away from isolated approaches and toward systemic, scenario-based planning. It ensures that resource use is optimized not in isolation but in a way that respects ecological thresholds, maximizes co-benefits, and improves overall resilience and sustainability [2], [21] .

Global institutions, including the FAO, UNECE, and IPCC, as well as regional policymakers and academic communities, are increasingly advocating for nexus-based strategies as essential to achieving the SDGs. The WEFE nexus is now recognized not only as a theoretical framework, but also as a practical instrument for translating climate targets into coordinated investment and policy actions, particularly at the interface of resource systems and human well-being.

1.2 Motivation and general overview

As mentioned in previous sections, increasing complexity and interdependence of modern infrastructure systems require a shift away from traditional, single-sector planning approaches toward more holistic and integrated strategies. Energy, water, food, and land systems are interconnected through physical, economic, and environmental linkages that demand systems-level understanding and coordination. As societies face mounting pressures from climate change, market volatility, and resource scarcity, the urgency for models and tools that reflect these interdependencies has become more evident than ever.

Current approaches are still predominantly sectoral, lacking the ability to fully capture the cascading effects that decisions in one system may have on others, especially under climate uncertainty and volatile market conditions. Planning within sectoral boundaries is often insufficient to address the kinds of challenges emerging from climate change, market volatility, and resource scarcity. For example, decisions made to optimize energy systems, such as the deployment of new technologies for heating or cooling, can have significant implications for water resources and land use. Similarly, expanding water supply through desalination or pumping can affect electricity demand, emissions, and long-term system flexibility. Without coordinated planning, these interdependencies can result in unintended trade-offs, inefficient investment, or increased vulnerability to external effects.

A more comprehensive approach is therefore needed, one that can simultaneously account for technical, economic, and environmental dimensions across multiple sectors. This includes the ability to evaluate scenarios under uncertain conditions, integrate emerging technologies like renewable energy systems (RES) and storage, and reflect spatial and temporal variability in demand and resource availability. Such an approach supports better-informed decisions,

improves the alignment of infrastructure development with sustainability goals, and enhances resilience at both local and regional scales.

The WEFE nexus has emerged as a prominent example of this kind of systems thinking. It provides a structured way to explore the interactions among resource sectors, promoting integrated solutions that can balance competing needs. While the WEFE concept has gained recognition in global policy and research agendas, turning it into a practical tool for planning and optimization under uncertainty remains a significant challenge, particularly when it comes to developing effective modelling frameworks.

This research was initiated in response to these broader needs. It is grounded in the understanding that achieving sustainability and resilience requires modelling approaches that go beyond optimizing individual technologies or sectors. Instead, it seeks to develop and apply tools that reflect real-world complexity, capturing cross-sectoral interactions, variable boundary conditions, and the implications of technological choices across multiple domains. Additionally, while much attention has been given to high-level nexus policy frameworks, fewer studies translate this into actionable modelling approaches that support scenario analysis, infrastructure design, and optimal operation under uncertainty. This research responds to both a scientific and societal need by aiming to advance methodological tools that enable decision makers to navigate complex trade-offs, explore adaptation strategies, and pursue sustainability goals in a way that is both technically sound and practically relevant.

By focusing on the intersection of energy, water, and ecosystem systems, particularly in contexts where heating, cooling, water production such as desalination, and RES integration come together, this work contributes to bridging the gap between theory and practice in WEFE nexus modelling. It responds directly to the growing consensus among scientific, policy, and funding communities that cross-sectoral, systemic planning is essential for delivering on climate goals and sustainable development pathways.

1.2.1 Holistic energy system modelling on urban level

Holistic energy system modelling at the urban level is essential for understanding and managing the complex interactions among district heating (DH), cooling systems, electricity networks, and water distribution infrastructures. Integrated modelling approaches allow for capturing synergies between these interconnected systems, optimizing resource use, and minimizing environmental impacts.

The authors in [22] emphasize the benefits of smart energy systems, demonstrating their potential in significantly enhancing RES integration and transport solutions at the urban scale.

Their research highlights coordinated interactions among heating, electricity, and transport sectors to achieve greater overall system efficiency and sustainability. Optimization methodologies specifically tailored for DH and cooling thermal networks are presented in [23]. The study introduces various optimization algorithms and frameworks that facilitate efficient resource allocation and operational management in urban thermal networks, resulting in substantial energy savings and improved system reliability. The practical application of integrated energy and water systems through demand response mechanisms is illustrated by the study in [24]. This research demonstrates significant potential for reducing electricity consumption and operational costs via optimized pump scheduling in water distribution systems, highlighting the importance of cross-sectoral integration. Study [25] examines variable taxation strategies designed to promote flexibility within DH systems using heat pumps. By leveraging policy mechanisms, this approach successfully incentivizes the integration of renewable heat sources and energy storage, enhancing system flexibility and resilience to demand fluctuations. The optimisation of multi-energy microgrids through mixed-integer linear programming (MILP) is detailed in [26]. The study explores optimal portfolios, sizing, and placement of distributed energy resources, emphasizing an integrated approach that balances economic viability with environmental considerations, providing robust solutions for urban-scale energy planning.

District heating traditionally relies on combined heat and power plants, waste-to-heat plants, and industrial sources. Recently, it has expanded to include RES such as biomass, geothermal energy, and solar thermal systems, reflecting a broader shift towards sustainable urban energy systems [27], [28]. This transition aligns closely with the emergence of 4th Generation District Heating systems, emphasizing integration across heating, electricity, and transport sectors to create comprehensive smart energy solutions [29]. Such systems require careful strategic planning, effective operational incentives, and robust investment frameworks to ensure their feasibility and economic viability [30], [31].

An extensive review of modelling approaches and tools for designing and simulating DH networks is provided in [32]. This work evaluates steady-state, quasi-dynamic, and fully dynamic simulation methods, along with numerical techniques like the Hardy-Cross method and node-element methods. It identifies critical research gaps, including insufficient standardization of benchmarks and limited integration of environmental assessments like life-cycle analyses, underscoring the need for further development in DH modelling tools. Similarly, a comprehensive meta-review of software tools for urban energy system planning,

specifically for DH and cooling systems, is conducted in [33]. The review emphasizes the growing importance of open-source tools and object-oriented frameworks, such as Modelica and Python-based solutions, highlighting their flexibility and suitability for complex urban-scale energy system analyses. However, it also highlights ongoing gaps related to integration with environmental impact assessments and standardization of software functionalities.

A simplified modelling approach utilizing archetype-based analyses for assessing the feasibility of DH networks in urban and rural contexts is proposed in [34]. This study emphasizes significant differences in heat demand patterns and network characteristics based on population density, stressing the importance of accurate building-level data integration to improve model reliability. An advanced MILP model for optimizing hourly operations and long-term strategic planning of DH systems, explicitly considering building refurbishment scenarios, is developed in [35]. Applied in a Zagreb, the model demonstrates substantial reductions in operational costs and emissions through integrated utilization of heat pumps, electric heaters, solar thermal collectors, and thermal storage, underscoring the benefits of comprehensive energy planning models. An exploration of multiple successful European DH markets is carried out in [36], identifying local dynamics as a critical determinant of system effectiveness. The study concludes that tailored, municipality-specific strategies are indispensable due to distinct local conditions, reinforcing the importance of context-specific planning and implementation approaches. The necessity of municipal-level decision-making and targeted local studies for effective DH systems is further supported in [37]. This work underlines local features and conditions as vital considerations in developing efficient, sustainable urban energy systems.

The analysis of benefits arising from interconnecting geographically distributed DH grids is presented in [38], promoting structural evolution from tree-like to ring-like or fully meshed configurations. Improvements in heat transfer capacity, system reliability, and operational flexibility resulting from strategic thermal energy storage (TES) integration are highlighted. Supporting this view, the role of TES in buffering heat demand fluctuations, enhancing combined heat and power (CHP) plant efficiencies, and reducing operational costs is further elaborated in [39]. Optimization methods critical to achieving urban sustainability goals are explored in [40], which employs MILP models to optimize configurations and operations of distributed energy supply systems, addressing both economic efficiency and carbon emission reductions. Similarly, [41] utilizes MILP modelling for the structural and operational optimization of energy systems, demonstrating cost and operational benefits in complex urban environments. Multi-objective MILP models designed to optimize the economic and

environmental performance of distributed energy resources integrated with DH networks are contributed by [42]. This approach effectively balances multiple competing objectives, ensuring both cost-efficiency and environmental sustainability. Studies [43], [44], and [45] employ MILP and heuristic optimization models, such as genetic algorithms, to optimize DH network designs, pipe diameters, and operational strategies. These methods provide robust, balanced solutions, addressing economic and environmental objectives within urban energy planning effectively.

Despite significant advancements, critical gaps remain in current urban energy system modelling approaches. Short-term operational optimization often overshadows comprehensive long-term strategic planning, and critical sub-hourly temporal dynamics are insufficiently addressed. Additionally, broader integration of water-energy nexus interactions and environmental impacts, including biodiversity considerations, remains underdeveloped. Addressing these gaps through enhanced modelling techniques and advanced uncertainty analyses will empower urban planners and policymakers, facilitating resilient, sustainable, and efficiently integrated urban energy infrastructures.

1.2.2 Renewable energy and water system integration in remote areas

The integration of RES with water supply infrastructure has become a significant research focus, especially in remote and island areas where conventional energy supply and freshwater resources are limited. Islands as isolated regions often suffer from high costs associated with fossil fuel imports and face increasing pressures from climate variability and tourism-driven seasonal demands, making them ideal testbeds for innovative solutions that couple local RES with essential services like water production.

Early methodological developments have provided a structured approach to assess the feasibility of sustainable energy and water systems for islands. A prominent example is the RenewIslands methodology, which established a four-step framework including the mapping of local demands, resource assessment, technological scenario development, and system modelling, offering a versatile tool adaptable to diverse island contexts such as Corvo, Porto Santo, and Mljet [46]. This holistic view underlined the potential for resource integration but also emphasized the site-specific nature of solutions. Building on this foundation, subsequent work has expanded into exploring interconnections between multiple islands to leverage shared resources. For example, the study in [47] proposed interconnected energy systems across island groups, enabling higher penetration of local RES and utilizing electric vehicles as storage assets through vehicle-to-grid strategies. Simulation tools such as EnergyPLAN and the MultiNode

extension facilitated analysis of power flows and interconnection impacts, revealing that increased RES deployment can reduce critical excess electricity and improve overall system efficiency.

Sector coupling has further evolved to include not only electricity but also heating, cooling, and transport services. The research in [48] investigated integration of the power, heating, cooling, and transport sectors on an island targeting carbon neutrality with exclusive reliance on intermittent RES. Using EnergyPLAN, the authors demonstrated how a series of simulations can approximate near-optimal solutions by balancing investment costs and electricity imports and exports. Similarly, the modelling approach in [49] applied PLEXOS to analyse a Caribbean island nation, where an integrated energy system included power, transport, cooling, and desalination sectors. The model revealed that high shares of RES could cover 78.1% of electricity demand with only one percent curtailment. When socio-economic factors such as CO_2 costs were incorporated, the RES system proved 2.5% more cost-effective than the fossil fuel alternative.

Desalination has emerged as a central technology in addressing water scarcity on islands, where traditional supply methods such as water transport by ship are both economically and environmentally unsustainable [50]. Desalination processes broadly fall into thermal-based and membrane-based categories, each with distinct energy requirements and operational characteristics. Thermal processes typically demand higher energy inputs, approximately 20 kWh/m^3 of freshwater, whereas membrane-based processes, particularly reverse osmosis (RO), operate in the range of 1-6 kWh/m^3 [51]. Recent reviews have underscored the growing interest in innovative desalination technologies such as forward osmosis, membrane distillation, and electrochemical processes, as well as the adoption of smart process monitoring and control systems to reduce operational costs and enhance system resilience [52]. These emerging technologies show promise for reducing the high energy intensity that has historically constrained desalination's economic viability in remote contexts.

Given the inherent energy requirements of desalination, the integration of RES has become an increasingly important research field, offering opportunities to decarbonize water production while mitigating fossil fuel dependence. Numerous comprehensive reviews have systematically evaluated RES integration with desalination technologies, exploring both technical and economic dimensions. For instance, the study in [53] provided a detailed survey of various combinations of RES resources such as wind, solar thermal, photovoltaics (PV), geothermal, and wave energy with desalination methods like RO, multi-stage flash distillation, multiple-

effect distillation, membrane distillation, and electrodialysis. This work clarified the advantages, disadvantages, and cost implications of different configurations, emphasizing the critical role of system design in achieving efficient and cost-effective solutions. Likewise, the reviews in [54] and [55] highlighted key challenges associated with the variability of RES, the importance of energy and water storage systems, and the optimization of hybrid systems for stable and economical operation.

Empirical studies have further advanced understanding of hybrid systems tailored for island conditions. In [56], a stand-alone RO system was designed for a Greek island of approximately 5,000 residents, integrating PV, wind, and hydropower within a stochastic optimization framework. The findings indicated that local RES generation coupled with desalination is more cost-effective than importing water, validating the potential for self-sufficient island systems. Similar insights emerged from [57], where a microgrid on Gran Canaria was modelled to supply an RO desalination plant using wind and PV. The analysis concluded that battery energy storage systems (BES) were not essential for optimal operation under certain scenarios, suggesting that proper system design can offset the need for costly storage investments. Another example is the study in [58], where a hybrid PV and wind system was evaluated for an island community, comparing three desalination technologies. RO again emerged as the most cost-effective solution, particularly when combined with hybrid renewable generation and BES. Although HOMER software facilitated optimization, the authors noted that such tools often rely on a simulation-based approach where multiple configurations are evaluated rather than solving a formal mathematical optimization problem.

Hybrid systems combining desalination with RES have also explored novel configurations and operational strategies. For instance, research in [59] reviewed decades of wind-driven desalination projects in the Canary Islands, identifying factors critical to system success such as technological modernization, siting decisions, and BES sizing. These insights offer valuable guidance for designing future systems in similar island contexts. The study in [60] developed a mathematical model to optimize the energy mix for desalination plants, considering scenarios with and without PV and incorporating time-of-use tariffs to enhance cost-effectiveness. Advanced solutions such as photovoltaic-thermal (PVT) systems have also been examined for their dual capability to supply both electrical and thermal energy, potentially improving efficiency and reducing costs in solar-powered desalination [61].

Optimization approaches have become essential in designing and operating hybrid RES-desalination systems, although the literature reveals diverse methodologies and varying levels

of rigor. The review in [62] documented mathematical and optimization models for desalination systems, discussing challenges related to energy consumption, fouling, and integration with renewable power sources. Another review in [63] offered a structured analysis of optimization techniques, distinguishing between classical mathematical methods and artificial intelligence-based algorithms such as Particle Swarm Optimization (PSO), Evolutionary Algorithms (EA), and Simulated Annealing (SA). The literature shows that optimization efforts typically focus on system sizing, operational planning, and thermodynamic performance, with increasing attention to dynamic and stochastic modelling to address the uncertainty inherent in RES availability.

The diversity of optimization tools and methods is evident across recent studies. Metaheuristic algorithms have gained prominence due to their ability to handle non-linear, multi-objective problems with numerous constraints. For example, the work in [64] applied the improved bees algorithm to optimize a hybrid RES-RO system, comparing it favourably against harmony search techniques. Similarly, hybrid methods combining different optimization strategies have shown superior performance, as illustrated in [65], where a combination of harmony search and chaotic search yielded better results than single algorithms alone. Comprehensive evaluations of multiple metaheuristic methods were performed in [66], demonstrating the advantages of hybrid algorithms for achieving faster convergence and higher accuracy in system design. Additionally, studies such as [60] have explored innovative two-loop optimization approaches where MILP models determine operational strategies within a broader heuristic framework, reflecting a growing trend towards integrated and hierarchical optimization structures.

Linear programming, particularly Mixed-Integer Linear Programming (MILP), has emerged as a valuable tool for modelling operational flexibility and demand response within the water-energy (WE) nexus. Research in [24] addressed pump scheduling in water networks as a demand response mechanism, offering grid services and cost savings. The study in [67] applied MILP to evaluate the combined impact of PV and wind energy on water supply systems in the Canary Islands, finding that demand shifting significantly improves RES energy self-sufficiency. More sophisticated models have been developed, as in [68], where MILP formulations incorporated water and energy storage dynamics, thermal unit commitment, and power flow constraints. Such studies underscore the potential of advanced optimization to reconcile competing objectives, minimize operational costs, and enhance resilience in integrated WE systems.

Flexibility remains a central challenge in hybrid systems combining RES and desalination, particularly in remote areas where grid support is limited or absent. Energy storage technologies, demand side management (DSM), and flexible system operation are key enablers for addressing the variability of RES. The review in [69] underscored the importance of energy storage and DSM in ensuring operational reliability for islands, while also highlighting the potential of RO units to function as flexible loads that can store energy in the form of water. Studies such as [70] and [71] further demonstrated the value of coordinated system designs that leverage both BES and water storage to enhance flexibility and reduce reliance on oversized renewable installations. Innovative approaches focusing on seasonal water storage as an alternative to expensive BES have been proposed in [72], suggesting practical pathways for reducing costs while maintaining reliability. Demand response strategies tailored to island networks have also been explored, as in [73], revealing economic incentives that can unlock system flexibility and enhance RES integration. The conceptual proposal in [74] introduced a modular RO design that accommodates fluctuating RES availability, further demonstrating how desalination systems can support grid stability while lowering costs. Technical reviews such as [75] have highlighted the critical need for future studies to address membrane performance under variable power inputs, control system adaptations, and integration of RES variability into system models.

The integration of renewable energy sources with desalination and water systems in remote areas represents a dynamic and evolving research field. Significant progress has been made in understanding technical configurations, optimization strategies, and flexibility solutions. Yet, challenges remain in bridging the gap between conceptual studies and practical implementations, particularly in developing robust, cost-effective systems capable of handling the variability of both demand and supply under real-world constraints. The growing body of literature demonstrates not only the feasibility of RES-powered water systems for remote regions but also the necessity of continued innovation in modelling, optimization, and systems integration to achieve sustainable and resilient infrastructure solutions.

1.2.3 Renewable energy system and storage integration

The integration of RES with effective storage solutions has emerged as a crucial aspect of energy research, particularly vital in isolated, remote, and island communities due to challenges such as resource intermittency and limited infrastructure. This integration involves diverse storage methodologies, notably BES, hydrogen storage, and water-based storage, all critical in maintaining grid stability and enhancing overall system resilience.

Comprehensive studies highlight that achieving grid flexibility through optimal storage integration significantly enhances RES viability. A detailed literature review in [69] categorizes flexibility into electricity storage, supply-side solutions, and sector coupling. Particularly, the role of flexible water systems, such as RO based desalination, has become pronounced in island communities. These systems can transform surplus RES generated electricity into stored potable water, effectively balancing energy supply and seasonal demand fluctuations. Hybrid RES energy configurations integrating BES, hydrogen storage, and desalination units have been extensively studied. For instance, research in [64] examined six configurations incorporating wind energy, PV, BES, and hydrogen storage. Utilizing optimization approaches with discrete and continuous variables, the study concluded that the PV-BES hybrid system presented superior cost-effectiveness.

The role of PV systems specifically tailored to power RO desalination units has also gained substantial attention. Study [76] presented a case study on Nisyros Island, showcasing a scalable and sustainable PV-RO integration applicable to other Mediterranean islands experiencing similar water scarcity issues. On Gran Canaria Island, a similar exploration in [57] evaluated wind and PV integration along with BES and grid connections, but interestingly concluded BES storage was not always economically favourable, indicating the necessity for context-specific assessments. Water storage, particularly when integrated with desalination technologies, effectively mitigates RES intermittency by converting surplus electricity into potable water reserves. Highlighting this, study [70] demonstrated that integrating smaller BES units with water storage effectively managed intermittent RES output, significantly enhancing overall system flexibility. Further, seasonal water storage explored in [72] confirmed economic competitiveness, albeit noting high levels of energy curtailment.

Advanced optimization methodologies have significantly contributed to the effective design and management of hybrid RES-storage systems. PSO, for instance, has been effectively employed in several case studies, including study [77], which assessed a hybrid RES microgrid integrating PV, wind, BES, and RO desalination systems tailored for small islands. This research demonstrated strong technical and economic feasibility but also noted limitations due to the predefined RES energy capacities used as fixed parameters instead of optimized variables. Similarly, study [78] applied PSO to optimize a PV-based pumping system combined with hydro storage in rural Nigeria. Despite the optimization of BES sizing, the analysis was constrained by limited optimization horizons, highlighting common limitations across similar studies. Additionally, comparative research by [79] evaluated PSO against HOMER software

in optimizing PV and hydrogen-based RO systems, identifying PSO as superior but highlighting limitations due to predefined renewable capacities.

MILP and hybrid optimization algorithms have played a pivotal role in enhancing BES operational efficiency and system economics. Study [80] employed MILP to minimize energy consumption within micro water-energy systems, although RES energy capacities remained fixed parameters. Another MILP-based approach, presented in study [81], optimized the integration of BES and water storage within remote microgrids. However, this approach similarly faced constraints, notably using fixed RES capacities and short-term optimization horizons. Studies [82] and [83] extended MILP optimization to multi-energy complementary systems, aiming for co-optimization of BES and thermal energy storage, but often maintaining RES capacities as fixed inputs.

The placement, sizing, and operational scheduling of BES in distribution networks with high-RES penetration have been studied extensively. For example, research by [84] aimed to optimize BES placement and sizing within high-PV environments, yet limitations included assumptions of fixed daily charge/discharge patterns extrapolated to annual scenarios. Study [85] developed a hybrid tabu search and PSO algorithm to determine BES sizing and location, though this approach constrained operational flexibility by allowing only one charge/discharge cycle daily and predefined RES capacities. Further, study [86] examined decentralized BES integration within medium voltage grids but faced similar restrictions concerning fixed RES parameters and limited simulation horizons.

Hydrogen storage complements BES, addressing seasonal energy variability and offering long-term stability. Study [87] introduced a combined system integrating wind energy, hydrogen storage, and RO desalination, achieving optimal cost-effectiveness despite restricting analysis to short-term scenarios. Iterative optimization methodologies explored by [88] and [89] further demonstrated practical applications of PV/wind/hydrogen hybrid systems, underscoring the feasibility and adaptability of hydrogen storage solutions in remote locations.

DSM has also emerged as essential for balancing RES generation and storage capabilities. DSM implementations examined in study [73] revealed significant economic advantages even at lower incentive thresholds. Study [67] validated DSM's effectiveness in improving RES utilization and energy self-sufficiency within the Canary Islands. Moreover, study [68] integrated BES and water storage in thermal unit scheduling, resulting in marked operational cost reductions, advocating broader DSM integration.

Despite considerable advancements, existing research indicates persistent gaps, notably in explicitly optimizing RES energy capacities within integrated WE models. Future studies must prioritize the explicit optimization of RES capacities, extending analyses to longer-term horizons. Addressing these research gaps will markedly improve the economic and operational effectiveness, reliability, and practical applicability of hybrid RES energy and storage solutions for remote and isolated communities.

1.2.4 Hydropower as a cross-sectoral nexus component

Hydropower plays a pivotal role in the WEFE nexus, serving as a flexible and reliable component in hybrid RES that integrate variable sources. Its ability to provide dispatchable power and energy storage through pumped storage hydropower (PSH) makes it a cornerstone for enhancing system resilience, particularly in remote areas where energy and water demands are tightly coupled. Recent literature has advanced the modelling of hydropower's integration with variable RES, but significant gaps remain in addressing cross-sectoral interactions, uncertainty management, and long-term planning within the WEFE framework.

Modelling efforts have primarily focused on energy-centric coordination of hydropower with wind and PV. For instance, a study [90] developed a robust day-ahead dispatch model for cascaded hydropower-PV systems, incorporating PV uncertainty through non-parametric ambiguity sets within a MILP framework. The model accounts for operational constraints such as reservoir limits and startup penalties, improving short-term dispatch reliability. Similarly, the authors in [91] proposed a multi-objective stochastic scheduling model for cascade hydropower-PV systems with pumping capabilities, optimizing for reduced output deviation and enhanced peak shaving. However, both studies are limited to short-term energy metrics and exclude broader WEFE dynamics, such as water allocation for irrigation or ecosystem services.

To address longer-term planning, the authors in [92] presented a two-stage stochastic MILP model for generation and transmission expansion planning, integrating PSH with wind, PV, and thermal power. While this approach provides detailed insights into electricity storage, it overlooks water use beyond hydropower and fails to incorporate food or ecosystem considerations. Similarly, in [93] a long-term sequential simulation is to evaluate three PSH retrofit options within a cascaded hydropower-wind-PV hybrid system. Their deterministic model, with weekly re-optimization cycles, offers valuable comparisons of seasonal and structural flexibility but lacks stochastic uncertainty modelling and cross-sectoral integration.

Uncertainty management is a critical aspect of hybrid system modelling, particularly under climate variability. The authors in [94] applied a two-stage stochastic model to explore climate

adaptation strategies in a hydro-dominated power system, incorporating uncertainties in hydropower generation, gas prices, and policy. However, the annual time step and fixed capacities limit operational insights, though the authors advocate for a WEFE-oriented perspective in future planning. In [95] proposed a two-stage stochastic multi-criteria framework to evaluate wind-PV-hydropower configurations, effectively managing preference uncertainty but omitting system dispatch and storage dynamics. Study shown in [96] co-optimized wind, thermal, hydropower, and PSH units using a two-stage stochastic approach with reserve allocation, treating wind and hydropower as zero-cost units. Despite capturing reservoir constraints, the model excludes food and ecosystem integration. Formulation of a chance-constrained MILP for hourly coordination of wind and PSH is shown in [97], addressing uncertainty via scenario clustering and sequence analysis to maximize generation, but it remains focused on short-term energy balancing.

More comprehensive approaches have emerged to tackle uncertainty and system integration. A two-stage stochastic model combining cascade hydropower, PV, wind, and BES, using probabilistic sampling and scenario reduction to handle medium and long-term load growth uncertainties is proposed in [98]. While this study advances operational coordination, it does not account for evaporative losses or agricultural water demands. The authors in [99] used a two-stage stochastic optimization to determine water value in a diesel-wind-PSH hybrid system over a two-week period, incorporating uncertainty but omitting water allocation and evaporative losses, which are critical.

Recent reviews [100] and [101] highlight the fragmented state of modelling practices for PSH-RES hybrid systems. They note a reliance on closed-source software, lack of methodological transparency, and limited real-world case studies. Most studies focus on short operational horizons and rarely address PSH configurations with PV or floating photovoltaic (FPV), despite their potential to reduce evaporative losses and land-use conflicts in water-constrained regions. The authors in [102] proposed a qualitative site selection framework for FPV-PSH integration based on multi-criteria decision-making, but it lacks system dynamics or cross-sectoral modelling. Similarly, in [103] a hybrid FPV-PSH system with hydrogen and thermal production is analysed, yet their deterministic model excludes optimization and WEFE linkages.

Across these studies, a clear emphasis on energy-system coordination and uncertainty management emerges, but integration of water, food, and ecosystem dynamics remains limited. Most models prioritize energy metrics, neglecting evaporative water losses, irrigation demands, or land-use impacts, which are critical for holistic WEFE nexus assessments. We here propose

to address these gaps by developing a stochastic optimization framework that integrates PSH with FPV, explicitly modelling evaporative water loss, irrigation demand, and land-use savings. This approach enables a comprehensive evaluation of hybrid system performance under technical and environmental constraints, aligning with the needs of remote areas where water and energy solutions must be co-optimized.

1.2.5 Modelling the water-energy-food-ecosystem nexus under climate and economic uncertainty

The WEFE nexus provides a sophisticated framework for addressing the interlinked challenges of water, energy, food, and ecosystem resources, particularly under climate and economic uncertainty. Unlike sector-specific approaches, such as RES integration or desalination discussed in prior sections, the WEFE nexus captures cross-sectoral interdependencies and their cascading effects across multiple domains. This demands advanced optimization techniques and robust uncertainty modelling to support resilient infrastructure planning and operational strategies. Below written synthesizes recent advancements in WEFE nexus modelling, emphasizing integrated approaches and the application of stochastic and robust optimization to manage uncertainty, while identifying critical research gaps and future directions.

The WEFE nexus excels in modelling interdependencies to ensure that decisions in one sector do not compromise others. For instance, the study in [104] develops a multi-objective optimization framework that integrates RES with agricultural and livestock production, balancing cost, emissions, and water sustainability. Its deterministic formulation, however, limits its ability to address climate or economic variability. Research in [105] employs a nonlinear multi-objective optimization model to evaluate trade-offs between hydropower generation and consumptive water demands, incorporating irrigation, municipal, livestock, and industrial requirements while accounting for monthly evaporation losses. This model estimates significant energy losses of 10,520 GWh annually during drought years but lacks stochastic uncertainty treatment and non-hydropower RES integration. The study in [106] introduces a modular, surrogate-based MILP framework to capture hourly interactions within the WEFE nexus, achieving computational scalability but relying on deterministic assumptions. These efforts highlight the complexity of cross-sectoral modelling while underscoring the need for uncertainty-aware frameworks.

Uncertainty modelling is essential for WEFE nexus applications due to the stochastic nature of climate and economic factors. Deterministic models often fail to capture these dynamics. For example, the study in [107] proposes a high-resolution LP model for national energy planning,

integrating hourly techno-economic details and sectoral coupling, but relies on sensitivity analyses rather than probabilistic methods, constraining its robustness. Similarly, research in [108] uses a scenario ensemble approach to assess weather variability in wind and solar systems through out-of-sample simulations across 10 weather years, enhancing risk evaluation but omitting stochasticity within the optimization framework. These studies advance system resolution but fall short of addressing probabilistic WEFE interactions.

Stochastic and robust optimization techniques offer promising solutions for uncertainty management. The research in [109] develops a two-stage stochastic model for water allocation, integrating interval parameters and fuzzy logic to address probabilistic inflows and imprecise constraints. This approach optimizes water management effectively but excludes energy and ecosystem considerations. A stochastic flexible programming framework, as explored in [110], addresses municipal-scale energy-water nexus planning by incorporating interval analysis, joint probabilistic risk modelling, and fuzzy constraints to manage multiple uncertainties. Its exclusion of agriculture and reliance on coarse yearly time steps, however, limit its applicability to dynamic WEFE systems. The study in [111] presents a data-driven multistage adaptive robust optimization framework for energy system transitions, leveraging machine learning-based uncertainty sets and affine decision rules for tractability, but its energy-centric focus neglects broader WEFE interactions. Study [112] employs a stochastic programming model to optimize hydropower dispatch under uncertainties in stream flows and electricity prices, outperforming conventional methods but omitting food and ecosystem dynamics. These methodologies advance uncertainty handling but reveal challenges in developing comprehensive WEFE models.

Integrated WEFE models that incorporate ecosystem services and food production are emerging, though uncertainty modelling remains limited. For instance, the study in [113] assesses the circular economy potential in Turkey's water and agriculture sectors through the WEFE lens, using the Circularity Assessment for Potential Application index to integrate regional data. Its static structure lacks stochastic modelling and high-resolution temporal dynamics. The study [114] develops a multi-reservoir optimization framework to maximize hydropower releases while ensuring environmental flow requirements and addressing irrigation and municipal water demands. This approach overlooks crop-specific outcomes and non-hydropower renewables, constraining its WEFE scope. The study in [115] proposes a hydro-economic water allocation model to quantify economic trade-offs across urban, irrigation, and hydropower sectors, achieving a 7% improvement in allocation efficiency, but it lacks

stochastic risk modelling. These frameworks emphasize ecosystem and food integration but require uncertainty-aware methodologies.

A comprehensive review, as conducted in [116], identifies a persistent gap in incorporating stochastic uncertainty modelling to capture variability and risks across all sectors. Similarly, the research in [117] integrates life cycle assessment, circular economy principles, and resource security into multi-objective optimization, but relies on predefined scenarios rather than probabilistic methods. These analyses highlight the challenge of balancing computational complexity with comprehensive sectoral coverage and robust uncertainty frameworks.

Current WEFE nexus modelling reveals significant limitations. Most studies prioritize operational optimization over system configuration, limiting their utility for long-term planning. Temporal resolution is often coarse, failing to capture sub-daily dynamics critical for energy and irrigation systems. Ecosystem services and food production are underexplored, with few models addressing biodiversity or crop-specific outcomes. While stochastic and robust optimization techniques are gaining traction, their application to holistic WEFE systems remains limited, with many studies focusing on single sectors or scenario-based approaches rather than fully probabilistic models. Future research should develop hybrid models that integrate high-resolution temporal dynamics, comprehensive sectoral coupling, and advanced uncertainty modelling, such as stochastic and robust optimization frameworks. Such models would enable decision-makers to navigate complex intersectoral trade-offs, align infrastructure planning with sustainability objectives, and enhance resilience under climate and economic uncertainty across diverse contexts.

1.3 Objective and hypotheses of research

The objectives of the research include:

- validation of the model of the complex connection of water and energy systems
- improving planning and reducing the cost of building infrastructure
- ensuring more complete integration of available water resources and renewable energy sources through optimal planning and management of the system, and
- adaptation scenario analysis of energy and water systems to climate change and related extreme weather conditions.

This research hypothesis is that using a detailed analysis of water and energy systems, including a data-mining approach for complex nexus between the two sectors, and available climate model forecasts, models to plan optimal operation of water and energy systems can be created,

which will result in minimal water and energy consumption, greater security of supply when compared to the existing one, maximum nexus efficiency, and maximum integration of variable renewable energy sources

1.4 Scientific contribution

The expected scientific contributions of this research are improved and developed models for the optimization of water and energy systems operation under different market and climate circumstances, conditions of extreme climate change, and cases of different water and energy demands in the sectors of agriculture, tourism, industry, and urban and rural settlements.

2 METHODS

The methods section presents the modelling frameworks and optimisation approaches developed to analyse the interactions among WEFE sectors. It introduces a progressive methodological structure that begins with an optimisation of urban district heating, extends to the integrated optimisation of RES and water systems with storage, and culminates in a stochastic two-stage optimisation of the WEFE nexus under climate and market uncertainty. Together, these methods establish a unified framework for evaluating technical, economic, and environmental performance across different spatial and sectoral contexts.

2.1 Technical, economic and environmental optimization method for district heating system in urban agglomeration

This subsection provides an overview of the optimization method applied for the analysis of DH system expansions within urban agglomerations. The method integrates technical, economic, and environmental dimensions, aiming to achieve the most efficient configuration of interconnected DH systems, incorporating RES and minimizing environmental impact.

The applied approach is based on MILP, explicitly designed to support decision-making regarding district heating network expansion and operational optimization. This methodology enhances previous optimization models by introducing endogenous decision-making capabilities, specifically addressing the automatic dimensioning of interconnecting pipes between different DH systems, as well as integrating TES solutions. The model employs binary variables to evaluate the feasibility and socio-economic justification of investments in connecting pipelines shown in equation (1), allowing the exploration of multiple configurations for network interconnection.

$$q_{conPipe,l}^{cap,maximum} \cdot a_l \geq q_{conPipe,l}^{cap} \geq q_{conPipe,l}^{cap,minimum} \cdot a_l \ , \quad (\forall\, l \in L, a \in \{0,1\}) \qquad (1)$$

The objective function of the model is structured to minimize the total socio-economic costs of district heating systems and shown in equation (2). This includes annualized investment costs, both fixed and variable operating and maintenance (O&M) costs, unit start-up costs, carbon emissions, fuel costs, and annualized sunk costs associated with investment decisions in new pipeline infrastructures. The optimization accounts for revenues generated from electricity sales derived from CHP plants, effectively linking the DH system's financial performance with electricity market dynamics.

$$min \sum_{l\in L}\sum_{n\in N}\sum_{t\in T}[\left(C_{l,n,t}^{VO\&M} + C_{l,n,t}^{fuel} + C_{t}^{CO2}\,K_{l,n} - R_{l,n,t}^{ele}L_n + c_{l,n,t}\cdot C_{l,n}^{startup}\right) q_{l,n,t}H + \left(C_{l,n}^{cap} + C_{l,n}^{FO\&M}\right)q_{l,n}^{cap} + a_l\,S_l\big]\,, (\forall l \in L, \forall n \in N, \forall t \in T) \quad (2)$$

where N represents a set of technologies ($n \in N$) installed at a location l for a set of locations L ($l \in L$), while T represents an hourly time set ($t \in T$). The case study developed had four different DH locations.

The method integrates detailed energy balancing constraints to ensure accurate representation of heat supply and demand dynamics at hourly resolution throughout the entire year and shown in equation (3). The model captures the interplay between heat generation, storage, and consumption, to maximize system flexibility and efficiency. The constraints ensure sufficient heat generation capacity at each location to satisfy the heating demand, accounting for the capacities and operational limits of individual heating units. Furthermore, the operational dynamics of CHP units, electric boilers, heat pumps, and TES are modelled to reflect realistic operational scenarios and can in detail be seen in PAPER 1.

$$q_{n,t,l}\cdot t = E_{l,t} + s_{l,t}^{ch} - s_{l,t}^{dis}, \quad (\forall\, t \in T, \forall\, n \in N, \forall\, l \in L), \quad (3)$$

To enhance realism and relevance to actual urban contexts, the methodology incorporates a steam demand component tailored for industrial purposes, allowing the evaluation of CHP units' operational strategies and economic viability under conditions that closely reflect real-world district heating demands. This aspect significantly enriches the model, making it suitable for practical urban planning and policy-making scenarios.

The model was implemented using Python 3 with the Gurobi optimization solver, ensuring robust computational efficiency and scalability. Its performance was validated on a detailed case study for the City of Zagreb and its neighbouring cities, Velika Gorica and Zaprešić, in Croatia. The studied scenarios included a baseline scenario representing existing capacities and two future-oriented scenarios incorporating additional RES technologies, TES, and the possibility of interconnecting DH networks, additionally shown in Table 1.

Table 1. Descriptions of scenarios

Scenario	Description
I	Baseline, business as usual case scenario
II	Future district heating networks with possibility of using new thermal energy storage, electrical boilers and heat pumps, but not allowing for interconnections

III	Future district heating networks with possibility of using new thermal energy storage, electrical boilers and heat pumps and allowing for interconnections

Detailed results and an extensive sensitivity analysis from this method are presented in the published paper PAPER 1. The paper provides comprehensive insights into the impact of various investment strategies and interconnection options on cost savings, environmental benefits, and operational efficiency. Key findings indicate substantial economic savings and notable reductions in CO_2 emissions achievable through optimized integration and expansion strategies.

Presented MILP-based optimization methodology represents a significant advancement in the strategic planning and operational optimization of urban district heating systems. It enables urban planners and decision-makers to effectively balance technical feasibility, economic competitiveness, and environmental sustainability, laying a robust foundation for future development and expansion of DH networks.

2.2 Integrated optimization of renewable energy and storage in desalination-based water system for water-energy nexus representation

This subsection elaborates on a sophisticated methodological framework designed to optimize the integration of RES and storage technologies within desalination-based water systems. This integrated optimization explicitly addresses the complexities and interdependencies characteristic of the WE nexus. The primary motivation behind such an approach is the need for reliable, economically viable, and environmentally sustainable solutions, particularly for isolated regions with fluctuating demand patterns, such as tourist-dependent islands.

The modelling approach is grounded in MILP optimisation framework that simultaneously addresses both capacity sizing and operational dispatch across energy and water domains. The model is designed to flexibly accommodate a wide range of water and energy technologies, including production, treatment, and storage components, as well as the interconnection between energy and water systems. Its main purpose is to simultaneously determine both the optimal system capacities and the optimal hourly dispatch of energy and water flows. Due to its modular nature, the framework can be easily adapted to different system configurations by including or excluding technologies as needed.

The framework was applied to optimize the operation of desalination-based water infrastructure and RES technologies. Specifically, it identifies the optimal sizing of PV generation, BES capacity and power, and the key parameters of the freshwater supply system. PV is chosen as the main electricity source in this configuration, supporting the study's objective of exploring

RES integration for sustainability. In addition to PV, a grid connection is included in the system to assess the economic trade-offs of RES integration versus reliance on conventional grid or fossil-based electricity sources, particularly in island or remote contexts where such dependence is typical.

To understand the role of Power-to-Water (PtW) applications, particularly through desalination and water storage, freshwater storage is included in the model as an essential system component. The integration of BES allows the model to capture the dynamic relationship between RES electricity supply, energy storage, and water production. Both the energy capacity and power output of the BES are decision variables in the optimization process. This dual optimization provides a more accurate representation of real-world constraints, avoiding the simplifications that can arise when only capacity is considered. By doing so, the model accounts for real operational limits, such as maximum allowable charge and discharge rates, thus capturing the technical nuances of BES operation. All relevant parameters, variables, and sets used in the model are systematically defined in the PAPER 2.

The optimization is performed over a one-year period using hourly time steps. This temporal resolution provides a good compromise between accuracy in capturing hourly variations (e.g., solar radiation, demand fluctuations) and computational tractability. While MILP models are more demanding than simpler linear formulations, the framework is designed to be flexible, and users can adjust the time resolution according to their computational resources. In this study, all simulations were conducted using Python 3.7 and the Gurobi solver. The Gurobi Python interface (gurobipy) was used for implementation, and the simulations were run on a workstation equipped with two Intel Xeon E5-2623 v3 CPUs and 64 GB of RAM. On average, each optimization run took about 30 minutes. The general structure of the model is illustrated in Figure 2.

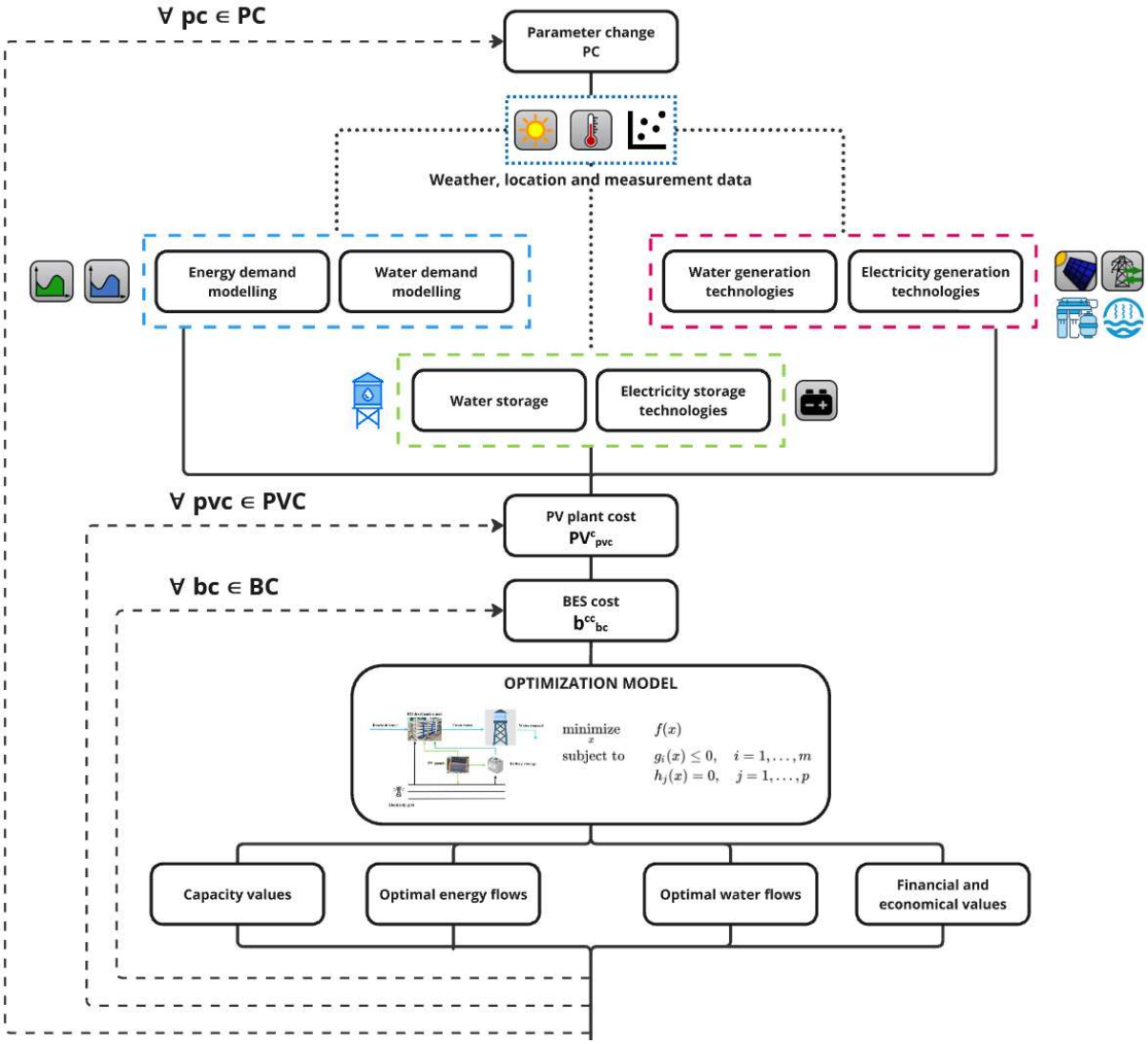

Figure 2. Schematic of the water-energy nexus modelling and optimization approach

The overall modelling and optimization process, shown in Figure 2, consists of three main stages. The first stage involves selecting the system technologies, defining input parameters, and preparing relevant time-series datasets. This includes the selection of desalination units and energy components, along with their associated storage technologies. These are visually marked within the red and green dashed rectangles. Depending on the specific system boundary, inputs such as water demand and, in broader cases, energy demand are introduced. To generate these inputs, real-world weather data, site-specific characteristics, and empirical measurements are used to construct demand profiles, highlighted in the blue dotted rectangle.

In the case study developed using this model, the defined water system includes the desalination unit, the water pipeline infrastructure, and a freshwater storage tank. Accordingly, water demand is treated as a fixed input, while electricity demand is an output generated by the model. This electricity demand is a function of how the desalination unit operates over time, influenced

by the availability of solar energy and storage capacity. If the modelled boundary is expanded to include additional energy-consuming processes, external energy demand inputs can also be incorporated, as noted in Figure 2.

The second stage describes the optimization process itself, which is structured around a multi-loop simulation to explore the sensitivity of the system to key input parameters. The outer loop varies high-impact parameters within the parameter change set ($pc \in PC$), such as grid electricity price, PV potential, and water demand. Each of these variations is defined as a set of discrete changes that the model evaluates in sequence. Nested within the outer loop are two inner loops that alter the investment cost assumptions. One for PV ($pvc \in PVC$) and one for BES ($bc \in BC$). For each unique combination of parameter variation, PV cost, and BES cost, the model runs a full optimization to identify the best-performing system design. These loops are represented by the black dashed lines in Figure 2.

Proposed nested-loop approach allows for a systematic evaluation of how economic and technical uncertainties affect optimal system configurations. In total, the model generates a set of results that include optimal technology sizes, time-resolved energy and water flow patterns, and key financial metrics such as system costs and potential savings. The third and final stage of the framework outputs these results, which are then used to assess the trade-offs between different investment strategies and system behaviours.

Finally, the mathematical formulation of the model includes the objective function and a comprehensive set of system constraints. The objective function, shown in Equation (4), minimizes total annual system costs. It includes components such as electricity purchase costs, backup water supply costs (e.g., boat carriers), lost load penalties, PV and BES operating and maintenance expenses, and annualized investment and replacement costs. It also accounts for financial gains from PV electricity used directly or sold to the grid, and savings from using stored energy during peak periods. The economic perspective is critical, particularly for remote locations where infrastructure costs are high and energy imports are often expensive. Importantly, the objective function also reflects a trade-off between up-front capital investment and operational cost savings, thereby supporting long-term planning strategies.

$$\begin{aligned}\min \quad & \sum_t e^{P}{}_t \cdot G^{D}{}_{pvc,\,bc,\,t} + \sum_t e^{P}{}_t \cdot B^{CH,G}{}_{pvc,\,bc,\,t} + \sum_t w^{BC} \cdot W^{B}{}_{pvc,\,bc,\,t} + \sum_t ll^{c} \cdot LL_{pvc,\,bc,\,t} + \\ & \sum_t pv^{var} \cdot PV^{E}{}_{pvc,\,bc,\,t} + B^{C}{}_{pvc,\,bc} \cdot b^{MCC} + B^{NP}{}_{pvc,\,bc} \cdot b^{MPC} - \sum_t e^{P}{}_t \cdot PV^{D}{}_{pvc,\,bc,\,t} - \sum_t e^{S}{}_t \cdot PV^{G}{}_{pvc,\,bc,\,t} - \\ & \sum_t e^{P}{}_t \cdot B^{DC}{}_{pvc,\,bc,\,t} + B^{C}{}_{pvc,\,bc} \cdot b^{CC}{}_{bc} \cdot \zeta \cdot cr + B^{NP}{}_{pvc,\,bc} \cdot b^{PC}{}_{bc} \cdot (1-\zeta) \cdot cr + \\ & PV^{P}{}_{pvc,\,bc} \cdot pv^{C}{}_{pvc} \cdot cr + B^{C}{}_{pvc,\,bc} \cdot b^{CC}{}_{bc} \cdot icdf \cdot pvf \cdot \zeta \cdot cr + B^{NP}{}_{pvc,\,bc} \cdot b^{PC}{}_{bc} \cdot icdf \cdot pvf \cdot (1-\zeta) \cdot cr \end{aligned} \tag{4}$$

$$, \quad \forall\, pvc \in PVC, \forall\, bc \in BC, \forall\, t \in T$$

A central element of the model is the energy balance constraint shown in Equation (5), which ensures that electricity demand for water production and system operations is met through a combination of PV, BES discharge, and grid electricity. This constraint is applied hourly and includes operational losses such as inverter efficiency and self-discharge. In this way, the model realistically reflects the limits of system autonomy and identifies when external grid support is necessary.

$$PV^{D}_{pc,\,pvc,\,bc,\,t} + B^{DC}_{pc,\,pvc,\,bc,\,t} + G^{D}_{pc,\,pvc,\,bc,\,t} = E^{D}_{pc,\,pvc,\,bc,\,t} - LL_{pc,\,pvc,\,bc,\,t}, \quad \forall\, pvc \in PVC, \forall\, bc \in BC, \forall\, t \in T \tag{5}$$

BES operational constraints include state-of-charge tracking, charge/discharge limits, efficiency losses, and self-discharge. The power constraint ensures that energy flows do not exceed physical capabilities. These constraints collectively prevent overestimation of BES flexibility and enforce system stability. Additionally, including both capacity and power variables enables the exploration of different BES technology configurations, such as high-power/low-capacity systems versus high-capacity/low-power ones.

Desalination dynamics are integrated via constraints on production rates, specific energy consumption, and water storage. The desalination units operate in response to available energy and demand profiles, and water can be stored to cover peak demands or periods of limited generation. This approach allows the system to shift water production to periods of RES surplus, reducing reliance on grid electricity or transported water. The model assumes RO desalination, though the structure is generalizable to other technologies. Detailed overview model constraint can be found in published PAPER 2.

The methodology is applied in a case study on the island of Unije, Croatia. The island's high seasonal variation in both water and electricity demand, driven by tourism, makes it an ideal candidate for demonstrating the model's strengths. Proposed comprehensive framework enables a robust evaluation of integrated WE systems, especially in remote or resource-constrained environments where infrastructure investment and operational efficiency are tightly coupled.

2.3 Uncertainty included optimal design and operation of integrated water-energy-food-ecosystem nexus

Building upon the optimisation structures developed in PAPER 2 and extended through the stochastic WEFE framework introduced in PAPER 3, this part of the research expands the methodological scope toward a more comprehensive representation of interdependent resource systems. The framework integrates stochastic programming to capture the influence of climatic

and market uncertainties while maintaining a multi-objective balance between technical, economic, and environmental performance. In this context, the approach is further enhanced by insights from PAPER 4, which analysed the technological and environmental potentials of FPV systems. FPV technology provides a dual benefit of RES and water conservation by reducing evaporation losses and improving photovoltaic efficiency through enhanced cooling on water surfaces.

A comprehensive modelling framework has been developed to guide the optimal design and operation of integrated WEFE systems under climate and market uncertainty. The approach is built around a hybrid infrastructure model that couples FPV technology with PSH, enabling optimisation across multiple resource domains. Central to the framework is a two-stage stochastic optimisation method, which supports robust planning by evaluating infrastructure sizing and system operation across a spectrum of plausible future scenarios.

The model is designed to integrate technical, environmental, financial, and economic considerations into a single optimisation environment. This unified structure allows for a holistic assessment of how interdependent variables across the WEFE sectors influence the performance and viability of complex infrastructure configurations. Through this formulation, the model determines the optimal combination of infrastructure investments and dispatch strategies that balance competing demands and maximise cross-sectoral efficiency.

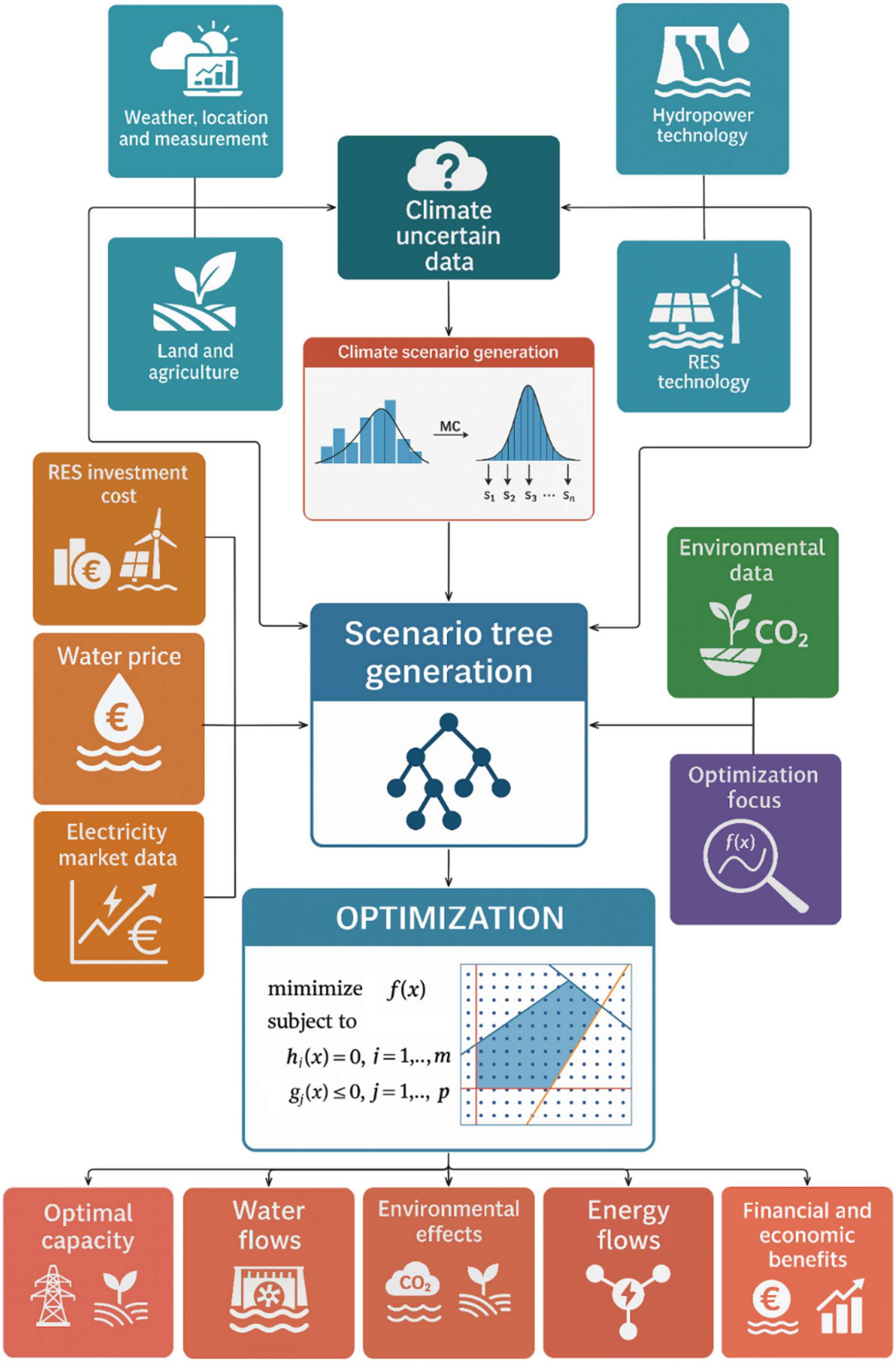
Weather, location and measurement
Hydropower technology
Climate uncertain data
Land and agriculture
RES technology
Climate scenario generation
MC
s_1 s_2 s_3 ⋯ s_n
RES investment cost
Environmental data
CO_2
Water price
Scenario tree generation
Optimization focus
$f(x)$
Electricity market data
OPTIMIZATION
mimimize $f(x)$
subject to
$h_i(x) = 0,\ i = 1,..,m$
$g_j(x) \le 0,\ j = 1,..,\ p$
Optimal capacity
Water flows
Environmental effects
CO_2
Energy flows
Financial and economic benefits

Figure 3. Schematic of the WEFE modelling and optimisation approach.

The overarching structure of the modelling framework is depicted in Figure 3. The upper section of the schematic outlines the input domains and pre-processing layers that supply the data required for optimisation. These inputs are organised into distinct categories, each playing a specific role in defining system characteristics, constraints, and uncertainties. Among the fundamental data layers, visually represented in blue, are meteorological inputs such as temperature, wind speed, solar radiation, and precipitation, which influence both energy generation and water balance. Additional spatial and physical information, such as geolocation coordinates, land use characteristics, reservoir data, and technical specifications of hydropower and solar technologies, are also included. Together, these inputs define the physical boundary conditions for the model and constrain feasible system behaviour.

To capture the effects of natural variability and climate uncertainty, the framework includes a dedicated module for uncertain environmental parameters. These are grouped as a set of climate-sensitive variables and visualised in the dark blue block of Figure 3. The uncertain parameters include:

- River inflow into the reservoir system,
- Precipitation contributing to water accumulation,
- Evaporation losses from water surfaces,
- Solar resource potential for RES generation,
- Water demand for residential, tourism, and industrial use,
- Irrigation water requirements for agricultural land.

These parameters are processed using a Monte Carlo (MC) simulation technique that generates a finite but statistically representative set of future climate states, each corresponding to one scenario $s \in S$. By using this probabilistic approach, the model captures the full range of variability in hydrological and meteorological inputs, allowing the optimisation to identify robust infrastructure designs that perform well across diverse future conditions.

In parallel with the climate uncertainty inputs, a separate set of economic and financial parameters is developed. This component is represented in orange in Figure 3. It includes capital investment costs for RES technologies, as well as assumptions regarding electricity market prices and equivalent water pricing (EWP) structures. To reflect volatility in energy markets, a separate MC simulation is used to generate a synthetic hourly electricity price series, which reflects real-world fluctuations and peaks. These economic inputs directly influence cost-

benefit assessments within the optimisation and affect prioritisation of specific system configurations.

Environmental co-benefits are integrated into the model using a dedicated set of inputs, highlighted in green. These reflect the ecological impacts of system design choices, including reductions in greenhouse gas emissions and land-use savings. For instance, FPV installations reduce reliance on grid-supplied electricity, thereby avoiding CO_2 emissions, and their placement on water surfaces mitigates the need for land acquisition compared to ground-mounted systems. These environmental benefits are quantified and included in the objective function, particularly when the broader WEFE nexus configuration is used.

Strategic decision-making is guided by a separate block of model inputs, shown in purple, which defines the optimisation's sectoral priorities. These priorities are established through the selection of objective function structures aligned with specific nexus perspectives. The model is capable of shifting among four main configurations starting from energy only, to full WEFE nexus optimisation.

By comparing these configurations, the model enables detailed exploration of the trade-offs that arise when system boundaries are expanded, and multiple sectors are jointly considered in infrastructure planning.

All input data streams feed into the scenario tree generation module, which forms the structural core of the stochastic optimisation framework. This tree maps the relationships between uncertain input conditions and corresponding system responses, enabling the evaluation of many plausible futures in a single model. First-stage decisions, made prior to the realisation of uncertainties, include the sizing of FPV capacity and the total irrigated agricultural area. Once the uncertainty is revealed in each scenario, the model then determines the optimal operational schedules for energy generation, water streams, reservoir operation, and irrigation delivery.

This structure follows the standard logic of two-stage stochastic programming, where infrastructure sizing must anticipate and withstand a wide range of operational conditions. The result is a robust system design that accounts for climatic variability, market dynamics, and cross-sectoral interactions.

The model evaluates the integrated operation of FPV-PSH systems in coordination with irrigation networks and environmental impact assessments. The final outputs from the model are grouped into five primary result categories:

- System capacity outcomes, such as optimal FPV area, rated power of pumping and generating units, and size of irrigated land.

- Water resource allocations, including hourly reservoir inflows and outflows, prioritisation of water use among sectors, and potential spillage events.
- Energy system flows, covering hourly electricity production, consumption, and exchange with the grid.
- Environmental metrics, which quantify system-wide emissions reductions, and the physical area of land saved through floating infrastructure.
- Financial and economic indicators, such as total system cost, operational expenditures, and benefit and cost ratios under uncertainty.

This output structure allows stakeholders to evaluate the benefits of integrated system design not only in terms of technical feasibility, but also in relation to environmental policy objectives and long-term economic resilience. The methodology is designed to support high-resolution, data-driven decision-making for the planning and operation of multi-sectoral infrastructure, particularly in regions sensitive to climate variability and resource competition

2.3.1 Evaporation modelling and agricultural irrigation needs estimation

A fundamental component of accurate hydrological and WEFE system modelling is the reliable estimation of evaporation losses from open water surfaces. This is particularly relevant for reservoirs used in PSH systems and in semi-arid or arid environments where evaporation represents a significant portion of water loss. Several modelling techniques have been developed for estimating evaporation, broadly classified into empirical, direct measurement, and physically based approaches, each with specific benefits and limitations.

Empirical methods such as the pan evaporation approach and simple adjustment of potential evapotranspiration using fixed coefficients are widely employed due to their minimal data requirements and ease of use. Class-A evaporation pans are a common reference instrument. However, their measurements often overestimate actual evaporation from large water bodies. This discrepancy is attributed to scale effects, wind exposure differences, and thermal properties, which necessitate the use of site-specific pan coefficients. These corrections, however, may not be universally applicable and can lead to inaccuracies, especially when applied outside of their calibration context [118], [119].

Physically based approaches, on the other hand, incorporate principles of energy and mass conservation to derive evaporation estimates. The energy balance method calculates evaporation by evaluating net radiation, heat fluxes, and heat storage within the water column. While this technique is theoretically robust, its application is constrained by its sensitivity to

measurement errors and the need for detailed and often unavailable meteorological and hydrological data [120]. Mass transfer models, which estimate evaporation as a function of vapor pressure gradient and wind speed, also require calibration and perform inconsistently under calm or sheltered conditions [118], [120]. To overcome these limitations, combination models such as the Penman and Priestley-Taylor methods have been developed. These models integrate both energy availability and aerodynamic factors, providing improved generalisation across different climates. The Priestley-Taylor formulation performs particularly well in humid environments but is less accurate in arid regions due to its simplified assumptions [121]. Meanwhile, the original Penman model, though comprehensive, may overstate evaporation in high-wind environments owing to the sensitivity of its aerodynamic term [120].

A refinement of these earlier models is provided by the FAO-56 Penman-Monteith method, developed by the Food and Agriculture Organization [122]. This formulation standardises assumptions regarding surface and aerodynamic resistances and was originally designed to estimate reference crop evapotranspiration (ET_0). Its methodological rigour, combined with operational practicality, has led to its widespread adoption in both agricultural and hydrological modelling. When adapted for open water bodies by setting surface resistance to zero, the FAO-56 Penman-Monteith method has shown strong alignment with observed evaporation measurements, often within a 10 % error margin [123]. Comparative studies using high-precision water level monitoring in reservoirs have consistently demonstrated its superior performance relative to other models, including standard Penman and modified open-water variants, which can overestimate evaporation by up to 40 % in certain contexts [123], [124].

Given its physical consistency, adaptability to varying climatic inputs, and compatibility with widely available meteorological datasets, the FAO-56 Penman-Monteith method is widely recognised as one of the most reliable tools for estimating open water evaporation [122]. It effectively balances theoretical accuracy with practical usability and can be applied across different temporal scales, from daily to hourly resolution, depending on the quality and granularity of the input data.

The FAO-56 formulation is based on the original Penman-Monteith equation but tailored for a reference surface of well-watered grass, 0.12 m in height, with a surface resistance of 70 s m^{-1} and an albedo of 0.23, shown in Equation (6) [122], [125]. The equation can be applied across various timescales; however, the hourly formulation offers improved accuracy in climates where weather conditions fluctuate rapidly throughout the day. This is especially critical in

Mediterranean and arid regions, where evaporation is not evenly distributed over the diurnal cycle [122], [126].

The FAO-56 Penman-Monteith equation for hourly reference evapotranspiration is given as:

$$ET_0 = \frac{0.408 \cdot \Delta \cdot (R_n - G) + \gamma \cdot \frac{37}{T_{hr} + 273} \cdot u_2 \cdot (e^0[T_{hr}] - e_a)}{\Delta + \gamma \cdot (1 + 0.34 \cdot u_2)} \quad (6)$$

This hourly formulation uses real-time data for solar radiation, air temperature, humidity, and wind speed to capture the sub-daily variability in evaporative demand. Averaging these parameters over a full day can lead to systematic under or overestimation, particularly when peak evaporative conditions occur in narrow time windows around solar noon. By resolving evapotranspiration at the hourly level, the model better reflects dynamic atmospheric processes and improves alignment with observed data, especially during periods of high demand.

The theoretical underpinning of the hourly approach lies in the quasi-steady assumption of the Penman-Monteith model, which is more accurately fulfilled on short time intervals. Field validation studies in regions characterised by significant diurnal fluctuations in solar radiation and vapour pressure have shown that the hourly FAO-56 formulation yields evapotranspiration estimates that closely match lysimeter measurements, particularly during dry, high-evaporation periods [126]. This improved temporal resolution not only enhances physical realism but also supports better integration into operational decision-making for water resource management.

The FAO-56 method's versatility and strong empirical performance have led to its inclusion in several globally used agricultural planning tools, such as CROPWAT and AquaCrop. These applications rely on accurate ET_0 estimation to simulate irrigation requirements, water balance, and crop performance. The growing availability of gridded, high-frequency meteorological data further supports the application of this method in regional and site-specific studies, offering decision-makers a robust foundation for water allocation strategies under changing climatic conditions [125].

Following the estimation of reference evapotranspiration (ET_0), crop-specific irrigation requirements can be calculated per Equation (7). In the FAO-56 approach, this is done by determining the crop evapotranspiration (ET_c), which represents the total water demand of a crop under optimal growing conditions. ET_c is estimated using the crop coefficient method, which scales ET_0 by a dimensionless coefficient (K_c) reflecting the crop's characteristics and growth stage [122].

The hourly crop evapotranspiration is expressed as:

$$ET_{c_{s,t}} = K_{c_{stage}} \cdot ET_{0_{s,t}} \quad (\forall\, s \in S, \forall\, t \in T) \tag{7}$$

The crop coefficient method accounts for both plant physiology and soil evaporation, encapsulated in a single K_c value. The FAO-56 framework segments the growing season into three key phases, each with an associated coefficient: the initial (K_{c_ini}), mid-season (K_{c_mid}), and late-season (K_{c_lat}) stages. Standard values for these coefficients are provided for a wide range of crops and climatic conditions. These reference values assume optimal conditions: healthy, unstressed plants grown with sufficient water and nutrients. Where local conditions differ, adjustments may be made based on wind speed, humidity, temperature, and field conditions [122], [125].

The estimated crop evapotranspiration forms the foundation for determining the actual irrigation requirement. This requirement is defined as the difference between ET_c and the effective portion of rainfall that is available for crop use, known as effective precipitation (P_{eff}), shown in Equation (8).

$$w_{s,t}^{agri} = ET_{c_{s,t}} - P_{eff_{s,t}} \quad (\forall\, s \in S, \forall\, t \in T) \tag{8}$$

Effective precipitation represents the share of total rainfall that is stored in the root zone and used for evapotranspiration. It excludes losses due to surface runoff, deep percolation, or interception. Several empirical and semi-empirical models exist for estimating P_{eff}, among which the CROPWAT method has emerged as a practical and accurate approach [124], [127].

CROPWAT offers an effective way to estimate P_{eff} using monthly rainfall data. Its formulation adapts depending on the total monthly precipitation, applying Equations (9) and (10).

$$P_{eff_{s,t}} = P_{tot_{s,t}} \cdot \frac{125 - 0.2 \cdot P_{tot_{s,t}}}{125} \quad for\ P_{tot_{s,t}} < 250\ mm \quad (\forall\, s \in S, \forall\, t \in T) \tag{9}$$

$$P_{eff_{s,t}} = \left(125 + 0.1 \cdot P_{tot_{s,t}}\right)\ for\ P_{tot_{s,t}} > 250\ mm \quad (\forall\, s \in S, \forall\, t \in T) \tag{10}$$

This method has shown high accuracy when compared to soil water balance measurements, particularly in semi-arid regions, with reported deviations often within 5% [127]. Unlike the USDA-SCS method, which is sometimes incorrectly equated with CROPWAT in literature, the latter applies a distinct approach to partition rainfall and is better suited to operational irrigation scheduling.

To harmonise temporal scales within the modelling framework, daily P_{eff} values calculated through the CROPWAT approach are proportionally disaggregated to match the hourly resolution of ET_0 and ET_c, ensuring consistency across all water balance components. This

facilitates integration with the hourly dispatch model used in the stochastic optimisation framework and allows for more responsive water management under varying climate scenarios.

Taken together, the FAO-56 Penman-Monteith method for ET_0, the crop coefficient approach for ET_c, and the CROPWAT-based estimation of P_{eff} provide a coherent and validated basis for estimating irrigation water requirements at high temporal resolution. This integration is essential for coupling agricultural water use with energy and environmental system models, as part of a broader WEFE nexus framework.

2.3.2 Climate uncertain scenario generation and two-stage optimisation model

The uncertainty-aware structure of the modelling framework is based on a scenario-generation approach that incorporates climate variability into second-stage operational decisions. This is achieved by identifying key climate-sensitive parameters, such as accumulation inflows, precipitation, evaporation rates, FPV generation potential, and sectoral water demands, and translating their variability into a set of representative scenarios. These uncertain parameters reflect both upper and lower reservoir conditions and are synthesised to form robust hydrological inputs that drive system optimisation.

To generate these scenarios, historical hourly inflow data are first statistically analysed to identify the best-fitting probability distribution, Figure 4. A MC simulation is then performed by sampling from this distribution, producing a broad range of synthetic inflow outcomes. From this simulated distribution, discrete hydrological scenarios are selected by sampling percentiles corresponding to extremely dry, dry, average, wet, and extremely wet conditions. The resulting scenarios form the core of the climate uncertainty module and are scaled to reflect realistic, system-wide inflow conditions over a full annual cycle. Other climate-sensitive variables are derived by aligning them with the most closely correlated historical inflow profiles, thus preserving interdependencies across meteorological factors.

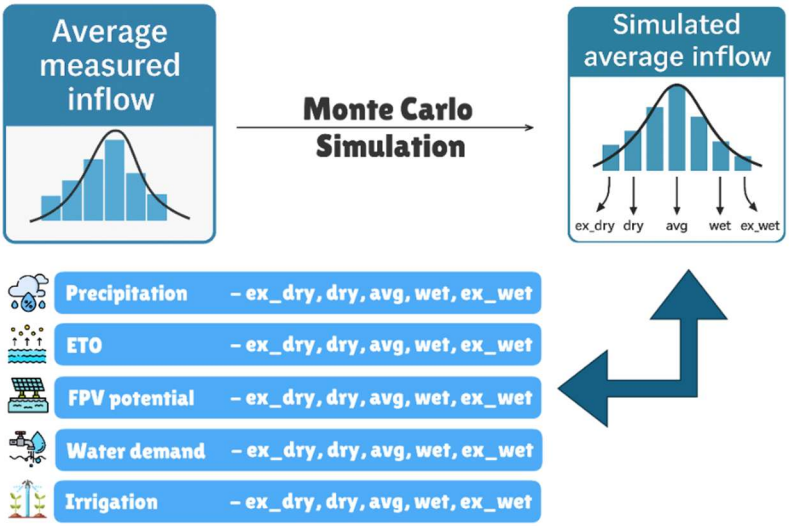

Figure 4. Climate uncertain data scenario generation approach.

This probabilistic sampling and matching strategy provide a diverse yet coherent set of operational contexts for optimisation. By capturing the non-linear and coupled behaviour of climate variables across multiple sectors, the scenario generation process enables the modelling framework to reflect both the temporal dynamics and stochastic nature of system drivers.

The core optimisation model follows a two-stage stochastic programming approach. In the first stage, long-term infrastructure design decisions are made, including the sizing of the FPV system and the extent of irrigated agricultural area. These decisions must be made before the specific climate scenario is known. In the second stage, operational decisions are adapted based on the realised scenario. This framework ensures that infrastructure sizing is robust to future uncertainty, while allowing flexible operational responses once specific climate and market conditions unfold.

To understand the implications of different system planning priorities, the model incorporates four distinct optimisation perspectives. Each of these perspectives corresponds to a specific objective function structure and reflects a progressively broader integration of sectoral considerations:

1. Energy-centric perspective, prioritising electricity production and associated financial outcomes. The objective function for this case is defined in Equation (11).
2. Water-Energy nexus, integrating hydrological dynamics and monetised evaporation savings, as described in Equation (12).
3. Water-Energy-Food (WEF) nexus, which includes agricultural irrigation scheduling and its operational implications, represented by Equation (13).

4. Water-Energy-Food-Ecosystem nexus, which expands upon WEF by internalising land-use savings, avoided emissions and hydropower operation ecosystem costs. This comprehensive objective is defined in Equation (14).

Each of these formulations shares the same investment and operational cost terms but differs in the way system benefits are structured and calculated.

$$\max \quad \sum_s p_s \cdot Z_{s,t}^{E} - FPV^{p} \cdot ic^{FPV} \cdot cr - \sum_r FPV^{p} \cdot ic^{FPV} \cdot isc \cdot pvf_r \cdot cr, \quad (\forall\, s \in S, \forall\, t \in T) \tag{11}$$

$$\max \quad \sum_s p_s \cdot Z_{s,t}^{WE} - FPV^{p} \cdot ic^{FPV} \cdot cr - \sum_r FPV^{p} \cdot ic^{FPV} \cdot isc \cdot pvf_r \cdot cr, \quad (\forall\, s \in S, \forall\, t \in T) \tag{12}$$

$$\max \quad \sum_s p_s \cdot Z_{s,t}^{WEF} - FPV^{p} \cdot ic^{FPV} \cdot cr - \sum_r FPV^{p} \cdot ic^{FPV} \cdot isc \cdot pvf_r \cdot cr, \quad (\forall\, s \in S, \forall\, t \in T) \tag{13}$$

$$\max \quad \sum_s p_s \cdot Z_{s,t}^{WEFE} - FPV^{p} \cdot ic^{FPV} \cdot cr - \sum_r FPV^{p} \cdot ic^{FPV} \cdot isc \cdot pvf_r \cdot cr + A^{FPV_{tot}} \cdot lsr \cdot lus, \quad (\forall\, s \in S, \forall\, t \in T) \tag{14}$$

The operational revenue and cost streams for each of these perspectives are scenario dependent. They are defined respectively in Equations (15) to (18) and represent the financial performance of the system under different sectoral assumptions. These expressions include revenue from electricity generation, water system contributions, irrigation demand impacts, and ecosystem service benefits, depending on the viewpoint considered.

$$Z_{s,t}^{E} = \sum_t \lambda_t^{emp} \cdot \left(E_{s,t}^{FPV_P} + bb \cdot E_{s,t}^{FPV_g} + E_{s,t}^{T} - E_{s,t}^{P_g}\right) - \sum_t hyd^{omc} \cdot E_{s,t}^{T} - \sum_t fpv^{omc} \cdot E_{s,t}^{FPV}, \quad (\forall\, s \in S, \forall\, t \in T) \tag{15}$$

$$Z_{s,t}^{WE} = Z_{s,t}^{E} + \sum_t \lambda^{ewp} \cdot W_{s,t}^{eva_{save}} - \sum_t \lambda^{spill} \cdot W_{s,t}^{spill} - \sum_t \lambda^{wll} \cdot W_{s,t}^{ll}, \quad (\forall\, s \in S, \forall\, t \in T) \tag{16}$$

$$Z_{s,t}^{WEF} = Z_{s,t}^{WE} + \sum_t sn \cdot W_{s,t}^{agri}, \quad (\forall\, s \in S, \forall\, t \in T) \tag{17}$$

$$Z_{s,t}^{WEFE} = Z_{s,t}^{WEF} + \left(co_2^{geq} - co_2^{FPV}\right) \cdot E_{s,t}^{FPV} \cdot co_{2_{cp}}^{c} + \left(co_2^{geq} - co_2^{hyd}\right) \cdot E_{s,t}^{T} \cdot co_{2_{cp}}^{c} - co_2^{geq} \cdot E_{s,t}^{P_g} \cdot co_{2_{cp}}^{c} - \lambda^{eco} \cdot E_{s,t}^{T}, \quad (\forall\, s \in S, \forall\, t \in T) \tag{18}$$

Operational feasibility across scenarios is ensured through a comprehensive set of constraints that govern water balance, energy dispatch, infrastructure limits, and sectoral demands. The reservoir subsystems, upper and lower, are modelled using mass balance principles, accounting for inflows from rivers and precipitation, outflows due to turbine discharge, pumping, evaporation, spillage, and sector-specific water consumption.

This complete set of constraints ensures that the model accurately represents the dynamic interactions between energy production, water use, land occupation, and ecosystem services

and is in detail shown in PAPER 3. By embedding these equations within the stochastic optimisation framework, the model provides a robust platform for evaluating complex infrastructure decisions under uncertainty.

3 SELECTED RESULTS AND DISCUSSION

Section 3 presents the key findings derived from the optimisation frameworks developed in this research, illustrating their application across urban, island, and regional contexts. The results demonstrate how integrated modelling enables simultaneous evaluation of technical, economic, and environmental objectives, highlighting the importance of flexibility, storage, and cross-sectoral coordination for system resilience. Through comparative analyses of district heating, desalination-based WE systems, and the stochastic WEFE nexus, the section synthesises the main insights that validate the methodological approach and confirm the research hypotheses.

3.1 Optimal configuration and dispatch of district heating system in urban agglomeration

The optimal configuration and dispatch of DH systems are crucial steps towards achieving cost-effective, environmentally sustainable, and resilient urban energy systems. This subsection presents a detailed case study of the City of Zagreb, Croatia, along with two adjacent urban areas, Velika Gorica and Zaprešić, to illustrate the practical applicability of the optimization method shown in Section 1.2.1. The case study provides insights into techno-economic and environmental benefits that can be attained through optimal sizing of DH components, including TES, CHP units, electrical boilers (EB), heat pumps (HP), and DH interconnectors. The scenario analysis approach is implemented to compare the current configuration with future-oriented scenarios aimed at higher RES integration and interconnection between separate DH networks.

The existing Zagreb district heating system is a large urban-scale network, supplying approximately 100,000 consumers across 274.41 km of distribution pipelines. Heat is primarily generated by two main CHP plants: TE TO Zagreb and EL TO Zagreb, both of which utilize natural gas and extra-light fuel oil as primary and backup fuels, respectively [128]. The TE TO Zagreb plant comprises multiple units, including combined-cycle gas turbines (CCGT) installed in 2003 and 2009, boilers for hot water generation, and ancillary steam boilers. In addition, TE TO Zagreb incorporates an existing TES unit with a capacity of 750 MWh, which plays a crucial role in enhancing operational flexibility [129].

The EL TO Zagreb facility includes CHP units and dedicated heat generation boilers, with nominal installed capacities of 90 MW_e for electricity and 491 MW_h for heat. Some older units (commissioned before 2000) have been decommissioned due to emissions regulations, driving the planning and construction of a new CCGT unit with 150 MW_e electrical and 114 MW_h thermal capacity [130]. The current state of the Zagreb district heating network is characterized by substantial heat and distribution losses, amounting to approximately 16.32%, indicating significant opportunities for efficiency improvements [128].

In contrast, Velika Gorica, located approximately 16 km south of Zagreb, operates a smaller, fragmented DH network. With a total installed heating power of 69.6 MW and a pipeline length of only 9.84 km, it covers roughly 32% of the city's heating demand. Historically, an interconnection with Zagreb's DH network was deemed economically unviable, yet the changing economic and technological landscape now warrants reconsideration. Similarly, Zaprešić, situated in the northwest part of Zagreb County, hosts an even smaller DH system, consisting of eight separate heating networks totalling 20.36 MW of heating capacity distributed over 2.37 km, supplying just 9.4% of the city's population [128].

To comprehensively evaluate optimal configurations, three scenarios were systematically investigated, and shown in Section 1.2.1. In future scenarios, outdated production units at EL TO and TE TO Zagreb plants commissioned before 2000 were assumed decommissioned due to non-compliance with emissions regulations, aligning the analysis with documented infrastructure development plans [130]. Detailed information on the generation units, including their types, fuels, capacities, and commissioning years, are provided in Table 3 of PAPER_1. Additional economic assumptions included a uniform CO_2 price of 25 EUR/t, electricity transmission and distribution fees of 20 EUR/MWh each, and discount rates of 6% for production equipment and 4% for interconnection piping, reflecting differential risk profiles of technology investments and infrastructure. Specific economic parameters such as investment costs, annualized investment costs, fixed and variable costs, and associated discount rates for different generation technologies are summarized in Table 4 of PAPER_1, while Table 5 of PAPER_1 details the economic parameters used specifically for district heating interconnectors.

Results from the optimization reveal significant shifts in heat generation patterns among the analysed scenarios (I, II, and III), as summarized in Table 2.

Table 2. Heat generation in DH for different scenarios, in GWh

Generation units	Scenario I	Scenario II	Scenario III

EL TO Zagreb	772.96	771.31	1,482.87
TE TO Zagreb	1,020.55	0	0
Zagreb Electric boilers	0	15.77	0
Zagreb Heat pumps	0	1,006.43	290.75
Velika Gorica Heating boilers (NG)	61.41	0	0
Velika Gorica Electric boilers	0	1.78	0.110
Velika Gorica Heat pumps	0	59.63	77.02
Zaprešić Heating boilers (NG)	17.46	0	0
Zaprešić Electric boilers	0	0.687	0.082
Zaprešić Heat pumps	0	16.77	21.46

NG – Natural gas

In Scenario II, aimed at maximizing RES and electrification without interconnections, natural gas boilers in Velika Gorica and Zaprešić were entirely replaced by EB and HP, complying with local environmental policies aimed at reducing air pollution. Detailed capacities and optimized configurations of generation units for Scenario II can be found in Table 7 in PAPER_1. Notably, TE TO Zagreb's generation capacity was shifted substantially, demonstrating a strategic preference for electrified heat production facilitated by TES enlargement (from 750 MWh to 4381 MWh) and significant new HP installations (294.5 MW). For EL TO Zagreb, the optimal scenario included a new CCGT CHP unit (114 MW thermal, 150 MW electric) and an expansion of the heat boiler capacity (Block K increased to 249.4 MW thermal). These investments not only align with existing infrastructure development plans by the Croatian energy company (HEP Group) but were also validated as economically justified by the optimization results.

Scenario III introduced the economic viability of physical interconnections between previously isolated DH networks. Results indicated that all evaluated interconnections were socio-economically feasible, with the largest interconnector (430.21 MW) established between Zagreb North and Zagreb South, a medium-capacity interconnector (10.54 MW) linking Zagreb South with Velika Gorica, and a smaller interconnector (2.98 MW) connecting Zagreb North with Zaprešić. Detailed optimized capacities of generation units resulting from Scenario III are shown in PAPER_1 illustrated in Table 8. These interconnections facilitate dynamic heat flow exchanges, optimizing energy flows in both directions based on seasonal and operational demands, significantly enhancing overall system flexibility. Specifically, heat exchange flows

between Zagreb North and Zagreb South are shown in Figure 5, between Zagreb South and Velika Gorica in Figure 6, and between Zagreb North and Zaprešić in Figure 7, clearly indicating the seasonal variability and bidirectional utilization of these interconnections.

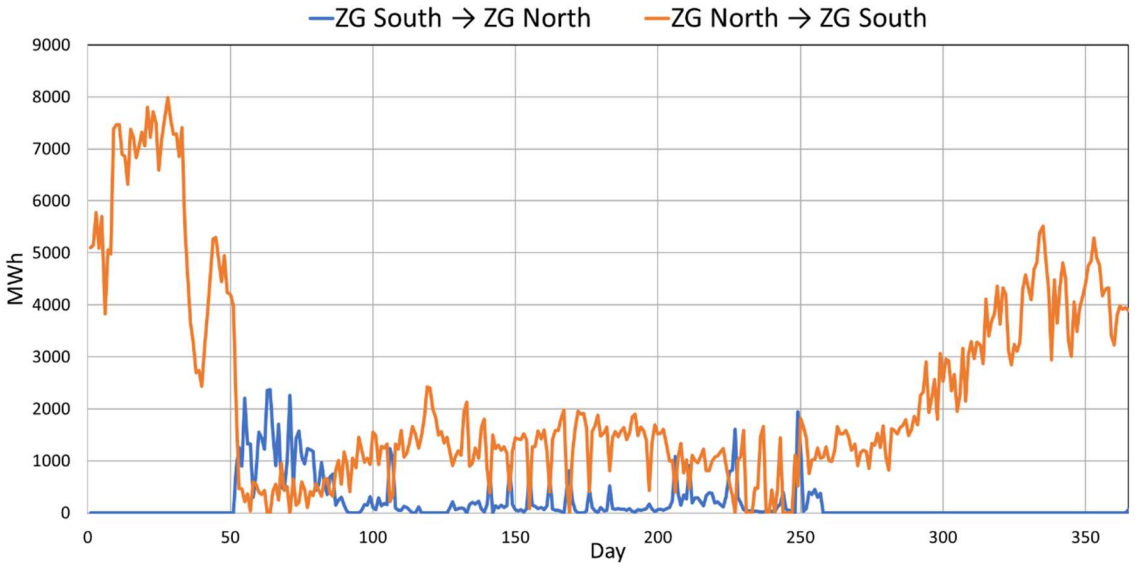

Figure 5. Heat flows between Zagreb South and Zagreb North for scenario III

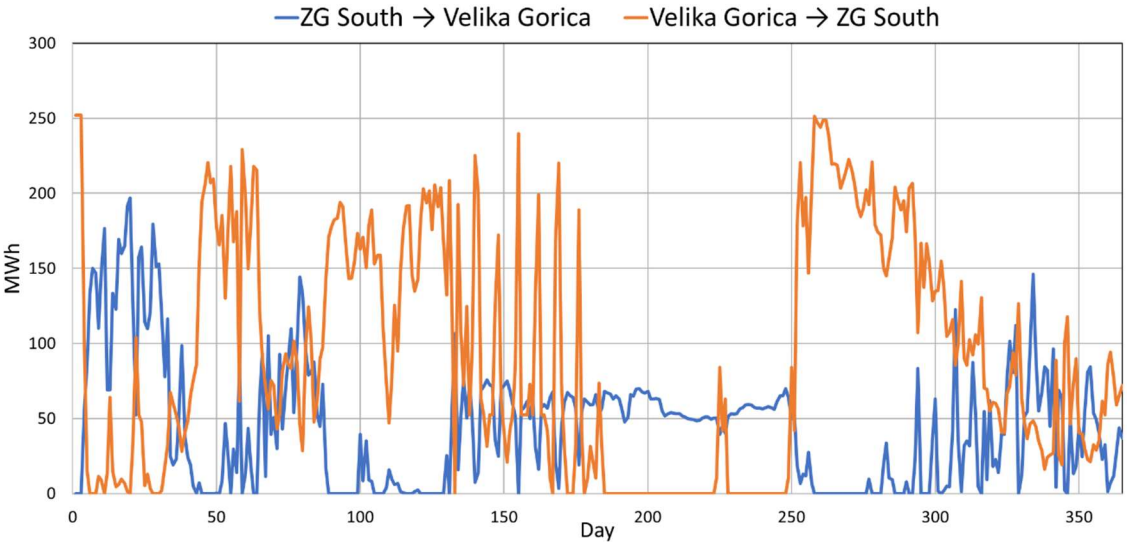

Figure 6. Heat flows between Zagreb South and Velika Gorica for scenario III

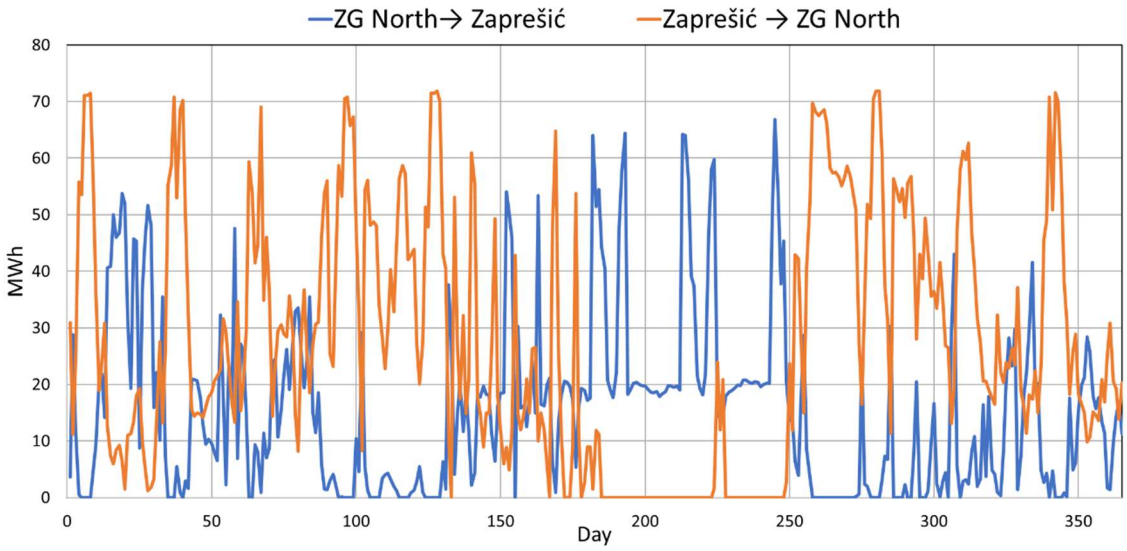

Figure 7. Heat flows between Zagreb North and Zaprešić for scenario III

The economic outcomes are particularly noteworthy, shown in Table 3. Scenario II resulted in an 11.2 million EUR reduction in total annualized system costs relative to the baseline, driven primarily by the increased electrification of heat supply and improved system efficiency. Scenario III demonstrated even greater economic benefits, with total system cost savings of 34.2 million EUR per annum, underscoring the substantial value added by interconnecting the district heating networks. These savings were accompanied by environmental co-benefits, including significant CO_2 emission reductions, 48.9% in Scenario II and 15.3% in Scenario III. The differential CO_2 reductions between these scenarios reflect the greater reliance on high-efficiency CHP units under Scenario III, which, despite increasing total emissions relative to Scenario II, still deliver substantial improvements over current operations.

Table 3. Economic and environmental results comparison across scenarios

Scenario	I	II	III
Total system cost (mil. EUR)	117	105.8	82.8
Savings (mil. EUR)	Reference	11.2	34.2
CO_2 emissions ($ktCO_2/a$)	356.34	181.87	301.97
Pipe length (km)	0	0	10.2 + 1 + 18.8

The analysis conclusively demonstrates the significant economic and environmental benefits achievable through strategic investments in DH infrastructure, particularly interconnections, thermal energy storage, and electrification technologies. The study clearly validates the initial hypothesis that integrating separate urban heating systems can provide substantial socio-economic savings, operational flexibility, and environmental performance improvements. These findings strongly advocate for policymakers and city planners to reconsider earlier evaluations of district heating interconnections, especially given advancements in technology

costs and evolving environmental policies. The methodological approach described in Section 1.2.1provided a robust framework to conduct this comprehensive techno-economic evaluation, enabling informed and economically justified infrastructure planning decisions in urban district heating contexts.

3.2 Optimal renewable energy sources and storage for flexible desalination in water-energy systems

The optimisation of RES generation and storage capacity for flexible desalination in WE systems was conducted using the MILP framework described in the Sections 1.2.2 and 1.2.3, applied to the case study of Unije Island in Croatia. The integrated model optimises the long-term capacities and the hourly operation of the coupled water and energy subsystems, explicitly including the PtW pathway through RO desalination and freshwater storage, in parallel with BES for electrical flexibility. The study considers the joint investment and operational decisions over a full year at hourly resolution, ensuring that both seasonal and diurnal variations in resource availability and demand are accurately represented.

Unije is a small island situated in the northern Adriatic Sea, forming part of Croatia's Cres–Lošinj archipelago. It covers an area of 16.77 km² and has an indented coastline stretching 36.6 km. According to the 2021 census, the island contains 35 private households with a total of 66 permanent residents. However, during the summer tourist season, the population can increase to around 500 people, with the number of households rising to 439 [131]. This pronounced seasonal variation in population reflects a common pattern observed across many Adriatic islands, where long-term trends of depopulation and an aging resident population are punctuated by short-lived surges driven by tourism. The island's climate is Mediterranean, characterised by hot, dry summers and mild, rainy winters. Such conditions support a variety of agricultural activities, particularly the cultivation of olives, grapes, and other crops important to the local economy. Average monthly temperatures range from 7.8 °C in January to 24.6 °C in August, with an annual mean temperature of approximately 15.3 °C. Unije receives an average of about 900 mm of precipitation annually, most of which occurs in autumn and early winter, consistent with typical Mediterranean climatic patterns [132].

Figure 8 presents a schematic of the modelled WE system for Unije Island. The water supply system comprises a RO desalination unit, a water pipeline network, and a primary freshwater storage tank. The energy system includes a PV plant, BES, and a grid connection. The desalination unit sources brackish water from the local aquifer, with a specific energy consumption of 2.5 kWh/m³. The existing freshwater storage tank has a capacity of 400 m³.

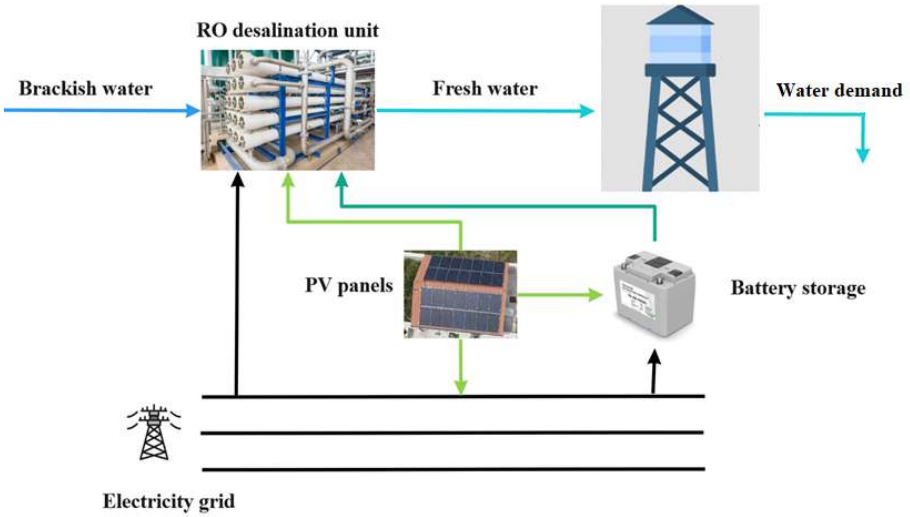

Figure 8. Schematic representation of the modelled water–energy flows for Unije Case Study

Hourly water demand data, provided by the local water utility, is shown in Figure 9. In addition to water demand profiles, Figure 9 also illustrates the number of people on the island and corresponding air temperature values, offering insight into seasonal variation and the influence of tourism. The principal water-side parameters used in the model are consistent with the system's physical constraints: the desalination unit capacity of 200 m^3/day, the annual water demand of 15,939.82 m^3, the storage capacity limit of 400 m^3, an initial storage level set at 40% of capacity, and allowable storage levels ranging from 20% to 100% of capacity. The cost of transporting water by carrier is set at 25 EUR/m^3. Further detailed parameter values related to the water system are summarised in Table 1 in PAPER 2.

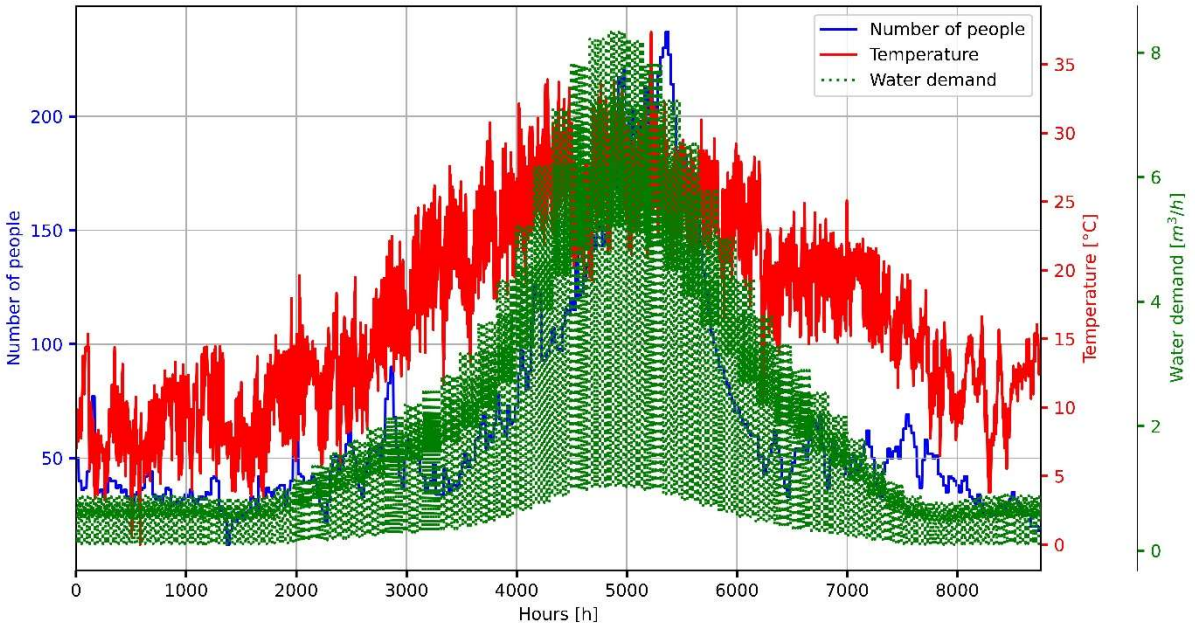

Figure 9. Hourly profiles for water demand, number of people, and air temperature for Unije case study

On the energy side, the model includes a PV plant, BES, and a grid connection. The Croatian electricity tariff structure is modelled with two time-of-use rates: a high tariff of 130 EUR/MWh for the day period (07:00–21:00) and a low tariff of 60 EUR/MWh for the night period (21:00–07:00), adjusted for daylight savings time changes. To reflect the asymmetry between purchase and sale prices, a buyback factor of 0.4 is applied, so that each kWh exported to the grid is valued at 40% of the equivalent cost of self-consumption. The hourly PV potential per unit capacity is derived using the approach referenced in [133], with PV investment costs varied between 900 and 1400 EUR/kW, encompassing the range currently observed in Croatia. The variable operation and maintenance cost for PV is set at 7.61 EUR/MWh, following NREL data. For BES, the capacity investment cost is varied between 50 and 600 EUR/kWh, covering the range observed in the Croatian market, which remains relatively high but is following global declining trends. BES power investment costs are derived through the capacity-to-power ratio *r*, with a replacement factor of 0.6 used to account for battery replacement in year 12 of the 25-year project lifetime. All capital and operational costs are discounted at a rate of 5%. The operational parameters for BES include minimum and maximum power limits, charging and discharging efficiencies of 90%, self-discharge of 1% per month, an initial state of charge of 50%, and bounds of 20% to 100% for the state of charge during operation. The fixed operation and maintenance costs are 0.38 EUR/kWh/year for capacity and 3.22 EUR/kW/year for power. These parameters are detailed in Table 2 in PAPER 2.

Figure 10 presents the main capacity optimisation results for the Unije Island case study, showing optimal PV power, BES capacity, and BES nominal power across a range of PV and BES investment costs. Each point on the three 3D surfaces corresponds to an optimal configuration from a separate optimisation run, with PV investment cost on one axis and BES investment cost on the other. The colour scale represents the negative of the objective function *(neg(objective)),* where positive values indicate profitable solutions and negative values non-profitable ones. This transformation is used because the original objective function is a cost minimisation where costs are positive and revenues or savings are negative; inverting the sign allows profitability to be interpreted more intuitively.

The first diagram in Figure 10 shows that lower PV investment costs lead to higher optimal PV capacities, but the rate of change depends significantly on BES cost. At fixed PV cost, PV capacity rises with decreasing BES cost, with an average increase of 0.124 kW per EUR/kWh for low BES costs, flattening to 0.049 kW per EUR/kWh for high BES costs. At fixed BES cost, PV capacity decreases with rising PV cost, with a steeper decline (–0.069 kW per EUR/kW) when BES cost is ≤ 200 EUR/kWh and a gentler slope (–0.055 kW per EUR/kW) above this threshold.

A comparison of the PV capacity and BES capacity surfaces in Figure 10 shows that the rate of change in PV capacity is strongly influenced by the corresponding BES capacity. At constant PV cost, a sharper drop in PV capacity is often matched by a rapid rise in BES capacity. This inverse relationship indicates that the system shifts from PV-dominated operation toward storage-driven flexibility when cost conditions favour BES. In such cases, PV generation remains the primary energy source for desalination, supported by flexibility from both PtW via water storage and electrical storage in the form of BES.

These results have important implications. First, they challenge the common assumption that lower BES costs, and therefore larger BES capacities, automatically lead to greater RES penetration. The findings here suggest that the most effective PV-BES configuration is not the one that maximises both capacities, but the one that yields the highest *neg(objective)* value, i.e., the best economic performance according to the optimisation. In some cases, reducing PV capacity while increasing BES capacity can improve overall profitability, because the storage allows more efficient use of generated energy. Conversely, there are scenarios where BES use is technically justified but the resulting profitability is modest. For example, in some high-PV-cost configurations, BES operation is beneficial but the *neg(objective)* is only around 500 EUR/year.

Another observation from Figure 10 is that as PV investment cost increases, BES becomes economically viable over a wider range of BES costs. This is because expensive PV shifts the economic balance toward making better use of each unit of PV-generated electricity through storage. However, the profitability gain from such configurations can be small if both PV and BES costs are high, reinforcing the need to evaluate capacity choices in the context of the overall objective function rather than focusing solely on maximising RES output.

The third diagram in Figure 10 shows the optimal BES nominal power. This follows similar trends to BES capacity but with greater sensitivity at high PV costs. Persistent PV capacity, even at higher PV costs, maintains the need for significant charging and discharging capability. As a result, BES nominal power reflects the combined influence of PV and BES capacities, and the sizing of BES power cannot be accurately determined without considering both. This interdependence underlines the importance of treating BES power and capacity as distinct decision variables, rather than relying on energy capacity alone to represent system flexibility.

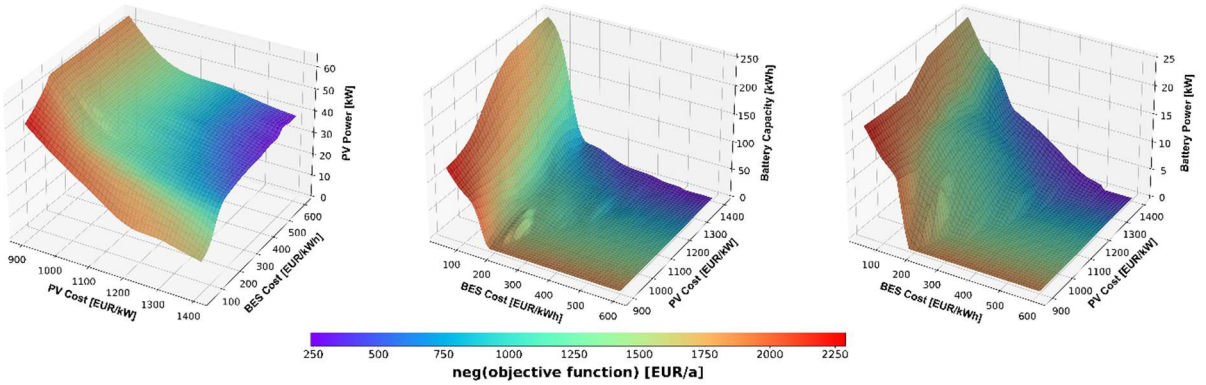

Figure 10. Range of optimal capacity results for Unije Island's water-energy system; PV power (left); BES capacity (middle); BES power (right)

A more detailed view of these relationships can be seen in the cross-section plots of BES capacity and PV power (and separately BES power) against BES capital cost, for several fixed PV capital costs. In these plots, solid lines represent BES capacity (left axis) and dashed lines represent either PV power or BES power (right axis).

The results in Figure 11 show that when PV investment costs are higher, the variation in PV power across the range of BES costs is more gradual, producing a smoother distribution of values. This behaviour is closely related to how the BES is utilised. When PV investment costs are lower, the final optimal PV power, visible as the horizontal segments of the dashed lines, is reached at much lower BES cost values. This indicates that in low-PV-cost scenarios, storage capacity requirements saturate quickly and further reductions in BES cost have limited

influence on PV capacity. In contrast, as both PV and BES investment costs increase, BES usage becomes more significant in maintaining system performance.

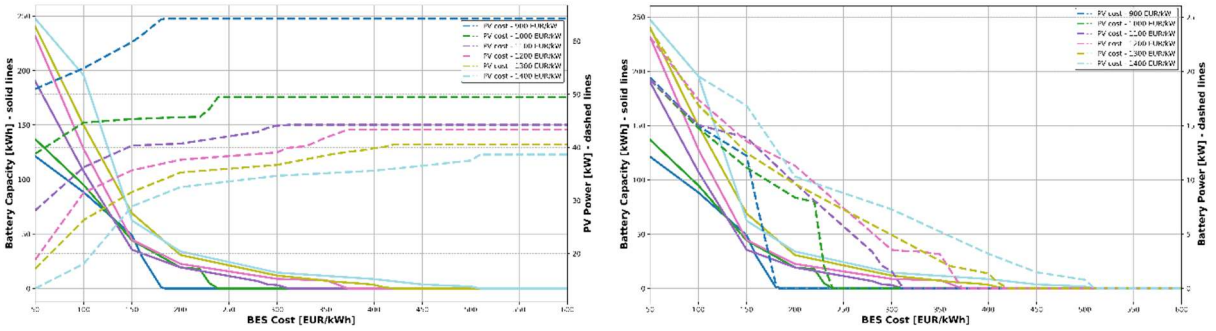

Figure 11. Detailed view on optimal water-energy system capacity values; BES capacity and PV power (left); BES Capacity and BES power (right)

The threshold BES cost values at which BES usage becomes economically justified, along with the corresponding optimal PV capacity without BES, and the maximum BES capacity at the lowest BES cost, can be found in Table 3 of PAPER 2. At this lowest BES cost, the highest utilisation of storage occurs. However, the installed BES capacity at this cost depends strongly on the PV investment cost. For example, when PV cost is 900 EUR/kW, the optimal BES capacity is 120.38 kWh, whereas for a PV cost of 1400 EUR/kW the optimal BES capacity increases to 247.60 kWh. This progression demonstrates that higher PV costs drive a greater reliance on storage to improve the value of each unit of PV-generated electricity. These findings underline the interdependence between PV and BES investment costs in determining optimal capacity values and highlight the increasingly critical role of BES when PV investment costs are high.

Figure 12 presents the results for BES utilisation, defined as the ratio of actual annual energy cycled through the BES to its theoretical maximum based on both capacity and power limits. The results show a clear upward trend in BES utilisation with increasing PV investment cost. This is consistent with the fact that higher PV costs are often accompanied by larger BES capacities, leading to a greater reliance on storage to meet system needs. In such scenarios, the optimisation tends to shift from solutions dominated by PV generation to those where BES plays a stronger supporting role, thereby increasing its share of the overall operation.

Interestingly, BES utilisation also increases with higher BES investment costs, even though BES capacity decreases under these conditions. This initially counterintuitive outcome can be explained by examining the BES nominal power results. The rate of decline in BES power is smaller than the rate of decline in BES capacity, so even with smaller storage volumes, the available power enables relatively high levels of cycling. The highest utilisation values tend to

occur at the threshold BES cost where storage first becomes economically justified. At these thresholds, the optimal solution typically involves modest BES capacities, which, when combined with limited reductions in BES power, result in proportionally higher utilisation rates.

The most profitable configuration overall, corresponding to the highest *neg(objective)* value, occurs at the lowest PV and BES investment costs, specifically a PV cost of 900 EUR/kW and a BES cost of 50 EUR/kWh. In this optimal case, PV generation contributes slightly more to the system, while BES is used to store excess PV output for use during higher-tariff periods. BES utilisation in this configuration also reflects the strong seasonality of the Unije Island system, where both energy and water demands fluctuate with the tourist season. This seasonality naturally lowers the annual utilisation percentage compared to a system with constant year-round demand.

It is important to emphasise that lower BES utilisation values do not indicate underuse of the storage potential or a need for larger BES capacities. The optimisation approach is designed to minimise the objective function, which represents the sum of all system costs and the potential financial and economic savings. From this perspective, high utilisation rates are not in themselves a requirement for economic justification. Instead, the results demonstrate that, for a highly seasonal island context, the joint deployment of RES generation and both water and energy storage delivers the most financially and economically optimal solution. In the best-performing cases, BES shares the operational role with PV generation in a balanced way.

Lower BES utilisation rates also have the practical advantage of potentially extending battery lifespan by reducing the number of annual cycles, while still maintaining strong economic performance. Furthermore, the current results do not account for external benefits such as avoided greenhouse gas emissions or public health improvements, which would likely strengthen the investment case for BES and RES even further. These additional benefits are intended to be considered in future work.

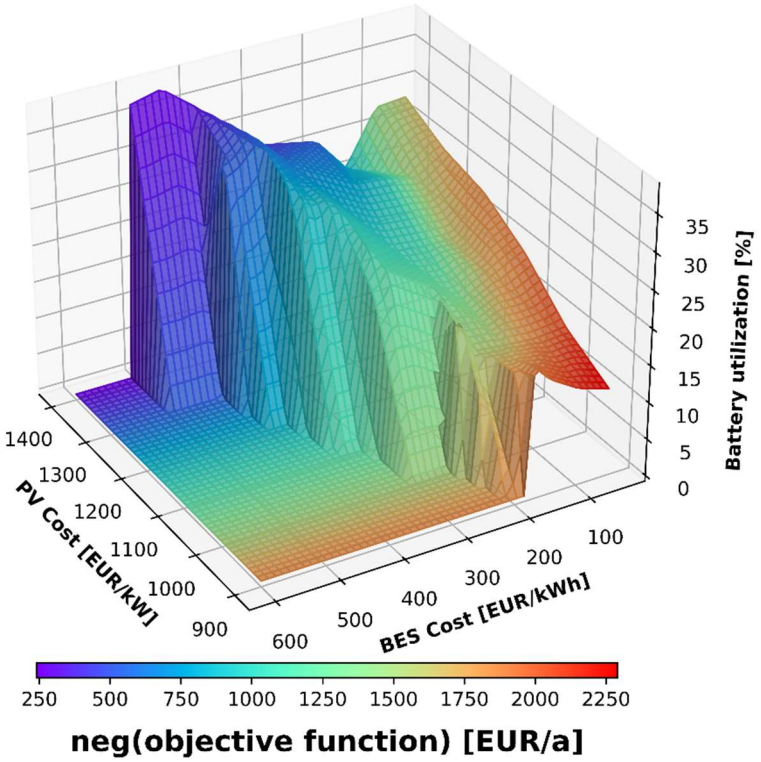

Figure 12. BES utilization parameter

Figure 13 presents the flexible operation savings of the optimised WE system for different combinations of PV and BES investment costs. Flexible operation savings are defined as the combined financial gains from using the two storage pathways represented in the model: water storage through desalination, and BES. Savings arise when RES electricity is used for desalination, with the water stored for later use, or when it is stored directly in BES. In both cases, the savings are calculated relative to the alternative of purchasing the same amount of electricity from the grid at the prevailing tariff in each time step. An additional source of savings comes from taking advantage of the time-of-use tariff difference, by charging BES or producing and storing water during low-tariff periods and using the stored energy or water when tariffs are higher.

The results show that the highest flexible operation savings occur at the lowest PV and BES investment costs, which also correspond to the highest *neg(objective)* values. This outcome is expected, as greater operational savings contribute directly to increased profitability. However, Figure 13 also reveals partial fluctuations in the total savings as BES capacity changes in response to lower BES costs. Because the total savings are the sum of PtW-related savings and BES-related savings, both of which depend primarily on PV generation, the specific PV-BES cost combination becomes the decisive factor.

Comparing these results with the PV power and BES capacity trends in Figure 10 helps explain the observed patterns. At a constant PV investment cost, the relationship between BES cost and savings changes markedly between different PV cost levels. For example, at a PV cost of 900 EUR/kW, flexible operation savings tend to decrease as BES cost falls. This is because the increase in PV power is smaller than the decrease in BES capacity, meaning that the gains from PtW storage grow more slowly than the losses in BES storage savings. In contrast, at a PV cost of 1400 EUR/kW, the trend reverses: as BES cost decreases, savings increase. In this case, the higher rate of change in PV and BES capacities at lower BES costs, and the smaller rate of change at higher BES costs, lead to a net increase in savings.

The interaction between PV cost and BES cost also explains why some high-PV-cost scenarios with large BES capacities still show relatively low overall flexible operation savings. The reduction in PV capacity at high PV cost limits the amount of RES electricity available for PtW storage, which reduces PtW-related savings. Even though BES-related savings can be substantial in such scenarios, reaching 1,411.89 EUR/year in the case of the largest BES capacity, these are not enough to fully offset the loss of PtW savings. This confirms that only the optimal pairing of RES generation and both storage types yields the highest total savings.

For constant PV cost across the BES cost range, another consistent pattern appears. As BES cost drops to around 100 EUR/kWh, there is a rapid increase in total savings, followed by a slower decline as BES cost decreases further. This behaviour mirrors the changes in PV and BES capacities: initially, falling BES costs enable both storage pathways to be used more effectively, but at very low BES costs, the marginal gains diminish.

For constant BES cost across the PV cost range, the results can also be divided into two regimes. At lower BES costs, savings decrease more sharply as PV cost rises. This is due to a steeper drop in PV capacity compared to the increase in BES capacity, which causes PtW savings to fall more than BES savings can compensate. At higher BES costs, the decrease in PV capacity with rising PV cost is less pronounced, and the increase in BES capacity is smaller, leading to a slower overall reduction in total savings.

It is important to note that each point in Figure 13 represents the optimal operation for a specific PV-BES cost combination, and all plotted results are associated with positive *neg(objective)* values, indicating system profitability. The absolute difference between the highest and lowest flexible operation savings in the dataset is 1,676.67 EUR/year. To improve the readability of the diagram, the z-axis scale was limited to 3,000 EUR/year.

The key conclusion from this analysis is that lowering both PV and BES investment costs consistently increases flexible operation savings, which in turn enhances system profitability. The results also underline that the maximum savings occur when the capacities of RES generation, PtW storage, and BES storage are optimally balanced. Although cost reductions can result in lower optimal PV capacity and higher BES capacity, the combination still maximises total savings and aligns with the highest *neg(objective)* values.

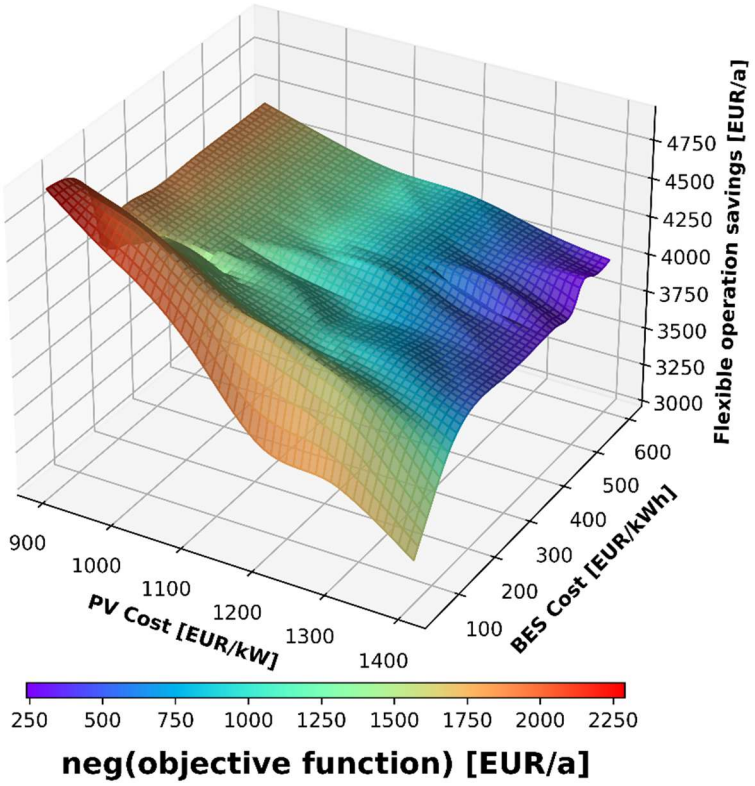

Figure 13. Flexible operation savings

This subsection analysed the optimal configuration of PV generation, BES, PtW through reverse osmosis for the Unije Island WE system. Results showed that the most profitable solutions balanced PV and BES capacities rather than maximising either. Lower investment costs for both PV and BES increased profitability, flexible operation savings, and overall system efficiency, with seasonal demand patterns influencing storage utilisation. The interplay between PV and BES costs determined capacity allocation, operational roles, and savings potential, highlighting that an optimal mix of renewable generation and both storage forms delivers the highest economic performance. Additional results and detailed are provided in PAPER 2.

The next subsection builds on findings by assessing the techno-economic resilience of desalination-based WE systems under uncertain conditions, focusing on parameter sensitivity to changes in grid electricity price, PV potential, and water demand.

3.3 Techno-economic resilience of desalination-based Water-Energy systems under uncertain conditions

Building on the baseline optimisation results from the Subsection 3.2, the analysis was extended to assess the techno-economic resilience of the Unije Island WE system under uncertainty in key external parameters. Three parameters were identified as critical drivers of system performance: grid electricity price, PV potential, and water demand. Each parameter was varied in the range of -30% to +30% relative to the base case, with the focus here placed on the boundary scenarios to illustrate the magnitude and nature of system response.

When grid electricity prices fall by 30 percent, as illustrated in Figure 14, the profitability of the optimal WE system changes dramatically. The range of *neg(objective)* values shifts from [240,2290] EUR/a range in the base case to [–770, 930] EUR/a range, signalling a substantial reduction in economic viability. The highest values still occur at the lowest PV and BES investment cost combination of 900 EUR/kW and 50 EUR/kWh, but the distribution of these top-performing configurations moves towards areas with lower BES costs. This shift indicates that under cheaper electricity prices from the grid, BES assumes a greater share of the flexibility role, displacing part of the operational space traditionally covered by PV generation and PtW. In effect, BES becomes the central mechanism for maintaining system adaptability, while PV's contribution to cost savings diminishes.

Even within similar profitability ranges, Figure 14 reveals considerable variability in the underlying capacity configurations. This illustrates that different capacity mixes can achieve comparable financial results, but the operational strategies and energy flows behind them would differ substantially. Such variability underlines the importance of detailed capacity and dispatch optimisation tailored to specific investment cost scenarios, rather than relying on generalised design rules.

Lower electricity prices also bring the first occurrence of a non-profitable configuration, appearing at 1100 EUR/kW for PV and 200 EUR/kWh for BES, with *neg(objective)* falling to –26.88 EUR/a. Above this point, further increases in either PV or BES cost deepen the losses. Figure 14 shows that BES plays a critical role in avoiding non-profitable outcomes under these conditions. For PV investment costs of 1100 EUR/kW and above, profitability is maintained only when BES cost is kept below roughly 130 EUR/kWh. This is evident in the green-shaded profitability zones, which represent the range where BES can offset the weaker returns from PV and PtW and keep the system in positive territory.

The capacity patterns in Figure 14 further highlight how system design priorities shift under low grid prices. At lower BES costs, PV becomes less viable as investment cost rises, with BES taking over the entire storage function. This is most visible at the outer cost boundaries, where PV capacity drops to zero for PV investment costs of 1200-1400 EUR/kW when BES costs are up to 110-170 EUR/kWh respectively. In these cases, the system relies exclusively on BES for storage, even though this results in lower absolute profitability.

A clear trend, consistent with the base case, is the tendency for optimal BES capacity to rise as PV costs increase. Figure 14 shows this rise occurring at a faster rate at higher PV costs, reflecting the reduced share of PtW savings and PV earnings and the greater dependence on BES to generate system revenues. Compared to the base case, BES capacities are not only larger but also occupy a wider cost spectrum, while PV capacities are reduced. This reduction in PV's role mirrors the decline in equivalent grid price revenues, which erodes the economic case for large PV installations when electricity prices are low.

The figure also demonstrates that BES can technically fulfil the role of energy storage even without PtW, although such configurations achieve much lower *neg(objective)* values. This confirms that in a low-price environment, PV and PtW are less competitive, and BES becomes the more viable, albeit less profitable, storage pathway. Larger BES capacities help partially offset the loss of PV and PtW contributions, and the resulting BES-driven savings play a central role in stabilising profitability.

Despite this compensatory function of BES, the overall profitability in the –30 % price scenario remains far below that of the base case. This outcome reinforces the pivotal role of grid electricity prices in determining both the optimal system configuration and the dispatch strategy. It also highlights the importance of careful planning in balancing PV and BES investments under different market conditions. For system designers and policymakers, these results indicate that low grid electricity prices significantly limit the financial headroom for RES and PtW, increasing the need for cost-effective BES deployment to sustain viability.

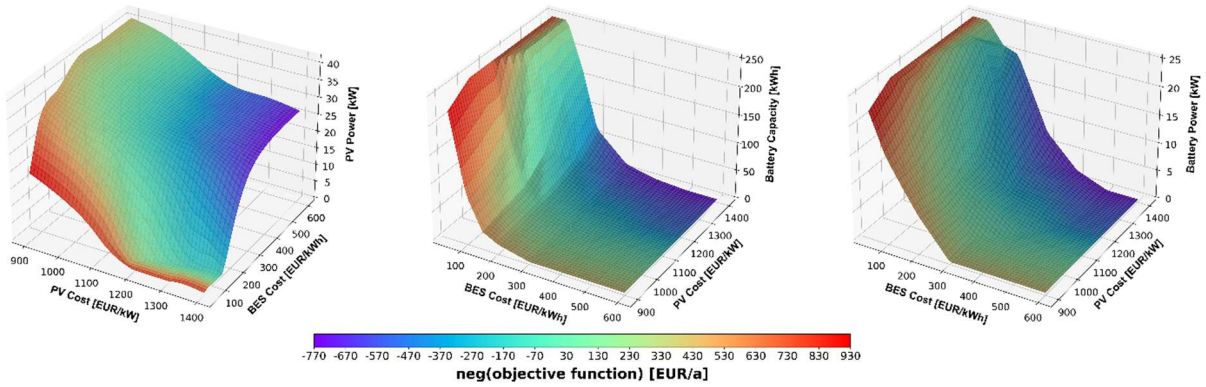

Figure 14. Range of optimal capacity results for Unije Island's water-energy system with 30% decrease in grid electricity price

When grid electricity prices rise by 30 percent, as shown in Figure 15, the profitability of the WE system increases substantially. The range of *neg(objective)* values shifts from [240, 2290] EUR/a range in the base case to [1560, 4810] EUR/a range, underscoring how sensitive the optimal configuration and dispatch are to market electricity prices. Unlike in the low-grid-price scenario shown in Figure 14, where BES assumed a greater role, the highest-value region in Figure 15 moves toward lower PV cost areas, signalling that PtW and PV generation take centre stage when grid prices are high. Under these conditions, RES electricity from PV displaces more expensive grid imports and yields higher revenues when sold back to the grid, making PtW and direct PV utilisation economically dominant. BES still contributes to flexibility, but its share in total system revenues is reduced as direct RES use becomes more attractive.

The magnitude of the price effect is notable: the peak profitability of 4810 EUR/a in Figure 15 is more than twice the base case maximum of 2290 EUR/a. Even configurations without BES can be highly profitable under high grid prices, as seen in the 900 EUR/kW and 210 EUR/kWh cost pair, which yields 4231.54 EUR/a. Tracing the most profitable base case configuration in Figure 15 reveals equivalent-profitability matches for the high-price scenario, such as the 1200 EUR/kW and 260 EUR/kWh pair with 2280.59 EUR/a, the 1300 EUR/kW and 130 EUR/kWh pair with 2296.75 EUR/a, and the 1400 EUR/kW and 85 EUR/kWh pair with 2292.08 EUR/a. These comparisons highlight that changes in grid electricity price not only shift the magnitude of profitability but also change the combinations of PV and BES investment costs that achieve it.

The capacity results in Figure 15 further supports this interpretation. PV deployment reaches its maximum capacity limit at PV costs of 900 and 1000 EUR/kW regardless of BES cost, showing that low-cost PV is so profitable under high grid prices that additional storage has minimal influence on sizing decisions. At a PV cost of 1100 EUR/kW, the maximum PV

capacity is reached when BES costs exceed 220 EUR/kWh, and no BES is deployed. When BES costs fall below this level, the system adopts an optimal PV-BES mix where PV capacity is slightly reduced but supported by storage to capture additional tariff arbitrage benefits.

BES capacities in Figure 15 are generally lower than in the base case, a direct consequence of PV and PtW dominating the operational strategy when grid prices are high. Nevertheless, BES retains importance, particularly at the lowest BES cost of 50 EUR/kWh, where optimal BES capacities range from 96.73 kWh to 210.90 kWh for PV costs between 900 and 1400 EUR/kW. This demonstrates that while BES becomes a smaller part of the total revenue picture, it still plays a complementary role in enabling maximum economic return, especially for investment scenarios with low storage costs and moderate to high PV costs.

The overall view emerging from Figure 15 is that high grid electricity prices create a strong incentive to maximise direct RES electricity use through PV and PtW, while maintaining BES primarily as a supplementary flexibility option. The economic hierarchy shifts in favour of generation rather than storage, but the most cost-effective solutions still rely on a balanced integration of both, ensuring that short-term variability and tariff differences can be exploited to their fullest. This complementary relationship between PV and BES is essential for sustaining high profitability even when market conditions strongly favour one over the other.

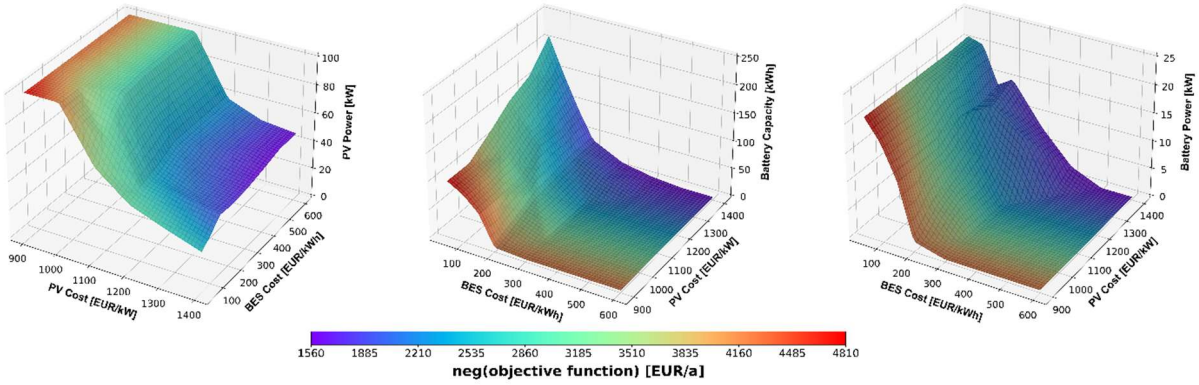

Figure 15. Range of optimal capacity results for Unije Island's water-energy system with 30% increase in grid electricity price

When PV potential decreases by 30 percent, as shown in Figure 16, the impact on system performance is evident. Profitability, expressed as *neg(objective),* shifts from [240, 2290] EUR/a range in the base case to [–1140, 1540] EUR/a range, signalling not only a sharp reduction in overall economic viability but also a wider spread of both profitable and unprofitable outcomes compared to the baseline. This pattern mirrors the response seen for the 30 percent decrease in grid electricity price in Figure 14 but with even greater magnitude, underlining PV potential as a more critical determinant of system behaviour.

Under this reduced PV potential, the most profitable configurations migrate towards lower BES cost regions. This shift shows that BES takes on a more dominant role in maintaining system flexibility and profitability when PV output is curtailed, while PV generation and PtW savings become less influential. Despite this adjustment in system strategy, the top *neg(objective)* values remain well below those in the base case, demonstrating the loss in economic headroom when solar resource availability declines.

The decrease in PV potential introduces a broader presence of non-profitable outcomes than in the low-grid-price scenario. The first non-profitable case occurs at the 1100/300 cost pair with –21.30 EUR/a. Beyond this point, higher PV or BES costs further reduce profitability. Any PV cost of 1100 EUR/kW or above leads to unprofitable results if no BES is deployed, confirming the dependence on storage to support PV viability under reduced generation conditions. In particular, BES maintains profitability within a narrow BES cost window, approximately 250 to 170 EUR/kWh, as PV cost increases from 1100 to 1400 EUR/kW.

A sharp reduction in PtW storage usage is visible in Figure 16 under the low-PV-potential scenario. As PV becomes less profitable, PtW output declines, reducing water storage's role in the operational mix. BES compensates for this loss by increasing its capacity and usage, resulting in higher BES-related savings. However, even with this compensation, the maximum profitability of 1540 EUR/a is far lower than the base case maximum. This reinforces the conclusion that PV potential is a foundational parameter for the economic viability of the integrated WE system.

The capacity distribution in Figure 16 shows that, similar to the low-grid-price case, rising PV costs make PV capacity less viable at low BES costs. At higher PV prices, BES fully takes over the storage function, and PV capacity drops to zero. The cost ranges where PV capacity is absent are wider here than Figure 14, extending to BES costs of 140 EUR/kWh for 1200 EUR/kW PV and up to 230 EUR/kWh for 1400 EUR/kW PV. This widening indicates that PV potential reduction has a stronger influence on the economic displacement of PV by BES than grid price changes do.

Overall, Figure 16 highlights the critical interplay between PV potential and BES in sustaining system profitability. With reduced PV output, BES becomes essential not just as a complement to PV but as the central driver of economic viability across a broad cost spectrum. While BES can fulfil the energy storage role alone, its ability to match the profitability of configurations with higher PV potential remains limited. These results confirm that safeguarding PV potential,

through site selection, maintenance, and performance optimisation, should be a primary strategic priority for ensuring the resilience and profitability of desalination-based WE systems.

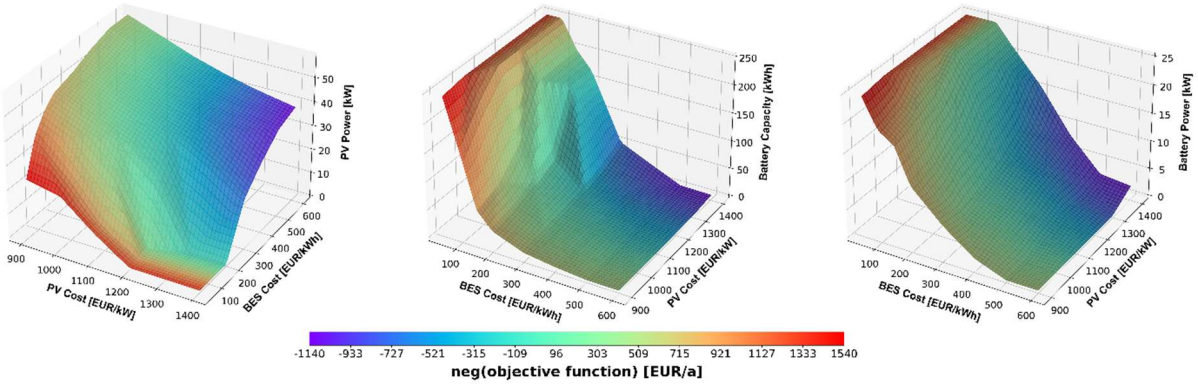

Figure 16. Range of optimal capacity results for Unije Island's water-energy system with 30% decrease in PV potential

When PV potential increases by 30 percent, as shown in Figure 17, system profitability improves significantly. The range of *neg(objective)* values shifts from [240, 2290] EUR/a range in the base case to [1200, 3920] EUR/a range, demonstrating the strong influence of PV potential on the optimal configuration and dispatch of the integrated WE system. This behaviour mirrors the pattern observed for the 30 percent increase in grid electricity price, but in contrast to scenarios involving reduced PV potential or grid electricity price, the distribution of the most profitable outcomes shifts toward lower PV investment cost regions. This shift reflects the greater economic dominance of PtW and PV generation, with BES playing a comparatively smaller role in the optimal mix.

The most profitable solution in this scenario, 3920 EUR/a, is lower than the maximum of 4810 EUR/a observed in the +30% grid price case. The difference arises mainly from the PV potential scenario reaching the upper limit of PV capacity earlier and having slightly lower BES capacities than in the grid price scenario. In the latter case, higher grid-equivalent savings boost both PtW and BES contributions. In the +30% PV potential scenario, the range of top-performing configurations extends from 3916.46 EUR/a for the 900 EUR/kW and 50 EUR/kWh PV-BES cost pair to 3575.31 EUR/a for the 900 EUR/kW and 170 EUR/kWh pair, where no BES is installed. All of these values comfortably exceed the highest base case profitability of 2290 EUR/a.

Following the most profitable base case configuration in Figure 17 shows that under increased PV potential, similar profitability levels are achieved for the wider range of PV/BES investment cost pairs. This reinforces the strong impact of PV potential on the arrangement of PV and BES

capacities, as higher RES availability shifts the balance towards generation rather than storage in the optimal design.

BES has a smaller relative impact on profitability in this scenario compared to the +30% grid electricity price case. The greater PV potential means PtW and PV savings account for a larger share of total revenues, while BES's contribution averages only 11.36 %. By comparison, in the high-grid-price scenario, BES savings are more significant due to higher tariff-based gains. Nevertheless, BES retains a role in the system, particularly in cost-effective investment regions, ensuring additional flexibility and storage capability when required.

Capacity results in Figure 17 show that, as in the high-grid-price scenario, PV capacity reaches its maximum for lower PV investment costs. However, a key difference is that in the PV potential scenario, the maximum PV capacity is achieved only when PV costs are at or below 1000 EUR/kW. In the grid price increase scenario, the upper PV capacity limit is reached even at 1200 EUR/kW when BES costs exceed 220 EUR/kWh. This broader high-capacity range in the grid price scenario explains its higher peak profitability compared to the PV potential case. Across the PV/BES cost spectrum, BES remains economically viable for costs below roughly 170 EUR/kWh, and for the lowest BES cost of 50 EUR/kWh, optimal BES capacity increases from 82.64 kWh to 192.78 kWh as PV costs rise from 900 EUR/kW to 1400 EUR/kW.

Taken together, the +30% PV potential case in Figure 17 confirms that greater PV resource availability enhances the economic case for maximising PV deployment, which in turn increases PtW savings and reduces the reliance on storage. Even so, BES continues to provide valuable flexibility and resilience, particularly at lower storage costs. While PV becomes the dominant component under higher potential conditions, a balanced configuration that retains BES ensures the system can adapt effectively to operational variability and tariff conditions.

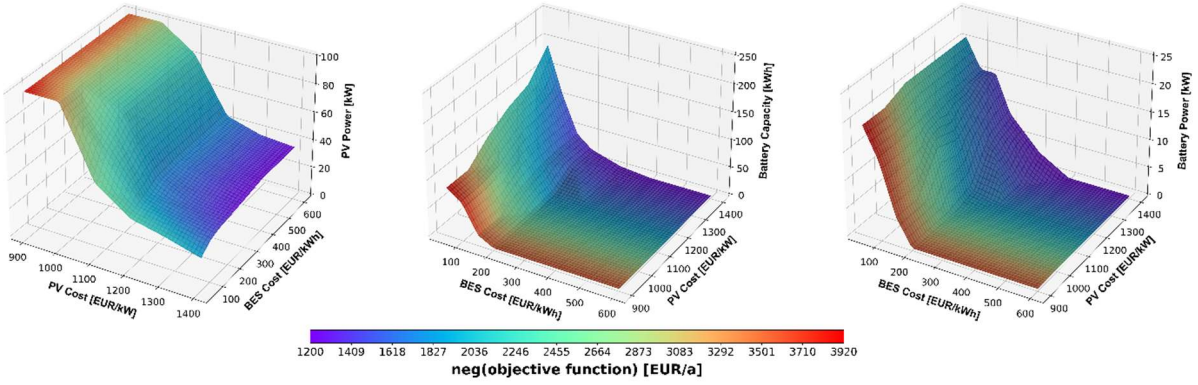

Figure 17. Range of optimal capacity results for Unije Island's water-energy system with 30% increase in PV potential

A 30% decrease in water demand, shown in Figure 18, produces a more modest change in system performance compared to variations in grid electricity price or PV potential. Profitability, shifts from [240, 2290] EUR/a range in the base case to [180, 1690] EUR/a range. The smaller change in both range and absolute values indicates that reductions in water demand have a relatively lower impact on the optimal system configuration and dispatch.

Lower water demand results in a greater proportional decline in revenues from PtW and PV usage compared to BES savings. While both revenue streams are reduced, PtW and PV savings experience a larger relative and absolute decrease. Across investment cost combinations, BES savings drop by an average of 14%, while PtW and PV savings decrease by approximately 31%. This difference reflects the fact that a reduction in water demand directly limits the utilisation of PV energy for desalination, reducing the scope for PtW-related cost offsets, while BES continues to provide flexibility benefits even under lower demand conditions. The most profitable configuration in the reduced demand scenario reaches a *neg(objective)* value of 1690 EUR/a.

An interesting marginal outcome appears for the 1400 EUR/kW and 50 EUR/kWh cost pair, where the optimal solution is based only on BES, with a capacity of 234.94 kWh, yet still achieves a positive *neg(objective)* of 1094.31 EUR/a. This demonstrates BES's ability to sustain profitability independently of PV when water demand is reduced, although at a lower absolute profit level.

Both PV and BES capacities decline compared to the baseline, with PV showing a larger relative reduction due to the greater loss in PtW and PV savings. BES capacities also decrease, but Figure 18 indicates a slightly broader range of BES usage for higher BES costs, implying that BES continues to play an important stabilising role in system profitability even with reduced demand.

Overall, the results for the –30% water demand scenario show that while reduced demand lowers both PtW and BES savings, the impact on overall profitability is moderate, and the system remains resilient. No non-profitable configurations emerge, confirming that water demand is a less critical parameter in determining viability. This highlights the stability of the optimal system configuration under demand-side fluctuations, in contrast to the greater sensitivity observed for changes in grid electricity price or PV potential.

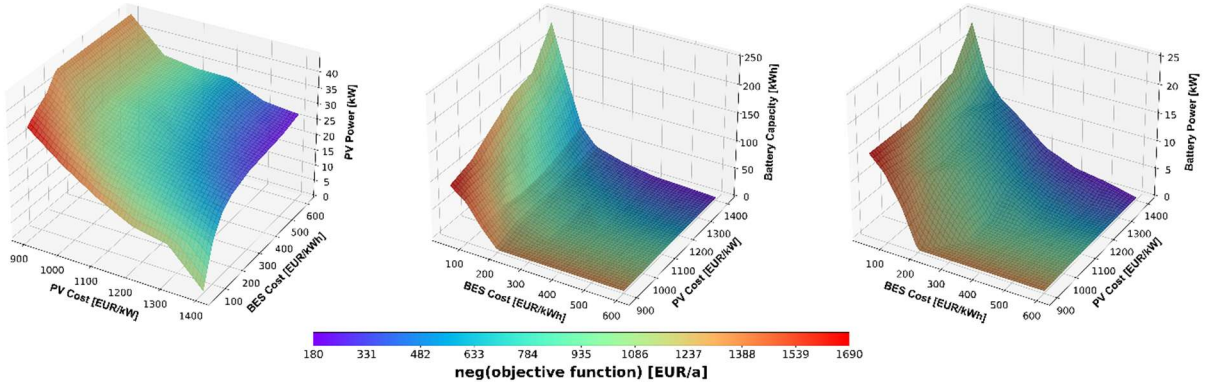

Figure 18. Range of optimal capacity results for Unije Island's water-energy system with 30% decrease in water demand

The 30% increase in water demand, shown in Figure 19, leads to a moderate improvement in system profitability compared to the base case. The range of *neg(objective)* values rises from [240, 2290] EUR/a range to [260, 3030] EUR/a. While this increase is notable, its magnitude remains smaller than the changes observed in scenarios involving grid electricity price or PV potential variation, confirming that water demand is a less influential parameter in determining the optimal system configuration and dispatch.

Higher water demand produces a more substantial absolute increase in savings and revenues from PtW and PV usage compared to those from BES. Although BES savings also rise noticeably, the percentage gain is greater for BES than for PtW and PV. Specifically, BES savings increase on average by 44.6%, while PtW and PV savings grow by 30.9%. This difference reflects the fact that increased demand allows more PV electricity to be channelled into desalination but also gives BES more opportunities for tariff optimisation and load shifting.

Both PV and BES capacities are higher than in the base case under increased demand, with the effect being more pronounced for PV. This is due to the direct link between water demand and the amount of PV electricity required for desalination, which raises PtW-related savings. BES deployment also expands, particularly at higher PV costs and lower BES costs, with capacities averaging around 240 kWh. However, for these cost ranges, the system approaches the upper limit of BES capacity, meaning that further demand increases would yield diminishing marginal savings from storage.

In summary, the 30% increase in water demand drives higher PV and BES capacities, resulting in greater overall savings, with PtW and PV providing the larger share in absolute terms. While both storage and generation benefit from higher utilisation, the scale of the impact remains modest compared to that of grid electricity price and PV potential changes, highlighting that water demand is a secondary driver of system-wide economic performance.

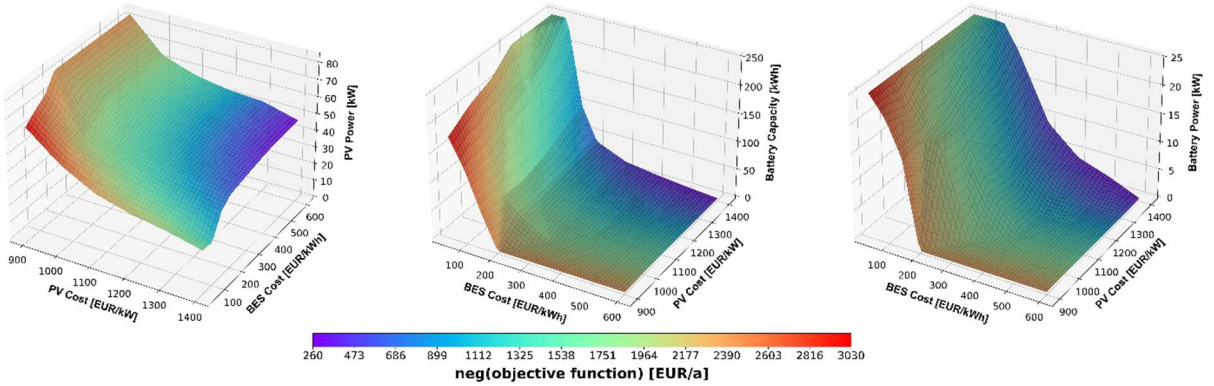

Figure 19. Range of optimal capacity results for Unije Island's water-energy system with 30% increase in water demand

The parameter sensitivity analysis shows that grid electricity price and PV potential are the most influential variables in determining profitability and optimal configuration. Increases in either parameter improve system viability by strengthening the case for PV and PtW, whereas decreases reduce economic performance and can result in non-profitable solutions for certain PV/BES cost combinations. In both reduced grid price and reduced potential cases, the system shifts towards greater reliance on BES, though often with lower profitability. Water demand changes affect the scale of both PV and BES capacities but have less influence on profitability than grid price or PV potential. Higher demand increases capacity and savings from both PtW and BES, while lower demand reduces utilisation but does not produce non-profitable results. This resilience to demand-side changes identifies water demand as a secondary factor in system viability compared to energy-related parameters.

Taken together, these findings confirm that optimal configurations for integrated WE systems emerge from the careful balancing of RES generation, water production, and storage capacities in response to both cost conditions and resource availability. These results highlight the importance of adapting investment and operational strategies to prevailing market and resource conditions to ensure long-term system resilience. More detailed results, including intermediate parameter variations, are provided in PAPER 2.

3.4 Stochastic optimal hybrid solar-hydro system under Water-Energy-Food-Ecosystem Nexus

PSH Velebit in Croatia was selected as the case study due to the availability of an upper storage area suitable for FPV installation, the highly variable and climate-dependent river inflow, and the presence of surrounding land suitable for agricultural development assessment. Its location in the Mediterranean region, projected to be significantly affected by climate change, further increases its relevance for integrated WEFE system analysis. PSH Velebit is situated in a

complex hydrogeographical setting in the southeast part of the Lika region, spanning the Gračac plateau and descending steeply into the lower basin of the Zrmanja River, within Zadar County, shown in Figure 20. The lower reservoir, Razovac, lies just above sea level, while the upper reservoir, Štikada, is located at over 550 m above sea level [134]. Environmental assessments indicate increasing climate variability, with projections of longer drought periods, more intense short-term rainfall events, and growing challenges for water quality and availability during dry seasons. These climatic and geographic characteristics are crucial for managing PSH Velebit and for understanding its interactions with downstream ecosystems and settlements

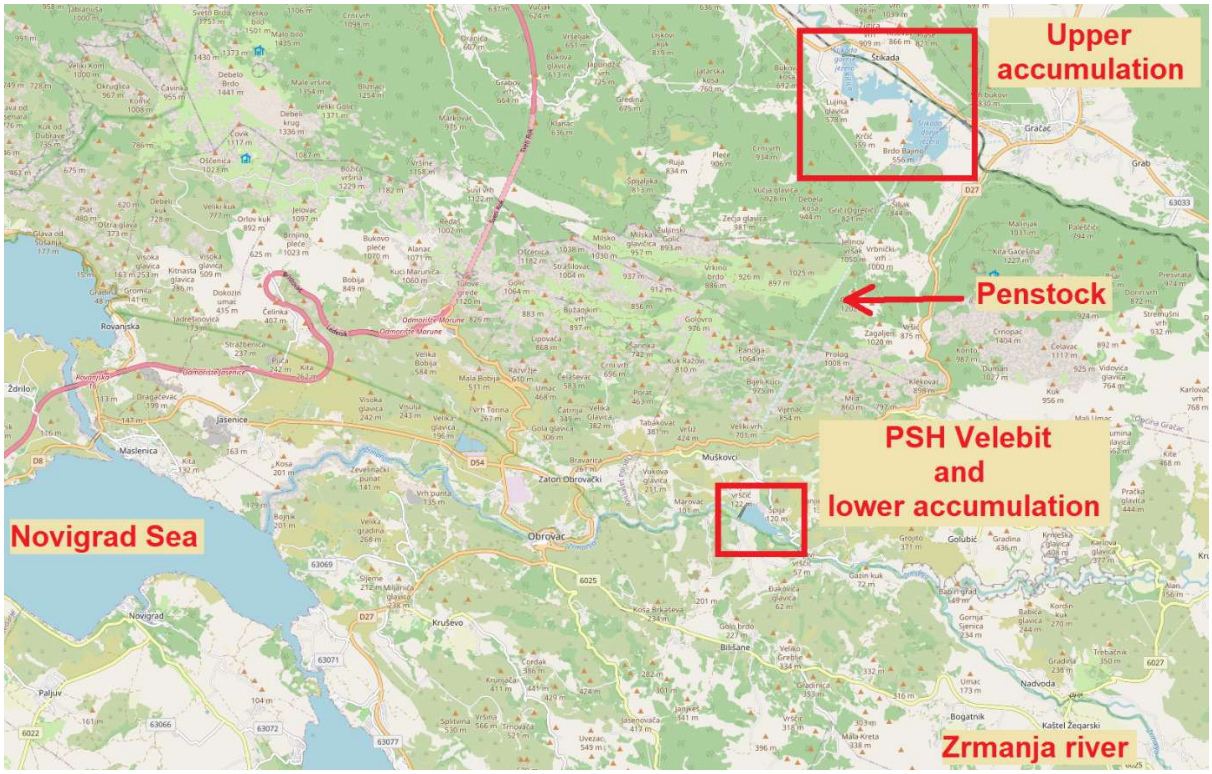

Figure 20. Case study geographic location for WEFE analysis - PSH Velebit - Croatia

PSH Velebit plays a strategic role in Croatia's energy system by delivering peak-load balancing, reserve capacity, and frequency regulation. The system uses the large elevation difference between reservoirs to store energy as gravitational potential. The upper reservoir, Štikada, formed by damming the Ričica River, is the only active upper storage used in this study. It has a total volume of 13.6 million m³, of which 9.6 million m³ is usable for energy generation [134], with an average surface area of 334 ha [135].

The lower reservoir, Razovac, situated at 9 m above sea level in the Zrmanja River valley, was created by an earth-fill dam and has a total volume of 1.84 million m³ and a surface area of 36 ha [134]. In the absence of literature data, the minimum lower storage level, was assumed to be 20% of total volume. These minimum levels define the natural accumulation outflow that is

always available. The facility is equipped with two reversible Francis pump–turbine units, operating in generation mode at up to 280 MW (maximum flow 60 m^3/s) and in pumping mode at up to 240 MW (maximum flow 40 m^3/s) [134].

Hourly inflow data for the lower and upper reservoirs covering 2001-2022 were provided by Croatian Waters, enabling detailed analysis of inflow variability, seasonal patterns, and operational effects [136]. Water demand data for residential, industrial, and tourism needs, equivalent to withdrawals from Razovac, were provided by the Zadar County water utility [137].

The FPV system potential was assessed following the approach in [133], with installation assumed at the Štikada reservoir elevation and configuration parameters as specified in the model. Evaporation modelling applied the FAO-56 ET_0 method with ERA5-Land meteorological inputs for 2001-2022, while evaporation suppression from FPV coverage was set at 87% in line with literature values. Agricultural irrigation needs were estimated using the single crop coefficient method and crop distribution data from [138] and [139]. The economic framework incorporated a 6% discount rate, 25-year project lifetime, hourly market prices from the Croatian Energy Exchange [140], and an equivalent water price range of 0-30 EUR/m^3. Ecosystem benefits were monetised through avoided CO_2 emissions (79.51 EUR/tCO_2 [141]) and land-use savings (2.96 EUR/m^2 [142]). Full modelling assumptions and parameter specifications are detailed in PAPER 3.

The optimisation modelling was carried out to determine the optimal configuration and operation of an integrated hybrid FPV-PSH system, progressively broadening the assessment scope through four optimisation viewpoints: Energy-centric (E), Water–Energy (WE), Water–Energy–Food (WEF), and Water–Energy–Food–Ecosystem (WEFE). Each viewpoint represents an incremental step in complexity and integration, beginning with a purely financial and operational focus on electricity generation and sequentially incorporating water management benefits, agricultural irrigation demands, and finally ecosystem-related benefits such as avoided CO_2 emissions, land-use savings, and hydropower generation ecosystem costs.

From the energy-centric viewpoint, corresponding to the objective function in equations (11) and (15), only the revenues and costs directly associated with electricity generation are considered. The investment cost of the FPV system is included, but no water-related, agricultural, or environmental benefits are accounted for. This allows for an isolated assessment of the financial viability of FPV integration driven solely by electricity market interactions and technical constraints.

The optimisation results indicate that FPV integration into the existing hydropower setup is financially justified only at the lowest investment cost examined (1000 EUR/kW). At higher investment costs, FPV installation is excluded from the optimal configuration, as the operational gains do not offset the increased capital expenditure. At 1000 EUR/kW, the optimal FPV capacity is 340.04 MW, corresponding to 1.911 km^2 of reservoir surface coverage and achieving annual evaporation savings of 1423 Mm^3.

Under this configuration, FPV electricity production totals 411.557 GWh/year, with 95.06% directly utilised for pump operations, reflecting high self-consumption. Hydropower generation increases slightly from 897.414 GWh/year in the hydro-only case to 903.701 GWh/year in the hybrid scenario, a 0.7% gain attributable to the operational flexibility introduced by FPV generation. As this analysis focuses exclusively on market prices and technical constraints, grid demand profiles are not explicitly modelled, although demand effects are indirectly captured within the market price data.

The financial comparison shows that hydropower-only operation yields an annual net benefit of 37.744 million EUR. The hybrid FPV-PSH system generates 67.295 million EUR/year in operational revenues; after subtracting the annualised FPV investment cost of 29.178 million EUR, the resulting net benefit is 38.117 million EUR/year. This represents an incremental financial advantage of 372.67 kEUR/year, or about 1% higher than the hydropower-only scenario.

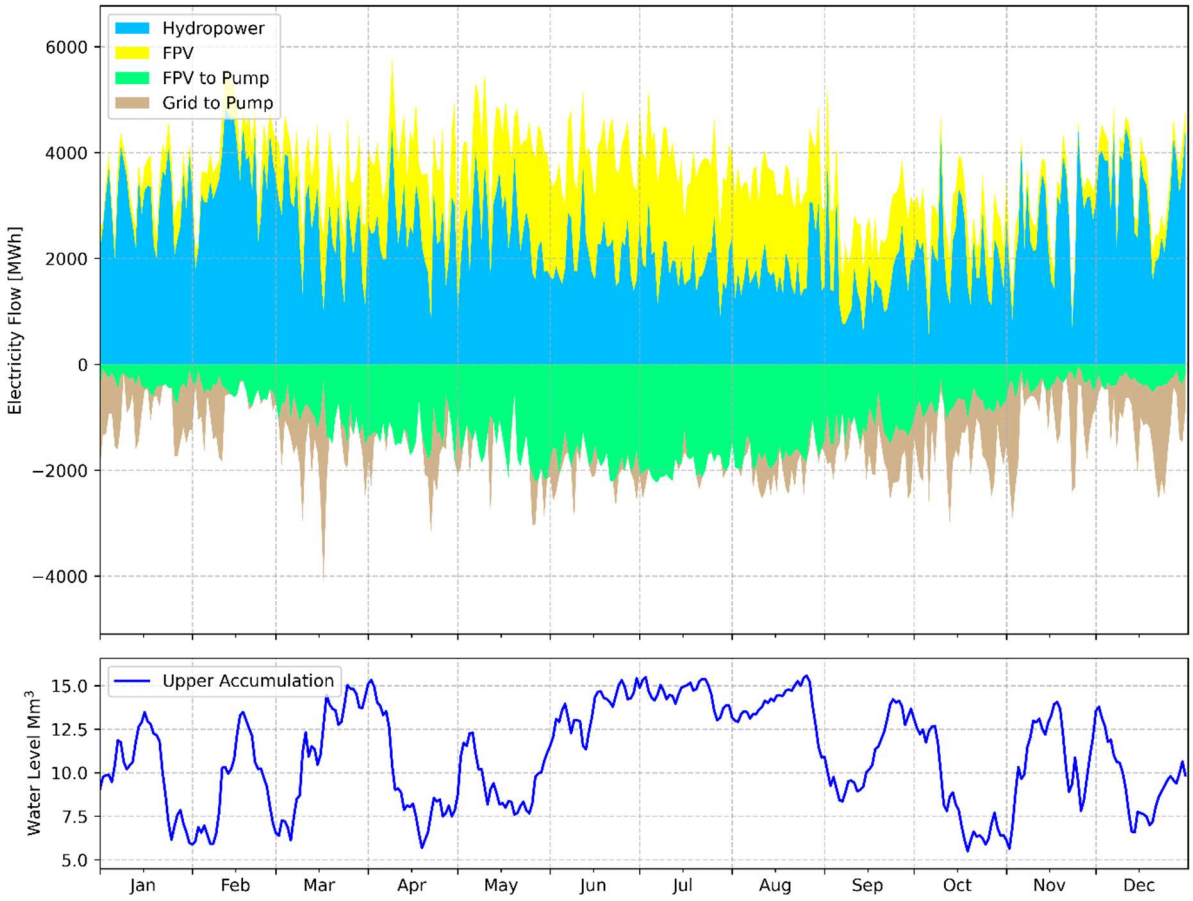

Figure 21. Optimal system dispatch under energy-centric viewpoint – daily aggregated

Operational dynamics over the year are illustrated in Figure 21, which shows daily aggregated electricity flows and reservoir levels for the hybrid case. Positive values denote PSH generation (blue) and FPV generation (yellow), while negative values indicate pumping, sourced either from FPV generation (green) or from the grid (brown). The lower part of Figure 4 shows daily water level variations in the upper reservoir, demonstrating compliance with operational limits. For direct comparison, Figure 22 presents the daily aggregated hydropower-only generation and reservoir level patterns.

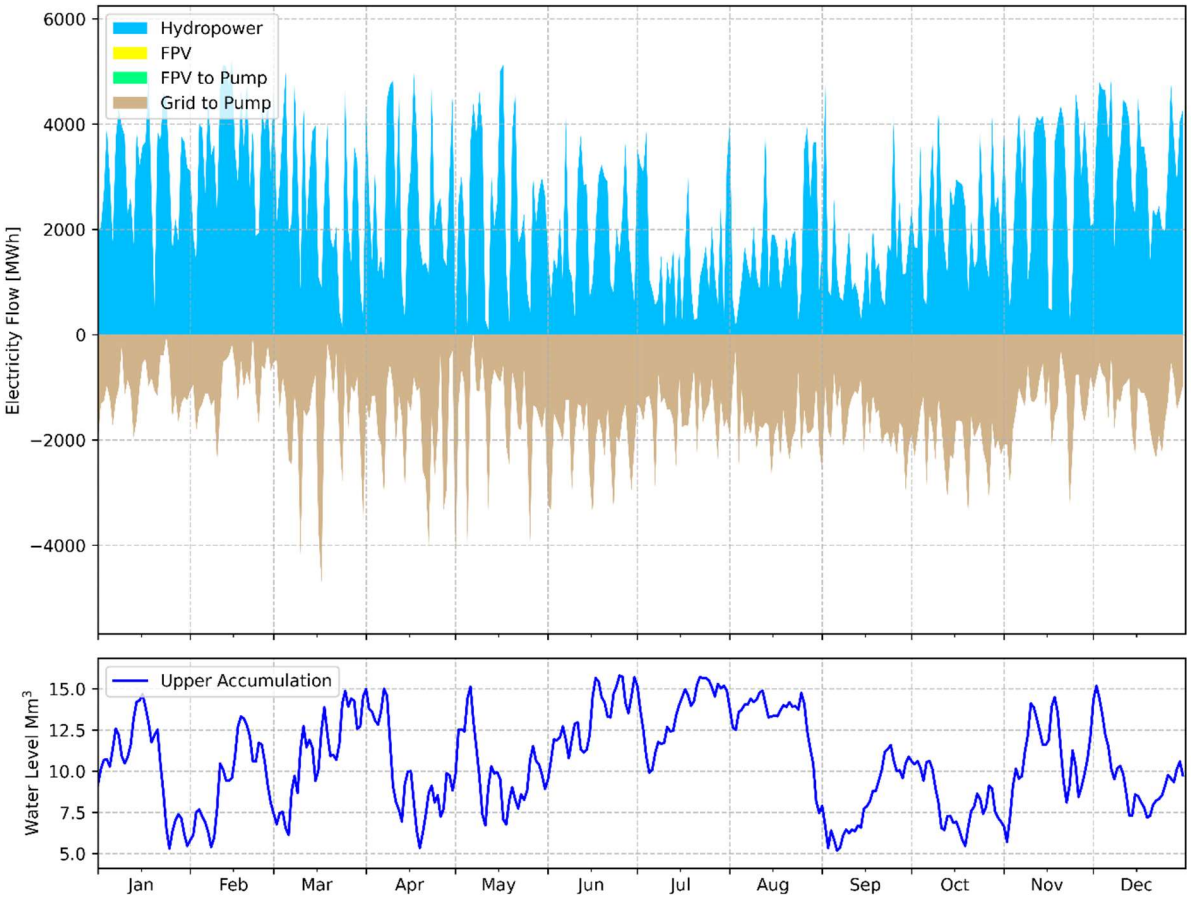

Figure 22. Optimal hydropower only system dispatch under energy-centric viewpoint – daily aggregated

This shift in generation patterns clearly demonstrates the potential of hybrid FPV–PSH operation to enable a smoother and less intermittent hydropower dispatch profile. The coordinated operation of these two technologies can serve to balance their respective intermittencies in a mutually beneficial way. Hydropower generation, with its flexibility and dispatchability, can stabilise both the hourly and seasonal fluctuations characteristic of FPV output. Conversely, FPV generation, which reaches its peak during late spring and summer months, can provide valuable support to hydropower operations by enabling more strategic water storage management during periods when water demand is at its highest and evaporation losses are most significant.

In addition to these operational synergies, it is important to recognise that optimised dispatch with reduced hydropower variability may yield further benefits. A less intermittent hydropower output profile can reduce the frequency and magnitude of rapid operational changes, thereby lowering mechanical stress on turbines and other system components. Over time, this reduction in operational stress has the potential to decrease wear and tear, improve the reliability of hydropower assets, and extend the effective service life of critical equipment.

The obtained results are consistent with findings presented in PAPER 4, which reviewed the technological development and operational feasibility of FPV systems and their hybridisation with hydropower plants. As demonstrated in PAPER 4, coupling FPV with existing reservoirs enables more efficient use of water surfaces by generating additional RES electricity while simultaneously reducing evaporation losses. These effects strengthen both the energy and water dimensions of the WEFE framework, particularly in regions with pronounced seasonal variability and water scarcity. The review further showed that hybrid FPV–hydropower configurations can increase total generation by up to 50 % of the hydropower output when covering only a fraction of the reservoir area, confirming the strong complementarity between the two resources.

In this research, the optimisation results reveal similar system behaviour. The stochastic model identifies FPV-PSH combinations that balance power production and water retention, yielding improved resource efficiency compared to individual systems. The methodological integration of FPV potential, as outlined in PAPER 4, provides validation for the modelling outcomes and underlines their practical relevance. It confirms that the simultaneous optimisation of solar generation and hydropower operation can deliver both economic and environmental benefits, contributing to evaporation mitigation, more stable electricity supply, and enhanced utilisation of existing water infrastructure. These findings further support the conclusion that the integration of FPV with PSH not only improves system flexibility and resource utilisation but also contributes to long-term operational sustainability and cost-effectiveness of the overall infrastructure.

These operational differences and their implications for long-term performance are explored further in the Subsection 3.5, where load duration curves (Figure 24) provide a detailed comparative view of dispatch characteristics under varying optimisation perspectives.

3.5 Influence of Water-Energy-Food-Ecosystem objectives and uncertainty on optimal hybrid solar-hydro system

The analysis in this subsection builds on the comprehensive WEFE framework developed in PAPER 3, which incorporates uncertainty in both climatic and market conditions through a two-stage stochastic optimisation approach. This method enables simultaneous consideration of technical, economic, environmental, and cross-sectoral interactions, ensuring that optimal system configurations are robust across a wide range of plausible future scenarios. By progressively expanding the optimisation perspective from a narrow, energy-only focus to the

full WEFE scope, the results highlight the trade-offs and synergies among competing objectives. Full details of the modelling formulation, data inputs, and scenario generation process are provided in the Method section and described in detail in PAPER 3.

From the WE perspective, the optimisation objective integrates both electricity-related financial streams and the economic benefits of water savings achieved through reduced reservoir evaporation. By assigning an economic value to conserved water, expressed as the EWP, this viewpoint extends the analysis beyond the purely energy-centric case to explicitly capture the interdependence between electricity production and water resource management.

Figure 23 presents the sensitivity of optimal FPV deployment and associated hydropower generation gains to variations in EWP and FPV investment costs (FPVC). The colour gradients in both panels represent the variation in the objective function value, providing a visual indication of financial and economic performance across the full scenario range. The left-hand-side (LHS) diagram shows the optimal FPV capacity, while the right-hand-side (RHS) panel depicts the percentage increase in hydropower generation relative to the hydro-only case.

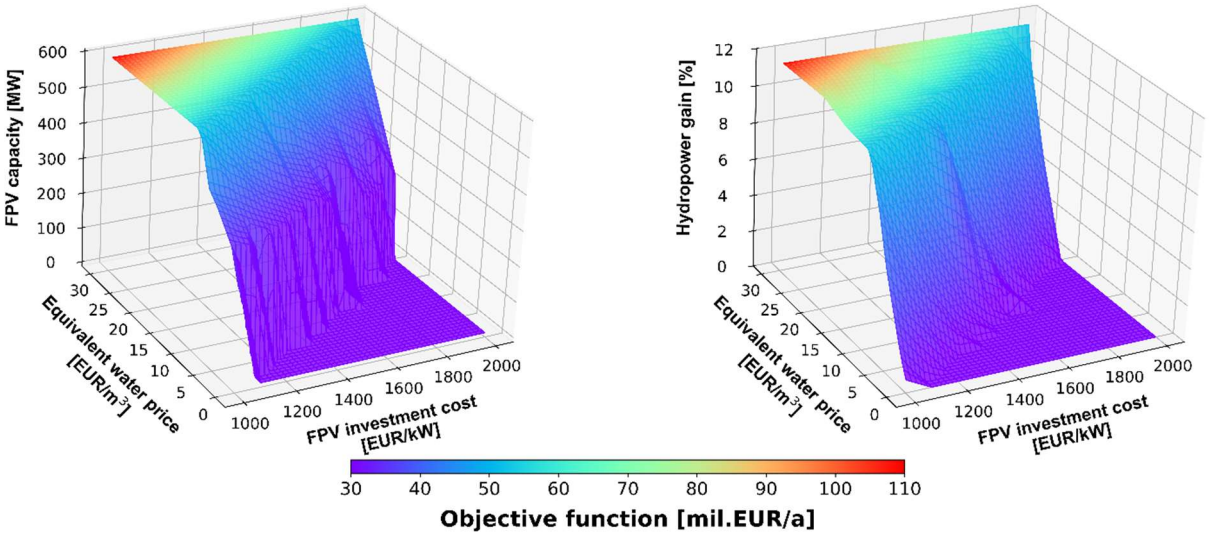

Figure 23. Range of optimal water-energy viewpoint results; FPV capacity (left); Hydropower generation gain (right)

The LHS diagram shows that, at an EWP of 0 EUR/m³, FPV deployment is economically justified only at the lowest investment cost considered (1 000 EUR/kW), resulting in an optimal capacity of 340.04 MW, consistent with the energy-centric findings. The diagram also reveals an upper plateau corresponding to the maximum available installation area, equal to an FPV capacity of 594.17 MW. As FPV investment costs increase, this plateau shifts towards higher EWP values, demonstrating that a higher valuation of water is required to offset increased capital expenditure. The results further indicate distinct sensitivities of optimal FPV capacity to EWP changes across different investment cost ranges. At FPV investment costs above 1600

EUR/kW, capacity changes occur at an average rate of 33.33 MW per EUR/m³ increase in EWP. For investment costs of 1500 EUR/kW and below, the rate of change decreases to an average of 25.61 MW per EUR/m³, suggesting that lower capital expenditure reduces sensitivity to water valuation.

The Figure 23 further shows that hydropower generation gains closely follow the trends in optimal FPV capacity, underscoring the direct relationship between FPV deployment and hydropower operational efficiency. In addition to providing renewable electricity, FPV coverage reduces reservoir evaporation, thereby conserving water that can be redirected towards hydropower generation. This secondary effect is clearly visible in the results, with an average increase in hydropower generation of approximately 11.44 % across the range of optimal FPV capacity configurations examined under varying combinations of FPV investment cost and EWP.

Further insight into the operational impacts of FPV integration on hydropower generation is provided by the load duration curves (LDC) shown in Figure 24. These curves capture the relationship between power output levels and their corresponding durations, allowing a detailed examination of how FPV deployment influences dispatch patterns and generation stability. Across the different FPVC analysed, the LDC profiles exhibit relatively limited sensitivity to FPVC variations. Instead, the EWP emerges as the dominant factor shaping both the form and magnitude of the curves for any fixed FPVC. Given this limited variability across different FPVC values, the LDC results are presented here specifically for the FPVC of 1000 EUR/kW, as FPV deployment remains economically optimal throughout the full analysed range of EWP at this investment cost. The rationale for this selection is to maintain clarity in the presentation of results and facilitate a straightforward interpretation.

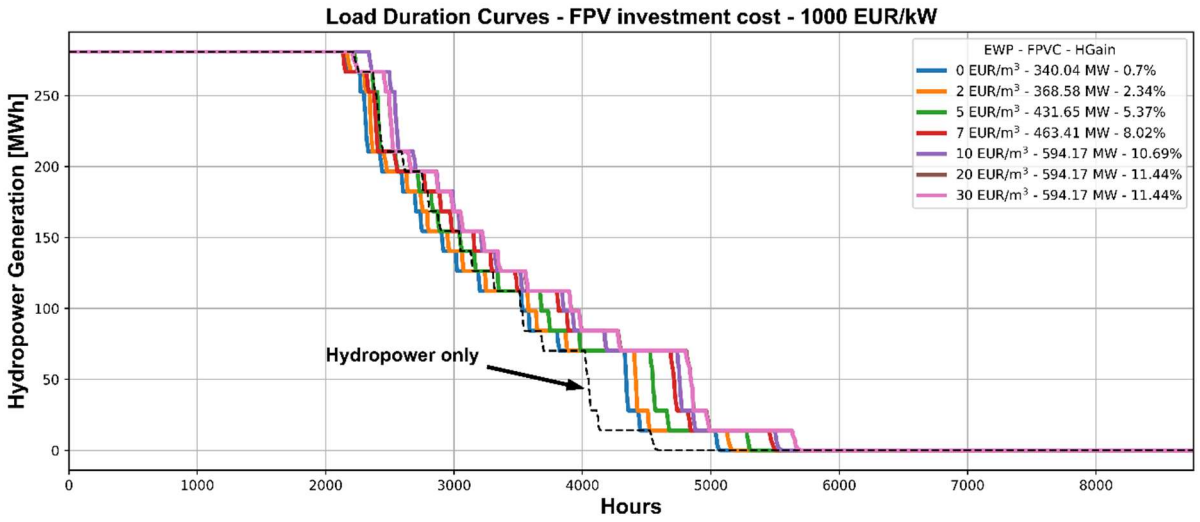

Figure 24. Load duration curves for hydropower generation

Figure 24 presents a series of LDCs for optimal hydropower generation under varying EWP values from 0 to 30 EUR/m³. The legend identifies each EWP scenario along with its corresponding optimal FPV capacity and the percentage gain in hydropower generation relative to the hydro-only baseline. Consistent with the daily aggregated results shown earlier for the energy-centric case (Figure 21), the integration of FPV reduces volatility in hydropower dispatch. This effect is clearly visible in the LDCs, where the curves for FPV-integrated scenarios shift to the right of the baseline (hydro-only) curve shown as a black dashed line. This rightward shift indicates that the additional hydropower generation made possible by FPV is primarily delivered at lower power output levels sustained over significantly longer periods, enhancing baseload capacity and demonstrating the complementary operational dynamics between FPV and hydropower, each technology offsetting the variability of the other.

For EWP values at or below 7 EUR/m³, the extension of generation durations at lower power outputs is accompanied by a reduction in the duration of peak or high-power generation compared to the hydro-only case. This suggests that at lower water valuations, FPV integration predominantly reallocates hydropower production towards more stable, sustained baseload operation rather than increasing peak output. In contrast, when EWP is 10 EUR/m³ or higher, the durations of peak and higher power generation are either maintained or slightly increased relative to the baseline, while the principal effect remains the marked extension of generation durations at lower outputs. Notably, the LDCs for EWP values of 20 EUR/m³ and above are almost indistinguishable, reflecting that under these conditions the system consistently reaches maximum FPV deployment capacity and delivers similar hydropower generation gains.

The operational effects of FPV integration on pumping activities within the hybrid FPV-PSH system are examined in Figure 25, which illustrates how variations in EWP and FPVC influence two key indicators: the pump load factor and the proportion of FPV-generated electricity directly utilised for pumping operations.

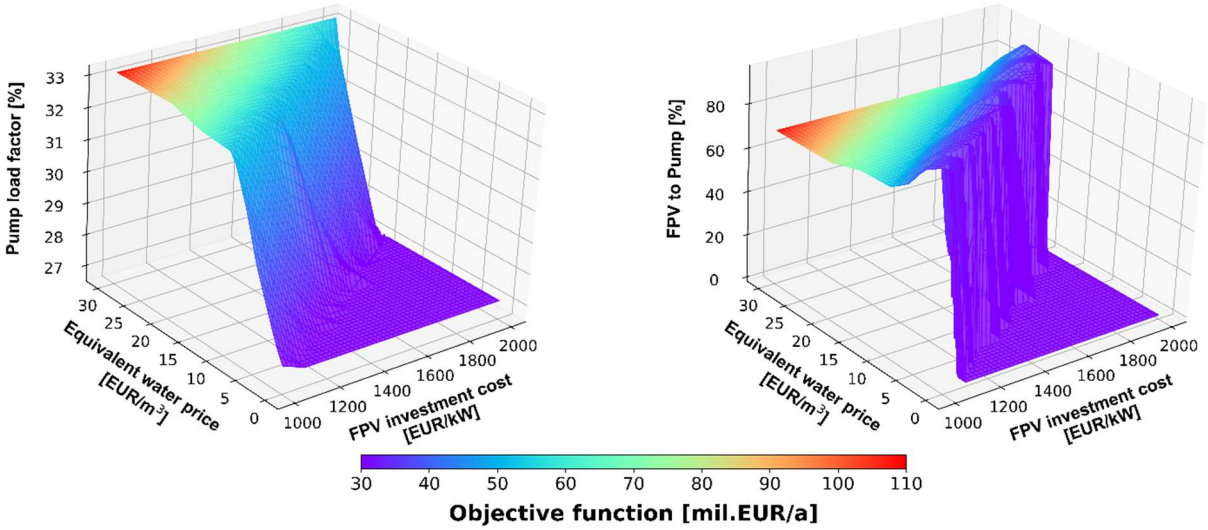

Figure 25. Range of optimal pump specific water-energy viewpoint results; Pump load factor (left); RES self-consumption for pump operation (right)

In the LHS diagram on Figure 25, the pump load factor is shown to increase from an initial value of 27.08% in the hydro-only scenario to a maximum of 33.15% as EWP rises and optimal FPV capacities expand. This upward trend highlights the role of FPV deployment in improving the consistency and overall utilisation of pumping operations. The increased availability of RES electricity from FPV directly supports pump operation, thereby raising self-consumption levels and reducing reliance on external grid electricity. The results also show that the sensitivity and rate of change in the pump load factor in response to increasing EWP become particularly pronounced at higher FPVC values, mirroring the trends previously observed for changes in optimal FPV capacity.

When FPV deployment first becomes economically optimal, the FPV-to-pump ratio attains very high levels, averaging above 90% across all FPV investment cost scenarios, as shown in RHS diagram in Figure 25. This strong initial self-consumption indicates a deliberate operational strategy in which newly installed RES capacity is channelled primarily into pump operation, thereby substantially reducing reliance on grid electricity. As EWP rises and FPV capacity approaches its maximum feasible level, the ratio gradually declines, eventually stabilising at an average of 69.03%. This downward shift reflects a change in operational priorities, driven by the growing economic value of conserved water. Under these conditions, system management increasingly focuses on maximising evaporation reduction to preserve

reservoir volumes, thereby enhancing hydropower generation potential. Although the proportion of FPV electricity used directly for pumping decreases slightly at higher EWP values, the associated indirect benefits, namely improved hydropower generation efficiency and increased water availability for generation, enhance overall system performance. This outcome demonstrates how operational strategies in the integrated WE system adapts dynamically to the relative economic importance of electricity generation and water conservation objectives.

Building on the results presented for the previous figures, the analysis is now extended by adding the food dimension to the optimisation framework, thereby accounting for agricultural irrigation water demands alongside energy and water objectives. Within the WEF approach, the model simultaneously determines the optimal operational strategy for hydropower and FPV generation, the optimal agricultural irrigation area, and the corresponding FPV deployment capacity. Given the similarity between the WEF optimisation outputs and the previously presented WE results, graphical representations analogous to the WE figures are omitted for clarity reasons. Instead, the discussion focuses on key differences between the WEF and WE scenarios, with particular attention to the implications of additional irrigation water demand on lower reservoir spillage and water lost load under varying irrigation area allocations.

The integration of agricultural water requirements in the WEF framework results in an optimised irrigation area in addition to the previously established FPV-PSH configuration. Across the full range of FPVC and EWP values considered, the model consistently identifies an optimal agricultural area of 130.54 km², with a very small standard deviation of 0.522 km². This consistency highlights the robustness of the WEF optimisation formulation, indicating that both the constraints and the objective function converge reliably towards the same solution regardless of parameter variations.

Compared to the WE scenario, the WEF case shows a similar overall trend in optimal FPV capacity, with the main difference occurring at lower EWP values. Here, additional irrigation demand reduces water availability for hydropower generation, limiting the benefit of FPV-induced evaporation savings and resulting in smaller optimal FPV capacities. Hydropower gains follow the same pattern, with a reduced plateau of 10.71% compared to 11.44% in the WE case. Pump operation metrics remain broadly consistent between scenarios, with only small differences. Across the entire FPVC-EWP range, differences are within 1%, indicating that agricultural water demand has only a modest influence on pumping dynamics relative to its effect on FPV capacity and hydropower output. For a broader comparison and detailed analysis, see PAPER 3.

The impact of incorporating agricultural water demand into the optimisation is most evident in the monthly lower reservoir spillage patterns shown in Figure 26. To effectively illustrate these implications, monthly spillage values are presented for a representative FPVC/EWP pair of 1000 EUR/kW and 30 EUR/m³, corresponding to conditions that allow for maximal FPV capacity deployment. Additionally, to illustrate the impact of agricultural irrigation water demand, optimization analyses were performed for predetermined agricultural areas of 0, 50, 100, 150, and 200 km², alongside the optimal case of 130.54 km².

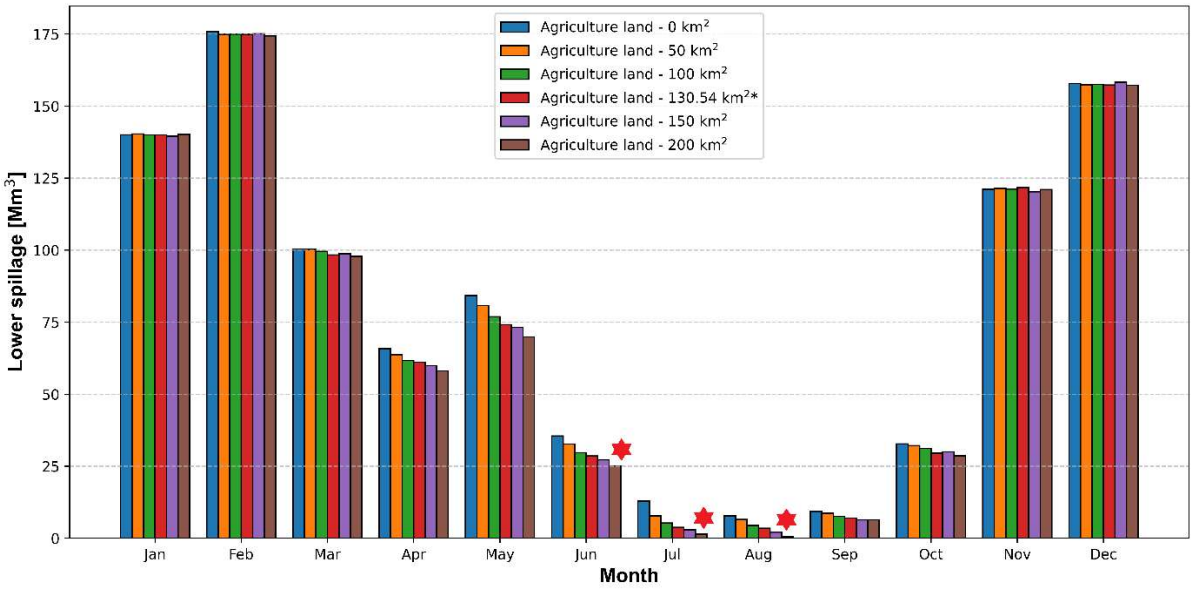

Figure 26. Monthly lower accumulation spillage volumes for different agriculture irrigation areas

The results show that the most significant constraints on hybrid FPV-PSH operation occur in the summer months. During this period, high irrigation water demand coincides with peak electricity demand, low precipitation, and reduced river inflows, creating severe operational limitations. The role of RES energy integration is reinforced by the fact that FPV output peaks during late spring and summer, enabling partial compensation for restricted hydropower generation and facilitating shifts in generation to less critical months. However, these benefits are limited by reservoir storage capacity, which constrains the extent of possible temporal shifting. Figure 26 also highlights the clear operational thresholds imposed by excessive agricultural land use. For irrigation areas of 150 km² and 200 km², water shortages occur in June, July, and August, indicated by red stars, underscoring the system's inability to reliably meet agricultural demand beyond the optimised area.

Addressing such seasonal constraints could involve exploring alternative agricultural management strategies. Given that most crops in the study have planting schedules concentrated in March and April, peak water demand currently coincides with periods of highest electricity

demand and lowest water availability. Diversifying crop types to include those with growth cycles outside the spring and summer months, or adopting technologies that enable year-round production, could help redistribute water demand towards periods of higher inflows, such as early spring or late autumn. While these options lie outside the scope of this study, they represent promising directions for future research aimed at improving the resilience and flexibility of integrated WEF systems.

Building on the preceding results for the WE and WEF scenarios, the analysis is now extended to include the ecosystem dimension within the optimisation framework. In the WEFE perspective, economic values associated with CO_2 emission costs and reductions, as well as land-use savings from FPV deployment, are explicitly incorporated alongside the water, energy, and agricultural considerations already discussed. This integration results in a more holistic optimisation approach, enabling the quantification of ecological and environmental benefits in parallel with technical and economic performance. The addition of these ecosystem-related parameters produces notable changes in optimal system configurations, as detailed below.

Figure 27 presents the optimal FPV capacities and hydropower generation gains obtained under varying FPVC and EWP values, allowing direct comparison with the earlier WE and WEF results. The inclusion of CO_2-related costs and savings, both from avoided grid emissions and from RES generation by FPV and hydropower, together with the value of land-use savings from FPV installation, leads to a substantial increase in optimal FPV deployment across most of the examined FPVC/EWP space.

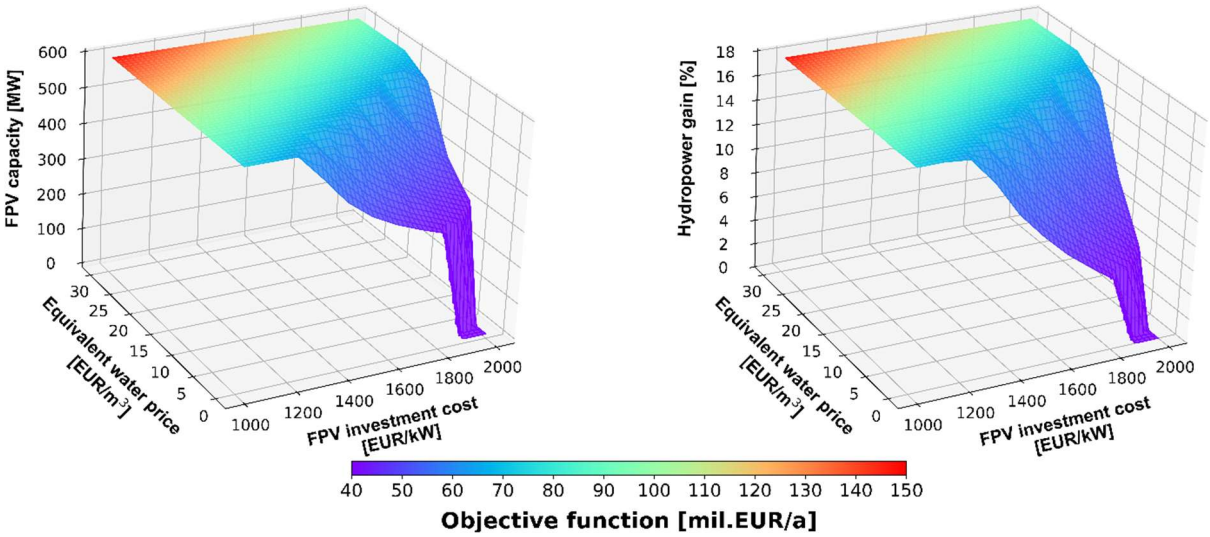

Figure 27. Range of optimal water-energy-food-ecosystem viewpoint results; FPV capacity (left); Hydropower generation gain (right)

For all FPVC values at or below 1200 EUR/kW, the optimal FPV capacity reaches the maximum allowable 594.17 MW. This contrasts sharply with the WE scenario, in which large-

scale FPV deployment only appears at lower investment costs and higher water valuations. In the WEFE case, optimal FPV capacity starts high even at low EWP levels and increases more rapidly with EWP. The only condition under which FPV is excluded from the optimal solution occurs at FPVC above 1900 EUR/kW combined with very low EWP values below 2 EUR/m³, underlining the strong influence of ecosystem valuation in supporting RES integration even under less favourable financial conditions. Hydropower generation gains, shown alongside FPV capacity in Figure 27, follow the same general pattern as FPV deployment. Gains rise quickly with the initial addition of FPV and then stabilise at a plateau once maximum FPV capacity is reached. In the WEFE scenario, this plateau corresponds to an average hydropower gain of approximately 17.74% relative to the hydro-only baseline.

The inclusion of ecosystem benefits also broadens the range of objective function values, further strengthening the financial case for hybrid FPV-PSH systems. In the WEFE scenario, annual objective function values range from 37 to 143 million EUR, compared to the narrower range of 37 to 105 million EUR observed for the WE and WEF scenarios. This wider range reflects the substantial additional value unlocked when ecological impacts and environmental savings are explicitly monetised, underscoring the potential of integrated WEFE optimisation to deliver both higher economic returns and greater sustainability co-benefits.

In addition to assessing absolute performance metrics such as FPV capacity, hydropower generation gains, and total objective function values, it is equally important to understand how the overall benefits of the WEFE optimisation are distributed among its three main value categories: Energy, Water, and Ecosystem. Figure 28 provides this breakdown, showing how the relative shares of these components shift across the full range of FPVC and EWP values. Energy savings reflect the net financial and economic outcomes directly linked to electricity generation from hydropower and FPV (Equation (15)), water savings capture the monetised value of evaporation reductions from FPV deployment (Equation (16)), and ecosystem savings represent the combined economic benefits of avoided CO_2 emissions and land-use savings from FPV installation (Equation (18)). These relative percentages offer insight into the changing balance of priorities and benefits under different economic and technical conditions and should be interpreted alongside changes in the total objective function value.

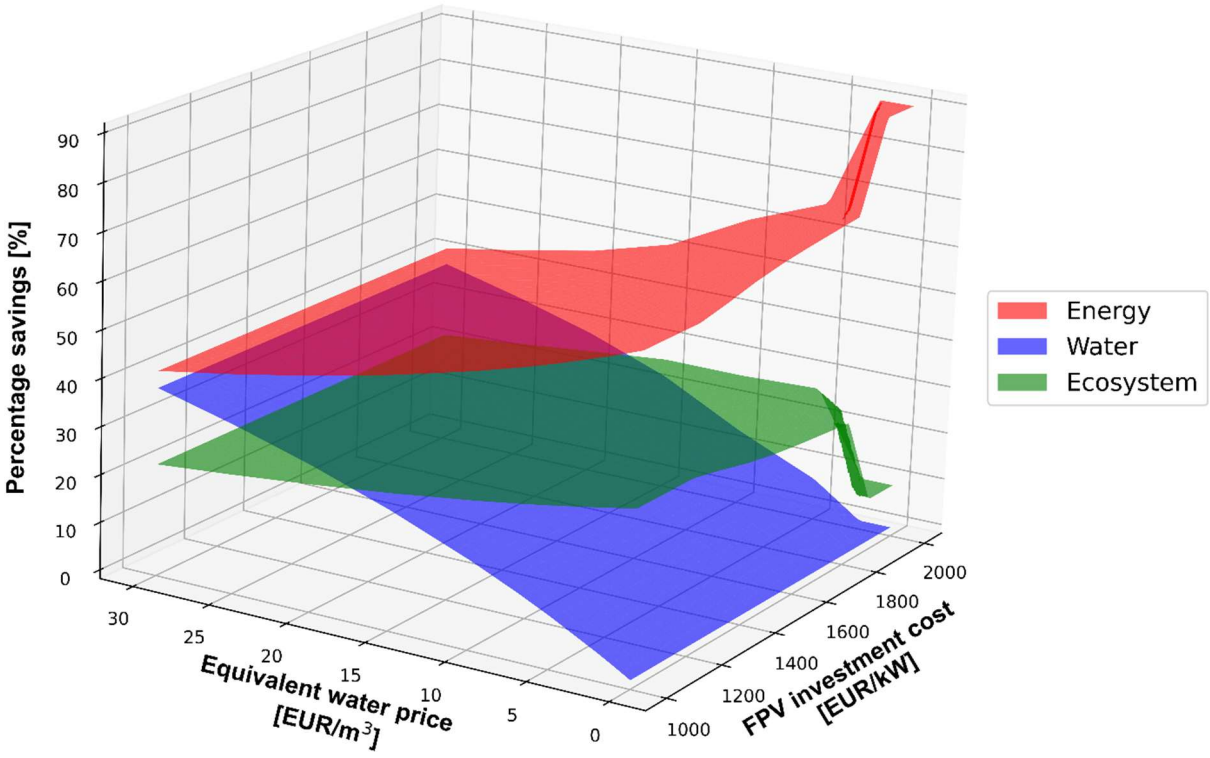

Figure 28. Relative savings divided into categories Energy, Water and Ecosystem

At high FPVC and low EWP, where no FPV is deployed, energy savings dominate at 90.44%, with negligible water and limited ecosystem contributions. As FPV deployment increases, the share of energy savings declines while water savings grow, and ecosystem savings remain relatively stable. This pattern reflects the trade-off between direct energy revenues and the additional value created by water and environmental benefits once FPV becomes economically viable.

Ecosystem savings average around 25.67% across all scenarios, maintaining stability due to maximum FPV deployment being achieved over a broad FPVC/EWP range, which sustains high levels of CO_2 reduction, land-use savings, and hydropower generation gains. Water savings rise steadily with EWP, reaching about 38.03% at the maximum EWP considered. As water savings increase, the energy savings share falls to about 40.92%, with a notable crossover point at EWP value of 16.34 EUR/m³ where water and ecosystem savings contribute equally, indicating a balance between economic incentives for water conservation and environmental benefits.

In scenarios with low or zero water savings, the interaction between energy and ecosystem benefits is particularly evident. For example, at EWP = 0 EUR/m³, increasing FPV capacity reduces the energy savings share from 95.92% to 66.32%, while ecosystem savings grow from 4.47% to 33.67%. This shift is driven by substantial gains in land-use savings and CO_2 emission

reductions, emphasising the important role that ecosystem benefits can play in determining optimal FPV-PSH configurations and dispatch strategies.

In summary, the WEFE optimisation demonstrates the value of expanding the decision-making scope to include water, food, and ecosystem dimensions under uncertainty. Incorporating water valuation shows evaporation reduction as a key driver for increasing FPV capacity, with hydropower gains over 11% and improved dispatch stability. Adding irrigation demands slightly reduces FPV capacity at low EWP and limits hydropower gains to about 10.7%, while highlighting seasonal constraints and water shortages when agricultural areas exceed the optimal 130.54 km². The full WEFE perspective, monetising CO_2 reductions and land-use savings, delivers the largest transformation, maximising FPV capacity across much of the FPVC-EWP range, raising hydropower gains to nearly 18%, and shifting benefits from energy-only to a balanced mix of energy, water, and ecosystem savings.

4 CONCLUSIONS AND FUTURE WORK

The research presented in this thesis aimed to model the optimal interconnection between water and energy systems in order to maximise social welfare under uncertain climatic and market conditions. The work was founded on the hypothesis that detailed, data-driven analysis of coupled water and energy systems can generate planning and operational models that reduce total resource use, strengthen supply security, and support greater penetration of renewable energy sources. The scientific contribution was the development of advanced optimisation frameworks for the operation and expansion of integrated systems exposed to fluctuating prices, variable resources, and climate extremes. Throughout the research, the methodological focus was on establishing a unified modelling approach capable of describing technical performance, economic behaviour, and environmental outcomes with consistent temporal and sectoral resolution. The optimisation structure developed for the thesis joined investment and operational decisions within the same framework. This methodological consistency made it possible to compare and interpret results across urban, island, and regional contexts, revealing common patterns in the behaviour of multi-sector systems under uncertainty.

The overall findings confirm the validity of the initial hypothesis. When design and operation are optimised simultaneously, rather than treated as sequential steps, systems achieve lower cost, lower emissions, and higher flexibility. This pattern was evident across all analysed applications. The joint treatment of capacity, operation, and interconnection proved essential for identifying economically and environmentally optimal configurations. Sectoral boundaries that are traditionally fixed, between heat and power, water and energy, or energy and ecosystems, can be relaxed through optimisation, yielding solutions that make better use of RES and storage resources.

A major insight of the research concerns the role of flexibility and its representation within optimisation models. The results demonstrate that storage in its various forms, thermal, electrical, or water, provides the main instrument through which RES variability and temporal mismatches between supply and demand are reconciled. The work shows that flexibility does not depend solely on electrical storage technologies, but is embedded in the coordinated use of multiple energy and water storages. When different storage media are optimised together, the

system can shift resources over time and across sectors, increasing the utilisation of RES and reducing the need for fossil back-up capacity.

Another key conclusion relates to the treatment of uncertainty. The modelling frameworks confirmed that uncertainty in climate and market conditions must be addressed within the optimisation process rather than analysed afterwards. In deterministic settings, the optimal configuration is narrowly defined and sensitive to single assumptions. Once uncertainty is represented through stochastic programming or systematic sensitivity analysis, the results become more robust and reveal how the value of flexibility increases with volatility. This insight supports the broader argument that uncertainty is not an external disturbance but an intrinsic design parameter for sustainable system planning..

The thesis also contributes to understanding how valuation scope affects planning outcomes. When objectives are extended beyond energy cost minimisation to include water, food, and ecosystem benefits, the optimal configuration and operation of the system change markedly. The results demonstrate that decisions justified purely on energy terms can underestimate the social and environmental value of integrated solutions. Broader objectives that reflect water conservation, food production, or carbon and land-use benefits lead to designs that are more resilient and more aligned with long-term sustainability goals. This behaviour was consistent across modelling approaches and confirms that multi-sector optimisation is a practical route for implementing the WEFE nexus in quantitative planning.

A cross-cutting conclusion emerging from the research is that system integration yields the largest efficiency gains when accompanied by spatial and temporal coupling. In the urban energy context, network interconnection and optimal storage placement achieve both cost reduction and emission mitigation. In water-energy systems, coordinated operation of PV generation, BES, and desalination allows RES electricity to serve water demand with minimal curtailment and grid dependence. In regional WEFE systems, coupling of FPV and PSH demonstrates how one technology can support another through evaporation reduction, seasonal energy shifting, and improved reservoir management. These findings emphasise that nexus integration is not only conceptual but operationally measurable through optimisation results.

The methodological contribution of the thesis lies in establishing optimisation as a unifying tool for analysing water and energy systems of different scales and functions. By keeping the same temporal resolution and optimisation logic across cases, the models bridge the gap between detailed engineering analysis and policy-relevant planning. The results demonstrate that

sectoral optimisation performed within isolated boundaries often leads to suboptimal global outcomes, whereas integrated optimisation captures synergies that translate into tangible cost savings and environmental benefits. The research therefore contributes both to the academic understanding of multi-sector system design and to the practical task of guiding investment and operation under uncertainty. Beyond quantitative outcomes, the thesis contributes conceptually to the evolving definition of resilience in the WE nexus. The presented frameworks show that resilience is a property that emerges from diversification of resources, storage, and cross-sector connections. Systems designed with multiple conversion and storage pathways can maintain service levels under volatile conditions and extreme events. This insight reinforces the relevance of optimisation modelling not only for cost minimisation but also for ensuring reliability and adaptability in the face of climate variability.

While the developed models achieve the objectives stated in the thesis, their application also revealed several limitations that define directions for future research. The DH framework would benefit from the inclusion of electrical and hydraulic network constraints and from explicit coupling with market dynamics at sub-hourly timescales. The desalination model could be refined by integrating process-level dynamics and by linking the optimisation results to the technical behaviour of RO systems under variable power operation. The stochastic WEFE framework could be extended to multistage formulations and to wider ecosystem indicators that include biodiversity and water quality. These extensions would preserve the methodological consistency of the thesis while improving realism and policy applicability and will be included in future research. Future research should also explore ways of connecting optimisation models with governance and social-science perspectives. The inclusion of participatory decision parameters, such as stakeholder preferences and distributional equity, would allow the frameworks to serve as decision-support tools in planning processes. Integration with life-cycle and environmental assessment would further strengthen their capacity to evaluate sustainability across economic, environmental, and social dimensions.

The collective findings demonstrate that uncertainty-aware, optimisation-based planning can provide actionable guidance for designing low-carbon, resource-efficient, and resilient systems. The developed frameworks quantify how technological, economic, and environmental interactions evolve when sectors are optimised together. They translate abstract nexus concepts into measurable performance improvements and deliver modelling evidence that supports integrated planning at multiple scales. The outcomes confirm the thesis objective and validate the hypothesis that cross-sectoral modelling can enhance the efficiency and sustainability of

water and energy systems under uncertain future conditions. Through its methodological advances and empirical insights, the research contributes to the scientific foundation needed for a more integrated and adaptive approach to resource planning in a changing climate.

5 LITERATURE

[1] European Commission, “Fit for 55.” https://www.consilium.europa.eu/en/policies/green-deal/fit-for-55-the-eu-plan-for-a-green-transition/

[2] C. E. Mooren *et al.*, “Water–energy–food–ecosystem nexus: how to frame and how to govern,” *Sustain. Sci.*, May 2025, doi: 10.1007/s11625-025-01691-x.

[3] C. Carmona-Moreno, C. Dondeynaz, and M. Biedler, “Position Paper on Water, Energy, Food, and Ecosystem (WEFE) Nexus and Sustainable development Goals (SDGs).,” 2019. doi: 10.2760/5295.

[4] World Economic Forum, *Global Risks 2011 Sixth Edition*. 2011. [Online]. Available: https://www3.weforum.org/docs/WEF_Global_Risks_Report_2011.pdf

[5] World Economic Forum, *Water security: the water-energy-food climate nexus*. 2011. [Online]. Available: https://www3.weforum.org/docs/WEF_WI_WaterSecurity_WaterFoodEnergyClimateNexus_2011.pdf

[6] D. M. Kammen, “Turning words into action on climate change,” *Carbon Manag.*, vol. 4, no. 2, pp. 139–142, Apr. 2013, doi: 10.4155/cmt.13.6.

[7] C. Yupanqui, N. Dias, M. R. Goodarzi, S. Sharma, H. Vagheei, and R. Mohtar, “A review of water-energy-food nexus frameworks, models, challenges and future opportunities to create an integrated, national security-based development index,” *Energy Nexus*, vol. 18, p. 100409, Jun. 2025, doi: 10.1016/j.nexus.2025.100409.

[8] A. Endo *et al.*, “Methods of the Water-Energy-Food Nexus,” *Water*, vol. 7, no. 10, pp. 5806–5830, Oct. 2015, doi: 10.3390/w7105806.

[9] R. Rosen and R. Mohtar, “Resource Nexus: Water, Energy, Food. Water Forum and Technology Roadmap.,” 2015. [Online]. Available: https://www.researchgate.net/publication/298787221_Resource_Nexus_Water_Energy_Food_Water_Forum_and_Technology_Roadmap

[10] R. H. Mohtar, “A call for a new business model valuing water use and production: the

Water, Energy and Food Nexus holistic system approach," *Water Int.*, vol. 42, no. 6, pp. 773–776, Aug. 2017, doi: 10.1080/02508060.2017.1353238.

[11] R. H. Mohtar and R. Lawford, "Present and future of the water-energy-food nexus and the role of the community of practice," *J. Environ. Stud. Sci.*, vol. 6, no. 1, pp. 192–199, Mar. 2016, doi: 10.1007/s13412-016-0378-5.

[12] European Commission, "Partnership for Research and Innovation in the Mediterranean Area (PRIMA)." https://research-and-innovation.ec.europa.eu/research-area/environment/prima_en

[13] E. Lucca *et al.*, "A review of water-energy-food-ecosystems Nexus research in the Mediterranean: evolution, gaps and applications," *Environ. Res. Lett.*, vol. 18, no. 8, p. 083001, Aug. 2023, doi: 10.1088/1748-9326/ace375.

[14] UNESCO and European Commission, "Implementing the Water–Energy–Food–Ecosystems Nexus and achieving the Sustainable Development Goals," 2021. [Online]. Available: https://unesdoc.unesco.org/ark:/48223/pf0000379588

[15] B. Daher and R. H. Mohtar, "Water-Energy-Food Sustainable Development Goals in Morocco," 2021, pp. 1–18. doi: 10.1007/978-3-319-70061-8_133-1.

[16] R. Mohtar, "The importance of the Water-Energy-Food Nexus in the implementation of The Sustainable Development Goals (SDGs)," 2016. [Online]. Available: https://www.policycenter.ma/sites/default/files/OCPPC-PB1630_0.pdf

[17] D. Magagna *et al.*, "Water-Energy Nexus in Europe," 2019. [Online]. Available: https://uploads.water-energy-food.org/resources/online_ecj095x_policy_report_interactive_4-2.pdf

[18] M. Clausse *et al.*, "River water heat pumps to decarbonise district heating and promote the resilience of hydrosystems: Technico-economic, environmental and sociological challenges," *Energy Nexus*, vol. 16, p. 100325, Dec. 2024, doi: 10.1016/j.nexus.2024.100325.

[19] Food and Agriculture Organization of the United Nations, "The Water-Energy-Food Nexus - A new approach in support of food security and sustainable agriculture," 2014. [Online]. Available:

https://openknowledge.fao.org/server/api/core/bitstreams/86fe97cc-4a38-4511-a37f-8eb8ea8fe941/content

[20] IPCC, “Climate Change 2021 - The Physical Science Basis,” 2021. [Online]. Available: https://www.ipcc.ch/report/ar6/wg1/downloads/report/IPCC_AR6_WGI_FullReport.pdf

[21] G. C. de Oliveira, E. Bertone, and R. A. Stewart, “Challenges, opportunities, and strategies for undertaking integrated precinct-scale energy–water system planning,” *Renew. Sustain. Energy Rev.*, vol. 161, p. 112297, Jun. 2022, doi: 10.1016/j.rser.2022.112297.

[22] B. V. Mathiesen *et al.*, “Smart Energy Systems for coherent 100% renewable energy and transport solutions,” *Appl. Energy*, vol. 145, pp. 139–154, May 2015, doi: 10.1016/j.apenergy.2015.01.075.

[23] M. Sameti and F. Haghighat, “Optimization approaches in district heating and cooling thermal network,” *Energy Build.*, vol. 140, pp. 121–130, Apr. 2017, doi: 10.1016/j.enbuild.2017.01.062.

[24] R. Menke, E. Abraham, P. Parpas, and I. Stoianov, “Demonstrating demand response from water distribution system through pump scheduling,” *Appl. Energy*, vol. 170, pp. 377–387, May 2016, doi: 10.1016/j.apenergy.2016.02.136.

[25] P. A. Østergaard and A. N. Andersen, “Variable taxes promoting district heating heat pump flexibility,” *Energy*, vol. 221, p. 119839, Apr. 2021, doi: 10.1016/j.energy.2021.119839.

[26] S. Mashayekh, M. Stadler, G. Cardoso, and M. Heleno, “A mixed integer linear programming approach for optimal DER portfolio, sizing, and placement in multi-energy microgrids,” *Appl. Energy*, vol. 187, pp. 154–168, Feb. 2017, doi: 10.1016/j.apenergy.2016.11.020.

[27] S. Frederiksen and S. Werner, *District Heating and Cooling*. Studentlitteratur AB, 2013.

[28] S. Werner, “International review of district heating and cooling,” *Energy*, vol. 137, pp.

617–631, 2017, doi: 10.1016/j.energy.2017.04.045.

[29] H. Lund *et al.*, “4th Generation District Heating (4GDH). Integrating smart thermal grids into future sustainable energy systems.,” *Energy*, vol. 68, pp. 1–11, 2014, doi: 10.1016/j.energy.2014.02.089.

[30] H. Lund, *Renewable energy systems: a smart energy systems approach to the choice and modeling of 100% renewable solutions. 2nd ed.* Academic Press, 2014.

[31] H. Lund *et al.*, “The status of 4th generation district heating: Research and results,” *Energy*, vol. 164, pp. 147–159, 2018, doi: 10.1016/j.energy.2018.08.206.

[32] S. Kuntuarova, T. Licklederer, T. Huynh, D. Zinsmeister, T. Hamacher, and V. Perić, “Design and simulation of district heating networks: A review of modeling approaches and tools,” *Energy*, vol. 305, p. 132189, Oct. 2024, doi: 10.1016/j.energy.2024.132189.

[33] D. Höffner and S. Glombik, “Energy system planning and analysis software—A comprehensive meta-review with special attention to urban energy systems and district heating,” *Energy*, vol. 307, p. 132542, Oct. 2024, doi: 10.1016/j.energy.2024.132542.

[34] I. Brocklebank, S. B. M. Beck, and P. Styring, “A Simple Approach to Modeling Rural and Urban District Heating,” *Front. Energy Res.*, vol. 6, Oct. 2018, doi: 10.3389/fenrg.2018.00103.

[35] M. Pavičević, T. Novosel, T. Pukšec, and N. Duić, “Hourly optimization and sizing of district heating systems considering building refurbishment – Case study for the city of Zagreb,” *Energy*, vol. 137, pp. 1264–1276, Oct. 2017, doi: 10.1016/j.energy.2017.06.105.

[36] M. GALINDO FERNÁNDEZ, C. ROGER-LACAN, U. GÄHRS, and V. AUMAITRE, *Efficient district heating and cooling markets in the EU: Case studies analysis, replicable key success factors and potential policy implications*, no. December. 2016. doi: 10.2760/371045.

[37] A. Hast, S. Syri, V. Lekavičius, and A. Galinis, “District heating in cities as a part of low-carbon energy system,” *Energy*, vol. 152, pp. 627–639, 2018, doi: 10.1016/j.energy.2018.03.156.

[38] D. F. Dominković, I. Bačeković, D. Sveinbjörnsson, A. S. Pedersen, and G. Krajačić,

"On the way towards smart energy supply in cities: The impact of interconnecting geographically distributed district heating grids on the energy system," *Energy*, vol. 137, pp. 941–960, 2017, doi: 10.1016/j.energy.2017.02.162.

[39] E. Guelpa and V. Verda, "Thermal energy storage in district heating and cooling systems: A review," *Appl. Energy*, vol. 252, no. June, p. 113474, 2019, doi: 10.1016/j.apenergy.2019.113474.

[40] D. Buoro, M. Casisi, A. De Nardi, P. Pinamonti, and M. Reini, "Multicriteria optimization of a distributed energy supply system for an industrial area," *Energy*, vol. 58, pp. 128–137, Sep. 2013, doi: 10.1016/j.energy.2012.12.003.

[41] C. Haikarainen, F. Pettersson, and H. Saxén, "A model for structural and operational optimization of distributed energy systems," *Appl. Therm. Eng.*, vol. 70, no. 1, pp. 211–218, Sep. 2014, doi: 10.1016/j.applthermaleng.2014.04.049.

[42] L. Li, H. Mu, N. Li, and M. Li, "Economic and environmental optimization for distributed energy resource systems coupled with district energy networks," *Energy*, vol. 109, pp. 947–960, Aug. 2016, doi: 10.1016/j.energy.2016.05.026.

[43] B. Morvaj, R. Evins, and J. Carmeliet, "Optimising urban energy systems: Simultaneous system sizing, operation and district heating network layout," *Energy*, vol. 116, pp. 619–636, Dec. 2016, doi: 10.1016/j.energy.2016.09.139.

[44] C. Bordin, A. Gordini, and D. Vigo, "An optimization approach for district heating strategic network design," *Eur. J. Oper. Res.*, vol. 252, no. 1, pp. 296–307, Jul. 2016, doi: 10.1016/j.ejor.2015.12.049.

[45] J. Zeng, J. Han, and G. Zhang, "Diameter optimization of district heating and cooling piping network based on hourly load," *Appl. Therm. Eng.*, vol. 107, pp. 750–757, Aug. 2016, doi: 10.1016/j.applthermaleng.2016.07.037.

[46] N. Duić, G. Krajačić, and M. da Graça Carvalho, "RenewIslands methodology for sustainable energy and resource planning for islands," *Renew. Sustain. Energy Rev.*, vol. 12, no. 4, pp. 1032–1062, May 2008, doi: 10.1016/j.rser.2006.10.015.

[47] A. Pfeifer, V. Dobravec, L. Pavlinek, G. Krajačić, and N. Duić, "Integration of renewable energy and demand response technologies in interconnected energy

systems," *Energy*, vol. 161, pp. 447–455, Oct. 2018, doi: 10.1016/j.energy.2018.07.134.

[48] H. Dorotić, B. Doračić, V. Dobravec, T. Pukšec, G. Krajačić, and N. Duić, "Integration of transport and energy sectors in island communities with 100% intermittent renewable energy sources," *Renew. Sustain. Energy Rev.*, vol. 99, pp. 109–124, Jan. 2019, doi: 10.1016/j.rser.2018.09.033.

[49] D. Dominković, G. Stark, B.-M. Hodge, and A. Pedersen, "Integrated Energy Planning with a High Share of Variable Renewable Energy Sources for a Caribbean Island," *Energies*, vol. 11, no. 9, p. 2193, Aug. 2018, doi: 10.3390/en11092193.

[50] H. Kariman, A. Shafieian, and M. Khiadani, "Small scale desalination technologies: A comprehensive review," *Desalination*, vol. 567, p. 116985, Dec. 2023, doi: 10.1016/j.desal.2023.116985.

[51] M. A. Abdelkareem, M. El Haj Assad, E. T. Sayed, and B. Soudan, "Recent progress in the use of renewable energy sources to power water desalination plants," *Desalination*, vol. 435, pp. 97–113, Jun. 2018, doi: 10.1016/j.desal.2017.11.018.

[52] F. E. Ahmed, A. Khalil, and N. Hilal, "Emerging desalination technologies: Current status, challenges and future trends," *Desalination*, vol. 517, p. 115183, Dec. 2021, doi: 10.1016/j.desal.2021.115183.

[53] Z. M. Ghazi, S. W. F. Rizvi, W. M. Shahid, A. M. Abdulhameed, H. Saleem, and S. J. Zaidi, "An overview of water desalination systems integrated with renewable energy sources," *Desalination*, vol. 542, p. 116063, Nov. 2022, doi: 10.1016/j.desal.2022.116063.

[54] J. Bundschuh, M. Kaczmarczyk, N. Ghaffour, and B. Tomaszewska, "State-of-the-art of renewable energy sources used in water desalination: Present and future prospects," *Desalination*, vol. 508, p. 115035, Jul. 2021, doi: 10.1016/j.desal.2021.115035.

[55] I. Nurjanah, T.-T. Chang, S.-J. You, C.-Y. Huang, and W.-Y. Sean, "Reverse osmosis integrated with renewable energy as sustainable technology: A review," *Desalination*, vol. 581, p. 117590, Jul. 2024, doi: 10.1016/j.desal.2024.117590.

[56] I. D. Spyrou and J. S. Anagnostopoulos, "Design study of a stand-alone desalination

system powered by renewable energy sources and a pumped storage unit," *Desalination*, vol. 257, no. 1–3, pp. 137–149, Jul. 2010, doi: 10.1016/j.desal.2010.02.033.

[57] E. Rosales-Asensio, A.-E. Rosales, and A. Colmenar-Santos, "Surrogate optimization of coupled energy sources in a desalination microgrid based on solar PV and wind energy," *Desalination*, vol. 500, p. 114882, Mar. 2021, doi: 10.1016/j.desal.2020.114882.

[58] H. Mehrjerdi, "Modeling and optimization of an island water-energy nexus powered by a hybrid solar-wind renewable system," *Energy*, vol. 197, p. 117217, Apr. 2020, doi: 10.1016/j.energy.2020.117217.

[59] P. Cabrera, J. A. Carta, C. Matos, and H. Lund, "Lessons learned in wind-driven desalination systems in the Canary Islands: Useful knowledge for other world islands," *Desalination*, vol. 583, p. 117697, Aug. 2024, doi: 10.1016/j.desal.2024.117697.

[60] E. J. Okampo and N. I. Nwulu, "Optimal energy mix for a reverse osmosis desalination unit considering demand response," *J. Eng. Des. Technol.*, vol. 18, no. 5, pp. 1287–1303, Apr. 2020, doi: 10.1108/JEDT-01-2020-0025.

[61] W. He, G. Huang, and C. N. Markides, "Synergies and potential of hybrid solar photovoltaic-thermal desalination technologies," *Desalination*, vol. 552, p. 116424, Apr. 2023, doi: 10.1016/j.desal.2023.116424.

[62] F. E. Ahmed, R. Hashaikeh, A. Diabat, and N. Hilal, "Mathematical and optimization modelling in desalination: State-of-the-art and future direction," *Desalination*, vol. 469, p. 114092, Nov. 2019, doi: 10.1016/j.desal.2019.114092.

[63] E. J. Okampo and N. Nwulu, "Optimisation of renewable energy powered reverse osmosis desalination systems: A state-of-the-art review," *Renew. Sustain. Energy Rev.*, vol. 140, p. 110712, Apr. 2021, doi: 10.1016/j.rser.2021.110712.

[64] A. Maleki, "Design and optimization of autonomous solar-wind-reverse osmosis desalination systems coupling battery and hydrogen energy storage by an improved bee algorithm," *Desalination*, vol. 435, pp. 221–234, Jun. 2018, doi: 10.1016/j.desal.2017.05.034.

[65] A. Maleki, M. G. Khajeh, and M. A. Rosen, “Weather forecasting for optimization of a hybrid solar-wind–powered reverse osmosis water desalination system using a novel optimizer approach,” *Energy*, vol. 114, pp. 1120–1134, Nov. 2016, doi: 10.1016/j.energy.2016.06.134.

[66] W. Peng, A. Maleki, M. A. Rosen, and P. Azarikhah, “Optimization of a hybrid system for solar-wind-based water desalination by reverse osmosis: Comparison of approaches,” *Desalination*, vol. 442, pp. 16–31, Sep. 2018, doi: 10.1016/j.desal.2018.03.021.

[67] H. Meschede, “Increased utilisation of renewable energies through demand response in the water supply sector – A case study,” *Energy*, vol. 175, pp. 810–817, May 2019, doi: 10.1016/j.energy.2019.03.137.

[68] H. Mehrjerdi, “Modeling and integration of water desalination units in thermal unit commitment considering energy and water storage,” *Desalination*, vol. 483, p. 114411, Jun. 2020, doi: 10.1016/j.desal.2020.114411.

[69] D. Groppi, A. Pfeifer, D. A. Garcia, G. Krajačić, and N. Duić, “A review on energy storage and demand side management solutions in smart energy islands,” *Renew. Sustain. Energy Rev.*, vol. 135, p. 110183, Jan. 2021, doi: 10.1016/j.rser.2020.110183.

[70] A. Sanna, B. Buchspies, M. Ernst, and M. Kaltschmitt, “Decentralized brackish water reverse osmosis desalination plant based on PV and pumped storage - Technical analysis,” *Desalination*, vol. 516, p. 115232, Nov. 2021, doi: 10.1016/j.desal.2021.115232.

[71] A. H. Ba-Alawi, H.-T. Nguyen, and C. Yoo, “Sustainable design of a solar/wind-powered reverse osmosis system with cooperative demand-side water management: A coordinated sizing approach with a fuzzy decision-making model,” *Energy Convers. Manag.*, vol. 295, p. 117624, Nov. 2023, doi: 10.1016/j.enconman.2023.117624.

[72] T. A. Ajiwiguna, G.-R. Lee, B.-J. Lim, S.-H. Cho, and C.-D. Park, “Optimization of battery-less PV-RO system with seasonal water storage tank,” *Desalination*, vol. 503, p. 114934, May 2021, doi: 10.1016/j.desal.2021.114934.

[73] M. Mimica, D. F. Dominković, T. Capuder, and G. Krajačić, “On the value and potential of demand response in the smart island archipelago,” *Renew. Energy*, vol.

176, pp. 153–168, Oct. 2021, doi: 10.1016/j.renene.2021.05.043.

[74] Y. Kunczynski and B. Burger, “Demand Response Desalination - A multi-module approach to reverse osmosis desalination offering a flexible energy demand.” [Online]. Available: http://renewabledesalination.com/wp-content/uploads/2015/06/Demand-Response-Desalination.pdf

[75] M. T. Mito, X. Ma, H. Albuflasa, and P. A. Davies, “Reverse osmosis (RO) membrane desalination driven by wind and solar photovoltaic (PV) energy: State of the art and challenges for large-scale implementation,” *Renew. Sustain. Energy Rev.*, vol. 112, pp. 669–685, Sep. 2019, doi: 10.1016/j.rser.2019.06.008.

[76] P. Triantafyllou *et al.*, “Optimum green energy solution to address the remote islands’ water-energy nexus: the case study of Nisyros island,” *Heliyon*, vol. 7, no. 9, p. e07838, Sep. 2021, doi: 10.1016/j.heliyon.2021.e07838.

[77] G. Kyriakarakos, A. I. Dounis, S. Rozakis, K. G. Arvanitis, and G. Papadakis, “Polygeneration microgrids: A viable solution in remote areas for supplying power, potable water and hydrogen as transportation fuel,” *Appl. Energy*, vol. 88, no. 12, pp. 4517–4526, Dec. 2011, doi: 10.1016/j.apenergy.2011.05.038.

[78] A. Stoppato, G. Cavazzini, G. Ardizzon, and A. Rossetti, “A PSO (particle swarm optimization)-based model for the optimal management of a small PV(Photovoltaic)-pump hydro energy storage in a rural dry area,” *Energy*, vol. 76, pp. 168–174, Nov. 2014, doi: 10.1016/j.energy.2014.06.004.

[79] D. P. Clarke, Y. M. Al-Abdeli, and G. Kothapalli, “Multi-objective optimisation of renewable hybrid energy systems with desalination,” *Energy*, vol. 88, pp. 457–468, Aug. 2015, doi: 10.1016/j.energy.2015.05.065.

[80] F. Moazeni, J. Khazaei, and J. P. Pera Mendes, “Maximizing energy efficiency of islanded micro water-energy nexus using co-optimization of water demand and energy consumption,” *Appl. Energy*, vol. 266, p. 114863, May 2020, doi: 10.1016/j.apenergy.2020.114863.

[81] A. Valencia-Díaz, E. M. Toro, and R. A. Hincapié, “Optimal planning and management of the energy–water–carbon nexus in hybrid AC/DC microgrids for sustainable development of remote communities,” *Appl. Energy*, vol. 377, p. 124517,

Jan. 2025, doi: 10.1016/j.apenergy.2024.124517.

[82] Y. Huang, P. Li, W. Wang, and L. Dong, “Capacity Optimization of Battery Energy Storage System in Multi-energy Complementary System Based on Time Series Simulation Method,” in *2019 IEEE Innovative Smart Grid Technologies - Asia (ISGT Asia)*, IEEE, May 2019, pp. 3804–3809. doi: 10.1109/ISGT-Asia.2019.8881502.

[83] P. Li, Y. Huang, W. Qi, and J. Gan, “Capacity Co-Optimization of Thermal and Battery Energy Storage System in Multi-energy Complementary System,” in *2019 IEEE Innovative Smart Grid Technologies - Asia (ISGT Asia)*, IEEE, May 2019, pp. 3815–3819. doi: 10.1109/ISGT-Asia.2019.8881407.

[84] M. R. Jannesar, A. Sedighi, M. Savaghebi, and J. M. Guerrero, “Optimal placement, sizing, and daily charge/discharge of battery energy storage in low voltage distribution network with high photovoltaic penetration,” *Appl. Energy*, vol. 226, pp. 957–966, Sep. 2018, doi: 10.1016/j.apenergy.2018.06.036.

[85] M. Sedghi, A. Ahmadian, and M. Aliakbar-Golkar, “Optimal Storage Planning in Active Distribution Network Considering Uncertainty of Wind Power Distributed Generation,” *IEEE Trans. Power Syst.*, vol. 31, no. 1, pp. 304–316, Jan. 2016, doi: 10.1109/TPWRS.2015.2404533.

[86] E. Grover-Silva, R. Girard, and G. Kariniotakis, “Optimal sizing and placement of distribution grid connected battery systems through an SOCP optimal power flow algorithm,” *Appl. Energy*, vol. 219, pp. 385–393, Jun. 2018, doi: 10.1016/j.apenergy.2017.09.008.

[87] Z. Liu, W. Zheng, J. Yuan, B. Zhang, B. Lv, and J. Sun, “Optimal Configuration of Island Water-Energy Nexus Systems Considering Multistage Desalination,” in *2024 9th Asia Conference on Power and Electrical Engineering (ACPEE)*, IEEE, Apr. 2024, pp. 278–283. doi: 10.1109/ACPEE60788.2024.10532570.

[88] M. Smaoui, A. Abdelkafi, and L. Krichen, “Optimal sizing of stand-alone photovoltaic/wind/hydrogen hybrid system supplying a desalination unit,” *Sol. Energy*, vol. 120, pp. 263–276, Oct. 2015, doi: 10.1016/j.solener.2015.07.032.

[89] A. M. Bilton and L. C. Kelley, “Design of power systems for reverse osmosis desalination in remote communities,” *Desalin. Water Treat.*, vol. 55, no. 10, pp. 2868–

2883, Aug. 2015, doi: 10.1080/19443994.2014.940641.

[90] Z. Wang, F. Wu, Y. Li, J. Li, Y. Liu, and W. Liu, “Day-ahead dispatch approach for cascaded hydropower-photovoltaic complementary system based on two-stage robust optimization,” *Energy*, vol. 265, p. 126145, Feb. 2023, doi: 10.1016/j.energy.2022.126145.

[91] Z. Wang, Y. Li, F. Wu, J. Wu, L. Shi, and K. Lin, “Multi-objective day-ahead scheduling of cascade hydropower-photovoltaic complementary system with pumping installation,” *Energy*, vol. 290, p. 130258, Mar. 2024, doi: 10.1016/j.energy.2024.130258.

[92] G. Micheli, M. T. Vespucci, M. Stabile, C. Puglisi, and A. Ramos, “A two-stage stochastic MILP model for generation and transmission expansion planning with high shares of renewables,” *Energy Syst.*, vol. 14, no. 3, pp. 663–705, Aug. 2023, doi: 10.1007/s12667-020-00404-w.

[93] M. He, S. Han, Y. Gao, Z. Zhao, D. Chen, and M. Deng, “Exploring the impact of three representative pumped storage retrofits on the economic-technical-energy efficiency of cascaded hydropower-VRE hybrid systems,” *Energy Convers. Manag.*, vol. 322, p. 119107, Dec. 2024, doi: 10.1016/j.enconman.2024.119107.

[94] O. J. Guerra, D. A. Tejada, and G. V. Reklaitis, “Climate change impacts and adaptation strategies for a hydro-dominated power system via stochastic optimization,” *Appl. Energy*, vol. 233–234, pp. 584–598, Jan. 2019, doi: 10.1016/j.apenergy.2018.10.045.

[95] W. Liu *et al.*, “Two-stage stochastic multi-criteria group decision making for wind-photovoltaic-hydropower scheduling,” *Energy Reports*, vol. 12, pp. 3732–3742, Dec. 2024, doi: 10.1016/j.egyr.2024.09.068.

[96] M. Daneshvar, B. Mohammadi-Ivatloo, K. Zare, and S. Asadi, “Two-stage stochastic programming model for optimal scheduling of the wind-thermal-hydropower-pumped storage system considering the flexibility assessment,” *Energy*, vol. 193, p. 116657, Feb. 2020, doi: 10.1016/j.energy.2019.116657.

[97] N. Lu, C. Su, C. Guo, P. Wang, H. Wu, and Q. Sui, “Stochastic optimal scheduling of wind power and pumped-storage hydropower complementary systems with multiple

uncertainties," *J. Energy Storage*, vol. 78, p. 110060, Feb. 2024, doi: 10.1016/j.est.2023.110060.

[98] Y. Shi, H. Wang, C. Li, M. Negnevitsky, and X. Wang, "Stochastic optimization of system configurations and operation of hybrid cascade hydro-wind-photovoltaic with battery for uncertain medium- and long-term load growth," *Appl. Energy*, vol. 364, p. 123127, Jun. 2024, doi: 10.1016/j.apenergy.2024.123127.

[99] D. Fernández-Muñoz, J. I. Pérez-Díaz, and M. Chazarra, "A two-stage stochastic optimisation model for the water value calculation in a hybrid diesel/wind/pumped-storage power system," *IET Renew. Power Gener.*, vol. 13, no. 12, pp. 2156–2165, Sep. 2019, doi: 10.1049/iet-rpg.2018.6151.

[100] R. J. Mahfoud, N. F. Alkayem, Y. Zhang, Y. Zheng, Y. Sun, and H. H. Alhelou, "Optimal operation of pumped hydro storage-based energy systems: A compendium of current challenges and future perspectives," *Renew. Sustain. Energy Rev.*, vol. 178, p. 113267, May 2023, doi: 10.1016/j.rser.2023.113267.

[101] P. Toufani, E. C. Karakoyun, E. Nadar, O. B. Fosso, and A. S. Kocaman, "Optimization of pumped hydro energy storage systems under uncertainty: A review," *J. Energy Storage*, vol. 73, p. 109306, Dec. 2023, doi: 10.1016/j.est.2023.109306.

[102] F. Guo, J. Gao, H. Men, Y. Fan, and H. Liu, "Large-scale group decision-making framework for the site selection of integrated floating photovoltaic-pumped storage power system," *J. Energy Storage*, vol. 43, p. 103125, Nov. 2021, doi: 10.1016/j.est.2021.103125.

[103] M. Temiz and I. Dincer, "Design and analysis of a floating photovoltaic based energy system with underground energy storage options for remote communities," *J. Energy Storage*, vol. 55, p. 105733, Nov. 2022, doi: 10.1016/j.est.2022.105733.

[104] F. Mansour, M. Al-Hindi, M. A. Najm, and A. Yassine, "Multi-objective optimization for comprehensive water, energy, food nexus modeling," *Sustain. Prod. Consum.*, vol. 38, pp. 295–311, Jun. 2023, doi: 10.1016/j.spc.2023.04.013.

[105] L. A. Mendes, M. T. L. de Barros, R. C. Zambon, and W. W.-G. Yeh, "Trade-Off Analysis among Multiple Water Uses in a Hydropower System: Case of São Francisco River Basin, Brazil," *J. Water Resour. Plan. Manag.*, vol. 141, no. 10, Oct. 2015, doi:

10.1061/(ASCE)WR.1943-5452.0000527.

[106] M. Di Martino, P. Linke, and E. N. Pistikopoulos, “Overcoming modeling and computational complexity challenges in food–energy–water nexus optimization,” *Comput. Chem. Eng.*, vol. 192, p. 108902, Jan. 2025, doi: 10.1016/j.compchemeng.2024.108902.

[107] M. Sánchez Diéguez, A. Fattahi, J. Sijm, G. Morales España, and A. Faaij, “Modelling of decarbonisation transition in national integrated energy system with hourly operational resolution,” *Adv. Appl. Energy*, vol. 3, p. 100043, Aug. 2021, doi: 10.1016/j.adapen.2021.100043.

[108] T. H. Ruggles *et al.*, “Planning reliable wind- and solar-based electricity systems,” *Adv. Appl. Energy*, vol. 15, p. 100185, Sep. 2024, doi: 10.1016/j.adapen.2024.100185.

[109] T. Khosrojerdi, S. H. Moosavirad, S. Ariafar, and M. Ghaeini-Hessaroeyeh, “Optimal Allocation of Water Resources Using a Two-Stage Stochastic Programming Method with Interval and Fuzzy Parameters,” *Nat. Resour. Res.*, vol. 28, no. 3, pp. 1107–1124, Jul. 2019, doi: 10.1007/s11053-018-9440-1.

[110] X. X. Ma, J. W. Zhang, L. Yu, Y. R. Fan, and J. P. Zhang, “An interval joint-probabilistic stochastic flexible programming method for planning municipal-scale energy-water nexus system under uncertainty,” *Energy Convers. Manag.*, vol. 208, p. 112576, Mar. 2020, doi: 10.1016/j.enconman.2020.112576.

[111] N. Zhao and F. You, “New York State’s 100% renewable electricity transition planning under uncertainty using a data-driven multistage adaptive robust optimization approach with machine-learning,” *Adv. Appl. Energy*, vol. 2, p. 100019, May 2021, doi: 10.1016/j.adapen.2021.100019.

[112] B. Xu *et al.*, “Analysis of a Stochastic Programming Model for Optimal Hydropower System Operation under a Deregulated Electricity Market by Considering Forecasting Uncertainty,” *Water*, vol. 10, no. 7, p. 885, Jul. 2018, doi: 10.3390/w10070885.

[113] E. Demir and E. Alp, “A framework for assessing the circular economy potential in the water and agriculture sectors in Türkiye through the water-energy-food-ecosystem nexus,” *Sustain. Prod. Consum.*, vol. 54, pp. 335–347, Mar. 2025, doi: 10.1016/j.spc.2025.01.009.

[114] P. D. Dabhade and D. G. Regulwar, “Multi-Reservoir Optimization for Maximization of Releases for Hydropower Generation Considering Environmental Flow,” *J. Water Resour. Prot.*, vol. 13, no. 12, pp. 931–944, 2021, doi: 10.4236/jwarp.2021.1312050.

[115] W. D. Vichete, A. V. Méllo Júnior, and G. A. dos S. Soares, “A Water Allocation Model for Multiple Uses Based on a Proposed Hydro-Economic Method,” *Water*, vol. 15, no. 6, p. 1170, Mar. 2023, doi: 10.3390/w15061170.

[116] D. Peña-Torres, M. Boix, and L. Montastruc, “Optimization approaches to design water-energy-food nexus: A litterature review,” *Comput. Chem. Eng.*, vol. 167, p. 108025, Nov. 2022, doi: 10.1016/j.compchemeng.2022.108025.

[117] X. G. Sánchez-Zarco and J. M. Ponce-Ortega, “Water-energy-food-ecosystem nexus: An optimization approach incorporating life cycle, security and sustainability assessment,” *J. Clean. Prod.*, vol. 414, p. 137534, Aug. 2023, doi: 10.1016/j.jclepro.2023.137534.

[118] W. Finch, J and L. Hall,R, “Estimation of Open Water Evaporation,” 2001. [Online]. Available: https://assets.publishing.service.gov.uk/media/5a7b90d4e5274a7202e17ff6/sw6-043-tr-e-e.pdf

[119] J. Finch and A. Calver, “Methods for the quantification of evaporation from lakes,” 2008. [Online]. Available: https://nora.nerc.ac.uk/id/eprint/14359/1/wmoevap_271008.pdf

[120] B. Gallego-Elvira, A. Baille, B. Martín-Gorriz, J. F. Maestre-Valero, and V. Martínez-Alvarez, “Evaluation of evaporation estimation methods for a covered reservoir in a semi-arid climate (south-eastern Spain),” *J. Hydrol.*, vol. 458–459, pp. 59–67, Aug. 2012, doi: 10.1016/j.jhydrol.2012.06.035.

[121] A. Pérez, O. Lagos, M. Lillo-Saavedra, C. Souto, J. Paredes, and J. L. Arumí, “Mountain Lake Evaporation: A Comparative Study between Hourly Estimations Models and In Situ Measurements,” *Water*, vol. 12, no. 9, p. 2648, Sep. 2020, doi: 10.3390/w12092648.

[122] G. Allen, Richard, S. Pereira, Luis, D. Raes, and M. Smith, *Crop evapotranspiration-Guidelines for computing crop water requirements-FAO Irrigation and drainage paper*

56. 1998. [Online]. Available: https://www.researchgate.net/publication/235704197_Crop_evapotranspiration-Guidelines_for_computing_crop_water_requirements-FAO_Irrigation_and_drainage_paper_56

[123] I. P. Craig, "Comparison of precise water depth measurements on agricultural storages with open water evaporation estimates," *Agric. Water Manag.*, vol. 85, no. 1–2, pp. 193–200, Sep. 2006, doi: 10.1016/j.agwat.2006.04.010.

[124] M. O. FARUQ, S. A. TURASH, N. FATTAH, and I. K. NAHID, "ESTIMATION OF CROP WATER REQUIREMENT FOR BORO RICE IN BANDARBAN, BANGLADESH BASED ON CROPWAT 8.0 MODEL," *Asian J. Plant Soil Sci.*, vol. 6, no. 1, pp. 31–38, Aug. 2021, doi: 10.56557/ajopss/2021/v6i147.

[125] L. S. Pereira, P. Paredes, D. J. Hunsaker, R. López-Urrea, and N. Jovanovic, "Updates and advances to the FAO56 crop water requirements method," *Agric. Water Manag.*, vol. 248, p. 106697, Apr. 2021, doi: 10.1016/j.agwat.2020.106697.

[126] N. Katerji and G. Rana, "FAO-56 methodology for determining water requirement of irrigated crops: critical examination of the concepts, alternative proposals and validation in Mediterranean region," *Theor. Appl. Climatol.*, vol. 116, no. 3–4, pp. 515–536, May 2014, doi: 10.1007/s00704-013-0972-3.

[127] A. Muratoglu, G. K. Bilgen, I. Angin, and S. Kodal, "Performance analyses of effective rainfall estimation methods for accurate quantification of agricultural water footprint," *Water Res.*, vol. 238, p. 120011, Jun. 2023, doi: 10.1016/j.watres.2023.120011.

[128] Energetski institut Hrvoje Požar, "Analiza sektora toplinarstva i iskorištavanja potencijala geotermalnih izvora na području Urbane aglomeracije Zagreb," 2017.

[129] HEP Proizvodnja, "TE TO Zagreb - Technical Data."

[130] EKONERG – Institut za energetiku i zaštitu okoliša d.o.o, "NETEHNIČKI SAŽETAK - ZAMJENA BLOKA "A" NOVOM KOMBI KOGENERACIJSKOM ELEKTRANOM U EL-TO ZAGREB," 2017. [Online]. Available: http://www.hep.hr/UserDocsImages/projekti/kke-zg/NTS_2017_HRV_FINAL.pdf

[131] Croatian Bureau of Statistics, "Croatia 2021 Census," 2022. [Online]. Available:

https://podaci.dzs.hr/media/ixpn5qzo/si-1711-popis-stanovnistva-kucanstava-i-stanova-2021-prvi-rezultati-po-naseljima.pdf

[132] Croatian Meteorological and Hydrological Service, “Weather data - Unije island.” https://meteo.hr/klima.php?section=klima_podaci&param=k1&Grad=mali_losinj

[133] M. Wirtz, P. Remmen, and D. Müller, “EHDO: A free and open-source webtool for designing and optimizing multi-energy systems based on MILP,” *Comput. Appl. Eng. Educ.*, vol. 29, no. 5, pp. 983–993, Sep. 2021, doi: 10.1002/cae.22352.

[134] Elektroprojekt d.d., “PSHP Velebit,” 2014. [Online]. Available: https://hro-cigre.hr/wp-content/uploads/2020/04/RHE_Velebit_v2.pdf

[135] Opcina Lovinac, “Lov i ribolov na području općine Lovinac.” https://www.lovinac.hr/page/lov-i-ribolov-na-podrucju-opcine-lovinac

[136] Hrvatske Vode, “Hrvatske Vode.” https://www.voda.hr/hr

[137] Zadar Vodovod d.o.o., “Zadar Vodovod d.o.o.” https://www.vodovod-zadar.hr/

[138] D. Segarić *et al.*, “PROGRAM RURALNOG RAZVOJA ZADARSKE ŽUPANIJE,” 2012. [Online]. Available: https://www.zadra.hr/images/dokumenti/izradeni_strateski_dokunmenti/9.pdf

[139] D. Romić, “PLAN NAVODNJAVANJA ZA PODRUČJE ZADARSKE ŽUPANIJE,” 2006. [Online]. Available: https://www.voda.hr/sites/default/files/2022-05/plan_navodnjavanja_za_podrucje_zadarska_zupanije.pdf

[140] CROPEX, “Croatian Power Exchange.” https://www.cropex.hr/en/

[141] Trading Economics, “ETS - EU Carbon Permits.” https://tradingeconomics.com/commodity/carbon

[142] V. Ramasamy, D. Feldman, J. Desai, and R. Margolis, “U.S. Solar Photovoltaic System and Energy Storage Cost Benchmarks: Q1 2021,” 2021. [Online]. Available: https://docs.nrel.gov/docs/fy22osti/80694.pdf

6 CURRICULUM VITAE

Goran Stunjek was born on 4 October 1994 in Zagreb, Croatia. He completed primary and secondary education in Zagreb. In 2013 year, he enrolled at the Faculty of Mechanical Engineering and Naval Architecture, University of Zagreb, where he developed a strong interest in energy systems and sustainability. He obtained his Bachelor's degree in Energy Engineering in 2017 with summa cum laude honours, defending a thesis entitled "*Solar thermal power plant operation with different thermal storages*". During his undergraduate studies, he consistently ranked among the top students of his generation and received several institutional and national awards, including the Davorin Bazjanac Award for Excellence and the Faculty Medal for Outstanding Achievement.

Continuing his academic path at the same Faculty, he completed his Master's degree in 2019, again with summa cum laude honours. His Master's thesis, "*Applying the Dispa-SET model to the analysis of the water-power nexus in the Western Balkan and neighbouring countries*", combined optimisation techniques with regional water-energy interaction analysis, which laid the foundation for his later research work. During his graduate studies, he was awarded numerous scholarships and distinctions, including those from the City of Zagreb, the Croatian Energy Association (Hrvoje Požar Foundation), and the Faculty of Mechanical Engineering and Naval Architecture. He also received the Annual Award of Croatian Water for the best Master's thesis related to water management and the Medal for Outstanding Achievement at Graduate Level.

In October 2019, Goran Stunjek enrolled in the doctoral programme at the Faculty of Mechanical Engineering and Naval Architecture under the supervision of Professor Goran Krajačić. He defended his doctoral thesis topic in January 2021 titled "*Modeling the optimal water-energy nexus to maximize social welfare under uncertainty of climate change forecasting and market prices*" and has since been employed as a Research and Project Assistant at the Department of Energy, Power and Environmental Engineering. His scientific focus lies in the optimisation and modelling of integrated water–energy systems within the broader Water-Energy-Food-Ecosystem (WEFE) nexus, with a particular emphasis on uncertainty modelling, stochastic optimisation, and multi-objective decision analysis. His work combines economic, environmental, and technical perspectives to support sustainable energy transition and climate-resilient infrastructure planning.

He has actively participated in several international and national research projects financed through the Horizon 2020 and Horizon Europe programmes, including KeepWarm, PHOENIX, INSULAE, META BUILD, INITIATE, and EMERGE. His role within these projects involved system modelling, optimisation analysis, and the preparation of new project proposals within EU frameworks. He has also been involved in the development of research tools for energy system modelling and leads the development of the optimisation tool GREENADVISE.

As part of his academic duties, Goran assisted in teaching undergraduate and graduate courses including "*Energy Systems 101*", "*Energy Economics*", and "*Energy Planning*". He has co-mentored 9 bachelor's and 8 master's theses, providing guidance in optimisation methods, data modelling, and energy system analysis. In addition, he contributes to the organisation of the SDEWES Conference series as a member of the local organising committee, facilitating the exchange of knowledge and collaboration among researchers in the field of sustainable development.

Goran Stunjek is the author or co-author of 7 scientific papers and reports and has presented his research at more than 10 international conferences. He serves as a peer reviewer for several leading international journals, including "*Energy*", "*Energy Conversion and Management*", "*Smart Energy*", "*Desalination*", and "*Energy Nexus*", and others.

List of publications:

- Stunjek, Goran; Krajačić, Goran; Stochastic Optimal Design and Operation of Floating Solar and Hydropower System for Integrated Water-Energy-Food-Ecosystem Planning//Energy Nexus, (2025), doi: 10.1016/j.nexus.2025.100570

- Stunjek, Goran; Krajačić, Goran; Optimisation of desalination-based water system with integrated renewable energy and storage within the water-energy nexus//Desalination, 600 (2025), 118474, 21. doi: 10.1016/j.desal.2024.118474

- Herc, Luka; Feijoo, Felipe; Kodba, Ana; Dorotić, Hrvoje; Stunjek, Goran; Beljan, Doris; Pukšec, Tomislav; Krajačić, Goran; Pfeifer, Antun; Duić, Neven, The management of an energy system in the realm of rapid energy transition and degasification as a consequence of energy crisis, examination in H2RES energy model // Energy conversion and management, 315 (2024), 118782, 49. doi: 10.1016/j.enconman.2024.118782

- Vidović, Vladimir; Krajačić, Goran; Matak, Nikola; Stunjek, Goran; Mimica, Marko, Review of the potentials for implementation of floating solar panels on lakes and water reservoirs // Renewable & sustainable energy reviews, 178 (2023), 113237, 22. doi: 10.1016/j.rser.2023.113237

- Stunjek, Goran ; Pfeifer, Antun ; Krajačić, Goran ; Duić, Neven, Analysis of the Water-Power Nexus of the Balkan Peninsula Power System // Springer Proceedings in Energy. Springer, 2020. str. 235-257. doi: 10.1007/978-3-030-55757-7_17

- Dominković, Dominik Franjo ; Stunjek, Goran ; Blanco, Ignacio ; Madsen, Henrik ; Krajačić, Goran, Technical, economic and environmental optimization of district heating expansion in an urban agglomeration // Energy (Oxford), 197 (2020), 117243, 10. doi: 10.1016/j.energy.2020.117243

7 SUMMARY OF PAPERS

PAPER 1

Dominković, Dominik Franjo; Stunjek, Goran; Blanco, Ignacio; Madsen, Henrik; Krajačić, Goran; Technical, economic and environmental optimization of district heating expansion in an urban agglomeration // Energy (Oxford), 197 (2020), 117243, 10. doi: 10.1016/j.energy.2020.117243

In order to integrate large shares of variable renewable energy sources, district heating can play an important role. Furthermore, in order to increase the efficiency of district heating systems, interconnecting adjacent system could be socio-economically justified. In order to assess the economic and environmental consequences of the latter, a mixed linear integer optimization model was developed with the endogenous decision on the potential interconnectors. The case study was carried out for the city of Zagreb, Croatia. The results showed that all three studied interconnections are economically viable, while the socio-economic cost was 29.2% lower in the case of the implemented interconnectors, all other capacities being equal. Moreover, the optimal thermal energy storage capacity was found to be equal to 25 and 24 days of average heating demand in two alternative scenarios. Finally, compared to the reference case, the CO_2 emissions could be lowered by 15.3%. CO_2 savings derive mainly from better utilization of low carbon capacities after interconnecting the systems, as well as from installation of heat pumps and electric boilers.

In this paper optimisation method was developed by Goran Stunjek and, Dominik Franjo Dominković. Ignacio Blanco, Henrik Madsen and Goran Krajačić reviewed the model and the results. The paper was written by Goran Stunjek and in reviewed by Dominik Franjo Dominković, and Goran Krajačić.

PAPER 2

Stunjek, Goran; Krajačić, Goran; Optimisation of desalination-based water system with integrated renewable energy and storage within the water-energy nexus // Desalination, 600 (2025), 118474, 21. doi: 10.1016/j.desal.2024.118474

This study presents a comprehensive optimization framework for integrated water and energy systems. It offers a novel implementation to determining the optimal dispatch of water and energy streams and sizing Battery Energy Storage (BES) and Renewable Energy Systems (RES). The proposed Mixed-Integer Linear Programming model integrates RES and BES with water systems through Reverse Osmosis desalination units and water storage supported by Power-to-Water technology. Unlike traditional models, the framework considers both BES capacity and power rating as variables while incorporating RES capacity optimization, water system modelling, and water storage integration. The integrated water-energy system model is particularly suited to addressing the unique challenges of smaller-scale island systems, often overlooked in larger-scale analyses. The methodology is applied to Unije Island, Croatia, characterized by significant seasonal demand fluctuations due to tourism. The results demonstrate the effectiveness of power-to-water and BES technology in increasing system flexibility and economic performance and provide a comprehensive analysis of the impact of varying RES and BES investment costs on optimal system configuration, and financial and economic outcomes. Lower RES investment costs lead to higher RES capacities, but the rate of change is significantly influenced by BES investment costs, highlighting the importance of an optimal RES-BES pair for maximizing financial and economic performance. Furthermore, the results emphasize that the highest financial and economic benefits are achieved not by maximizing both RES and storage capacities, but by finding an optimal balance between them, demonstrating the critical role of BES and water storage utilization in enhancing system efficiency. Change in specific parameters showed that grid electricity and PV potential effect final system profitability more than change in water demand defining two parameters as critical. Proposed study offers valuable insights into the optimization of water-energy systems on islands and other isolated regions, emphasizing the importance of integrated planning for sustainable development, and offering strategic insights for future infrastructure development.

Goran Stunjek: project administration, supervision, writing–review & editing, resources, validation, methodology, conceptualization, visualization, formal analysis

Goran Krajačić: funding acquisition, project administration, supervision, writing–review & editing, resources, validation.

PAPER 3

Stunjek, Goran; Krajačić, Goran; Stochastic Optimal Design and Operation of Floating Solar and Hydropower System for Integrated Water-Energy-Food-Ecosystem Planning // Energy Nexus, 20 (2025), 100570, 21. doi: 10.1016/j.nexus.2025.100570

This study presents a high-resolution, two-stage stochastic optimisation framework for the configuration and operation of a hybrid floating photovoltaic (FPV) and pumped-storage hydropower (PSH) system. The model captures interdependencies among sectors through progressive optimisation perspectives, including energy-only (E), water-energy (WE), water-energy-food (WEF), and water-energy-food-ecosystem (WEFE), each expanding the system boundary and revealing cross-sectoral trade-offs. Methodological innovations include endogenising evaporation losses within the optimisation dynamically linked to FPV deployment, optimising agricultural area as decision variable, and embedding ecosystem values such as avoided CO_2 emissions, land-use savings, and biodiversity costs directly into the optimisation objective. Uncertainty is addressed through Monte Carlo-based hourly scenario generation, while a layered objective function systematically expands system integration. Results show that broader perspectives substantially shift optimal FPV capacity and hydropower dispatch, while enhancing the economic viability of hybrid configurations. In the WE case, evaporation savings drive larger FPV deployment and increase PSH output by over 11% on average, while integration of irrigation constraints in the WEF case highlights seasonal trade-offs and optimal irrigation areas. Incorporating ecosystem values in the WEFE case leads to maximum FPV deployment across wide cost ranges, with hydropower ramp rate reduced by 16.4%. CO_2-price sensitivity further confirms that higher carbon valuation widens the feasible deployment space, increasing FPV power by 15.84% on average. The framework advances WEFE-integrated planning by linking high-resolution sectoral interactions with ecosystem valuation, offering practical insights for resource-efficient, low-carbon systems that balance competing demands under uncertainty and support long-term sustainability goals.

Goran Stunjek: Writing – review & editing, Writing – original draft, Visualization, Validation, Software, Resources, Methodology, Investigation, Formal analysis, Data curation, Conceptualization.

Goran Krajačić: Writing – review & editing, Validation, Supervision, Project administration, Investigation, Funding acquisition, Conceptualization.

PAPER 4

Vidović, Vladimir; Krajačić, Goran; Matak, Nikola; Stunjek, Goran; Mimica, Marko, Review of the potentials for implementation of floating solar panels on lakes and water reservoirs // 178 (2023), 113237, 22. doi: 10.1016/j.rser.2023.113237

Many places are dealing with the problem of water scarcity, especially in the summer months. This occurs mostly in the dry areas with hot climates that are exposed to intensive solar insolation which are the main driver for the evaporation of water. Some companies that are in charge of water service, and are operating open water reservoirs, have developed a solution to cover the water with floating balls to limit the solar insolation and to mitigate the evaporation of water. Another good approach is using floating solar panels for the same cause, which will provide an additional power source. It can enhance the productivity of hydropower plants with reservoirs. An additional benefit of the solution is the amount of the available water surfaces for placing the solar panels, instead of potentially useful areas for other purposes (agriculture, buildings …). This paper reviews the current development of the technology, potentials, and best practices. It shows that this technology is feasible and can compete with other power sources, considering the cheapest LCOE being 46 USD/MWh for a 50 MW power plant in Uttar Pradesh, India.

Vladimir Vidović: Writing - Review & Editing, Resources, Validation, Conceptualization, Methodology

Goran Krajačić: Funding acquisition, Project administration, Supervision, Writing - Review & Editing, Resources, Validation, Conceptualization, Methodology

Nikola Matak: Project administration, Supervision, Writing - Review & Editing, Resources, Validation, Methodology,

Goran Stunjek: Visualization, Writing - Review & Editing, Resources,

Marko Mimica: Visualization, Writing - Review & Editing.

PAPER 1

"So it begins"

Théoden, King of Rohan

Energy 197 (2020) 117243

Contents lists available at ScienceDirect

Energy

journal homepage: www.elsevier.com/locate/energy

Technical, economic and environmental optimization of district heating expansion in an urban agglomeration

Dominik Franjo Dominković [a, *], Goran Stunjek [b], Ignacio Blanco [a], Henrik Madsen [a], Goran Krajačić [b]

[a] Technical University of Denmark, Department of Applied Mathematics and Computer Science, Denmark
[b] University of Zagreb, Faculty of Mechanical Engineering and Naval Architecture, Croatia

ARTICLE INFO

Article history:
Received 5 November 2019
Received in revised form
29 January 2020
Accepted 23 February 2020
Available online 24 February 2020

Keywords:
District heating expansion
Variable renewable energy
Capacity extension planning
Thermal energy storage
MILP programming
Interconnecting district heating systems

ABSTRACT

In order to integrate large shares of variable renewable energy sources, district heating can play an important role. Furthermore, in order to increase the efficiency of district heating systems, interconnecting adjacent system could be socio-economically justified. In order to assess the economic and environmental consequences of the latter, a mixed linear integer optimization model was developed with the endogenous decision on the potential interconnectors. The case study was carried out for the city of Zagreb, Croatia. The results showed that all three studied interconnections are economically viable, while the socio-economic cost was 29.2% lower in the case of the implemented interconnectors, all other capacities being equal. Moreover, the optimal thermal energy storage capacity was found to be equal to 25 and 24 days of average heating demand in two alternative scenarios. Finally, compared to the reference case, the CO_2 emissions could be lowered by 15.3%.CO_2 savings derive mainly from better utilization of low carbon capacities after interconnecting the systems, as well as from installation of heat pumps and electric boilers.

1. Introduction

Newly completed package Clean energy for all Europeans, presents an important step towards the implementation of the Energy Union strategy and it delivers to the Paris Agreement commitments for reducing greenhouse gas (GHG) emissions. In eight legislative acts, package addresses all 5 dimensions of the Energy Union: (*i*) energy security; (*ii*) international energy market; (*iii*) energy efficiency; (*iv*) decarbonisation of the economy; and (*v*) research, innovation and competitiveness. Increase in energy performance in buildings, 32% of renewable energy sources in EU's energy mix by 2030, building targets of at least 32.5% energy efficiency by 2030, robust governance system for the energy union and electricity market design are building elements of the Clean energy for all Europeans package [1].

Heating and cooling sector accounts for 50% of the EU's annual energy consumption. The largest primary energy source for heating and cooling is natural gas with 46% share, followed by coal, biomass and fuel oil with shares of 15, 11 and 10%, respectively. Renewable energy sources account for 18% of primary energy consumption, however, its potential is not even close to being fully utilized. Considering EU climate goals, heating and cooling demand is expected to fall by 42% by 2050 with a proportional reduction in CO_2 emissions. To achieve the latter mentioned, the EU identified actions in making the building renovations easier, increasing the share of renewables, higher use of waste heat from industry and involving consumers and industries. Mentioned actions were implemented in the first initiative in the EU that considered the energy used for heating and cooling in buildings and industry called Heating and Cooling Strategy[1] presented in February of 2016 by the European Commission. The strategy identifies actions that will transform heating and cooling sectors to smarter, more efficient and sustainable sector, while at the same time decreasing the energy imports, costs and CO_2 emissions. Mentioned actions are

* Corresponding author.
E-mail addresses: dodo@dtu.dk (D.F. Dominković), Goran.stunjek@fsb.hr (G. Stunjek), igbl@dtu.dk (I. Blanco), Hmad.dtu@gmail.com (H. Madsen), Goran.krajacic@fsb.hr (G. Krajačić).

[1] The EU strategy on heating and cooling, https://setis.ec.europa.eu/publications/setis-magazine/low-carbon-heating-cooling/eu-strategy-heating-and-cooling.

https://doi.org/10.1016/j.energy.2020.117243

Nomenclature

$C^{VO\&M}_{l,n,t}$ Variable operating and maintenance (O&M) cost of plant n in hour t at location l EUR/MWh_{heat}
$C^{fuel}_{l,n,t}$ The cost of fuel for plant n in hour t at location l EUR/MWh_{fuel}
C^{CO2}_{t} The cost of CO_2 emission in hour t EUR/ton_{CO2}
$K_{l,n}$ The CO_2 intensity of the plant n at location l ton_{CO2}/MWh_{heat}
$R^{ele}_{l,n,t}$ Revenues from electricity sales of plant n in hour t at location l EUR/MWh_{ele}
L_n Electricity-to-heat generation ratio of plant n MWh_{ele}/MWh_{heat}
$q_{l,n,t}\ \varepsilon\mathbb{R}+$ Heat power of plant n in hour t at location l MW_{heat}
$C^{cap}_{n,l}$ Annualized capacity cost of plant n at location l EUR/MW
$C^{FO\&M}_{n,l}$ Fixed O&M cost of plant n at location l EUR/MW
$C^{startup}_{l,n}$ Start-up cost of plant n at location l EUR
$q^{cap}_{n,l}$ The capacity of plant n at location l MW
$q^{minimum}_{n,l}\varepsilon\mathbb{R}+$ Minimum production of plant n at location l MW
$q^{cap,maximum}_{n,l}\varepsilon\mathbb{R}+$ The upper bound of generation capacity of plant n at location l MW
$q^{cap,\ maximum}_{conPipe,l}\varepsilon\mathbb{R}+$ The upper bound of the connecting pipe capacity at location l MW
$q^{cap,\ minimum}_{conPipe,l}\varepsilon\mathbb{R}+$ The lower bound of the connecting pipe capacity at location l MW
$q^{cap}_{conPipe,l}\varepsilon\mathbb{R}+$ The connecting pipe capacity at location l MW
$E_{l,t}$ District heating energy demand in hour t at location l MWh_{heat}
$s^{ch}_{l,t}\varepsilon\mathbb{R}+$ Heat charge of heat accumulator in hour t at location l MWh_{heat}
$s^{dis}_{l,t}\varepsilon\mathbb{R}+$ Heat discharge of heat accumulator in hour t at location l MWh_{heat}
$\eta_{st,n,l}$ Heat storage efficiency
$x_{n,l,t}\varepsilon\{0,1\}$ Binary variable: 1, if unit n in hour t is on, otherwise 0
$c_{n,l,t}\varepsilon\{0,1\}$ Start-up cost activation binary variable; 1 if the unit n in hour t was turned on, otherwise 0
$a_l\varepsilon\{0,1\}$ Binary variable (do invest, don't invest)
S_l Annualized sunk investment cost in the case of piping investment decision at location l EUR
H One hour (used for relating the energy generated (MWh) by using a certain power (MW) of the plant during the period of 1 h)
T A set of hours in a year
L A set of district heating locations
N A set of different energy plant generators

key actions incorporated in the Energy Union Framework Strategy[2] [2].

The basic idea of district heating (DH) is to use local waste heat sources in order to satisfy the local heating demand [3]. Traditional heat sources are combined heat and power, waste to heat and industrial plants. However, in the last decade, the higher share of renewable heat from biomass, geothermal wells and solar collectors was introduced in the DH system [4]. Smart energy system is the future energy system that challenges problems of integrating district heating with electricity sector and transport sector [5]. Smart energy systems can also integrate district cooling in the system [6]. Such a future system will be composed of smart district heating, electricity and gas networks which would be mutually coordinated to achieve an optimal solution for each sector and for the overall energy system [7]. List of studies mentioned in the review [5] concludes that district heating can, and will have an important role in the future energy systems, but they must undergo transition to low-temperature DH networks that will be part of the smart energy system. Hence, the needed transformation of the DH system can be defined under the term of 4th Generation District Heating Technologies and Systems (4GDH) [5]. As reviewed in Ref. [8], unlike the previous three generations, the 4GDH includes energy supply and conservation balancing, so the challenge of supplying more energy efficient buildings with space heating and domestic how water could be met. Moreover, the investments in reducing the district heating network losses should also be included, as well as the innovative and strategic integration of DH into the smart energy system [7]. Abilities needed for a future DH systems to be part of the smart energy system include: (*i*) supplying existing and newly built buildings with low-temperature DH; (*ii*) low grid losses; (*iii*) integration of renewable heat sources and utilization of recycle heat from low-temperature sources; (*iv*) participation in solving the problems of integrated fluctuating renewable energy sources; and (*v*) ensuring suitable planning and incentives for DH system operation, as well as strategic investment planning [8].

A study in Ref. [9] included design and operation analysis of eight efficient district heating markets in the EU. The study explored eight case studies from national policy frameworks to specific local business models to determine key factors that make them efficient, and to investigate if the best practices and business models could be transferred to the other Member States. The study has shown that district heating and cooling systems represent a powerful and cost-efficient measure to ensure the development of low-carbon and resilient local energy system. However, the study also concludes that there is no universal model to develop efficient DHC system, due to its distinctive architecture and reliance on the local dynamics. Hast et al. [10]. also adds to latter point concluding that it is not enough to perform country-level decision-making, since every municipality has its own local specific features. Therefore, case studies focusing on the municipality level are needed for a future development. Thus, case studies for several European countries have been tested.

This paper further investigates the impact of interconnecting geographically distributed district heating grids and expands methods used for the analysis of DH expansion in Sonderborg municipality [11]. Based on [3], proposed Sonderborg municipality interconnection represents tree-like structure in the development of district heating structures. Initially, district heating systems start in the form of a small tree-like structure, and by means of interconnections or expansion, it grows to ring-like structure, before it reaches the final fully meshed structure. Two main advantages of growth from tree to ring-like, or meshed structure are an increase in heat transfer capacity, and reduction of risk that large supply areas will not be served in case of major pipeline rupture [3]. Also, as addition to the previous research, impact of thermal energy

[2] The Energy Union Strategy, https://eur-lex.europa.eu/legal-content/EN/TXT/?uri=CELEX:52015DC0080.

storage placement is investigated, with a goal of lowering costs in a form of smaller pipe size for interconnection of multiple district heating networks. Thermal energy storage acts as buffer between heat demand and supply, and allows for maximization of DH system flexibility and performance, as well as utilizing the potential of connecting more buildings to existing system, which leads to decrease in operating costs and emissions [12]. Furthermore, the impact of interconnecting multiple DH networks and the use of thermal storage as a buffer to an operation of Combined Heat and Power (CHP) units was investigated. Proper thermal energy storage placement and design increases operating hours of a CHP unit, as well as allowing for a better management to shift production of electricity to hours when electricity price is higher [12]. Moreover, steam demand for industrial purposes has been added to a model and tested on a case study for a City of Zagreb and surrounding regions of Zagreb County.

Further three paragraphs describe the current state-of-the-art in the research on district heating. Two recent papers from Telebi B. et al. [13], and Sarbu I. and Mirza M [14]. provide extensive research on modelling and optimization of DH systems. In Ref. [13] authors provide a new approach in DH categorization including geographical variables, size of the DH system, DH heat density and consumer demand. The study also includes a research review of system and component modelling approaches, as well as a review of the state of the art in optimization-based. For each component in the DH system, the study provides equations and assumptions on how to model the whole DH system. Both, the deterministic and heuristic optimization solving techniques are reviewed, with deterministic methods being divided into complex, simplified and predictive models. Complex models include software such as Energy Plus[3] or TRNSYS[4] used for a building level modelling for a generation of consumer demand profile, but they are dependent on a quality of an input data and come with a high computational cost. Simplified models often use the assumption that simplifies building characteristics, while predictive models are used for demand profile generation using predictive methods such as Kalman filter or artificial intelligence methods [13]. Similarly to Ref. [13], authors in Ref. [14] divide optimization techniques into deterministic and heuristic, where heuristic techniques include genetic and evolutionary algorithms. Main advantages of heuristic approach are non-dependency on restrictive assumptions of the objective function and that results are not dependent on a initial values of the decision variables. However, this advantages come to a cost of a longer calculation times. Authors conclude that researchers generally take the approach of DH system optimizations under steady-state conditions using deterministic approaches, which generally don't guarantee a global optimal solution. However, recent research shows that researchers tend to use heuristic optimization techniques such as simulated annealing (SA), particle swarm (PSO) and ant colony optimization (ACO) [14].

Related to the modelling for the optimal configuration of the system, a number of researches have used deterministic or heuristic approaches. Sanaei S. M. and Nakata T. in Ref. [15] used generalised reduced gradient method (GRG) to calculate optimal choice of the system components solving minimum total cost equation. Boro D. et al. in Ref. [16] created mathematical mixed-integer linear programming (MILP) model that resulted in the optimal configuration and operation of the DH system. The objective function included total annual cost (TAC) and total CO_2 emissions. EnergyPLAN modelling tool and Matlab algorithms were developed to optimize the expansion of a district cooling system in the tropical region [17]. The authors in the latter case used a simulation tool for modelling the expansion of the district energy system. Haikarainen C. in Ref. [18] developed a model as a MILP problem for the optimization of a DH network, including the objective function made out of all construction and operation costs of new network components. Mertz T. et al. in Ref. [19] created a model described as mixed-integer nonlinear programming (MINLP) problem that optimized configuration and design of the DH system using objective function summed up of investment costs and operational costs, and used GAMS[5] software to solve optimization problem. Li. L et al. in Ref. [20] created a multi-objective MILP model to optimize distributed energy sources (DER) with neighbouring DH network. Authors used Matlab[6] software for solving the objective function composed of the sum of TAC and CO_2 emissions. Delangle A. et al. in Ref. [21] developed a MILP model in GAMS and solved for optimal expansion of the existing DH system with the objective of maximising cost savings or minimising greenhouse gas emissions using CPLEX solver.

Regarding the modelling of the DH network, researchers used both the heuristic and deterministic approaches. Earlier research by Weber C. et al. [22] divided multiobjective optimization problem into two problems, optimizing based on the minimum costs and CO_2 emissions and for the optimal choice of the DH system such as new heat pumps and characteristics of the pipe dimensions and pipe water temperatures. Authors used multiobjective evolutionary algorithm for solving the objective functions. Craus M. et al. in Ref. [23] developed a hybrid genetic algorithm to solve for the optimal network extension taking into the account the most profitable consumers and using the constraints on optimal pipe path. Zeng J. et all in Ref. [24] used hourly substation demand to develop an optimization model for DH network. Authors used a genetic algorithm to solve the objective function composed of the total annual costs and using results for a real DH network determining the optimal diameter of pipes. Dobersek D. and Goricanec D. developed a new approach for the optimal DH network design using a simplex algorithm to solve objective function composed of a sum of capitalised costs [25]. Morvaj B. et al. created a MILP model that included a selection of optimal technologies, network design and optimal operating conditions to satisfy the demand for electric and thermal energy. Authors implemented the model in AIMMS[7] and used CPLEX solver to find the optimal solution for the objective function composed of total costs and CO_2 emissions [26]. Bordin C. et al. proposed a new methodology by using graph theory and MILP model, using objective function to maximise earnings of connecting new consumers to existing DH network, simultaneously minimising the operation costs of the DH network [27]. Dorotić H. et al. in Ref. [28] analysed benefits of integration of DH and cooling systems. Authors developed hourly based multiobjective optimization model capable of defining supply capacities and their operation on a one-year period. They conclude that integrated DH and cooling systems can operate with the same CO_2 emissions, but with a lower total discount cost. Vesterlund M. and Toffolo A. developed a multiobjective evolutionary algorithm for the minimisation of DH network expansion costs. Authors used the real case of the DH network expansion in the town of Kiruna. Results of the case study show that the optimal solution is compromise between investment costs for the new pipes and the new technologies, and operating costs in the DH network [29].

The mentioned paper rarely address the interconnection of already existing district heating systems. Furthermore, no

[3] Energy Plus - https://energyplus.net/.
[4] TRNSYS - http://www.trnsys.com/.
[5] GAMS - https://www.gams.com/.
[6] Matlab - https://www.mathworks.com/products/matlab.html.
[7] AIMMS - https://www.aimms.com/.

mentioned paper in this area considered steam production optimization, on top of heat and electricity generation considerations. Finally, models from the papers mentioned in the state-of-the-art analysis do not take into account the Not-in-my-backyard movement due to which people resist having nearby installed generators that have flue gases that can pollute the air. In order to fill the mentioned gaps, and to improve the current models that were used for calculating the feasibility of interconnections between different district heating systems, this paper brings three main novelties.

To sum up, the main novelties in this paper are:

(i) developed mixed-integer linear optimization model with endogenous decision-making on investments in interconnecting different district heating systems,
(ii) considering thermal energy storage at each of the potentially interconnected district heating systems in order to potentially reduce the needed diameter of the connecting piping
(iii) heat generation supply from the newly connected areas fulfilled only by heat with no emissions produced at the location, forestalling any potential air pollution sources

To investigate aforementioned impacts, the case study for a City of Zagreb and surrounding regions of Zagreb County, the city of Velika Gorica and Zaprešić was carried out. The aim is to show if the interconnection of the multiple district heating systems can result in fuel-saving and/or reduced CO_2 emissions, while simultaneously ensuring the economic competitiveness of the connecting energy system.

Subsequently to the introduction, a model description is presented in chapter 2, while the case study is described in chapter 3. In chapter 4 one can find results and discussion on case study for the City of Zagreb, followed by conclusion in chapter 5.

2. Methods

A linear mixed-integer programming approach was used to develop a model used in this paper. This model presents an improvement in the model developed in Ref. [11]. The main improvement deals with the connecting piping dimensioning, which is now automatically calculated by the model. Furthermore, investments in the connecting piping between different district heating systems were modelled as a mixed-integer problem now, with binary variables used for the options of having or not having the investment in the connection piping. Moreover, steam demand for industrial purposes is introduced into the model.

The predefined technologies in the model were gas combined heat and power plants, gas boilers, electric boilers, electric heat pumps, heat accumulators and ancillary steam boilers. The model allowed for capacity extension and/or building interconnectors between different district heating systems. Sector coupling between power and heat sectors was modelled via CHPs, heat pumps and electric boilers. Revenues from electricity sales of CHPs on a day-ahead power market was modelled as an income in the district heating system, represented as the term.

$R^{ele}_{l,n,t}$ in the objective function (1). Consequently, the total CO_2 emissions and fuel costs from CHPs was assigned to the district heating system, when calculating the costs of CO_2 emission allowances. Including electricity sales as revenue in the system avoided the need for complicated calculations of splitting the cost of fuel and CO2 emissions on the power and heat systems. Electricity needed to power the electric heat pumps and electric boilers were priced according to the day-ahead power prices, with additional transmission and distribution fees. Due to the combined production of electricity, heat and steam in CHP units, the coefficient that calculates the loss of electricity produced per each MWh of steam sold for industrial purposes, was used to account for the amount of electricity lost as an additional variable cost.

The objective function was set to minimize the total socio-economic costs of the system. It included the annualized investment cost, fixed and variable operating and maintenance costs (O&M), unit start-up costs, carbon and fuel costs, as well as the annualized sunk costs associated with the investment decision for building the piping connection (1).

$$minimize \sum_{l\in L}\sum_{n\in N}\sum_{t\in T}\left[\left(C^{VO\&M}_{l,n,t}+C^{fuel}_{l,n,t}+C^{CO2}_{t}K_{l,n}-R^{ele}_{l,n,t}L_n+c_{l,n,t}\cdot C^{startup}_{l,n}\right)q_{l,n,t}H+\left(C^{cap}_{l,n}+C^{FO\&M}_{l,n}\right)q^{cap}_{l,n}+a_l S_l\right],\ (\forall\, l\in L,\forall\, n\in N,\forall\, t\in T) \tag{1}$$

Where N represents a set of technologies installed at a location l, while T represents a time set (8760 h of a year). The case study developed for this paper had four different district heating locations.

Several different constraints were used in this model. The heat energy balance is represented by (2).

$$q_{n,t,l}H = E_{l,t}+s^{ch}_{l,t}-s^{dis}_{l,t}, \qquad (\forall\ t\in T,\ \forall\ n\in N,\ \forall\ l\in L), \tag{2}$$

Where $H = 1\ hour$. Hence, all the generators n located at a certain location l needed to generate enough heat to cover the total heat demand plus the additional demand for charging the heat accumulator minus the heat discharged from the heat accumulator.

The heat balance equation for heat accumulators is represented by (3).

$$s^{level}_{n,l,t}=s^{level}_{n,l,t-1}+s^{ch}_{n,l,t}-s^{dis}_{n,l,t}\Big/\eta_{st,n,l},\ (\forall\, n\in N,\forall\, l\in L,\forall\, t\in T) \tag{3}$$

The capacity of each plant needed to be sufficient to generate the heat in every hour of the year (4)

$$0\le q_{n,t,l}\le q^{cap}_{n,l}, \quad (\forall n\in N,\forall t\in T,\ \forall\ l\in L) \tag{4}$$

Units needed to produce within the minimum and maximum power (lower and upper bounds) [30]. The minimum power for CHP units, if turned on, was 20%, while for boilers the minimum production was 0.

$$q^{minimum}_{n,l}\cdot x_{n,l,t}\le q_{n,l,t}\le q^{cap,maximum}_{n,l}x_{n,l,t},\ (\forall n\in N,\ \forall\, l\in L,\forall t\in T) \tag{5}$$

Binary variable $c_{l,n,t}$ was activated if the plant n was just turned on in hour t (6).

$$c_{l,n,t}\ge x_{l,n,t}-x_{l,n,(t-1)},\ (\forall n\in N,\ \forall\ l\in L,\forall t\in T) \tag{6}$$

A maximum discharge (and charge) of the storage during 1 h

was constrained to 20% of the total storage capacity (5).

$$s_{l,t}^{dis} H \leq q_{storage,l}^{cap} \ , (\forall\ l \in L) \tag{7}$$

Investments in the connecting piping between different district heating systems were modelled with binary variables. More precisely, there was a sunk cost S_l associated with the investment as soon as the decision was made. Technically, the binary variables a_l were modelled as shown in (6).

$$q_{conPipe,l}^{cap,maximum} \cdot a_l \geq q_{conPipe,l}^{cap} \geq q_{conPipe,l}^{cap,minimum} \cdot a_l \ , \ (\forall\ l \in L, a \in \{0,1\}) \tag{8}$$

Capacities of connecting piping needed to be sufficient for the heat flow at every time point of the year (7).

$$q_{conPipe,l}^{cap} \geq q_{ConPipeFlow,t,l}, \quad (\forall t \in T,\ \forall\ l \in L) \tag{9}$$

The model described here was implemented in Python 3 with Gurobi solver. The optimization was run on a personal computer with Intel Core i7 4-core processor, 16 GB RAM and 500 GB SSD disc.

3. Case study

The City of Zagreb is the capital and the largest city of Croatia. The total city area is 641 km^2 with a population of 790,017, based on the last census from 2011 [31]. Heating for Zagreb district heating network is being produced in CHP units TE TO Zagreb and EL TO Zagreb. District heating network is divided into three hot water networks and two steam networks. Steam network is mostly being used for industrial purposes with its small part being utilized for space heating purposes. The total length of the Zagreb district heating network is 274.41 km, while the total installed heating power is equal to 1,349.23 MW$_h$. Zagreb district heating network is supplying around 100,000 customers [32]. Production units are gas-fired units with the possibility of using extra-light fuel oil as a replacement fuel [33].

TE TO Zagreb power plant has seven electricity/heat-producing units, and those can be observed in Table 3. Units K and L are combined cycle gas turbine power plants (CCGT) commissioned in 2001 and 2009, respectively. Additionally, Unit C is also utilized for electricity and heat production. Units VK3, VK4, VK5 and VK6 are heat generation boilers for a hot water network. TE TO power unit is also equipped with thermal energy storage of 750 MWh capacity [34]. Additional to electricity and heat production units, five units produce steam for industrial purposes. TE TO power plant produces steam with constant parameters of 230 °C and 9 bar, while the produced amount depends on the consumers' demand [35]. Mentioned units K, L and C, besides electricity and hot water production, produce steam with a capacity of 140, 70 and 70 t/h, respectively. Two additional steam boilers, units PK3 and M produce steam with a capacity of 64 and 60 t/h, respectively.

EL TO Zagreb power station has a nominal power output of 90 MW$_e$ and 491 MW$_h$ and numbers four units for joint production of electricity, how water and steam, two units for hot water generation and two additional units for steam generation. Unit specifications can be seen in Table 3. Units A, B, H and J are used for joint production of electricity, hot water and steam, while Units G and K are utilized for heat generation only. Units M and N are utilized for steam production for industrial purposes. Steam produced has constant parameters of 225 °C and 16 bar, while the produced amount depends on the consumers demand. Since the first of January 2018, units A and B are not being utilized since they are not in compliance with the regulations on emissions [36]. Due to the non-profitable revitalization of the Units A and B, planning and construction of additional CCGT CHP unit with a power output of 150 MW$_e$ and 114 MW$_h$ started in 2018. Commissioning is expected to happen in 2021 [37]. The main goals of the revitalization of the existing system are guided by the efforts to increase energy efficiency, especially in the part of production and distribution. It is of high importance to lower generation and distribution losses, which are especially high considering its value of 16.32% [33]. In Ref. [38] authors made detailed comparison between district heating systems in Zagreb and Aalborg, using comparative analyses. They conclude that a number of good practices used in Aalborg case, such as the importance of lowering specific heat and water losses and charging customers according to the cubic metres of hot water used, could improve Zagreb DH system operation.

The City of Velika Gorica is located 16 km south of the Zagreb. The city area is 328.65 km^2 with a population of 31,553, while the municipality counts 63,517 inhabitants [39]. Heat consumption of a city is 197.34 GWh and the district heating system supplies 32% of the demand [40]. Close urban area is covered with 14 district heating networks, only partially interconnected. The total length of the DH network is 9.84 km, while its total heating power output is 69.6 MW, and heating units are mostly gas-fired. In 2016 DH system produced 59.18 GWh of heating energy. Idea of interconnecting Zagreb and Velika Gorica DH networks was studied more than ten years ago, and conclusions was that interconnection was not profitable. However, market prices of the equipment and changes in technologies, as well as results of this study, might be used to revaluate the proposed interconnection [33].

Zaprešić is a town in northwest Croatia and is part of the Zagreb County. It covers an area of 52.60 km^2, while the inner-city area is 18.96 km^2. Population equals 25,223 inhabitants and it is the third-largest city in terms of population in Zagreb County [41]. District heating network consists of 8 individual heating systems which are not connected by a common district heating network. Boilers are mostly gas-fired with a possibility to use extra-light heating oil as fuel. Heating systems counts 2,372 customers which represent a share of 9.4%. Total "district" heating system is 2.37 km long and has 20.36 MW of installed heating power. Yearly heat production for the year 2016 was 16.53 GWh [33].

Following the validated methods used in analysis on Sonderborg municipality [11], a significantly updated model used in this paper focuses on the analysis of the district heating networks of City of Zagreb and two cities in Zagreb County, City of Velika Gorica and City of Zaprešić (see Table 1). Three scenarios were investigated. First one represents a baseline scenario with current installed capacities, while two additional scenarios represent future district heating system that will boost renewable energy utilization for district heating systems. Hence, the second scenario represents future district heating networks with no interconnections between Zagreb (Zagreb South and Zagreb North), Velika Gorica and Zaprešić, while the third scenario considers the possibility of mutual interconnections. Future scenarios represent the year 2025. Scenarios analysed are listed in Table 2.

Starting capacities in future scenarios are constrained by some production units not following the regulations on emissions. Data on development plant of EL TO Zagreb from document [37] suggests that only units commissioned after 2000 will be producing. According to decommissioned units for EL TO power plant case, which was commissioned before 2000, and due to missing data on TE TO power station development plan, we assumed that TE TO units commissioned before 2000 are also decommissioned by 2025. Details on production units can be seen in **Table 3**. Dual values for heat and electric capacities suggests the difference in starting values for the scenario I, and scenarios II and III, where first values represent starting capacities (sunk costs or forced investments) for the scenario I, while second value represents starting capacities for

Table 1
General data on district heating systems in Zagreb, Velika Gorica and Zaprešić for 2016 [33].

City	No. Consumers	Network length (km)	Heating capacity (MW_h)	Generated heat (GWh/a)	Supplied heat (GWh/a)
Zagreb	100,871	274.41	1,349.23	1,873.57	1,548.76
Velika Gorica	5,902	9.84	69.61	59.18	53.21
Zaprešić	2,372	2.37	20.36	16.53	15.86

Table 2
Description of investigated scenarios.

Scenario	Description
I	Baseline, business as a usual case scenario
II	Future district heating networks with the possibility of using new thermal energy storage, electric boilers and heat pumps, but not allowing for interconnections
III	Future district heating networks with the possibility of using new thermal energy storage, electric boilers and heat pumps and allowing for interconnections

Table 3
Details on generation units for scenario I [34,36,37]. EL TO and TE TO Zagreb units need to satisfy both heating and steam demand, while in Zaprešić and Velika Gorica only heat demand needs to be satisfied.

	Unit type	Fuel	Heat Capacity (MW)	Electric capacity (MW)	Steam production capacity (t/h)	Commissioned
EL TO Zagreb						
Block A	Back-pressure steam turbine	NG/FO	71/0	12/0	100/0	1970
Block B	Condensing steam turbine	NG/FO	162/0	30/0	200/0	1980
Block H	CHP	NG	10.25/0	25/0	64/0	1998
Block J	CHP	NG	10.25/0	25/0	64/0	1971
Block G	Heat boiler	NG/FO	116/0	–	–	1991
Block K	Heat boiler	NG/FO	121/121	–	–	2010
Block M	Ancillary steam boiler	NG	–	–	39/39	2016
Block N	Ancillary steam boiler	NG	–	–	39/39	2018
TE TO Zagreb						
Block C	Back-pressure steam turbine	NG/ELFO	200/0	120/0	70/0	1979
Block VK3	Heat boiler	NG/ELFO	58/0	–	–	1977
Block VK4	Heat boiler	NG/ELFO	58/0	–	–	1978
Block VK5	Heat boiler	NG/ELFO	116/0	–	–	1982
Block VK6	Heat boiler	NG/ELFO	116/0	–	–	1990
Block K	CCGT CHP	NG/ELFO	80/80	202/202	140/140	2003
Block L	CCGT CHP	NG	80/80	110/110	70/70	2009
Block PK3	Ancillary steam boiler	NG	–	–	64/0	1985
Block M	Ancillary steam boiler	NG	–	–	60/60	2018
TES	TES	–	750[1]	–	–	2015
Velika Gorica						
	Heat boilers	NG	26.3/0	–	–	–
Zaprešić						
	Heat boilers	NG	9/0	–	–	–

(1) The capacity of thermal energy storage (MWh), NG – Natural gas, FO – Fuel oil, ELFO – Extra-light fuel oil, TES – thermal energy storage.

scenarios II and III. The difference between the latter values arises due to different plants decommissioning.

Furthermore, in all the scenarios the assumed CO_2 price was 25 EUR/t, while both electricity transmission and distribution fees were set to 20 EUR/MWh, respectively. The discount rate for all the technologies was set to 6%, except for connecting piping which was set to 4%, as it was considered to be a long-term infrastructure investment that does not share the same risk as to the investments in different generation plants. Finally, the economic figures on different technologies can be seen in Table 4.

The potential investment in connecting piping consisted of the fixed part and the linear part dependent on the installed capacity, as seen in equation *(1)* and Table 5.

4. Results and discussion

Results on heat generation for three different scenarios can be observed in Table 6. In scenarios II and III, natural gas boilers were replaced by electric boilers and/or heat pumps in both Zaprešić and Velika Gorica. The latter was the result of the implemented policy

Table 4
Economic parameters used in the study [42].

Type of the plant	Investment cost (EUR/MW)	Annualized investment cost (EUR/(MWyear))	Fixed cost (EUR/(MWyear))	Variable cost (EUR/MWh)	Discount rate
Back pressure[a] cogeneration plant	720,000	61,784	30,000	4.5	6%
Combined cycle[a] cogeneration plant	1,350,000	115,844	30,000	4.5	6%
Gas boiler	100,000	8,059	2,000	0.9–1.1	6%
Thermal storage	3,000	225	8.6	0.1	6%
Electric boiler	75,000	7,079	1,100	0.8	6%
Heat pump	700,000	60,067	2,000	2	6%

[a] Combined heat and power plant included start-up costs of 6,746 EUR [43].

Table 5
Economic cost parameters for district heating interconnectors. Cost included a fixed part of the investment (a sunk cost) and incremental cost dependent on the optimal interconnector capacity.

	Fixed annualized investment (EUR)	Piping annualized cost (EUR/MW)
Zagreb north to south	19,561	1,766
Zagreb north to Zaprešić	359,137	32,435
Zagreb south to Velika Gorica	195,610	17,666

Table 6
Heat generation in DH for different scenarios and different regions, in GWh.

Generation units	Scenario I	Scenario II	Scenario III
EL TO Zagreb	772.96	771.31	1,482.87
TE TO Zagreb	1,020.55	0	0
Zagreb Electric boilers	0	15.77	0
Zagreb Heat pumps	0	1,006.43	290.75
Velika Gorica Heating boilers (NG)	61.41	0	0
Velika Gorica Electric boilers	0	1.78	0.110
Velika Gorica Heat pumps	0	59.63	77.02
Zaprešić Heating boilers (NG)	17.46	0	0
Zaprešić Electric boilers	0	0.687	0.082
Zaprešić Heat pumps	0	16.77	21.46

NG – Natural gas.

that no emissions should be allowed in the newly connected areas, in order to remove any potential source of the air pollution, a common complaint nowadays of the citizens.

Units that were generating in scenario II are shown in Table 7. One can observe that only the unit K, M and N from EL TO, and units K, L and M from TE TO were modelled as sunk costs (forced investments). To compensate for the missing capacity for EL TO, based on [37] and assumptions for loss of capacities for TE TO, the addition of CCGT CHP unit (Block KKF) in EL TO was the optimal result of the model .

Based on the model results for the EL TO power station we can observe: (i) the addition of CCGT CHP unit with heat capacity of 114 MW and electric capacity of 150 MW; (ii) the increase in heat capacity of the Block K from 121 MW to 249.4 MW; (iii) the addition of 66.4 MW heat capacity electric boiler (North ZG EB). It is worthwhile to mention that HEP group, a heat and power generation company, is planning the construction of the new CCGT CHP block in EL TO power station, and our model showed that the investment is socio-economically justified.

Results on the TE TO power station capacities showed: (*i*) the addition of the 51.9 MW heat capacity electric boiler (South ZG EB); (*ii*) the increase in thermal energy storage capacity from 750 MWh to 4381 MWh and (*iii*) the addition of 294.5 MW heat capacity heat pump (South ZG HP).

As previously mentioned, to boost electrification and lower fossil fuel usage, the model considered the use of electric boilers and/or heat pumps with the possibility of additional thermal energy storage for Zaprešić and Velika Gorica locations. Hence, the results on generation capacities for Velika Gorica showed the replacement of natural gas-fired heating boilers with an electric boiler and a heat pump, with installed capacities of 9.7 and 16.6 MW, respectively. The case for the city of Zaprešić showed the replacement of 9 MW heating boiler with an electric boiler and a heat pump with both having the heat capacities of 4.2 MW. Additionally, the thermal energy storage of 2.8 MWh capacity is added in Zaprešić.

Similar to scenario II, the model allowed additional installed capacities in scenario III, as well as the investment in additional interconnectors between district heating systems. Hence, the potential connections between Zagreb North and Zaprešić, Zagreb South and Zagreb North, and Zagreb South and Velika Gorica were assessed (Table 8).

Based on the results for the EL TO power station we can observe: (i) the addition of CCGT CHP unit with the heat capacity of 114 MW and electric capacity of 150 MW; (ii) the increase in heat capacity of Block K from 121 MW to 415.7 MW.

Results on TE TO power station capacities showed: (i) the increase in thermal energy storage capacity from 750 MWh to 4124 MWh and (ii) the addition of 51.36 MW heat capacity heat

Table 7
Generation units as results from model for scenario II in different regions.

	Unit type	Fuel	Heat Capacity (MW)	Electric capacity (MW)	Steam production capacity (t/h)
EL TO Zagreb					
Block KKE	CCGT CHP	NG	114	150	70
Block K	Heat boiler	NG/FO	121 + 128.4	–	–
North ZG EB	Electric boiler	–	66.4	–	–
Block M	Ancillary steam boiler	NG	–	–	39
Block N	Ancillary steam boiler	NG	–	–	39
TE TO Zagreb					
Block K	CCGT CHP	NG/ELFO	80	202	140
Block L	CCGT CHP	NG	80	110	70
ZG TES	TES	–	750 + 3,631[a]	–	–
South ZG EB	Electric boiler	–	51.9	–	–
South ZG HP	Heat pump	–	294.5	–	–
Block M	Ancillary steam boiler	NG	–	–	60
Velika Gorica					
	Electric boiler	–	9.7	–	–
	Heat pump	–	16.6	–	–
Zaprešić					
	Electric boiler	–	4.2	–	–
	Heat pump	–	4.2	–	–
	TES	–	2.8	–	–

[a] The capacity of thermal energy storage (MWh), NG – Natural gas, FO – Fuel oil, ELFO – Extra-light fuel oil, TES – thermal energy storage.

Table 8
Generation units as results from the model for scenario III in different regions.

	Unit type	Fuel	Heat Capacity (MW)	Electric capacity (MW)	Steam production capacity (t/h)
EL TO Zagreb					
Block KKE	CCGT CHP	NG	114	150	70
Block K	Heat boiler	NG/FO	121 + 294.7	–	–
Block M	Ancillary steam boiler	NG	–	–	39
Block N	Ancillary steam boiler	NG	–	–	39
TE TO Zagreb					
Block K	CCGT CHP	NG/ELFO	80	202	140
Block L	CCGT CHP	NG	80	110	70
ZG TES	TES	–	750 + 3,374[a]	–	–
South ZG HP	Heat pump	–	51.6	–	–
Block M	Ancillary steam boiler	NG	–	–	60
Velika Gorica					
	Electric boiler	–	2.8	–	–
	Heat pump	–	13.5	–	–
Zaprešić					
	Electric boiler	–	2.4	–	–
	Heat pump	–	3.7	–	–

[a] The capacity of thermal energy storage (MWh), NG – Natural gas, FO – Fuel oil, ELFO – Extra-light fuel oil, TES – thermal energy storage.

pump (South ZG HP).

Results on generation capacities for Velika Gorica showed the replacement of natural gas-fired heating boilers with an electric boiler and a heat pump, with installed capacities of 2.8 and 13.5 MW, respectively. The case for the city of Zaprešić showed the replacement of 9 MW heating boiler with an electric boiler and a heat pump with heat capacities of 2.4 and 3.7 MW, respectively.

Regarding the interconnections, one can notice that all proposed connection were economically viable, and their capacities were (i) 430.21 MW capacity connection between Zagreb North and Zagreb South; (ii) 10.54 MW capacity connection between Zagreb South and Velika Gorica and (iii) 2.98 MW capacity connection between Zagreb North and Zaprešić. Heat flows between Zagreb South and Zagreb North aggregated on a daily basis can be seen in Fig. 1, while heat flows between Zagreb South and Velika Gorica can be observed in Fig. 2. Additionally, a smaller capacity connection between Zagreb South and Zaprešić can be seen in Fig. 3. One can see that all three of the interconnections are used for heat transfer in both ways, depending on the different period of the year. Furthermore, it can be noticed that interconnections are used less during the summer season.

Regarding the economical results from the model, one can observe that total system cost decreases from 117 m EUR for the scenario I to 105.8 and 82.8 m EUR for scenarios II and III, respectively. These values can also be expressed as savings for future scenarios (II and III) regarding the business as usual scenario (I). In Table 9, the additional economic and environmental data is shown. One can note that future systems, both in the case of interconnecting district heating systems, and not interconnecting them, can be significantly cheaper than the current one. Results show that total system cost for scenario II is 11.2 m EUR lower, while the savings for the scenario III are 34.2 m EUR. Moreover, CO_2 emissions are lower in both future scenarios. In scenario II CO_2 emissions are 48.9% lower, while for the scenario III reduction in CO_2 emissions are 15.3%. The main reason why the CO_2 emissions are much lower in the second scenario, is the difference in installed capacities between the second and third scenario. In the second scenario there is total of 447.5 MW of installed capacities in form of heat pumps or electric boilers, while in the third scenario only 74 MW of newly installed heat pumps or electric boilers are available. That difference is also due to the model allowed connection in the third scenario, which results with the higher CCGT CHP production, which in turn gives higher CO_2 emissions. The CO_2 emissions for CHP units were calculated using the efficiency method [44].

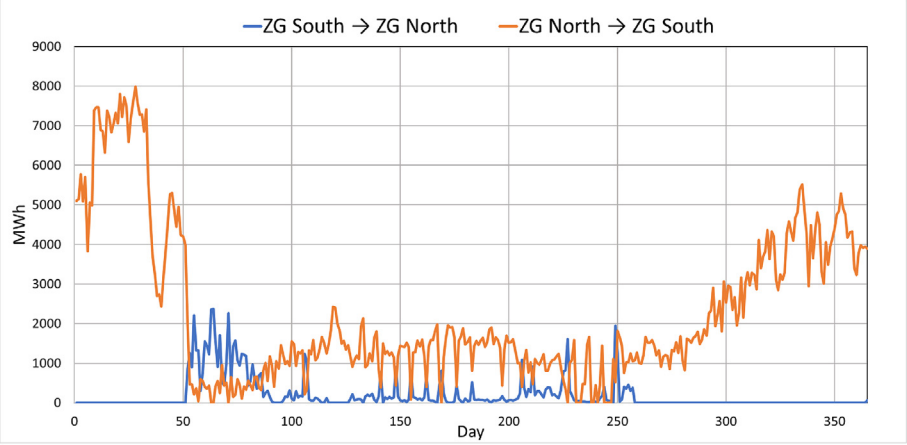

Fig. 1. Heat flows between Zagreb South and Zagreb North for scenario III. The data points are represented on the daily time resolution.

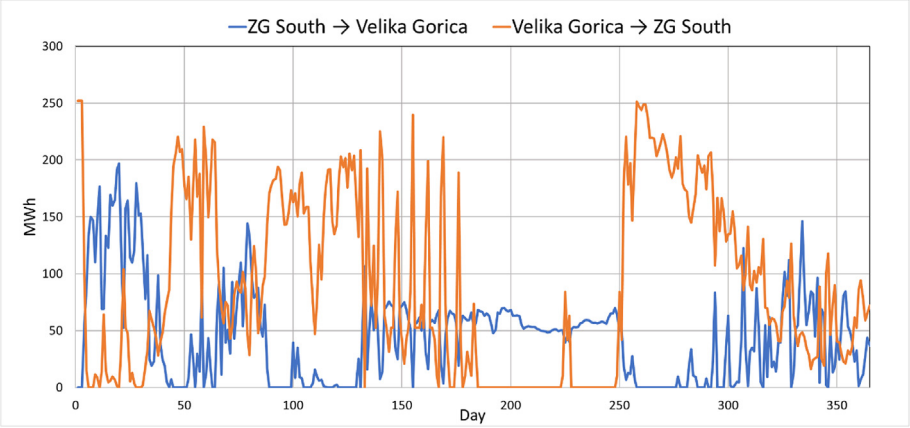

Fig. 2. Heat flows between Zagreb South and Velika Gorica for scenario III. The data points are represented on the daily time resolution.

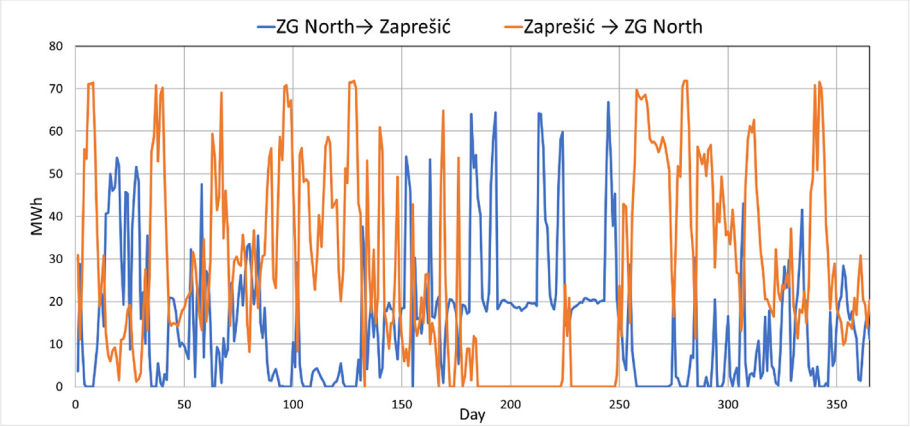

Fig. 3. Heat flows between Zagreb North and Zaprešić for scenario III. The data points are represented on the daily time resolution.

Table 9
Results on costs and CO_2 emissions for three different scenarios.

Scenario	I	II	III
Total system cost (m EUR)	117	105.8	82.8
Savings (m EUR)	Reference	11.2	34.2
CO_2 emissions ($ktCO_2/a$)	356.34	181.87	301.97
Pipe length (km)	0	0	10.2 + 1 + 18.8

5. Conclusion

In this paper, a mixed-integer linear program with endogenous decision-making on building district heating interconnectors was successfully developed. The model was applied for the case of the City of Zagreb and the two adjacent smaller cities. There are three main conclusions that arose from this study.

First, when allowed in the model, it was optimal to install both heat pumps and electric boilers in all three geographic areas when interconnectors were not allowed. Electric boilers were covering peak demand while heat pumps were covering a significant share of the heat demand. In scenario III, the one in which interconnectors between the regions were allowed, electric boilers generation was almost negligible. On the other hand, the interconnectors allowed for much larger utilization of cogeneration units, making the system more profitable.

Second, it was socio-economically optimal to invest in all three possible interconnectors, both within two district heating regions of Zagreb that are located next to each other, as well as interconnector between the cities of Zagreb and Zaprešić that are distanced almost 19 km. The latter points out that urban agglomerations should more thoroughly assess the possibility of interconnecting its systems as those could bring significant benefits.

Third, the thermal energy storage significantly increased its size in both scenarios II and III. The optimal capacities amounted to the 25 days of the average heat demand in Scenario II and 24 days of the average demand in Scenario III.

Declaration of competing interest

The authors declare that they have no known competing financial interests or personal relationships that could have appeared to influence the work reported in this paper.

Acknowledgements

This work was financed as a part of the CITIES project No. DSF1305-00027B funded by the Danish Innovationsfonden and KeepWarm project that received funding from the European Union's Horizon 2020 research and innovation programme under grant agreement N784966. Those contributions are greatly acknowledged.

References

[1] European Commission. Clean energy for all Europeans package. 2019.
[2] European Commission. Towards a smart, efficient and sustainable heating and cooling sector. 2016. p. 21 [Online]. Available: https://www.google.com/url?sa=t&rct=j&q=&esrc=s&source=web&cd=1&ved=2ahUKEwi_gNXIwa3lAhXTMMAKHTe6DhcQFjAAegQIBRAC&url=http%3A%2F%2Feuropa.eu%2Frapid%2Fpress-release_MEMO-16-311_en.pdf&usg=AOvVaw22S-raeHXtzg2_bZtNxs7C. [Accessed October 2019].
[3] Frederiksen S, Werner S. District heating and cooling. Studentlitteratur AB; 2013.
[4] Werner S. International review of district heating and cooling. Energy 2017;137:617–31.
[5] Lund H, et al. 4th Generation District Heating (4GDH). Integrating smart thermal grids into future sustainable energy systems. Energy 2014;68:1–11.
[6] Dominković DF, Dobravec V, Jiang Y, Nielsen PS, Krajačić G. Modelling smart energy systems in tropical regions. Energy 2018;155:592–609.
[7] Lund H. Renewable energy systems: a smart energy systems approach to the choice and modeling of 100% renewable solutions. second ed. Academic Press; 2014.
[8] Lund H, et al. The status of 4th generation district heating: research and results. Energy 2018;164:147–59.
[9] Galindo Fernández M, Roger-Lacan C, Gährs U, Aumaitre V. Efficient district heating and cooling markets in the EU: case studies analysis, replicable key success factors and potential policy implications. 2016. December.
[10] Hast A, Syri S, Lekavičius V, Galinis A. District heating in cities as a part of low-carbon energy system. Energy 2018;152:627–39.
[11] Dominković DF, Bačeković I, Sveinbjörnsson D, Pedersen AS, Krajačić G. On the way towards smart energy supply in cities: the impact of interconnecting geographically distributed district heating grids on the energy system. Energy 2017;137:941–60.
[12] Guelpa E, Verda V. Thermal energy storage in district heating and cooling systems: a review. Appl Energy 2019;252:113474. June.
[13] Mirzaei PA. "A review of district heating Systems : modeling and optimization, vol. 2; October 2016. p. 1–14. 2020.
[14] Sarbu I, Mirza M, Crasmareanu E. A review of modelling and optimisation techniques for district heating systems. " no. April; 2019. p. 6572–98.
[15] Sanaei SM, Nakata T. "Optimum design of district heating : application of a novel methodology for improved design of community scale integrated energy systems. Energy 2012;38(1):190–204.
[16] Buoro D, Casisi M, De Nardi A, Pinamonti P, Reini M. Multicriteria optimization of a distributed energy supply system for an industrial area. " *Energy*; 2013. p. 1–10.
[17] Dominković DF, et al. Potential of district cooling in hot and humid climates. Appl Energy 2017;208:49–61.
[18] Haikarainen C, Pettersson F, Saxén H. A model for structural and operational optimization of distributed energy systems. Appl Therm Eng 2;70(1):211–8.
[19] Mertz T, SSHA, RJM. "A MINLP optimization of the configuration and the design of a district heating network : case on an existing site of a A MINLP optimization of the study configuration and. Energy Procedia 2017;116:236–48.
[20] Li L, Mu H, Li N, Li M. Economic and environmental optimization for distributed energy resource systems coupled with district energy networks. Energy 2016;109:947–60.
[21] Delangle A, Lambert RSC, Shah N, Acha S, Markides CN. Modelling and optimising the marginal expansion of an existing district heating network. Energy 2017;140:209–23.
[22] Weber C, Maréchal F, Favrat D. Design and optimization of district energy systems. 2007. p. 1127–32.
[23] Craus M, Leon F, Arot D. A new hybrid genetic algorithm for the district heating network problem. " no. July; 2015.
[24] Zeng J, Han J, Zhang G. Diameter optimization of district heating and cooling piping network based on hourly load. Appl Therm Eng 2016;107:750–7.
[25] Dobersek D, Goricanec D. Optimisation of tree path pipe network with nonlinear optimisation method Next pipe section. Appl Therm Eng 2009;29(8–9):1584–91.
[26] Morvaj B, Evins R, Carmeliet J. "Optimising urban energy systems : simultaneous system sizing , operation and district heating network layout. Energy 2016;116:619–36.
[27] Bordin C, Gordini A, Vigo D. An optimization approach for district heating strategic network design. Eur J Oper Res 2016;252(1):296–307.
[28] Dorotić H, Pukšec T, Duić N. Multi-objective optimization of district heating and cooling systems for a one-year time horizon. Energy Feb. 2019;169:319–28.
[29] Vesterlund M, Toffolo A. Design optimization of a district heating network expansion. ": a Case Study for the Town of Kiruna; 2017.
[30] Blanco I, Andersen AN, Guericke D, Madsen H. A novel bidding method for combined heat and power units in district heating systems. " *Energy Syst.*; 2019.
[31] Central Bureau of Statistics C. Croatia census 2011 - Zagreb. " [Online]. Available: https://www.dzs.hr/Eng/censuses/census2011/results/htm/E01_01_01/e01_01_01_zup21.html.
[32] Tomić T, Dominković DF, Pfeifer A, Schneider DR, Pedersen AS, Duić N. Waste to energy plant operation under the influence of market and legislation conditioned changes. Energy 2017;137:1119–29.
[33] Energy Institute Hrvoje Požar. Analiza sektora toplinarstva i iskorištavanja potencijala geotermalnih izvora na području Urbane aglomeracije Zagreb. 2017.
[34] Proizvodnja HEP. "TE TO Zagreb - Technical Data." [Online]. Available: http://www.hep.hr/proizvodnja/UserDocsImages/dokumenti/tehnicki_podaci_termoelektrane/TE-TO_Zagreb.pdf.
[35] EKONERG – Institut za energetiku i zaštitu okoliša d.o.o.. ELABORAT ZAŠTITE OKOLIŠA-Zahvat: zamjena toplinske mreže za područje Zagreba. 2018.
[36] Proizvodnja HEP. "EL TO Zagreb - Technical Data." [Online]. Available: http://www.hep.hr/proizvodnja/UserDocsImages/dokumenti/tehnicki_podaci_termoelektrane/EL-TO_Zagreb.pdf.
[37] EKONERG – Institut za energetiku i zaštitu okoliša d.o.o. "NETEHNIČKI sažetak - zamjena bloka "A" novom kombi KOGENERACIJSKOM ELEKTRANOM U el-to zagreb. "; 2017.
[38] Ćulig-Tokić D, Krajačić G, Doračić B, Mathiesen BV, Krklec R, Larsen JM. Comparative analysis of the district heating systems of two towns in Croatia and Denmark. Energy Dec. 2015;92:435–43.
[39] Central Bureau of Statistics. Croatia census 2011 - Velika Gorica. " [Online]. Available: https://www.dzs.hr/Eng/censuses/census2011/results/htm/E01_01_01/e01_01_01_zup01_5410.html.
[40] Felipe Andreu J, Schneider DR, Krajačić G. Evaluation of integration of solar energy into the district heating system of the city of Velika Gorica. Therm Sci 2016;20(4):1049–60.
[41] Vale C. Techno-economic analysis of solar district heating plant with sessional heat storage in Zaprešić. 2018.
[42] Dominković DF, Grønborg RJ, Byskov K, Madsen H. "Implementing flexibility into energy planning models : soft-linking of a high- level energy planning model and a short-term operational model. Appl Energy August 2019;260:114292. 2020.
[43] Heinisch V. Modeling the grid integration of power to gas: a case study of Denmark. " Chalmers University; 2014. http://publications.lib.chalmers.se/records/fulltext/211408/211408.pdf.
[44] Greenhouse gas protocol, allocation of GHG emissions from a combined heat and power (CHP) plant.

PAPER 2

"There is a difference between knowing the path and walking the path"

Morpheus

Optimisation of Desalination-Based Water System with Integrated Renewable Energy and Storage within the Water-Energy Nexus

Goran Stunjek*, University of Zagreb, Faculty of Mechanical Engineering and Naval Architecture, Croatia
goran.stunjek@fsb.hr

Goran Krajačić, University of Zagreb, Faculty of Mechanical Engineering and Naval Architecture, Croatia
goran.krajacic@fsb.hr

https://doi.org/10.1016/j.desal.2024.118474

Abstract

This study presents a comprehensive optimization framework for integrated water and energy systems. It offers a novel implementation to determining the optimal dispatch of water and energy streams and sizing Battery Energy Storage (BES)[1] and Renewable Energy Systems (RES)[2]. The proposed Mixed-Integer Linear Programming model integrates RES and BES with water systems through Reverse Osmosis desalination units and water storage supported by Power-to-Water technology. Unlike traditional models, the framework considers both BES capacity and power rating as variables while incorporating RES capacity optimization, water system modelling, and water storage integration. The integrated water-energy system model is particularly suited to addressing the unique challenges of smaller-scale island systems, often overlooked in larger-scale analyses. The methodology is applied to Unije Island, Croatia, characterized by significant seasonal demand fluctuations due to tourism. The results demonstrate the effectiveness of power-to-water and BES technology in increasing system flexibility and economic performance and provide a comprehensive analysis of the impact of varying RES and BES investment costs on optimal system configuration, and financial and economic outcomes. Lower RES investment costs lead to higher RES capacities, but the rate of change is significantly influenced by BES investment costs, highlighting the importance of an optimal RES-BES pair for maximizing financial and economic performance. Furthermore, the results emphasize that the highest financial and economic benefits are achieved not by maximizing both RES and storage capacities, but by finding an optimal balance between them, demonstrating the critical role of BES and water storage utilization in enhancing system efficiency. Change in specific parameters showed that grid electricity and PV potential effect final system profitability more than change in water demand defining two parameters as critical. Proposed study offers valuable insights into the optimization of water-energy systems on islands and other isolated regions, emphasizing the importance of integrated planning for sustainable development, and offering strategic insights for future infrastructure development.

Keywords: water-energy nexus, desalination, renewable energy sources, battery energy storage, power-to-water, flexibility

1. Introduction

All nations have agreed to reduce emissions in accordance with the goals of the Paris Agreement in order to keep global warming below 2 °C and, if at all possible, to keep it to 1.5 °C. A significant revamp of the EU's energy policy framework was launched to transition away from the heavy reliance on fossil fuels, building on the pledges made in the Paris Agreement. The eight pieces of legislation that make up the "Clean Energy for all Europeans" package [1] collectively represent the last steps in putting into practice the five pillars of the energy union strategy: security, solidarity, and trust; a fully integrated energy market; increased energy efficiency; climate action; and decarbonization; as well as research, innovation, and competitiveness [2].

[1] BES – Battery Energy Storage
[2] RES – Renewable Energy storage

The EU has more than 2,200 inhabited islands, and most of them have access to some form of renewable energy sources (RES), mostly wind and solar energy. However, many islands are still dependent on expensive imported energy sources, fossil fuels, and land-based energy supplies [3]. The EU has recognized the renewed need for island development with the legislative frameworks such as the "Smart Islands Declaration" [4] as the most important document for island development, and the "Clean Energy for European Islands" initiative [5]. The redevelopment of the island is a challenge due to the different geographical locations of the islands, different interests and requirements of the local population, and this challenge is recognized as an opportunity to learn, develop and implement new technologies. The Clean Energy for European Islands aims to reduce energy costs and increase energy production from RES, promote energy storage using the latest technologies to ensure better energy independence of the island, improve air quality, reduce greenhouse gas emissions and encourage economic transition in the context of job creation and business opportunities.

1.1. Renewable energy systems and storage integration

The integration of RES at the island level has been extensively studied. One of the pioneering approaches, the RenewIsland method, employs a four-step analysis to integrate energy and resource flows, demonstrated in case studies of Corvo, Porto Santo, and Mljet [6]. Further research explored interconnecting island groups to enhance RES utilization, incorporating electric vehicles as storage via vehicle-to-grid systems. This analysis used EnergyPLAN for scenario simulations and MultiNode for interconnection studies [7]. Similarly, [8] examined energy and transport sector integration on a carbon-neutral island reliant on intermittent RES, using EnergyPLAN to model power, cooling, heating, and transport systems. Another study developed an integrated energy system model with PLEXOS for a typical Caribbean island, incorporating power, transport, cooling, and water desalination sectors to achieve high RES penetration [9].

In [10] a review of energy storage and demand side management (DSM) highlighted the role of grid flexibility through storage, supply solutions, and sector integration. Flexible water systems and reverse osmosis (RO) based desalination were noted as key for remote islands, enabling electricity storage as water and reducing seasonal peak loads. In study [11], six hybrid RES-based RO configurations, combining wind, photo-voltaic (PV), battery energy storage (BES), and hydrogen storage, were proposed. An optimization problem is introduced where number of BES and hydrogen storage units represent two integer variables while wind turbine swept area and PV plant area represent two continuous variables. The study [12] evaluates the integration of PV system to sustainably power RO desalination units on Nisyros Island, addressing water scarcity while reducing environmental impacts. It highlights a scalable solution for other Mediterranean islands with abundant renewable energy resources. Authors in [13] present optimization model for minimizing energy consumption in micro water-energy systems, integrating RES and storage solutions. It highlights the potential of synchronized water and energy management to enhance efficiency and sustainability in interconnected systems. Although Mixed-Integer Linear Programming (MILP) optimisation approach with inclusion of BES and water storage was used, the proposed study lacks the optimisation of RES capacities which are used as parameters. A MILP model for optimizing the energy–water–carbon nexus in remote AC/DC microgrids, focusing on integrating RES and BES was developed in [14]. Similarly, even though study includes both water and energy system, as well as the energy and water storage, it is limited as RES capacities are parameters and only 24h analysis is suggested.

A study [15] examines the impact of energy and water storage on the co-optimization of water and power networks, introducing ramping constraints and storage facilities to enhance efficiency. Study suggests that only co-optimisation was performed, while power and storage capacities are represented as parameters. A hybrid RES microgrid in study [16] integrates PV, wind turbines, storage options, and RO desalination to meet electricity and potable water demands. Utilizing Particle Swarm Optimisation (PSO) approach, the system demonstrates technical feasibility and financial viability for small islands. However, RES capacities were used as parameters. Study [17] introduced a novel DSM model for the Cres-Lošinj archipelago, considering grid limitations. Results showed DSM activation at incentives below 23% of day-ahead market prices, suggesting benefits for all stakeholders from distribution-level DSM implementation. The authors in [18] applied PSO to optimize a PV-based pumping system with

hydro storage for a rural village in Nigeria. Only BES capacity was used as variable and simpler 24h only hour optimisation was proposed. A optimal dispatch integrating RES, desalination, and brine storage was done in [19]. The method was tested on a hypothetical case of Jordan for different levels of installed wind and PV capacities, as well as different sizes of the brine storage. However, no capacity optimisation was performed.

An optimization approach for the placement, sizing, and daily operation of BES to address challenges in distribution networks with high PV penetration was proposed in [20]. A proposed optimisation lacks in not having the hourly BES power variable and assumes only 1 daily charge and discharge rate. Daily curve is further multiplied by 365 to represent yearly distribution which limits the study approach. Furthermore, RES capacities are represented as parameters. Focus on optimal BES planning in distribution grids with RES to minimize costs and meet technical constraints was proposed in [21]. The study uses a hybrid tabu search/PSO algorithm to determine the ideal location, capacity, and power rating of BES. Although it uses both BES capacity and power as variable, it lacks as RES capacities are used as parameters and only 24h is proposed. Furthermore, it limits BES operation to only one daily charge/discharge operation and allows BES discharge only if BES is on max capacity.

Authors in [22] propose a MILP method for optimizing the BES capacity in a multi-energy complementary system with wind, PV, and concentrating solar power. It uses both BES capacity and power as variables, and limits BES charge and discharge with binary variables. Although similar to our proposed modelling approach, it lacks in having RES as parameters. A study [23] presents an algorithm for the simultaneous optimal sizing, placement, and operational strategy of decentralized BES systems in medium voltage distribution grids. Approach uses both BES capacity and power as variable but lacks in only having 24h horizon which is further simulated to whole year period. Objective function lacks the BES power variable, while RES capacities are parameters. A method to co-optimize BES and thermal energy storage capacities in a multi-RES-energy complementary system was proposed in [24]. Using a MILP model, it aims to maximize the system's annual profit while considering energy curtailment and operational constraints. Although suggesting that RES capacities are part of the objective function, it seems that RES capacities are used as parameters. Furthermore, only BES capacity is in objective function without BES power variable. It uses binary variables for BES charge/discharge operation. The authors in [25] present an integer-programming model for optimizing the mix of RES, conventional generation, and BES. The model minimizes capital, operational, and utility costs while meeting system constraints and demand. Although it uses both BES capacity and power as variable in objective function, RES capacity is used as parameter and no investment cost is in objective function. Additionally, no water storage is accessed. Still, study offers high level BES modelling as a main problem evaluation.

A MILP model for planning a local community's water and energy resources, focusing on the energy-water-carbon nexus was proposed in [26]. The model optimizes the sizing of components such as RES and desalination plants while minimizing costs and carbon emissions. Both BES capacity and power are variables and modelled in objective function as investment cost, but BES is limited for daily usage avoid the possibility to take seasonality into consideration. Still, binary variables were used for BES charging and discharge. Furthermore, proposed analysis tends to be only on 24h basis providing water scenario, energy scenario and water-energy nexus scenario separately. A MILP optimization model for wind-powered desalination units, where the number and type of turbines are optimized based on technical and economic factors is presented in [27]. The model includes the integration of a diesel generator, BES, and a water storage tank to reduce costs and improve reliability. Approach uses both BES capacity and power as variable and uses binary variables for charge and discharge options. However, RES capacities are not variables, but number of RES options. Furthermore, it uses 24h equivalents and not whole year horizon period.

1.2. Desalination and Water-Energy Nexus approach

Remote islands often face freshwater shortages due to limited resources, exacerbated by the seasonality of tourism. Traditionally, many islands relied on transporting water via boats, significantly increasing costs. As a result, desalination has emerged as a cost-effective and sustainable solution to meet freshwater demands efficiently [28].

Islands face energy resource constraints, making energy-intensive desalination a challenge. A sustainable solution is pairing RES with desalination, addressing water shortages while avoiding fossil fuel dependence and ensuring environmental sustainability. The authors in [29] give a detailed review of different desalination and RES technologies focusing mostly on RO desalination. Similarly, the authors in [30] review existing desalination and RES applications, emphasizing energy storage and process optimization for greater efficiency and cost-effectiveness. Detailed overview of the RES integration with a highlight on technical issues, environmental, and economic impact was further shown in [31]. Authors give a more thorough view on technical issues, environmental and economic impact. The authors in [32] tested a stand-alone wind-powered desalination prototype on Gran Canaria, evaluating reverse osmosis, electrodialysis reversal, and vacuum vapor compression. Reverse osmosis proved the most effective for intermittent wind energy, offering stable water quality and efficient operation. The study [33] reviews over a decade of work on RES powered desalination, testing different desalination technologies using wind and solar energy. Findings from pilot projects in the Canary Islands and Africa show the viability of autonomous desalination, highlighting cost and environmental benefits in off-grid areas.

The authors in [34] optimized the design of a stand-alone RO desalination unit for a Greek island using PV, wind, and hydropower, finding it more cost-effective than water transport. For Gran Canaria, [35] examined a RES-powered microgrid for RO, using wind and PV with grid connection and BES, concluding BES was unnecessary. In [36] a hybrid PV-wind-diesel system with BES was modelled for isolated islands, identifying RO as the most cost-effective desalination method. While HOMER software was used stating the optimisation approach, the study indicates a simulation approach for determining the optimal number of PV and wind units. Comprehensive analysis of wind energy-driven desalination projects in the Canary Archipelago, spanning from 1984 to the present was assessed in [37]. Authors in [38] studied the operation of desalination unit using RES with the implementation of BES, grid connection, and smaller internal combustion engines. The authors used HOMER software for optimisation. However, a study is missing the objective function and what is being optimized. The study [39] applied a Pareto front optimization approach with automated EnergyPLAN simulations to determine optimal capacities for water-energy systems on Lanzarote Island. By integrating flexible desalination as a load, the method increases renewable energy contribution from 5.14% to 24.6%, balancing wind and PV capacities, water storage, and desalination to maximize renewables while minimizing CO2 emissions, fossil fuel use, and costs.

Authors in [40] a continuously operated RO model with PV power, BES, and water storage showed that a smaller BES suffices without grid connection. To tackle the problem of higher BES costs that are generally used as a flexibility resource on the energy system side, a study of using only seasonal water storage for PV based RO system is shown in [41]. Even though authors mention optimization, it seems they used brute-force approach to determine the number of PV panels. Study [42] addresses water and energy challenges on Greek islands by developing an optimal desalination systems powered by RES. Although no optimisation approach was used, authors simulate water storage and RES integration.

Authors in [43] propose a method for optimizing island water-energy systems by integrating wind, hydrogen storage, and RO desalination. Optimization aims to minimize the total system cost and was tested on typical summer and winter days for a 24h periods. The study [44] compared PSO and HOMER software for optimizing the sizing and dispatch of PV and hydrogen based RO desalination system. Authors conclude how PSO optimisation approach outperforms HOMER. Although it uses PSO approach, optimal number of model actors is selected, and not optimal value capacities. Iterative "optimization" method for sizing a stand-alone hybrid PV/wind/hydrogen system to power a desalination unit was proposed in [45]. A case study on the Kerkennah islands was proposed. Like other semi-optimisation approaches, it uses iterative simulation approach to find the most cost-effective option for a number of investigated scenarios. Similarly, although mentioning optimisation of water and energy system approach, authors in [46] use iterative "optimization" approach to design power system for RO in remote communities, including Honduras, Eritrea, and Australia.

1.3. Optimisation approaches in Water-Energy system modelling

When studying the literature on desalination and water-energy nexus, even though one can still find a more basic simulation approaches, it is now a common thing to see the optimization approaches being used. It is also common to see authors use the optimization wording relatively "freely", sometimes not stating which optimization approach was used and what was the optimization problem. Hence, below we cover main optimization approaches used in field of water-energy nexus, and more specific the implementation of desalination, RES, storage, and DSM technologies.

The authors in [47] reviewed desalination optimization models, highlighting energy consumption, transport, fouling, and integration with RES. They pointed out that while hybrid desalination technologies show promise, the review lacks detailed optimization discussions. In [48] he authors offer an extensive review of optimization approaches in RES-RO modelling, categorizing methods into classical techniques (e.g., Newton's method, Simplex) and AI-based methods (e.g., Particle Swarm Optimization, Evolutionary Algorithms, Simulated Annealing).

We provide a brief review of recent optimization approaches for desalination, RES, and storage. We classify methods into two main types: those using commercial software and those based on custom models created with coding tools like Python, Matlab, or GAMS. The latter approach allows for transparency in the objective function and constraints, whereas commercial software like HOMER often lacks such detail. Many studies using HOMER, [36], [38], [49], appear to select the optimal scenario based on cost from multiple simulations, rather than a true optimization approach. Similarly, other approaches not related to HOMER, and previously mentioned, tend to mention optimisation while the methods suggest the iterative simulation approach was used [15],[34],[42],[45],[46].

A popular optimization technique seen in literature is the usage of iterative heuristic and meta-heuristic approaches. The authors in [50] put nineteen different heuristic and metaheuristic algorithms to the test to find the optimal RO-RES system. Included RES solutions were wind and PV power while also including a BES. Both the individual and hybrid heuristic and metaheuristic optimization approaches were assessed. The authors conclude that improved harmony search-based chaotic simulated annealing algorithm provided the best results in regards to the mean, min, and max values. Moreover, authors add that hybrid metaheuristic algorithms, the ones combining two or more single optimization approaches, are more superior to individual optimization algorithms due its faster convergence speed and calculation accuracy. Many authors in previously mentioned references use iterative heuristic and meta-heuristic approaches for water-energy system analysis [11],[16],[18],[20],[21],[35],[44]. Iterative heuristic and meta-heuristic approaches can be less efficient than linear programming methods because they often require more computational time to converge and do not guarantee optimal solutions. These methods rely on approximation and trial-and-error processes, which can lead to suboptimal results, whereas linear programming methods offer a systematic approach to find the best solution within given constraints, ensuring optimality and faster convergence. Therefore, a concept of linear programming has grown significantly in popularity during the last several years in the field of water-energy nexus.

In study [51], a MILP model was used to optimize RES dispatch through demand response in the Canary Islands' water supply sector. The results show that demand shifting increases self-sufficiency and RES utilization, with the highest self-sufficiency achieved by combining both PV and wind power. Authors in [52] proposed a MILP-based short-term scheduling approach for desalination unit operation and thermal power unit scheduling. It includes water energy storage and BES integration with power flow constraints. The authors demonstrate that the model significantly reduces system operation costs and recommend its use for future water-energy nexus challenges. Before mentioned studies in sections 1.1 and 1.2 deploy the LP optimisation approach for water-energy system analysis [13],[14],[17], [22],[24],[25],[27].

1.4. Proposed paper contribution

The proposed study presents a comprehensive assessment of water and energy systems through an optimization framework, providing the optimal dispatch of water and energy streams while determining

the optimal capacities for BES and RES. This approach incorporates water storage and PtW technology, offering a novel perspective on integrated water-energy system optimization.

Existing research highlights a gap in the holistic optimization of capacity and dispatch for islanded systems, particularly those experiencing pronounced seasonality.

While some studies focus on detailed optimization of energy systems or storage capacities, they often neglect the integration of water storage and water system optimization. Conversely, studies cantered on water systems rarely include RES or energy storage capacity optimization or extend their analyses to shorter time horizons.

The literature review underscores the absence of a broader optimization framework that simultaneously addresses water and energy system capacities and their operational dispatch, alongside storage solutions. To bridge this gap, this study proposes an innovative implementation of MILP model that optimizes RES and BES capacities, coupled with water systems through RO desalination unit and water storage supported by PtW technology.

Unlike the traditional approach in water-energy system analysis, which often focuses solely on BES capacity optimization, this study adopts a more detailed methodology. Similar to advanced studies [22],[25],[26],[27] the proposed model considers both BES capacity and power rating as variables. It extends this approach by including RES capacity optimization, water system modelling, and water storage integration. Additionally, the model provides an optimized hourly dispatch for RES (primarily PV power), BES, grid connection, and RO desalination for a full one-year period, offering insights into enhanced system flexibility and integration through PtW.

The proposed integrated water-energy system model delivers optimal system capacities and the dispatch of energy and water streams. Notably, the study addresses the unique challenges faced by smaller-scale island systems, which are often overlooked in larger-scale water-energy nexus analyses. These systems are particularly affected by tourism-induced demand fluctuations, which can cause up to tenfold variations in total system demand. By focusing on the Croatian island of Unije as a case study, the research provides valuable insights into island-specific dynamics, with detailed case data presented in Section 3.

Furthermore, the study explores the impact of varying PV and BES investment costs, offering a range of optimal solutions based on different cost scenarios. This analysis provides a comprehensive overview of system operational capacities and economic performance, which can inform practical assessments of water-energy systems in islands and remote areas. Finally, the effects of changes in grid electricity prices, PV potential, and water demand on optimal system configuration and financial outcomes are thoroughly evaluated, making the findings highly relevant for future applications and decision-making in water-energy system design.

1.5. Paper organization

The remainder of the proposed study is divided into: Section 2 where a detailed description of the proposed MILP based water-energy system optimisation model, and modelling framework is presented. The Section 3 follows with clarification on case study, used input data and assumptions for the specific parameters, demand curves, price curves etc. The Section 0 presents a detailed analysis and discussion of the optimal water-energy system configuration for Unije Island, focusing on the joint RES, water and BES storage operation. Additional change in grid electricity price, PV potential, and water demand is shown after base results. Finally, conclusion and future work is provided in the Section 5.

2. Method - Water-energy nexus model

A MILP optimisation approach for optimising integrated water and energy systems is proposed, offering the flexibility to incorporate any water production, treatment, or storage technology, as well as any electricity generation or storage technology, with the inclusion of energy to water system connection.

This model is designed to identify the optimal dispatch of water and energy streams while simultaneously determining the optimal system capacities. The framework is highly adaptable, enabling users to include various technologies depending on specific system requirements, as illustrated in Figure 1.

The model was applied to optimize the dispatch of water and energy system components while determining the optimal sizing of electricity generation technologies, storage power and energy capacities, and key water system parameters.

In the proposed setup, PV generation was selected as a main power source to support the sustainability and study the RES integration. Additionally, a grid connection was incorporated to evaluate the economic implications of RES and storage integration into existing island water-energy system, which traditionally rely heavily on grid connections and/or fossil electricity generation technologies.

To assess the impact of Power-to-Water (PtW) through the operation of a desalination unit, water storage was included as a component of the water-energy system optimization model. Furthermore, to explore the interactions between electricity generation and various storage options, a BES storage system was incorporated, with both its optimal capacity and power values modelled. The sets, variables, and parameters used in the model are comprehensively detailed in Nomenclature.

The modelling framework operates on a yearly time horizon, allowing the user to select a desired time step for their specific application. In this study, an hourly time step was chosen as a balance between achieving high temporal resolution and maintaining reasonable computational efficiency. This selection reflects the trade-offs inherent in optimization models, particularly MILP formulations, which are more computationally intensive than basic LP models and depend heavily on system hardware configurations. However, the framework is flexible, permitting the use of higher-resolution time steps if supported by advanced computational resources.

The optimization problem was implemented in Python 3.7 using the GUROBI solver for mathematical optimization. The GUROBI Python extension module (gurobipy) was installed and integrated into the Python environment to enable efficient execution. All optimizations were performed on a workstation equipped with two Intel Xeon E5-2623 v3 CPUs and 64 GB of RAM, with an average runtime of approximately 30 minutes per optimization run.

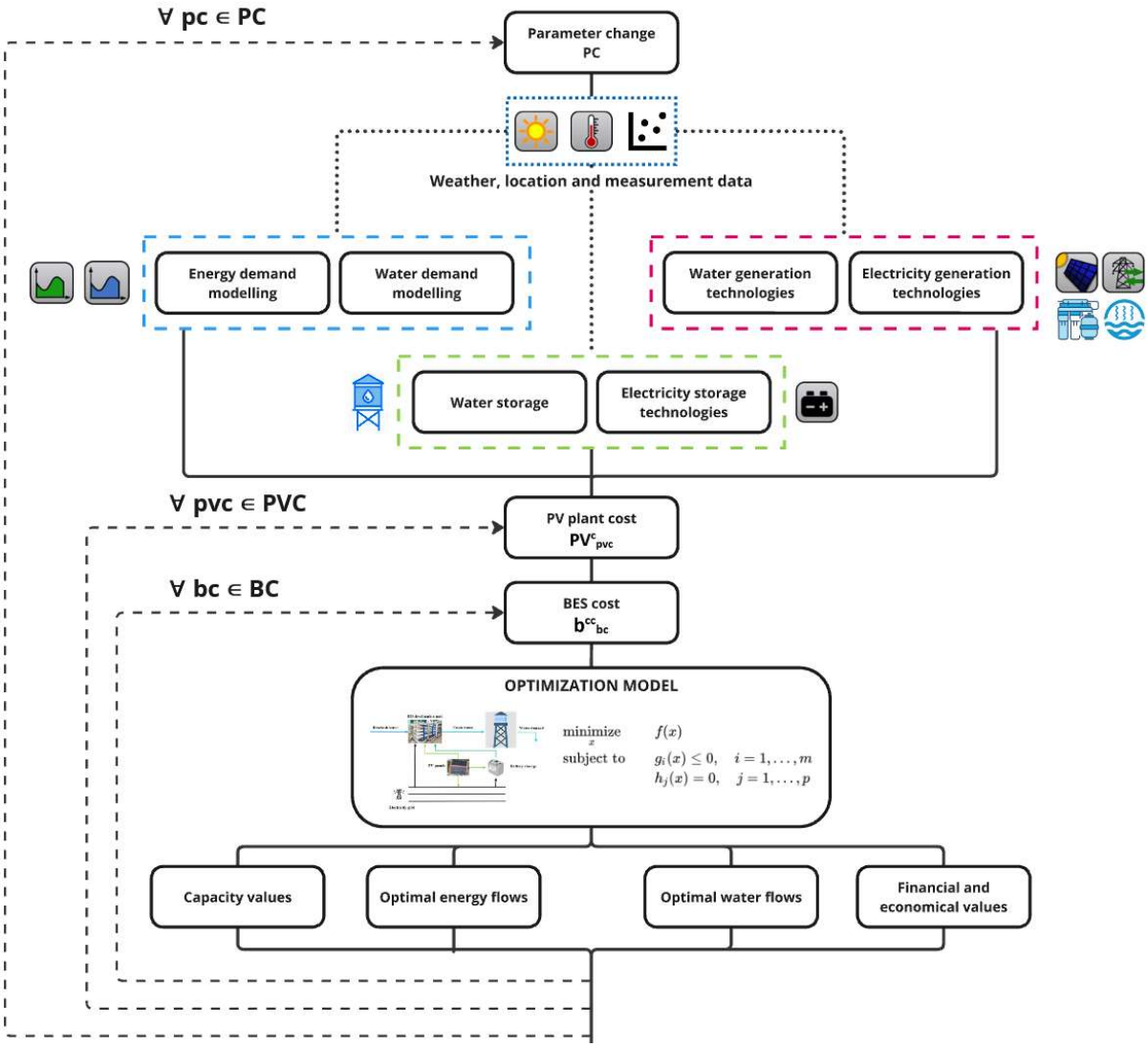

Figure 1. Schematic of the modelling and optimization approach

Figure 1 illustrates the schematic of the proposed modelling and optimization approach, which can be divided into three main sections.

The first section focuses on the selection of system-side technologies and the definition of input parameters along with representative time-series data. This includes identifying water generation and/or treatment technologies and energy system technologies, enclosed within the dashed red rectangle. Additionally, the selection of storage options, encompassing both water and energy storage systems, is highlighted within the dashed green rectangle. Depending on the defined system boundaries, inputs in the form of energy demand and/or water demand may be required. To address this, weather data, site-specific information, and existing measurement datasets are modelled to generate tailored demand profiles, represented within the dashed and dotted blue rectangles.

In the proposed case study, the system boundary encompasses the desalination unit, the associated water pipeline system, and water storage. Consequently, water demand is the primary input, while electricity demand is derived as an output of the optimization process, based on the optimal operation of the desalination unit and the selected PV and energy storage configurations. However, in cases where the system boundary includes broader energy systems, additional energy demand inputs may be necessary, as indicated in the Figure 1.

The second section outlines the optimization approach, which is structured around variations in specific parameters, PV investment cost, and BES investment cost. Changes in specific parameters are represented by the outermost loop, while changes in PV and BES investment costs are captured within two nested inner loops, illustrated with black dashed lines in the schematic.

The outermost loop represents variations in key parameters that significantly influence the optimal configuration and dispatch of the water-energy system. For each parameter change pc within the parameter change set (pc ∈ PC), a set of optimization runs is performed. Each selected parameter itself represents a set of different parameter changes based on which set of optimisation runs is made. Therefore, a set of grid electricity price change ($\varepsilon \in \Omega_E$), set of PV potential change ($\kappa \in \Omega_K$), and set of water demand change ($\psi \in \Omega_\Psi$) was selected as important parameters change.

The second loop corresponds to changes in PV investment cost. For each value pvc within the PV cost set (pvc ∈ PVC), an optimization run is executed. Nested within this loop, the third and innermost loop addresses variations in BES investment cost. For each value bc within the BES investment cost set (bc ∈ BC), an optimization run is initiated. Each run aims to minimize the objective function, ultimately determining the optimal configuration of the water-energy system under the given parameter conditions.

The third section presents the outputs of the proposed framework, including optimal system capacities, time-step-based energy and water flows, and key financial and economic indicators. By performing multiple optimization runs, the framework generates a comprehensive set of results detailing the optimal water-energy system configurations under varying PV and BES investment costs. Additionally, variations in the three key parameters provide insights into the impacts on overall system profitability, optimal renewable energy and storage capacities, and the dispatch of water and energy systems.

An optimisation model objective function and main model constraints are shown below. The first paragraph explains the main objective function and what it is composed of. The following paragraph shows the main constraints regarding the proposed energy system while the last paragraph discusses on the constraints for the water system and its connection to energy system.

The objective function is composed of the sum of the system costs, and potential financial and economical savings which can be seen in equation (1).

$$\begin{aligned}\min \quad & \sum_t e^{P}_t \cdot G^{D}_{pvc,\,bc,\,t} + \sum_t e^{P}_t \cdot B^{CH,G}_{pvc,\,bc,\,t} + \sum_t w^{BC} \cdot W^{B}_{pvc,\,bc,\,t} + \sum_t ll^{c} \cdot LL_{pvc,\,bc,\,t} + \\ & \sum_t pv^{var} \cdot PV^{E}_{pvc,\,bc,\,t} + B^{C}_{pvc,\,bc} \cdot b^{MCC} + B^{NP}_{pvc,\,bc} \cdot b^{MPC} - \sum_t e^{P}_t \cdot PV^{D}_{pvc,\,bc,\,t} - \sum_t e^{S}_t \cdot PV^{G}_{pvc,\,bc,\,t} - \\ & \sum_t e^{P}_t \cdot B^{DC}_{pvc,\,bc,\,t} + B^{C}_{pvc,\,bc} \cdot b^{CC}{}_{bc} \cdot \zeta \cdot cr + B^{NP}_{pvc,\,bc} \cdot b^{PC}{}_{bc} \cdot (1-\zeta) \cdot cr + \\ & PV^{P}_{pvc,\,bc} \cdot pv^{C}{}_{pvc} \cdot cr + B^{C}_{pvc,\,bc} \cdot b^{CC}{}_{bc} \cdot icdf \cdot pvf \cdot \zeta \cdot cr + B^{NP}_{pvc,\,bc} \cdot b^{PC}{}_{bc} \cdot icdf \cdot pvf \cdot (1- \\ & \zeta) \cdot cr, \quad (\forall\, pvc \in PVC, \forall\, bc \in BC, \forall\, t \in T)\end{aligned} \tag{1}$$

The objective function of the proposed problem is to minimize the total system cost on the annual basis. It encompasses several components, each representing a specific cost or saving within the system. These components can be categorized as follows:

- Grid electricity cost - the grid electricity cost is a significant component of the objective function. It is composed of two terms where the first one represents the cost of grid electricity required for running the desalination unit, while the second term represents the cumulative cost of grid electricity used for charging the BES. These costs directly impact the operational expenses of the system, and are shown as the first two summations in the equation 1,
- Cost of water boat carriers - in situations where the desalination unit cannot produce sufficient fresh water to meet the demand, water boat carriers are utilized. This component in the objective function represents the cost associated with employing water boat carriers for the transportation of water. It captures the expenses incurred when alternative means are required to fulfil the water demand. The water boat carriers in optimisation approach can also be seen as a loss of load on a water supply side,
- Lost load cost - the objective function includes a term that represents the lost load cost for electricity production. This cost arises when the system is unable to meet the electricity demand,

resulting in a loss of potential revenue. By considering this cost, the objective function accounts for the economic consequences of insufficient electricity production,

- Variable cost of PV electricity generation - the objective function incorporates a term that represents the variable cost associated with using PV for electricity generation. This component includes expenses related to the maintenance, operation, and other variable costs specific for the PV technology,
- BES maintenance cost
- Financial and economical savings - the summations with negative signs represent the financial or economical savings generated by the system operation. These savings can be further divided into savings due to the direct PV usage for desalination purposes, earnings from excess PV generation sold to the grid, and savings due to BES usage, respectively seen as a negative summation in the equation 1,
- Annualized investment cost - reflects the expenses incurred for the initial setup, installation, and financing of these renewable energy components. It is worth noting that the general approach of using only BES capacity as the variable in the objective function is here further divided into the battery storage capacity in kWh, and nominal BES power kW where ζ represents the weighting factor for the two battery storage costs. The base case value for the ζ is 0.5,
- Annualized BES replacement cost – reflects the annualised expenses for the replacement of BES in year *ry.* Factor *icdf* represents the BES investment cost decrease factor for a year *ry,* while present value factor *pvf* determines the present value of the future BES replacement cost.

Model is additionally constrained by the equations and inequalities (2)-(28) that are simulating the physical energy and water flows, as well as the physical boundaries for the water-energy system operation based on the RES and BES. Below are the main constraints regarding the energy system side.

Equation (2) represents the demand-supply balance where on the LHS of the equation are energy input variables such as PV generation, BES discharge and grid connection, while the RHS of the equation is composed of the electricity demand and lost load variables.

$$PV^{D}_{pc,\,pvc,\,bc,\,t} + B^{DC}_{pc,\,pvc,\,bc,\,t} + G^{D}_{pc,\,pvc,\,bc,\,t} = E^{D}_{pc,\,pvc,\,bc,\,t} - LL_{pc,\,pvc,\,bc,\,t}, \quad (\forall\, pvc \in PVC, \forall\, bc \in BC, \forall\, t \in T) \tag{2}$$

Constraints ranging from (3)-(16) describe the energy system side and specific limitations on BES operation. Equation (3) represents the BES state-of-charge (SOC) for each timestep t ∈ [1, T]. The RHS of the BES SOC equation is composed of the SOC in the previous time step with the inclusion of self-discharge, BES grid and PV charging and charging efficiency, and BES discharge and its corresponding discharge efficiency. Set of constraints from (4)-(7) gives further limits on the BES SOC and capacity. Equation (4) sets the starting SOC in time step t=0 as a percentage of global BES capacity while constraint (5) limits the final SOC in the time step t=T to values higher or equal to the staring BES SOC. To further model BES operation in a sense of capacity preservation, equations (6) and (7) limit the lower and upper usable BES capacity. As model differentiates BES power and capacity, further limitations on BES nominal power output are shown in constraints (8)-(11).

Constraints (8) and (9) represent the upper and lower limits on the time-step based power output, respectively. Global nominal BES power output is the upper limit for the time-step based power output values and shown in the constraint (10). Similarly, constraint (11) limits that time-step based power output is lower than the global nominal BES capacity.

$$B^{SOC}_{pvc,\,bc,\,t} = B^{SOC}_{pvc,\,bc,\,t-1}\cdot(1-b^{sd}) + (B^{CH,G}_{pvc,\,bc,\,t} + B^{CH,PV}_{pvc,\,bc,\,t})\cdot b^{ch,\eta} - {B^{DC}_{pvc,\,bc,\,t}}/{b^{dc,\eta}}, \quad (\forall\, pvc \in PVC, \forall\, bc \in BC, \forall\, t \in [1, T]) \tag{3}$$

$$B^{SOC}_{pvc,\,bc,\,t} = b^{SOC}_{t0}\cdot B^{C}_{pvc,\,bc}, \quad (\forall\, pvc \in PVC, \forall\, bc \in BC, t = 0) \tag{4}$$

$$B^{SOC}_{pvc,\,bc,\,t} \geq b^{SOC}_{t0} \cdot B^{C}_{pvc,\,bc}, \quad (\forall\, pvc \in PVC, \forall\, bc \in BC, t = T) \tag{5}$$

$$B^{C}_{pvc,\,bc} \cdot b^{SOC,max} \geq B^{SOC}_{pvc,\,bc,\,t}, \quad (\forall\, pvc \in PVC, \forall\, bc \in BC, \forall\, t \in T) \tag{6}$$

$$B^{C}_{pvc,\,bc} \cdot b^{SOC,min} \leq B^{SOC}_{pvc,\,bc,\,t}, \quad (\forall\, pvc \in PVC, \forall\, bc \in BC, \forall\, t \in T) \tag{7}$$

$$B^{P}_{pvc,\,bc,\,t} \leq b^{P,max}, \quad (\forall\, pvc \in PVC, \forall\, bc \in BC, \forall\, t \in T) \tag{8}$$

$$B^{P}_{pvc,\,bc,\,t} \geq b^{P,min}, \quad (\forall\, pvc \in PVC, \forall\, bc \in BC, \forall\, t \in T) \tag{9}$$

$$B^{NP}_{pvc,\,bc} \geq B^{P}_{pvc,\,bc,\,t}, \quad (\forall\, pvc \in PVC, \forall\, bc \in BC, \forall\, t \in T) \tag{10}$$

$$B^{C}_{pvc,\,bc} \geq B^{P}_{pvc,\,bc,\,t}, \quad (\forall\, pvc \in PVC, \forall\, bc \in BC, \forall\, t \in T) \tag{11}$$

Further constraints ranging from (12)-(14) show the connection between the time-step based BES power output/input and its energy equivalent for selected time-step Δt. X variables are binary variables limiting that only one operation, either BES charging or discharging, can be done in one time-step and it is shown in constraints (15) and (16). The abovementioned constrains are adding mixed-integer part in the linear programming problem. Furthermore, one can see that multiplication of variables sets this problem as quadratic, and not linear. Hence, this model can be expressed as MIQCP problem. Even though the GUROBI solver, which was used for this study, automatically does linearization of multiplication of two variables, additional linearization of constraints (12)-(14) can be done using upper and lower BES power limits per common linearization technique [53], making a problem MILP.

$$B^{CH,PV}_{pvc,\,bc,\,t} \leq B^{P}_{pvc,\,bc,\,t} \cdot \Delta t \cdot X^{PV}_{pvc,\,bc,\,t}, \quad (\forall\, pvc \in PVC, \forall\, bc \in BC, \forall\, t \in T) \tag{12}$$

$$B^{CH,G}_{pvc,\,bc,\,t} \leq B^{P}_{pvc,\,bc,\,t} \cdot \Delta t \cdot X^{G}_{pvc,\,bc,\,t}, \quad (\forall\, pvc \in PVC, \forall\, bc \in BC, \forall\, t \in T) \tag{13}$$

$$B^{DC}_{pvc,\,bc,\,t} \leq B^{P}_{pvc,\,bc,\,t} \cdot \Delta t \cdot X^{DC}_{pvc,\,bc,\,t}, \quad (\forall\, pvc \in PVC, \forall\, bc \in BC, \forall\, t \in T) \tag{14}$$

$$X^{PV}_{pvc,\,bc,\,t} + X^{DC}_{pvc,\,bc,\,t} \leq 1, \quad (\forall\, pvc \in PVC, \forall\, bc \in BC, \forall\, t \in T) \tag{15}$$

$$X^{G}_{pvc,\,bc,\,t} + X^{DC}_{pvc,\,bc,\,t} \leq 1, \quad (\forall\, pvc \in PVC, \forall\, bc \in BC, \forall\, t \in T) \tag{16}$$

Limitations and energy flows regarding the PV generation are shown in constraints (17)-(21). Equation (17) shows that energy generated from PV can be used for direct energy consumption, BES charging or be sold to the grid. Equation (18) shows a simple PV generation form through the usage of PV potential parameter $pv^{S}_{\kappa,t}$ in kWh/kW. The approach of open-source EHDO tool authors for PV generation was used [54]. The *solar_modelling.py* script uses data such as location, elevation, azimuth, weather data, PV module data etc. to find the time-step based PV potential and can be accessed on EHDO Github page [55]. The dependence between the nominal BES power cost and nominal BES capacity cost is shown in the equation (19) where the base value of 0.5 vas used. Equations (20) and (21) represent the grid electricity price curve and selling electricity price curve, respectively. The connection between the grid electricity price and selling electricity price is determined by the parameter γ, often recognised as buy-back factor.

$$PV^{D}_{pvc,\,bc,\,t} + B^{CH,PV}_{pvc,\,bc,\,t} + PV^{G}_{pvc,\,bc,\,t} = PV^{E}_{pvc,\,bc,\,t}, \quad (\forall\, pvc \in PVC, \forall\, bc \in BC, \forall\, t \in T) \tag{17}$$

$$PV^{E}_{pvc,\,bc,\,t} = PV^{P}_{pvc,\,bc,\,t} \cdot pv^{S}_{t}, \quad (\forall\, pvc \in PVC, \forall\, bc \in BC, \forall\, t \in T) \tag{18}$$

$$b^{PC}_{bc} = {}^{b^{CC}_{bc}}\!/_{r}, \quad (\forall\, bc \in BC) \tag{19}$$

$$e^{P}_{t} = e^{P}_{t} \cdot \varepsilon, \quad (\forall\, t \in T) \tag{20}$$

$$e^{S}_{t} = e^{P}_{t} \cdot \gamma, \quad (\forall\, t \in T) \tag{21}$$

Constraints on water system side are shown in set of equations ranging from (22) to (28). Equation (22) represents the water storage level for each timestep t ∈ [1, T]. The RHS of the water storage level is composed of the previous time step water level, addition of water production and water boat carriers' coverage, and subtracted by the water demand. The water production in proposed model is limited only to the water desalination, but further model development will include the other water production technologies to have wider water production possibilities similar to the energy system side.

Set of equations (23)-(26) further limit the water storage operation similarly to the energy system side for the BES SOC constraints. Equation (23) sets the starting water storage level in time step t=0 as a percentage of available water storage capacity while constraint (24) limits final water storage level, in the time step t=T, to values higher or equal to the staring water storage level. Further limitations shown in equations (25) and (26) limit the water storage level between the maximum and minimum values, respectively. Connection between the water and energy system can be observed in the equation (27) where electricity demand is dependent on water production and water production efficiency. The base water production efficiency is generally technology dependent, and here only the water desalination technology is being used. However, the model can include multiple water production and treatment options. Similar to connection between the time-step based BES power output/input and its energy equivalent, the equation (28) limits that the water production in time-step Δt cannot be higher than the installed water production technology generally displayed in m^3/h multiplied by the time-step Δt.

$$W^{L}_{pvc,\,bc,\,t} = W^{L}_{pvc,\,bc,\,t-1} + W^{D}_{pvc,\,bc,\,t} + W^{B}_{pvc,\,bc,\,t} - w^{D}_{t}, \quad (\forall\, pvc \in PVC, \forall\, bc \in BC, \forall\, t \in [1, T]) \tag{22}$$

$$W^{L}_{pvc,\,bc,\,t} = w^{LC} \cdot w^{L}_{t0}, \quad (\forall\, pvc \in PVC, \forall\, bc \in BC, t = 0) \tag{23}$$

$$W^{L}_{pvc,\,bc,\,t} \geq w^{LC} \cdot w^{L}_{t0}, \quad (\forall\, pvc \in PVC, \forall\, bc \in BC, t = T) \tag{24}$$

$$W^{L}_{pvc,\,bc,\,t} \leq w^{LC} \cdot w^{L,max}, \quad (\forall\, pvc \in PVC, \forall\, bc \in BC, \forall\, t \in T) \tag{25}$$

$$W^{L}_{pvc,\,bc,\,t} \geq w^{LC} \cdot w^{L,min}, \quad (\forall\, pvc \in PVC, \forall\, bc \in BC, \forall\, t \in T) \tag{26}$$

$$E^{D}_{pvc,\,bc,\,t} = W^{D}_{pvc,\,bc,\,t} \cdot d^{\eta}, \quad (\forall\, pvc \in PVC, \forall\, bc \in BC, \forall\, t \in T) \tag{27}$$

$$d^{C} \cdot \Delta t \geq W^{D}_{pvc,\,bc,\,t}, \quad (\forall\, pvc \in PVC, \forall\, bc \in BC, \forall\, t \in T) \tag{28}$$

3. Case study: Unije Island

The Unije island is a small island located in the northern part of the Adriatic Sea, part of the larger Cres-Lošinj archipelago, Croatia. The total island area is 16.77 km^2, with a 36.6 km long indented coast. Based on the 2021 census, Unije has 35 private households with 66 permanent inhabitants, while the total number of people in the summer months can rise up to 500 numbering total households to 439 [56].

The population has notable seasonal fluctuations, with an increase in numbers during the summer months brought on by the influx of tourists. This demographic pattern is representative of more general trends seen in many Adriatic islands, where aging and depopulation coexist with sporadic spikes in population brought on by tourism. The weather in Unije is Mediterranean, with hot, dry summers and warm, rainy winters. The climate of the island is suitable for a range of agricultural activities, especially for the cultivation of olives, grapes, and other commodities that are essential to the regional economy. The typical monthly average temperature varies from 7.8 °C in January to 24.6 °C in August, with an annual mean temperature of about 15.3 °C. The island experiences approximately 900 mm of precipitation on average per year, most of which falls in the fall and early winter, in line with the Mediterranean climate [57].

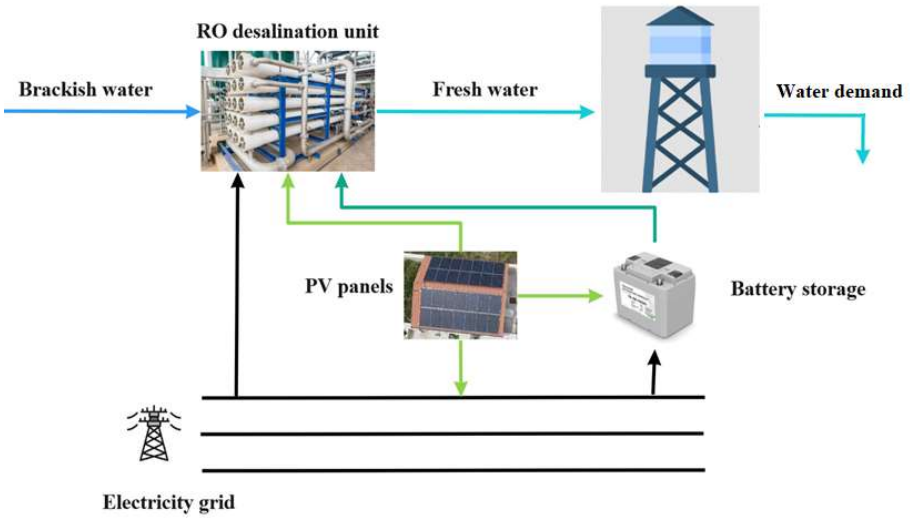

Figure 2. Schematics of water-energy flows for the Unije Island case study

Figure 2 provides a schematic representation of the modelled water-energy system on Unije Island. The water system consists of a RO desalination unit, a water pipeline network, and a primary water storage tank. The energy system includes a PV plant, BES storage and a grid connection. The desalination unit utilizes brackish water from the local aquifer, resulting in an overall energy consumption of 2.5 kWh/m³. The existing water storage tank has a capacity of 400 m³. Hourly water demand data, obtained from the local water utility, is presented in Figure 3. Besides the water hourly demand values, Figure 3 is showing data on number of people on the island and the air temperature values giving the view on the island seasonality and tourism effect. Additional parameter values related to the water system side can be seen in the Table 1.

Table 1. Water system input parameters

Water system input parameters	Model parameter name	Value	Unit
Desalination unit specific consumption	d^{η}	2.5	kWh/m^3
Desalination unit nominal capacity	d^{c}	200	m^3/day
Total water demand	w^{D}_{t}	15939.82	m^3/a
Water storage capacity	w^{LC}	400	m^3
Starting water level	w^{L}_{t0}	40%	% of WS
Max water level	$w^{L,max}$	100%	% of WS
Min water level	$w^{L,min}$	20%	% of WS
Water boat carrier cost	w^{BC}	25	EUR/m^3

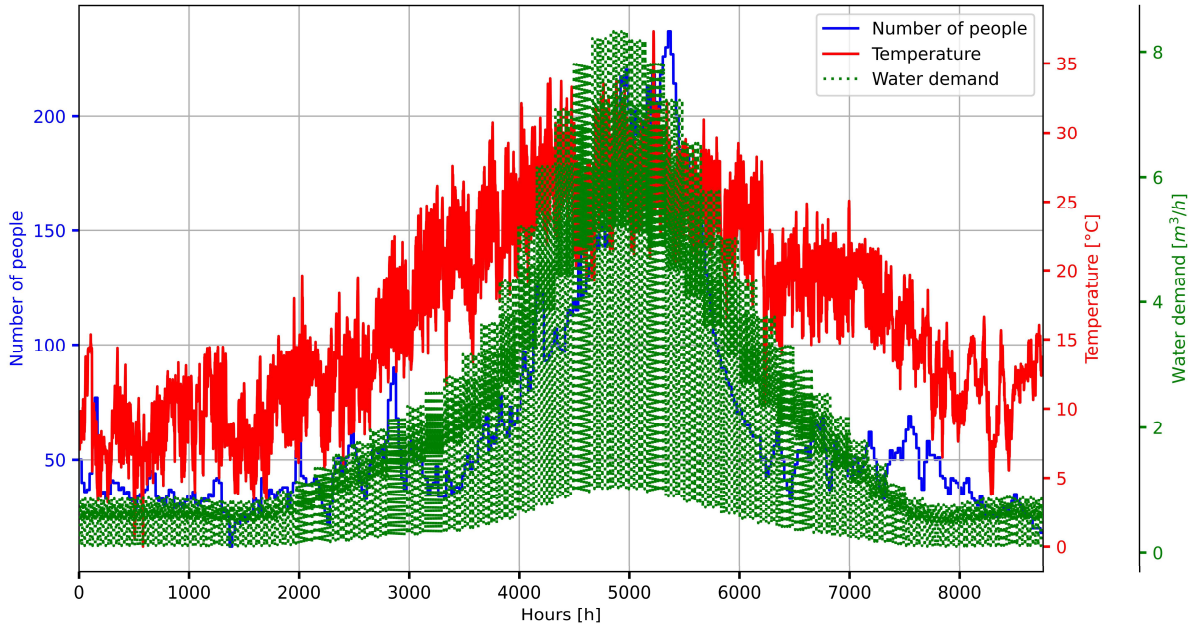

Figure 3. Input data curves for Unije Island

In Croatia, most electricity consumers use a two-tariff pricing model, which was adopted in this study. However, the framework is flexible and can accommodate any electricity price curve. A higher daytime tariff of 130 EUR/MWh was applied between 7 a.m. and 9 p.m., while a lower nighttime tariff of 60 EUR/MWh was applied from 9 p.m. to 7 a.m. The electricity price curve also accounted for daylight saving time adjustments.

To distinguish between electricity purchase and sale prices, a buyback parameter (γ) was introduced. For the Croatian case, any excess electricity sold back to the grid, rather than used for self-consumption, is multiplied by a buyback rate of 0.4. This implies that 60% of potential savings are lost for every kWh sold back to the grid instead of being utilized for self-consumption.

As outlined in Section 2, the methodology for calculating hourly PV generation potential in kWh/kW was adopted from the approach presented by the authors in [54]. The PV investment cost was treated as a variable parameter, reflecting the current market conditions and actual investment costs relevant to the Croatian context. Specifically, with average PV investment costs in Croatia ranging between 1100 and 1200 EUR/kW, the selected range extended from a minimum of 900 EUR/kW to a maximum of 1400 EUR/kW. Additionally, the NREL report [58] was referenced to determine the variable cost of PV power generation, which was calculated as 7.61 EUR/MWh.

Similarly to the PV investment cost range, the BES investment cost range was determined based on current market conditions and real-world investment costs specific to Croatia. As there are only a few existing BES projects in Croatia, available data indicate that BES capacity investment costs remain relatively high, averaging between 500 and 600 EUR/kWh. However, given global trends and the ongoing decline in BES costs, it was assumed that these costs would continue to decrease. Consequently, the selected range spans from a minimum investment cost of 50 EUR/kWh to a maximum of 600 EUR/kWh. Based on this defined BES capacity cost range and the parameter *r,* representing the ratio of BES capacity cost to BES power cost, the BES power investment cost was calculated. To calculate future investment cost for BES replacement, a NREL report [59] was used. A mid-cost decrease projection for BES investment was used resulting with the investment cost decrease factor *icdf* of 0.6. Additional input parameters related to BES utilization are provided in Table 2.

Table 2. BES usage input parameters

BES usage input parameters	Model parameter name	Value	Unit
Minimum BES power output	$b^{P,\,min}$	0	kW
Minimum BES power output	$b^{P,\,max}$	25	kW
BES charge efficiency	$b^{ch,\eta}$	90%	-
BES discharge efficiency	$b^{dc,\eta}$	90%	-
BES self-discharge rate	b^{sd}	1%	% of BES capacity per Month
BES starting SOC	$b^{soc}{}_{t0}$	50%	% of BES capacity
Minimum BES SOC	$b^{soc,\,min}$	20%	% of BES capacity
Maximum BES SOC	$b^{soc,\,max}$	100%	% of BES capacity
BES capacity maintenance cost	b^{MCC}	0.38	EUR/kWh/a [27]
BES power maintenance cost	b^{MPC}	3.22	EUR/kW/a [27]

Annualization of investment cost are with the life-time of technology of 25 years, and the average financial discount rate of 5%. It was assumed that BES replacement is needed in 12^{th} year of studied 25 years project life-time.

4. Results and discussion

The below section present a detailed analysis of the optimal water-energy system configuration for Unije Island, focusing on the joint PV and storage operation. The study examines how variations in PV and BES investment costs influence the system's operational capacities and its overall financial and economic performance. Through a series of optimization runs, the analysis provides insights into the optimal system operation under different cost scenarios, represented by 3D diagrams that map the relationships between PV power, BES storage, and investment costs. The below results and discussion explores how the optimal PV power values change in response to different BES and PV investment costs.

The analysis explores the influence of BES on system performance, emphasizing how variations in BES capacity affect the optimal PV power and the corresponding objective function values, which reflect the system's financial and economic outcomes. Additionally, the study examines BES utilization and its role in enhancing system efficiency, focusing on the interplay between BES power and capacity and their collective impact on storage utilization and overall system savings. This includes a detailed assessment of how BES capacity affects the required BES power and how these parameters together optimize energy storage performance.

The findings further highlight the broader implications for adopting renewable energy and storage solutions, particularly in regions like Unije Island, where seasonal variability significantly impacts energy and water demand. Finally, additional analysis was conducted to evaluate the impact of key parameter changes on the optimal configuration and economic profitability of the future water-energy system on the Unije island. Parameter change analysis systematically varied critical parameters, such as grid electricity price, PV potential, and water demand, to assess their effects on system capacities, dispatch, and overall economic performance. This analysis lays the groundwork for further discussions on the integration of renewable energy sources and storage technologies in contexts characterized by dynamic energy and resource demands.

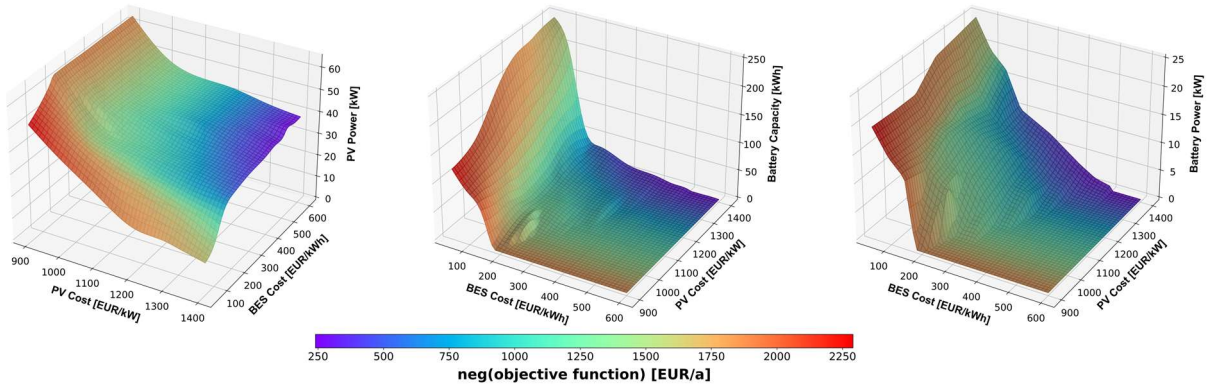

Figure 4. Range of optimal base case capacity results for Unije Island's water-energy system; PV power (left); BES capacity (middle); BES power (right)

The Figure 4 is showing main capacity results regarding the optimal water-energy system for the Unije Island case study. Each of the point is representing the optimal system operation based on the different PV and BES investment costs which are shown as x and y axes. Hence, the shown 3D diagrams are set of multiple optimization runs for different PV and BES investment costs. All shown results depict the optimal system values.

The objective function is composed of the sum of the system costs, and potential financial and economical savings. As the goal is to minimize the objective function, system costs in the objective function are represented with the plus sign while financial and economic revenues are represented with the negative sign. Therefore, if project is to be profitable, final objective function should be below zero. To make it easier for results representation and avoid negative objective function ranges, we display the negative of objective function (*neg(objective function)*) in the results. Therefore, when the overall system is profitable the *neg(objective function)* will be above zero, while for the ones not profitable will be below zero. In a sense, we display the final profitability indicator as negative of objective function that can be seen in equation (1). In the below results, all surface results will be coloured based on *the neg(objective function)* showing that optimal results for different investment cost pairs that are higher than zero as profitable, and those below zero as not profitable. Furthermore, in below results whenever a PV/BES investment cost pair is referenced in numbers, to maintain clarity, units may be not mentioned. However, whenever a PV/BES investment cost pair is mentioned it references the PV cost in EUR/kW and BES investment cost in EUR/kWh.

One of the main points of proposed research was to see the effect of investment cost change on optimal system values. Furthermore, the important part of the research was to study the effect of storage options, here BES and water storage, on RES implementation and total financial and economical profitability. The first diagram on Figure 4 presents the optimal PV power values across the range of selected PV and BES investment costs. As anticipated, lower PV investment costs correspond to higher optimal PV power capacities. However, the rate of change in PV power capacities exhibits notable variability depending on changes in PV and BES investment costs. For instance, when analysing PV power values at a fixed PV investment cost, it becomes evident that the rate of change in PV power is not uniform but is influenced by the associated BES investment cost. One can observe how PV power value rises with higher average rate of 0.124 kW per EUR/kWh for lower BES investment cost values and smooths out to average rate of 0.049 kW per EUR/kWh when approaching higher BES investment costs. In contrast, when observing PV power values for constant BES investment cost, one can observe that rate change is higher for BES cost values up to 200 EUR/kWh with the average rate decrease of -0.069 kW per EUR/kW increase in PV investment cost. Above the 200 EUR/kWh BES cost threshold, the PV

power rate change is lower with average rate decrease of -0.055 kW per EUR/kW increase in PV investment cost. These results are closely tied to BES usage and the second diagram showing the BES capacity in kWh dependent on the PV and BES investment cost.

It is important to note that the axes for “PV cost” and “BES cost” have been switched in the diagrams for clarity and ease of interpretation. A comparison of the first two diagrams reveals that the rate of change in PV power values is strongly influenced by the corresponding BES capacities. Specifically, a higher rate of decrease in PV power is inversely related to a sharp increase in optimal BES capacities when observing changes at a constant PV investment cost.

This relationship underscores that optimal PV and BES configurations exist where PV power serves as the primary energy producer, maximizing direct usage for desalination in a form PtW storage and storage in the form of BES. Consequently, a decrease in optimal PV power is often accompanied by an increase in BES storage, leading to higher *neg(objective function)* values. This observation challenges the common assumption that lower BES costs, and consequently higher BES capacities, always result in greater RES implementation. Instead, the findings suggest that from an optimization perspective, the most effective PV and BES pair does not necessarily maximize both capacities but achieves the best economic outcome as defined by the objective function.

The common conclusion is still relevant, but it is important to define the objective function which determines the optimal value pairs. Further analysis on financial and economical savings will be discussed further below, and are shown in Figure 7 and Figure 8. It is also relevant to notice that BES usage is justified in broader BES cost range with the increase in PV investment cost. However, it is worth noting that those PV and BES pairs result with quite low *neg(objective function)* values of around 500 EUR/a.

The third diagram in Figure 4 illustrates the relationship between BES nominal power and PV and BES investment costs. The BES nominal power results closely follow the trends observed in the BES capacity plane, with notable differences characterized by a higher rate of change at increased PV investment costs. This elevated rate of change is attributed to the continued presence of constant PV power, even at higher PV costs. Consequently, the BES nominal power distribution reflects a combination of the PV power and BES capacity planes. Scenarios with higher PV power, in conjunction with existing BES capacities, result in an increased requirement for BES nominal power, highlighting the interdependence between these variables. This relationship underscores the importance of simultaneously considering PV power and BES capacity when evaluating the optimal configuration of BES nominal power in the system.

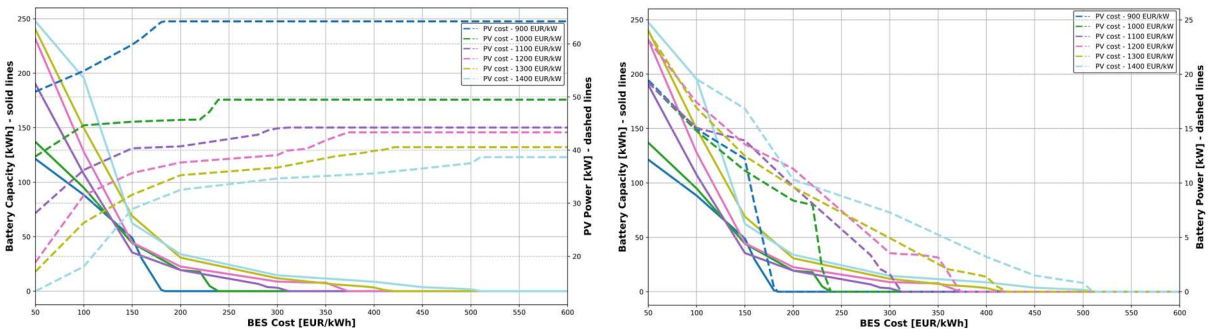

Figure 5. Detailed view on optimal water-energy system capacity values; BES capacity and PV power (left); BES Capacity and BES power (right)

A more detailed analysis of PV power, BES capacity, and BES power is presented in Figure 5. Both diagrams in the figure illustrate results as a function of BES investment costs, displayed along the x-axis. The results are represented as paired solid and dashed lines for each PV investment cost, with each pair distinguished by a consistent colour scheme.

The LHS y-axis in both diagrams corresponds to BES capacity, represented by the solid lines. In the first diagram, the dashed lines indicate PV power values, which are read from the RHS y-axis. Similarly, in the second diagram, the dashed lines represent BES nominal power values, also read from the RHS y-axis. This dual-axis representation provides a comprehensive view of how BES and PV capacities interact across varying BES investment costs, offering insights into their combined impact on system performance and optimization.

The results indicate that higher PV investment costs are associated with a smoother distribution of PV power values, which is directly linked to BES utilization. For lower PV investment costs, the final optimal PV power—represented by the horizontal segments of the dashed lines—is achieved at lower BES cost values. This demonstrates that BES usage becomes more prominent as both PV and BES investment costs increase. Table 3 provides threshold BES cost values below which BES usage is economically justified. In addition to the threshold values, Table 3 also presents the final optimal PV power when BES storage is not utilized and the maximum BES capacities at the lowest BES investment cost. As anticipated, the highest BES utilization occurs at the lowest BES cost of 50 EUR/kWh. However, an intriguing pattern emerges in the BES capacities at this cost. The influence of PV costs on final BES capacity is apparent, and a change from minimum optimal BES capacity of 120.38 kWh to overall maximum BES capacity of 247.60 kWh for PV cost ranges from 900 to 1400 EUR/kW, respectively. These observations highlight the interplay between PV and BES investment costs in determining the optimal capacities, emphasizing the critical role of BES in scenarios with higher investment costs for PV.

Table 3. Overview of base results for ranging PV investment cost – threshold results

PV Cost [EUR/kW]	BES Cost Threshold [EUR/kWh]	PV power w/o BES [kW]	Max BES capacity [kWh]
900	184	64.22	120.38
1000	239	49.48	136.41
1100	312	44.23	189.22
1200	373	43.33	231.49
1300	421	40.54	240.22
1400	510	38.66	247.6

The second diagram in Figure 5, alongside BES capacity, illustrates the BES nominal power values for various PV and BES investment costs. When compared to BES capacity change, we can see that BES power does not have such a high increase in BES power with the increase in PV cost. For example, one can see how BES power at lowest BES cost of 50 EUR/kWh starts with relatively high value of 19.45 kW which is close to the case-study limited power of 25 kW referring the power capacity of the installed desalination unit. With further increase in PV cost, highest BES power is achieved at value of 24.78 kW for PV cost of 1400 EUR/kW.

These findings highlight the necessity of treating BES power and capacity as distinct variables in modelling. In conventional BES modelling approaches that consider only BES capacity, the final optimal BES capacity would likely be underestimated because such models allow charging and discharging to exceed the physical power constraints of the unit. The observed distribution of BES power values, which differ from BES capacity, underscores the importance of explicitly incorporating BES power as an independent variable. This distinction ensures more accurate representation of the physical and operational limits of BES systems, contributing to more reliable optimization results.

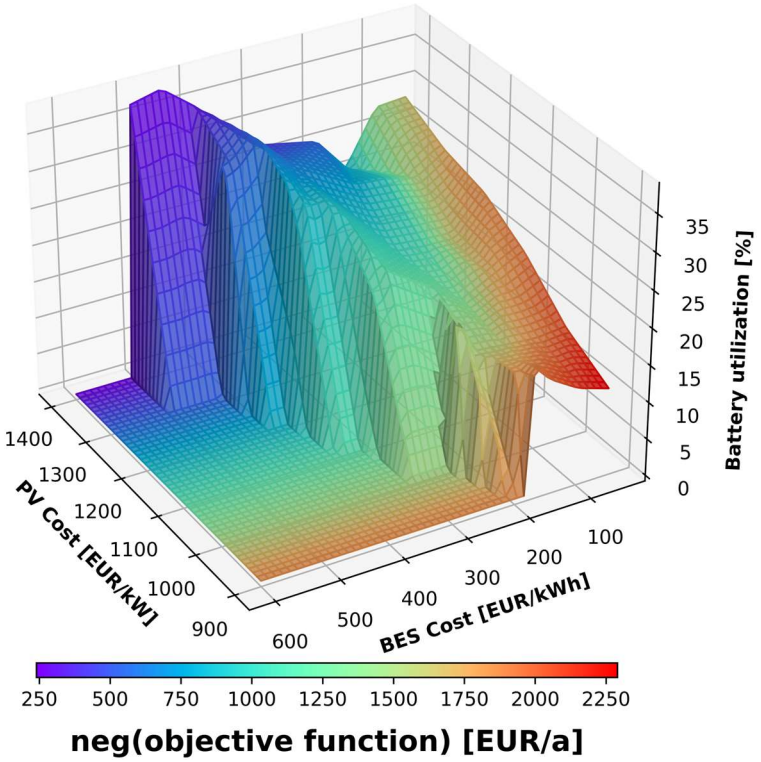

Figure 6. BES utilization parameter

To further evaluate storage utilization and its potential, a BES utilization parameter was developed and is depicted in Figure 6. The BES utilization is defined as the ratio of the energy stored in the BES to the maximum potential energy storage capacity of the BES, calculated on an annual basis and expressed as a percentage. A BES utilization rate of 100% indicates that the storage is being used at full capacity with constant charging and discharging cycles, irrespective of the optimal timing for its operation. While this assumption of full utilization is commonly adopted in research, it does not accurately represent real-world BES operation. The maximum potential energy storage in BES is determined by accounting for both BES power and capacity, under the assumption that every charging cycle is immediately followed by a discharge cycle. This represents the theoretical upper limit of BES cycling potential. Conversely, a BES utilization rate of 0% indicates that the BES is not employed in the optimal system configuration and is effectively excluded from operation. This parameter provides a valuable measure for analysing the role and efficiency of BES in various scenarios and investment cost configurations.

Analysis of BES utilization data reveals an upward trend, where BES utilization increases with higher PV investment costs. This behaviour corresponds to the increase in BES capacity that accompanies higher PV costs. Moreover, it can be concluded that an increase in PV investment cost leads to a shift towards an optimal solution that relies more on BES usage than PV generation, resulting in higher overall BES utilization. In contrast, BES utilization also rises with higher BES investment costs, which seems counterintuitive given the overall decrease in BES capacity. This paradox can be explained by examining the BES power results, where the rate of decline in BES power is smaller than that of BES capacity. Additionally, the highest BES utilization values are observed at threshold BES cost values, where the initial BES usage is economically justified. These optimal solutions typically involve relatively lower BES capacities, which, combined with a smaller rate of decline in BES power, lead to higher BES utilization. Thus, it can be concluded that the highest BES utilization occurs due to a combination of factors: a steeper rate of decline in BES capacity, a smaller decline in BES power, and the influence of lower BES capacity values at the BES cost threshold.

Further important and interesting result is the optimal BES utilization value at the highest *neg(objective function)* point. It is evident that the most profitable optimal solution occurs at the lowest PV and BES investment costs, specifically at a PV cost of 900 EUR/kW and a BES cost of 50 EUR/kWh. This optimal outcome arises from the favourable combination of PV and BES, where PV contributes slightly more to the final solution, while BES serves as storage for excess PV generation, particularly during periods of lower electricity grid tariffs. Moreover, BES utilization exhibits pronounced seasonal behaviour, which is directly tied to the energy and water demand characteristics of the tourist-dependent island of Unije, selected for the case study. Consequently, BES utilization values are expected to be lower, as illustrated in Figure 6, reflecting the system's adaptation to seasonal fluctuations in demand.

As a final remark and discussion starter, one could say that BES utilization results state contradictory conclusions that storage potential is not fully used and has more room for the higher financial and economical savings. However, we would point out reasons why that is not important and what are above results stating. Based on the shown results we state that high BES utilization values are not important for the BES usage justification because the optimization approach gives results that are based on minimisation of objective function which is the sum of all of system costs and potential financial and economical savings. Results are therefore showing that water and energy storage are financially and economically justified for the highly seasonal touristic island and that RES and storage options are jointly taking on the burden of the energy transition. Results of relatively lower BES utilization values for the highest *neg(objective function)* solution shows that there is the optimal PV and BES pair where both take part of the task in providing the financially and economically optimal solution. Therefore, the results are not stating that higher BES capacity are needed at higher PV cost values, but rather that for the optimal energy transition we need both the RES and storage options where with the decrease of investment costs we have optimal combination of RES and storage options that result with the highest financial and economical savings. One could also state that lower BES utilization values go in line with the higher BES lifespan due to the lower numbers of cycles while still achieving the financial and economical benefits. Also worth noting is that provided results do not include external economical benefits such as greenhouse gas emissions savings or health benefits but are to be included in future work expecting that RES and storage options have even higher investment justification.

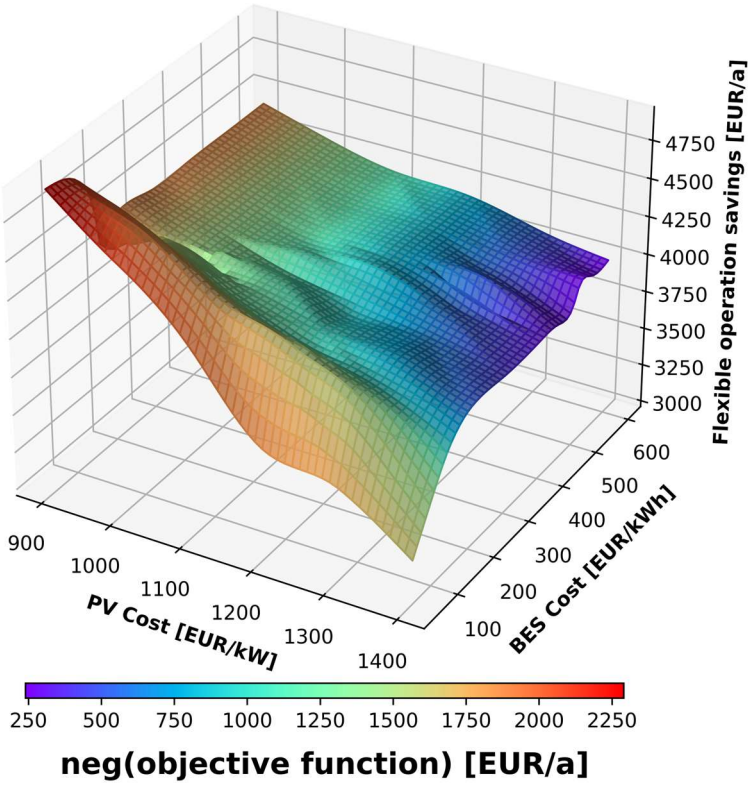

Figure 7. Flexible operation savings

Further below discussion and results follow more closely on financial and economical gains of optimally running water and energy system. Figure 7 is showing the flexible operation savings dependent on different PV and BES investment costs. Flexible operation saving represent a sum of savings due to the usage of storage options. Proposed model differentiates two types of storage options, one being water storage through means of desalination unit (PtW), and BES storage option. Therefore, flexible operation savings represent the sum of savings due to water storage usage where the generated electricity is stored in form of a water for later use, or directly stored in BES. Savings are recognised as any potential difference in RES generated electricity and grid alternative, or the savings due to the electricity tariff difference. To further clarify, any RES generated electricity that is used for the desalination usage, and consequently for water storage, is recognised as a potential saving where the grid electricity price for each time step is used as price alternative. Identical approach for savings due to RES generation being stored in BES was used. The electricity tariff price difference savings can be achieved through means of water or BES storage, where the grid electricity is being used for the desalination usage or BES storage in times of lower tariff, and subsequently used when the grid prices are higher.

Analysing the results in Figure 7, it is evident that the highest flexible operation savings occur at the lowest investment costs for both BES and PV, aligning with the highest *neg(objective function)* point. This behaviour is expected, as higher savings contribute directly to increased *neg(objective function)* values. However, an interesting pattern emerges in the partial fluctuations of overall flexible operation savings as BES capacity increases, which correlates with a reduction in BES investment cost. Since savings are derived from both PtW and BES storage savings, primarily due to PV usage, the main factor differentiating overall flexible operation savings is the specific PV and BES pair combination.

To better understand the behaviour of flexible operation savings, it is crucial to examine the changes in PV power and BES capacity, as shown in Figure 4. When analysing the change in flexible operation savings for a constant PV investment cost, it becomes apparent that the rate of change transitions from a constant decrease in savings at a PV cost of 900 EUR/kW to a constant increase in savings at a PV

cost of 1400 EUR/kW. The continuous decrease and subsequent increase in savings are directly related to the rate changes in PV power and BES capacity. For the 900 EUR/kW PV cost scenario, the increase in PV power is lower than the decrease in BES capacity. This results in a lower increase in PtW storage savings compared to the decrease in BES storage savings, ultimately leading to a reduction in flexible operation savings. In contrast, for a PV cost of 1400 EUR/kW, the higher rate of change for lower BES costs, coupled with the lower rate of change for higher BES costs, results in a positive trend in flexible operation savings.

The primary reason for the lower savings at high PV costs and low BES investment costs is the reduced PV power, which leads to lower PtW storage savings. Despite the highest BES storage savings of 1411.89 EUR/a, aligned with the highest BES capacity, the overall flexible operation savings remain relatively low. As with previous results, it can be concluded that only the optimal combination of both RES and storage yields the highest overall flexible operation savings. When examining the behaviour of flexible operation savings for constant PV costs across the range of investment costs, an interesting pattern emerges. Up to a threshold BES cost of 100 EUR/kWh, there is a rapid increase in savings, followed by a slower decrease in savings. This pattern is directly correlated with changes in PV and BES capacity, influencing the overall savings from RES to water and BES operation.

For constant BES investment costs, the results can be divided into two distinct scenarios. For lower BES costs, savings decrease more rapidly with increasing PV investment costs, which is primarily due to a sharper reduction in PV power compared to the increase in BES capacity. This results in a higher decrease in PtW savings than the increase in BES operation savings. On the other hand, as BES costs rise, the decrease in PV power becomes less pronounced, and the increase in BES capacity slows down, leading to a smaller overall decrease in flexible operation savings.

It is important to note that each data point in the provided results represents the optimal system operation across the entire range of PV and BES investment costs, yielding positive *neg(objective function)* values that state the system profitability. Additionally, when examining flexible operating savings, it is worth mentioning that the absolute difference between the highest and lowest savings is not substantial, amounting to 1676.67 EUR/a. To improve diagram clarity, the z-axis was set to a lower value of 3000 EUR/a. In conclusion, the key takeaway from the flexible system operation savings analysis is that a decrease in both PV and BES investment costs leads to an increase in flexible operation savings, reinforcing the importance of reducing RES and storage investment costs. Furthermore, these results emphasize the critical role of the optimal RES, PtW and BES storage pair, maximizing system performance. Although lower investment costs result in a decrease in optimal PV power and an increase in optimal BES capacity, the overall outcome is the maximization of flexible operation savings, which aligns with the highest *neg(objective function)* values.

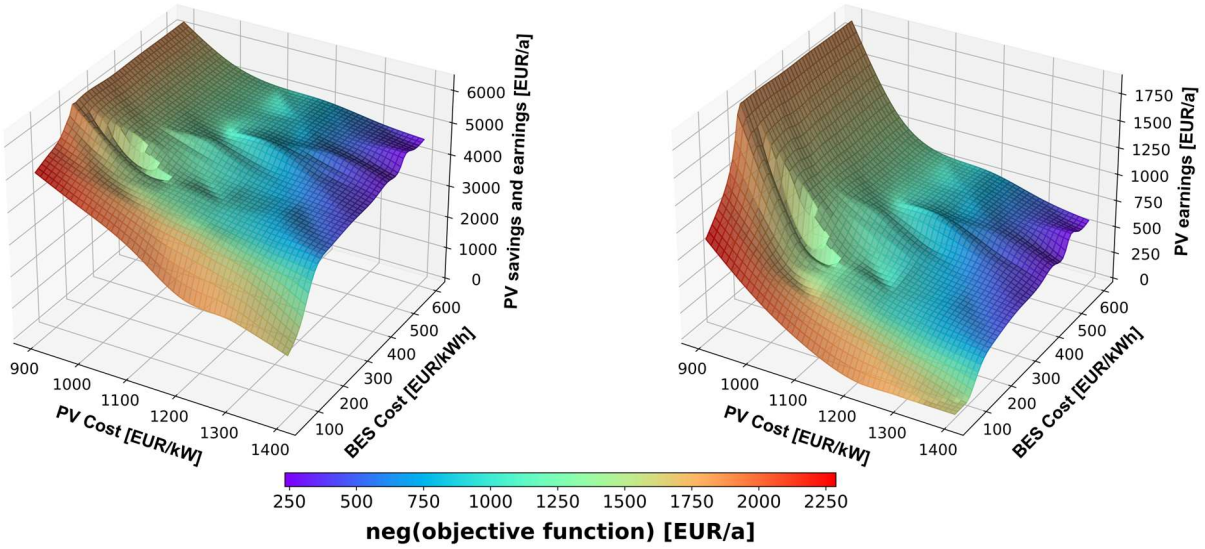

Figure 8. Financial and economical benefits of optimal water-energy system operation; PV savings and earnings (left); PV earnings (right)

Further analysis on financial and economical benefits of optimally running the water and energy system can be seen on Figure 8. Left diagram is showing the sum of savings and earnings due to the PV usage. Similar to flexible operation savings, savings represent economical savings as any potential difference in RES generated electricity and grid alternative. To further clarify, any PV generated electricity that is directly stored in water storage through means of desalination (PtW) is recognised as savings. On the contrary, any excess PV generated electricity that is sold to the grid is recognised as earnings as one directly receives remuneration for that energy stream and can further be seen on second diagram.

By comparing the distribution of PV power in Figure 4 with the first diagram on Figure 8, it is apparent that the PV savings and earnings follow a proportional pattern, with minor variations based on the amount of electricity sold to the grid. The lowest optimal PV power is observed at high PV investment costs and low BES investment costs, which corresponds to the lowest PV savings and earnings at the same investment cost values. As grid electricity is sold at a lower buyback rate, a slight discrepancy between PV power and PV savings and earnings can be observed.

The analysis of PV earnings reveals interesting trends based on different PV and BES investment costs. PV earnings, or the remuneration for electricity sold to the grid, generally follow an increase in PV power. However, the effect of higher BES capacity, driven by a decrease in BES investment costs, becomes evident. As BES investment costs decrease and BES capacity increases, PV earnings begin to drop, eventually reaching zero. This illustrates the relationship between BES capacity and PV earnings, highlighting how increasing BES capacity reduces the need to sell excess PV electricity to the grid.

Table 4. Boundary results for 50 EUR/kWh BES investment cost values

PV investment cost [EUR/kW]	Power to Water Storage		PV to Grid	
	kWh/a	EUR/a	kWh/a	EUR/a
900	32,763.33	4,207.73	17,477.92	908.87
1000	30,232.99	3,892.44	9,475.34	492.49
1100	26,042.44	3,358.26	3,767.93	195.89
1200	19,537.82	2,522.14	214.15	10.98
1300	18,125.28	2,339.15	0	0
1400	14,288.39	1,841.16	0	0

Table 4 presents the values for the boundary BES investment cost of 50 EUR/kWh, where the remuneration for excess PV electricity sold to the grid reaches zero. It is important to highlight that the buyback rate for excess electricity, which varies by country, is a critical parameter influencing the final PV earnings results. Lower buyback rates would likely lead to a scenario where the system favours PtW and BES storage, with zero PV earnings occurring over a broader range of investment costs. Finally, when comparing PV savings and earnings with flexible operation savings in Figure 7, it becomes evident that as BES capacity increases, and consequently BES usage rises, the PV savings and earnings distribution is reshaped into the flexible operation savings distribution. This shift results in the highest savings values being achieved at the lowest investment cost levels, reinforcing the importance of optimizing both PV and BES costs for maximum financial and operational efficiency.

The base results were provided above, and further below we follow with the representation of optimal water-energy system results based on the specific important parameter changes. Three parameters were recognised as important, and range between -30% and +30% change, with 10% step, was selected. Parameters being changed are:

- Grid electricity price - e^P_t
- PV power potential - pv^S_t
- Water demand - w^D_t

To maintain clarity and conciseness, the presentation of optimal capacity results will focus on boundary scenarios, specifically the cases representing -30% and +30% parameter changes.

4.1. Grid electricity price change

Grid electricity price is an important parameter because main revenues (savings and earnings) in provided approach are directly related to equivalent savings (or earnings) in grid electricity prices.

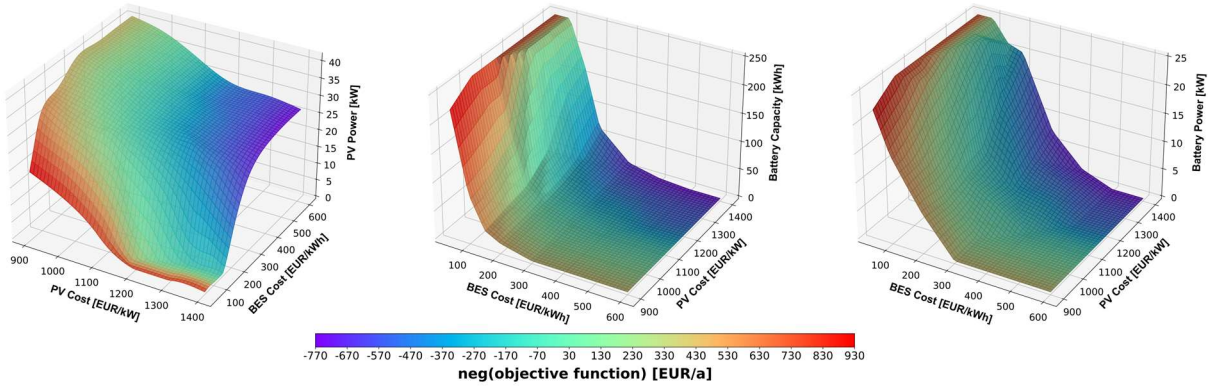

Figure 9. Range of optimal capacity results for Unije Island's water-energy system with 30% decrease in grid electricity price

When comparing the -30% scenario to the base case, the *neg(objective function)* values shift significantly from a range of [240, 2290] EUR/a in the base case to [-770, 930] EUR/a in the -30% scenario. This highlights the substantial impact of grid electricity price changes on the total optimal system capacities and dispatch. It is evident that the highest *neg(objective function)* are achieved at lowest PV/BES investment cost pairs of 900/50. However, the distribution of these highest values (depicted as the red-colored areas in Figure 9) shifts towards regions with lower BES investment costs, indicating that BES storage becomes more dominant in the final optimal solution compared to PV generation and PtW options. Despite this shift, it is important to note that the *neg(objective function)* values in the -30% scenario are still considerably lower than those in the base case, underscoring the reduced financial viability under lower grid electricity prices. Interestingly, the distribution of optimal

PV and BES capacities reveals variability for similar *neg(objective function)* values. For instance, a *neg(objective function)* value of approximately 750 EUR/a (light red area in Figure 9) is achieved at distinctly different investment cost combinations: at 900 EUR/kW for PV and 75 EUR/kWh for BES, and 1400 EUR/kW for PV and 50 EUR/kWh for BES. The respective *neg(objective function)* values for these cases are 776.26 EUR/year and 750.48 EUR/year. These results emphasize the importance of conducting detailed calculations for optimal capacities and dispatch configurations tailored to specific investment cost scenarios. Such analyses are crucial for identifying the most cost-effective solutions, especially under varying grid electricity price conditions.

An additional noteworthy observation is the first occurrence of a non-profitable solution, identified at the investment cost combination of 1100 EUR/kW for PV and 200 EUR/kWh for BES, where the neg(*objective function*) reaches a value of -26.88 EUR/a. Beyond this point, further increases in PV and/or BES investment costs result in increasingly negative neg(*objective function*) values, indicating non-profitability. It is also important to highlight the role of BES storage in maintaining the profitability of the system. For PV investment costs of 1100 EUR/kW and above, BES storage supports profitability within average BES cost ranges below 130 EUR/kWh, as illustrated by the green-coloured areas in Figure 9. This underscores the importance of BES in enabling PV generation and PtW options to remain financially viable under specific investment cost conditions.

From the analysis of optimal capacity values, it is evident that with increasing PV investment costs, PV becomes less viable as an optimal solution at lower BES costs, with BES taking over the entire storage role. This trend is observed in the edge regions of Figure 9, where the optimal PV capacity drops to zero. Specifically, for PV investment costs between 1200 EUR/kW and 1400 EUR/kW, zero PV capacity is seen within BES investment cost ranges of up to 110 EUR/kWh and 170 EUR/kWh, respectively.

A noticeable trend, similar to the base case, is the increase in optimal BES capacity, particularly at higher PV costs. This is evident in Figure 9, where a faster rate of increase in BES capacity is observed as PV costs rise. This phenomenon can be attributed to the higher share of PtW savings and PV earnings at lower PV costs, which diminish as PV costs increase, shifting the reliance on BES to generate greater savings within the total system revenues.

Compared to the base case, optimal BES capacities are generally more prominent, occupying higher values across a broader spectrum of BES investment costs. Conversely, PV capacities are reduced, reflecting a smaller contribution to system savings due to the relatively lower equivalent revenues from grid electricity prices. Notably, the analysis also demonstrates that BES alone can fulfil the role of energy storage, even in the absence of PtW through PV, albeit at significantly lower neg(*objective function*) values. This reinforces the notion that PV and PtW systems are less profitable under these conditions due to lower grid electricity price equivalents.

Furthermore, the reduction in PtW savings and PV earnings results in PV becoming a less competitive solution in the system. However, larger BES capacities compensate to some extent, as they contribute a greater share to total system savings. This increase in BES savings plays a critical role in maintaining profitability, particularly at higher BES capacities, where BES helps offset the diminishing contributions from PV and PtW.

Despite these compensatory effects, it is crucial to emphasize that the final neg(*objective function*) values in the 30% reduction scenario remain significantly lower than those of the base case. This highlights the pivotal role of grid electricity prices in determining the optimal configuration and dispatch of water-energy systems. The results underscore the need for strategic planning to balance the interplay between PV and BES to achieve an economically viable solution under varying electricity price scenarios.

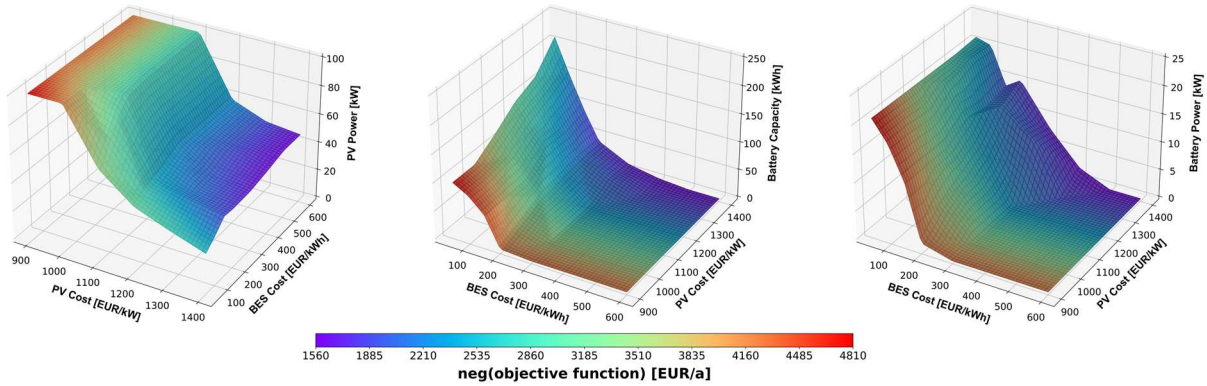

Figure 10. Range of optimal capacity results for Unije Island's water-energy system with 30% increase in grid electricity price

When comparing the +30% scenario to the base case, the *neg(objective function)* values exhibit a significant upward shift, increasing from a range of [240, 2290] EUR/a in the base case to [1560, 4810] EUR/a in the +30% scenario. This highlights the substantial impact of grid electricity price increases on the optimal system configuration and dispatch.

The highest *neg(objective function)* values are observed at the lowest PV and BES investment cost combination of 900 EUR/kW for PV and 50 EUR/kWh for BES. However, in contrast to the scenario with a grid electricity price decrease, the distribution of these highest values (represented as red-colored areas in Figure 10) shifts towards regions with lower PV investment costs. This shift indicates that PtW and PV usage become more dominant in the final optimal solution, while BES options contribute less significantly. This change reflects the increased economic competitiveness of PV and PtW under higher grid electricity prices, as these options provide greater savings and earnings within the overall system.

It is noteworthy that the most profitable solutions per *neg(objective function)* range from 4810 EUR/a for the PV/BES investment cost pair of 900/50 to 4231.54 EUR/a for the pair 900/210, where no BES is deployed. The highest profitability observed in the +30% scenario significantly exceeds the base case, where the maximum *neg(objective function)* reached value of 2290 EUR/a. It is interesting to follow the most profitable base case solution which is on a Figure 10 displayed in blue-teal colours. The closest *neg(objective function)* equal solutions for +30% increase in grid price is seen at PV/BES investment cost pairs of 1200/260 with value of 2280.59 EUR/a when also no BES storage is deployed, at pair 1300/130 with value of 2296.75 EUR/a , and at pair 1400/85 with *neg(objective function)* value of 2292.08 EUR/a. This further confirms that the change in grid electricity cost significantly affects the final optimal arrangement of production capacities and storage options.

The results further reveal that BES contributes less significantly to profitability under the +30% scenario. Instead, PtW and PV usage account for a larger share of revenues due to higher equivalent grid electricity price savings and earnings. Across the PV/BES investment cost range, BES capacities are generally lower compared to the base case. Consequently, BES savings are reduced, but the overall profitability improves as PtW and PV revenues dominate total system revenues.

When examining capacity values, PV deployment reaches its upper limit at lower PV investment costs. Specifically, at PV costs of 900 and 1000 EUR/kW, the PV capacity remains at its maximum irrespective of BES investment costs. At a PV cost of 1100 EUR/kW, maximum PV capacity is achieved for BES investment costs exceeding 220 EUR/kWh, with no BES deployed. For BES costs below 220 EUR/kWh, optimal PV and BES combination is observed, with the PV capacity being below its maximum level but supported by BES storage

Overall, BES appears optimal at slightly lower BES investment costs compared to the base case, as higher grid electricity prices make PtW and PV options more profitable. For the lowest BES cost of 50

EUR/kWh, optimal BES capacities range from 96.73 kWh to 210.90 kWh for PV costs between 900 and 1400 EUR/kW, respectively. On the other hand, PV capacities are higher due to the larger share of savings achieved from the increased grid electricity price. Nonetheless, BES continues to play a role in the optimal system mix, particularly at lower BES costs, generally below 220 EUR/kWh. This demonstrates the complementary relationship between BES and PV in achieving cost-effective solutions, even under scenarios of elevated grid electricity prices.

4.2. PV potential change

PV potential change was recognised as potential critical parameter. As main system revenues are related to PtW and PV generation, below are the optimal system results for the change in PV potential.

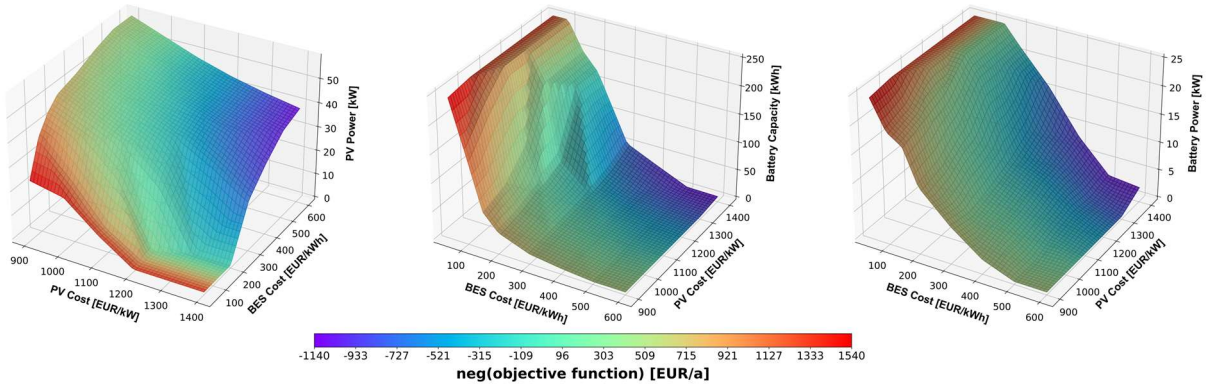

Figure 11. Range of optimal capacity results for Unije Island's water-energy system with 30% decrease in PV potential

Comparing the 30% decrease in PV potential to the base case, the *neg(objective function)* values shift significantly from a range of [240, 2290] EUR/a in the base case to [-1140, 1540] EUR/a in the 30% decrease scenario. Similar to the scenario involving a grid electricity price decrease, this emphasizes the critical impact of PV potential changes on the total optimal system capacities and dispatch. As with the grid electricity price change, a reduction in PV potential causes the distribution of the most profitable systems (depicted as the red-coloured areas in Figure 11) to shift towards regions with lower BES investment costs. This indicates that BES storage becomes more dominant in the final optimal solution compared to PV generation and PtW savings. However, it is important to note that the *neg(objective function)* values in the -30% PV potential decrease scenario are considerably lower than those in the base case, reflecting the diminished economical viability under reduced PV potential.

The 30% decrease in PV potential also reveals variability in the distribution of optimal water-energy system for similar *neg(objective function)* values. For instance, a PV/BES investment cost pair of 900/200 results with a *neg(objective function)* value of 772.61 EUR/a which is by profitability close to *neg(objective function)* value of 764.46 EUR/a seen for investment cost pair of 1400/100. These results further emphasize the importance of conducting detailed calculations for optimal capacities and dispatch configurations tailored to specific investment cost scenarios and identifying the crucial parameters that define the profitability of a water-energy system.

The presence of non-profitable system configurations is also observed in the 30% PV potential decrease scenario. The first occurrence of a non-profitable solution is identified at the investment cost pair of 1100/300, where the *neg(objective function)* reaches a value of -21.30 EUR/a. Beyond this point, further increases in PV and/or BES investment costs result in increasingly negative *neg(objective function)* values, indicating non-profitability. Additionally, for any PV cost equal to or greater than 1100 EUR/kW, configurations where only PV is deployed, and no BES is installed are also non-profitable.

It is worth emphasizing that, across a range of PV and BES investment costs, BES can support system profitability. For PV investment costs equal to or greater than 1100 EUR/kW, BES storage contributes to profitability within a marginal BES investment cost range of 250 to 170 EUR/kWh, corresponding to PV investment costs between 1100 and 1400 EUR/kW, respectively. These areas, depicted in teal colour on Figure 11, demonstrate the crucial role of BES in enabling PV generation and PtW options to remain economically viable under specific cost conditions.

When compared to the 30% decrease in grid electricity prices, it is evident that the impact of a decrease in PV potential is more substantial. The *neg(objective function)* range is wider for both negative and positive values, indicating that decrease in PV potential has a more pronounced influence on system profitability than grid electricity price decrease. This highlights the importance of PV potential in shaping the optimal capacities and annual dispatch.

A noticeable drop in PtW storage is observed under reduced PV potential, as PV becomes less profitable, leading to decreased PtW and PV usage. Conversely, larger BES capacities result in higher BES savings. However, it is crucial to consider that the *neg(objective function)* values are still lower in absolute terms compared to the base case. This can be illustrated by comparing the most profitable case under the 30% PV potential decrease, with a *neg(objective function)* value of 1540 EUR/a, to the green-to-yellow areas in the base case results, as shown in Figure 4. Furthermore, highly negative *neg(objective function)* values confirm that PV potential change is the crucial parameter and these findings further underscore the importance of PV potential in driving the profitability of the system and the critical interplay between PV and BES in achieving optimal water-energy system configurations.

Similar to the scenario of a decrease in grid electricity prices, it is evident that as PV investment costs increase, PV becomes less viable as an optimal solution at lower BES costs, with BES assuming the primary storage role. This trend is observed in the edge regions of Figure 11, where the optimal PV capacity drops to zero. Specifically, for PV investment costs between 1200 EUR/kW and 1400 EUR/kW, zero PV capacity is observed within BES investment cost ranges of up to 140 EUR/kWh and 230 EUR/kWh, respectively. Compared to the grid electricity price decrease scenario, the range of costs where optimal PV capacity equals zero is broader, further indicating that a reduction in PV potential has a more significant impact on the profitability of PtW and PV usage. As the decline in PV potential shifts the system toward greater reliance on BES storage at the expense of PtW and PV usage, higher BES usage is observed across a wider range of PV and BES costs. For instance, even in the boundary case with a PV investment cost of 1400 EUR/kW and a BES investment cost of 600 EUR/kWh, BES is utilized, albeit with a smaller capacity of 4.417 kWh.

As with the base case and the grid price change scenario, the rate of increase in optimal BES capacity varies with specific PV investment costs. This behaviour is apparent in Figure 11, where a faster rate of BES capacity increase is observed at higher PV costs. However, when compared to the base case and the 30% decrease in grid electricity prices, the maximum BES capacity is achieved across a broader range of PV investment costs. For example, for the PV/BES investment cost pair of 900/50, the optimal BES capacity is 243.49 kWh for the 30% decrease in PV potential, 221.73 kWh for the 30% decrease in grid electricity prices, and 121.38 kWh for the base case.

Finally, when compared to the base case and similarly to the grid electricity price decrease scenario, optimal BES capacities are generally more prominent, occupying higher values across a wider spectrum of BES investment costs. Conversely, PV capacities are reduced, reflecting a smaller share of PtW and PV earnings in total system revenues due to the diminished PV potential. Furthermore, the results demonstrate that BES alone can fulfil the role of energy storage even in the absence of PtW through PV, though this occurs at significantly lower *neg(objective function)* values. This highlights the critical role of PV potential decrease in determining the profitability of PtW and PV systems and the complementary role of BES in maintaining system viability under constrained PV conditions.

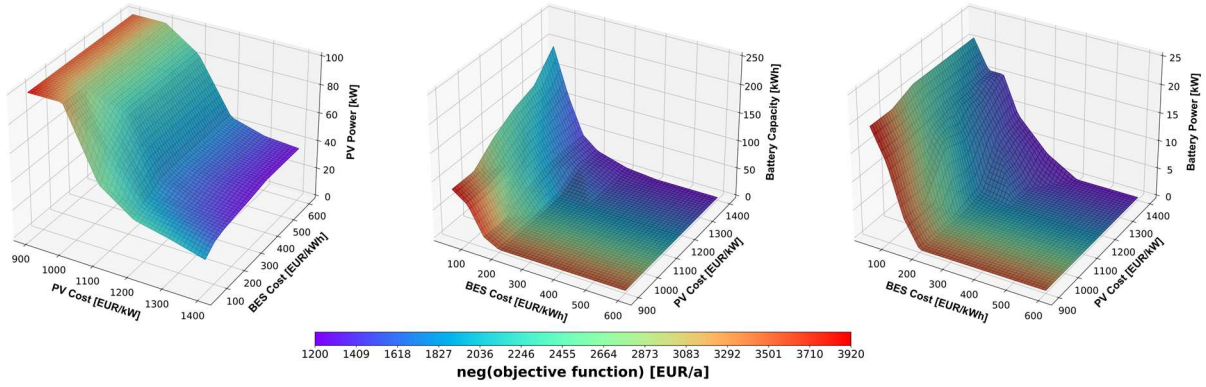

Figure 12. Range of optimal capacity results for Unije Island's water-energy system with 30% increase in PV potential

When comparing the +30% scenario in PV potential to the base case, the *neg(objective function)* values exhibit a significant upward shift, increasing from a range of [240, 2290] EUR/a in the base case to [1200, 3920] EUR/a in the +30% scenario. This highlights the substantial influence of PV potential changes on the optimal system capacities and dispatch. Similar to the 30% increase in grid electricity prices - and in contrast to the scenarios involving decreases in grid electricity price or PV potential - the distribution of the highest values (depicted as the red-coloured areas in Figure 12) shifts towards regions with lower PV investment costs. This shift indicates that PtW and PV generation become more dominant in the final optimal solution compared to BES options.

Notably, the most profitable solution in this scenario, with a *neg(objective function)* value of 3920 EUR/a, is lower than the maximum value achieved in the 30% increase in grid electricity price scenario, which reached 4810 EUR/a. This difference arises primarily due to the upper limit on PV capacity being reached in the PV potential scenario and the slightly higher optimal BES capacities in the grid electricity price increase scenario. The latter scenario benefits from greater PtW and BES savings, driven by higher grid-equivalent savings.

The range of the most profitable solutions in the +30% PV potential scenario spans from a maximum of 3916.46 EUR/a for the 900/50 PV/BES investment cost pair to 3575.31 EUR/a for the 900/170 pair, where no BES is installed. Importantly, the maximum profitability in this scenario exceeds that of the base case, where the highest *neg(objective function)* value is 2290 EUR/a.

It is also insightful to follow the most profitable base case solution, represented in teal colour on Figure 12. The closest *neg(objective function)* values in the +30% PV potential scenario are observed at the PV/BES investment cost pairs of 1100/150 with 2243.62 EUR/a and 1200/50 with 2284.31 EUR/a *neg(objective function)* values. This underscores the significant impact of PV potential changes on the arrangement of optimal production capacities and storage options.

Furthermore, the results indicate that BES has a smaller impact on final profitability in this scenario, as PtW and PV usage contribute a larger share of revenues due to the increased PV potential. However, BES operation and savings are more prominent in the 30% increase in grid electricity price scenario, owing to the higher grid-equivalent savings in that case. In the +30% PV potential scenario, the lower average BES capacities across the PV/BES investment cost range result in reduced BES savings, accounting for just 11.36% of total revenues. Despite this, overall profitability increases due to the greater contribution of PtW and PV earnings, which dominate total system revenues.

Comparing capacity values to the base case, and similar to the grid electricity price increase scenario, PV capacity in the +30% PV potential scenario reaches its upper limit for lower PV investment costs. However, a key difference between the two scenarios is that, under increased PV potential, the maximum PV capacity is achieved only at PV investment costs equal to or below 1000 EUR/kW. In

contrast, for the grid electricity price increase scenario, maximum PV capacity is observed at a PV investment cost of 1200 EUR/kW when BES costs are above 220 EUR/kWh. This broader range of maximum PV capacities and BES storage in the grid electricity price increase scenario results in higher overall profitability compared to the increased PV potential scenario. Across the entire PV/BES investment cost spectrum, BES is cost-effective for BES costs below an average of 170 EUR/kWh. For the lowest BES investment cost of 50 EUR/kWh, the optimal BES capacity ranges from 82.64 kWh to 192.78 kWh as PV investment costs increase from 900 EUR/kW to 1400 EUR/kW, respectively.

Overall, optimal BES capacities are more pronounced at lower levels, as higher PV capacities and the associated PtW savings prove more profitable across a broader range of variable investment costs. The increased PV potential allows PV to operate at higher capacities, generating a larger share of savings due to the enhanced availability of renewable energy. However, BES continues to play a critical role in the optimal system configuration. This demonstrates that while PV becomes increasingly dominant in higher PV potential scenarios, BES retains its importance as a complementary storage solution, especially in cost-effective investment ranges.

4.3. Water demand change

Water demand was recognised as potential critical parameter as it is a main driver for system consumption. Below results show optimal capacity and economic changes based on change in water demand.

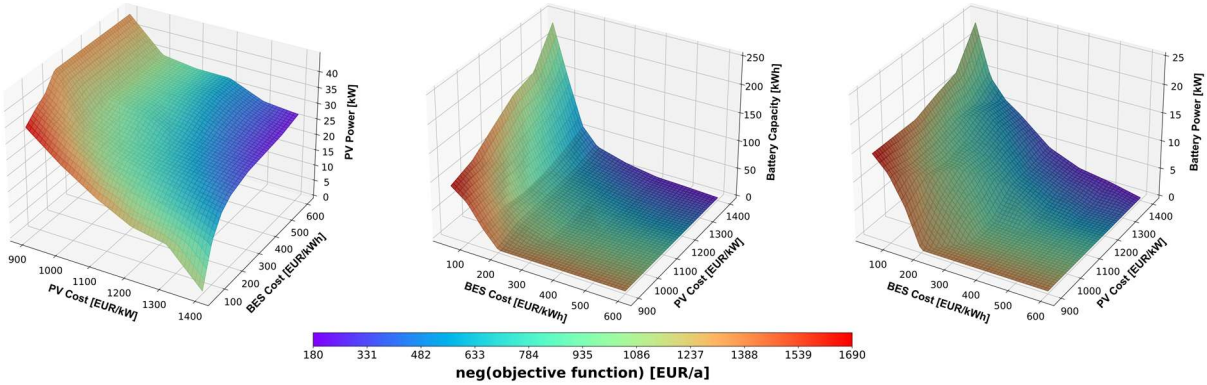

Figure 13. Range of optimal capacity results for Unije Island's water-energy system with 30% decrease in water demand

Comparing the 30% decrease in water demand in Figure 13 to the base case, the *neg(objective function)* values shift from a range of [240, 2290] EUR/a in the base case to [180, 1690] EUR/a in the 30% decrease scenario. This smaller change, compared to scenarios involving grid electricity price and PV potential variations, indicates that reductions in water demand have a relatively lower effect on the overall optimal system configuration and dispatch.

The reduced water demand leads to a greater proportional decrease in revenues from PtW and PV usage compared to savings from BES usage. While both categories experience declines, the impact is more pronounced for PtW and PV savings. Percentagewise, depending on the investment cost pair, BES savings decrease by an average of 14%, whereas PtW and PV savings are approximately 31% lower. In absolute terms, BES savings decrease by an average of 83.50 EUR/a, while PtW and PV usage savings drop by an average of 1378.46 EUR/a.

Following the most profitable solution in the 30% decrease scenario, with a *neg(objective function)* value of 1690 EUR/a, provides additional insights. This solution can be closely compared to its base case counterparts, as represented by the orange-coloured areas in base results Figure 4. In the base case, the closest *neg(objective function)* equal solutions for base case are seen at PV/BES investment cost pairs of 1000/130 with value of 1690.18 EUR/a, at pair 1100/105 with value of 1683.36 EUR/a, at pair

1200/85 with value of 1686 EUR/a, and at pair 1300/60 with 1688.83 EUR/a *neg(objective function)* value.

Overall, the 30% decrease in water demand results in a noticeable decline in revenues from both BES and, PtW and PV usage, with the drop being more significant for PtW and PV savings in both absolute and percentage terms. This is largely due to marginal cases with higher PV costs (≥ 1300 EUR/kW) and higher BES costs, where BES achieves higher savings than in the base case. An additional particularly interesting marginal result is observed for the investment cost pair of 1400/50, where only BES is utilized, achieving an optimal capacity of 234.94 kWh while PV capacity is zero. In this scenario, BES alone is sufficient to maintain a positive *neg(objective function)* value of 1094.31 EUR/a.

The decrease in water demand also leads to reductions in optimal PV and BES capacities compared to the baseline, with PV capacities experiencing a larger relative decline due to the greater drop in PtW and PV revenues. While BES capacities also decrease, a slightly broader range of BES usage is observed for higher BES costs, suggesting that BES remains an important component in the system even with reduced water demand.

These comparisons emphasize the nuanced impact of reduced water demand on the optimal system. While the reductions in PtW and PV savings are more pronounced in absolute terms, BES still plays a stabilizing role in the system's profitability, ensuring that even under reduced water demand scenarios, the system maintains relatively close profitability to the base case.

It is further evident that the decrease in water demand that results with reductions in PV and BES capacities, and the associated savings and revenues, is less impactful compared to the changes caused by reductions in grid electricity prices or PV potential. Furthermore, the analysis confirms that a 30% decrease in water demand does not lead to any non-profitable scenarios, indicating that water demand is a less critical parameter in determining system profitability. This finding highlights the resilience of the system to variations in water demand, underscoring the stability of the optimal configurations under such changes.

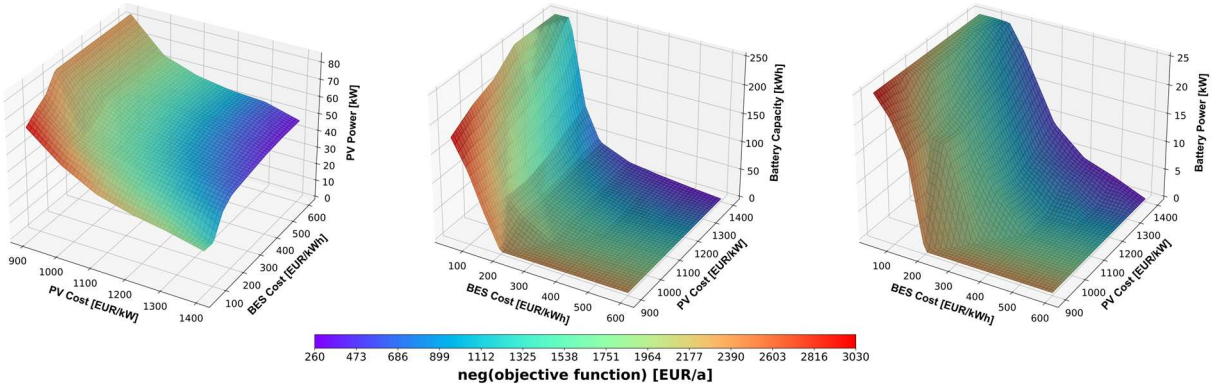

Figure 14. Range of optimal capacity results for Unije Island's water-energy system with 30% increase in water demand

When comparing the 30% increase in water demand to the base case, the *neg(objective function)* values shift from a range of [240, 2290] EUR/a in the base case to [260, 3030] EUR/a in the 30% increase scenario. This change, while notable, is smaller than the effects observed in scenarios involving grid electricity price and PV potential changes, further confirming that changes in water demand have a relatively lower effect on the total optimal system configuration and dispatch.

The higher water demand results in a more significant increase in savings and income from PtW and PV usage (in absolute terms) compared to the higher savings due to BES usage. Although there is also a noticeable increase in BES savings, the percentage increase in savings is more pronounced for PtW

and PV usage. Specifically, BES savings increase by an average of +44.6%, while PtW and PV usage savings rise by approximately +30.9%. In absolute terms, BES savings are higher by an average of 140.5 EUR/a, while PtW and PV usage savings increase by an average of 1356.27 EUR/a.

It is interesting to follow the most profitable solution in base case and compare it to the Figure 14 for an increase in water demand. The most profitable solution with *neg(objective function)* value equal to 2290 EUR/a can be closely followed by the profitable equivalent solution in water demand increase case by the orange colour. The closest *neg(objective function)* equal solutions for increase in water demand are seen at PV/BES investment cost pairs of 1000/118 with value of 2286.64 EUR/a, and at pair 1100/50 with 2283.81 EUR/a *neg(objective function)* value.

Overall, there is a noticeable increase in both PtW and BES revenues, with a higher average absolute increase for PtW and PV usage. However, the percentage increase in savings and earnings is higher for BES usage. As BES is deployed at higher PV costs and lower BES costs, with quite high capacities (on average 240 kWh), it is evident that with an increase in water demand and, consequently, electricity consumption for desalination, there is limited additional room for savings through BES for these cost pairs. This is because the savings are already relatively high, driven by the system nearing the upper BES capacity limit.

It is evident that both PV and BES capacities are higher than in the base case, indicating that the increase in water demand similarly affects the optimal PV and BES capacities. However, it is more noticeable that the impact on PV is slightly more pronounced, leading to a greater increase in optimal PV capacities. This, in turn, results in an increase in savings associated with the slightly higher PV output. The red area, representing the most unprofitable solutions across all optimal combinations, is located at the lowest PV cost, further emphasizing the significance of PV in this scenario.

Compared to the base case, although BES capacities are also higher, the range of BES usage is marginally greater for higher BES costs. This can be observed in the case of higher PV costs, where BES remains a viable option at higher BES costs, such as the cost combinations of 1300/450 or 1400/500, where BES would not have been optimal in the base case. However, it is important to note that the differences in the absolute values of BES capacity are minimal, meaning they have little impact on final profitability.

In conclusion, the primary impact on the increase in both PV and BES capacities, which leads to higher savings and income from both sources, is less significant compared to the effects of changes in other parameters. Thus, while the increase in PV and BES capacities contributes to profitability, it is the changes in other factors, such as grid electricity prices and PV potential, that have a more substantial effect on overall system performance.

5. Conclusion and future work

This study introduces the framework for optimizing integrated water-energy systems, applied to small-scale island with unique seasonal fluctuations. The research significantly advances the traditional approach by implementing a MILP model that not only determines the optimal capacities for RES and BES but also integrates these with water supply systems via a RO desalination unit and water storage highlighting the importance of PtW. Furthermore, unlike the traditional approach in water-energy system analyses, which often focuses solely on BES capacity optimization, this study adopts a more detailed methodology considering both BES capacity and power rating as variables.

This dynamic optimization framework contrasts with conventional methods that typically rely on predetermined capacities, instead offering a comprehensive strategy to optimize both system capacity and dispatch in response to varying energy and water demands on a yearly basis. The methodological approach is grounded in a MILP optimisation model, which facilitates the simultaneous optimization of multiple variables across interconnected energy and water systems. Additionally, the proposed RES

and BES range investment cost analysis enables a robust approach that can accommodate market volatility and technological advancements.

The case study of Unije Island underscores the practical applicability of the proposed model, demonstrating its effectiveness in optimizing an integrated water-energy system within a context characterized by seasonal population spikes due to tourism and a variable climate. The optimization results reveal the potential for enhanced system flexibility and economic performance, particularly through the deployment of PtW technologies and the efficient management of energy and water storage. The insights gained from this case study are not only applicable to the specific context of Unije Island but also offer broader implications for the optimization of water-energy systems on other islanded or remote areas.

The study comprehensively mapped how variations in investment cost impact system operation, financial viability, and broader economic outcomes, revealing a complex relationship between RES power generation and storage options. Significant observation was the non-linear influence of BES investment costs on the optimal PV power capacities. While lower PV costs generally incentivize higher PV power capacities, the rate of this increase is dependent on the BES investment costs. The study also highlights the importance of BES capacity and power as separate but interdependent variables in optimizing the system's performance.

The findings demonstrated that BES capacity influences not only the overall storage potential but also the required BES power, which must be adequately matched to avoid underutilization or overestimation of storage capabilities. This is particularly evident in scenarios where BES power follows the capacity trend, but with sharper changes, especially at lower PV investment costs. These results underscore the importance of treating BES power and capacity as distinct parameters in the optimization process to achieve accurate and efficient system configurations. Moreover, the analysis of BES utilization gives additional view on optimal storage usage. While high BES utilization is typically associated with efficient storage operation, the results indicated that maximum financial and economic benefits might not necessarily coincide with maximum BES usage. In fact, the highest objective function values, indicative of the most financially and economically optimal configurations, were observed at lower BES utilization levels. This counterintuitive finding, together with the findings showing decrease in optimal PV power with lower BES investment cost, suggests that the optimal integration of PV and BES does not simply depend on maximisation of PV and storage capacities but rather on achieving the right combination that maximizes financial and economic returns while minimizing costs.

Furthermore, the flexible operation savings, which capture the combined economic benefits of both PtW and BES storage, underscore the importance of integrating these technologies in a balanced manner. The highest flexible operation savings are achieved when both PV and BES investment costs are minimized, indicating that cost reductions in both areas are essential for maximizing system efficiency. Moreover, the results show that the PV savings and earnings decrease as BES capacity increases, particularly when BES investment costs are low. This trend further highlights the trade-off between direct PV utilization and storage options. Thus, the optimal system design must carefully balance these factors to achieve the greatest overall savings and earnings.

The results further highlight the sensitivity of the water-energy system's optimal configuration to changes in grid electricity price, PV potential, and water demand. Results indicate that an increase in grid electricity prices enhances the system’s profitability by incentivizing the use of PV and PtW further reducing reliance on grid electricity. Higher PV potential leads to increased PV installation, improving renewable energy utilization and overall system performance. Conversely, lower grid electricity prices or reduced PV potential diminish economic viability, shifting reliance to BES and raising operational costs. Furthermore, decrease in both grid electricity prices and PV potential in some investment cost pair combinations resulted with the non-profitable solution marking those parameter changes as critical.

Changes in water demand primarily influence the capacity requirements of system components. Higher demand necessitates scaling up both energy and water system capacities, which impacts revenues and

operational strategies. Lower demand reduces system load but may affect cost efficiency due to underutilized infrastructure. However, and contrary to grid electricity price and PV potential change, decrease in water demand does not result with non-profitable solutions which marks water demand as non-critical parameter. These findings emphasize the need for tailored strategies to adapt to varying cost and resource scenarios, ensuring optimal system performance and economic efficiency.

The contributions of this research extend beyond theoretical advancements, offering practical solutions and a versatile modelling framework that can be adapted to various areas. Furthermore, the findings provide valuable guidance for policymakers and stakeholders involved in the sustainable development of island communities, particularly in the face of evolving energy markets and climate challenges. Future research will expand this framework to include additional renewable energy sources, water production technologies, and additional external economical benefits, thereby enhancing its utility across a wider range of scenarios. Additionally, crucial input parameters change in future research will aim to show the effect on optimal solution distribution further increasing the robustness of the proposed modelling framework.

Abbreviations

Acronyms

EU	-	European Union
RES	-	Renewable energy sources
PV	-	Photovoltaic power plant
RO	-	Reverse osmosis desalination unit
BES	-	Battery energy storage
DSM	-	Demand-side management
PSO	-	Particle swarm optimisation
MILP	-	Mixed integer linear programming
PtW	-	Power-to-Water
MIQCP	-	Mixed-integer quadratically-constrained programming
SOC	-	State of charge
RHS	-	Right hand side
LHS	-	Left hand side

Nomenclature

Model sets

Name	**Description**
$t \in T$	Time periods
$pvc \in PVC$	PV power investment cost change
$bc \in BC$	Battery storage capacity investment cost change
$pc \in PC$	Important parameters
$\varepsilon \in \Omega_E$	Grid electricity price change
$\kappa \in \Omega_K$	PV potential change
$\psi \in \Omega_\Psi$	Water demand change

Model variables

Name	**Unit**	**Description**
$LL_{pvc,\,bc,\,t}$	kWh	Lost load
$G^{D}_{pvc,\,bc,\,t}$	kWh	Grid energy used for desalination electricity demand
$B^{DC}_{pvc,\,bc,\,t}$	kWh	Battery discharging
$B^{CH,G}_{pvc,\,bc,\,t}$	kWh	Battery charging from the grid
$B^{CH,PV}_{pvc,\,bc,\,t}$	kWh	Battery charging from available PV generation
$B^{SOC}_{pvc,\,bc,\,t}$	kWh	Battery state of charge

$B^{P}_{pvc, bc, t}$	kW	Battery power output
$PV^{D}_{pvc, bc, t}$	kWh	PV power used for the desalination electricity demand
$PV^{G}_{pvc, bc, t}$	kWh	PV power transferred to the grid
$PV^{E}_{pvc, bc, t}$	kWh	PV generation
$X^{PV}_{pvc, bc, t}$	{1,0}	Binary variable allowing PV battery charging
$X^{G}_{pvc, bc, t}$	{1,0}	Binary variable allowing grid battery charging
$X^{DC}_{pvc, bc, t}$	{1,0}	Binary variable allowing battery discharging
$E^{D}_{pvc, bc, t}$	kWh	Electricity demand
$B^{NP}_{pvc, bc}$	kW	Optimal battery power
$B^{C}_{pvc, bc}$	kWh	Optimal battery capacity
$PV^{P}_{pvc, bc}$	kW	Optimal PV power
$W^{L}_{pvc, bc, t}$	m^3	Water level values
$W^{D}_{pvc, bc, t}$	m^3	Water production
$W^{B}_{pvc, bc, t}$	m^3	Water boat carriers

Model parameters

Name	**Unit**	**Description**
ll^{c}	EUR/kWh	Lost load cost
e^{P}_{t}	EUR/kWh	Grid electricity price profile
e^{S}_{t}	EUR/kWh	Selling electricity price profile
pv^{S}_{t}	kWh/kW	PV power potential
pv^{C}_{pvc}	EUR/kW	PV power investment cost
pv^{var}	EUR/kWh	Variable PV cost
b^{CC}_{bc}	EUR/kWh	Battery storage capacity investment cost
b^{MCC}	EUR/kWh/a	Battery storage capacity maintenance cost
b^{PC}_{bc}	EUR/kW	Battery storage power investment cost
b^{MPC}	EUR/kW/a	Battery storage power maintenance cost
$b^{P, min}$	kW	Minimum battery power
$b^{P, max}$	kW	Maximum battery power
$b^{ch,\eta}$	%	Battery charge efficiency
$b^{dc,\eta}$	%	Battery discharge efficiency
b^{soc}_{t0}	%	Battery state of charge in the first time step in %
$b^{soc, min}$	%	Minimum battery state of charge in %
$b^{soc, max}$	%	Maximum battery state of charge in %
b^{sd}	%/month	Battery self-discharge
w^{D}_{t}	m^3	Water demand
w^{LC}	m^3	Water storage capacity
w^{L}_{t0}	%	Water level in the first time step in %
$w^{L,max}$	%	Maximum water level in %
$w^{L,min}$	%	Minimum water level in %
w^{BC}	EUR/m^3	Water boat carrier cost
d^{η}	kWh/m^3	Water production or treatment specific energy consumption
d^{c}	m^3/h	Water production or treatment unit nominal capacity
lf	years	Life-time of a technology
ry	year	Battery storage replacement year
dr	%	Discount rate
cr	-	Capital recovery factor
icdf	-	Battery storage investment cost decrease factor
pvf	-	Present value factor
Δt	h	Time-step in units of hour
γ	-	Ratio of electricity selling and purchase price

Acknowledgments

Contributions from companies Vodoopskrba i odvodnja Cres Lošinj d.o.o. and Ericsson Nikola Tesla d.d. regarding the data availability for the Unije Case study is greatly acknowledged. Furthermore, the contributions from European Union's Horizon Europe programme projects INITIATE, Grant agreement ID 101136775, as well as from the project EMERGE, Grand agreement ID 101118278 are greatly acknowledged.

Reference

[1] Directorate-General for Energy (European Commission). Clean energy for all Europeans. 2019. https://doi.org/10.2833/9937.

[2] European Commission. A Framework Strategy for a Resilient Energy Union with a Forward-Looking Climate Change Policy /* COM/2015/080 final */. n.d.

[3] Kotzebue JR, Weissenbacher M. The EU's Clean Energy strategy for islands: A policy perspective on Malta's spatial governance in energy transition. Energy Policy 2020;139:111361. https://doi.org/10.1016/j.enpol.2020.111361.

[4] Initiative SI. Smart Islands Declaration. n.d.

[5] European Commission. Clean energy for EU islands n.d. https://ec.europa.eu/energy/topics/markets-and-consumers/clean-energy-eu-islands_en.

[6] Duić N, Krajačić G, da Graça Carvalho M. RenewIslands methodology for sustainable energy and resource planning for islands. Renew Sustain Energy Rev 2008;12:1032–62. https://doi.org/10.1016/j.rser.2006.10.015.

[7] Pfeifer A, Dobravec V, Pavlinek L, Krajačić G, Duić N. Integration of renewable energy and demand response technologies in interconnected energy systems. Energy 2018;161:447–55. https://doi.org/10.1016/j.energy.2018.07.134.

[8] Dorotić H, Doračić B, Dobravec V, Pukšec T, Krajačić G, Duić N. Integration of transport and energy sectors in island communities with 100% intermittent renewable energy sources. Renew Sustain Energy Rev 2019;99:109–24. https://doi.org/10.1016/j.rser.2018.09.033.

[9] Dominković D, Stark G, Hodge B-M, Pedersen A. Integrated Energy Planning with a High Share of Variable Renewable Energy Sources for a Caribbean Island. Energies 2018;11:2193. https://doi.org/10.3390/en11092193.

[10] Groppi D, Pfeifer A, Garcia DA, Krajačić G, Duić N. A review on energy storage and demand side management solutions in smart energy islands. Renew Sustain Energy Rev 2021;135:110183. https://doi.org/10.1016/j.rser.2020.110183.

[11] Maleki A. Design and optimization of autonomous solar-wind-reverse osmosis desalination systems coupling battery and hydrogen energy storage by an improved bee algorithm. Desalination 2018;435:221–34. https://doi.org/10.1016/j.desal.2017.05.034.

[12] Triantafyllou P, Koroneos C, Kondili E, Kollas P, Zafirakis D, Ktenidis P, et al. Optimum green energy solution to address the remote islands' water-energy nexus: the case study of Nisyros island. Heliyon 2021;7:e07838. https://doi.org/10.1016/j.heliyon.2021.e07838.

[13] Moazeni F, Khazaei J, Pera Mendes JP. Maximizing energy efficiency of islanded micro water-energy nexus using co-optimization of water demand and energy consumption. Appl Energy 2020;266:114863. https://doi.org/10.1016/j.apenergy.2020.114863.

[14] Valencia-Díaz A, Toro EM, Hincapié RA. Optimal planning and management of the energy–water–carbon nexus in hybrid AC/DC microgrids for sustainable development of remote communities. Appl Energy 2025;377:124517. https://doi.org/10.1016/j.apenergy.2024.124517.

[15] Santhosh A, Farid AM, Youcef-Toumi K. The impact of storage facility capacity and ramping capabilities on the supply side economic dispatch of the energy–water nexus. Energy 2014;66:363–77. https://doi.org/10.1016/j.energy.2014.01.031.

[16] Kyriakarakos G, Dounis AI, Rozakis S, Arvanitis KG, Papadakis G. Polygeneration microgrids: A viable solution in remote areas for supplying power, potable water and hydrogen as transportation fuel. Appl Energy 2011;88:4517–26. https://doi.org/10.1016/j.apenergy.2011.05.038.

[17] Mimica M, Dominković DF, Capuder T, Krajačić G. On the value and potential of demand response in the smart island archipelago. Renew Energy 2021;176:153–68. https://doi.org/10.1016/j.renene.2021.05.043.

[18] Stoppato A, Cavazzini G, Ardizzon G, Rossetti A. A PSO (particle swarm optimization)-based model for the optimal management of a small PV(Photovoltaic)-pump hydro energy storage in a rural dry area. Energy 2014;76:168–74. https://doi.org/10.1016/j.energy.2014.06.004.

[19] Perković L, Novosel T, Pukšec T, Ćosić B, Mustafa M, Krajačić G, et al. Modeling of optimal energy flows for systems with close integration of sea water desalination and renewable energy sources: Case study for Jordan. Energy Convers Manag 2016;110:249–59. https://doi.org/10.1016/j.enconman.2015.12.029.

[20] Jannesar MR, Sedighi A, Savaghebi M, Guerrero JM. Optimal placement, sizing, and daily charge/discharge of battery energy storage in low voltage distribution network with high photovoltaic penetration. Appl Energy 2018;226:957–66. https://doi.org/10.1016/j.apenergy.2018.06.036.

[21] Sedghi M, Ahmadian A, Aliakbar-Golkar M. Optimal Storage Planning in Active Distribution Network Considering Uncertainty of Wind Power Distributed Generation. IEEE Trans Power Syst 2016;31:304–16. https://doi.org/10.1109/TPWRS.2015.2404533.

[22] Huang Y, Li P, Wang W, Dong L. Capacity Optimization of Battery Energy Storage System in Multi-energy Complementary System Based on Time Series Simulation Method. 2019 IEEE Innov. Smart Grid Technol. - Asia (ISGT Asia), IEEE; 2019, p. 3804–9. https://doi.org/10.1109/ISGT-Asia.2019.8881502.

[23] Grover-Silva E, Girard R, Kariniotakis G. Optimal sizing and placement of distribution grid connected battery systems through an SOCP optimal power flow algorithm. Appl Energy 2018;219:385–93. https://doi.org/10.1016/j.apenergy.2017.09.008.

[24] Li P, Huang Y, Qi W, Gan J. Capacity Co-Optimization of Thermal and Battery Energy Storage System in Multi-energy Complementary System. 2019 IEEE Innov. Smart Grid Technol. - Asia (ISGT Asia), IEEE; 2019, p. 3815–9. https://doi.org/10.1109/ISGT-Asia.2019.8881407.

[25] Ogunmodede O, Anderson K, Cutler D, Newman A. Optimizing design and dispatch of a renewable energy system. Appl Energy 2021;287:116527. https://doi.org/10.1016/j.apenergy.2021.116527.

[26] Mehrjerdi H, Aljabery AAM. Modeling and Optimal Planning of an Energy–Water–Carbon Nexus System for Sustainable Development of Local Communities. Adv Sustain Syst 2021;5. https://doi.org/10.1002/adsu.202100024.

[27] Mehrjerdi H, Aljabery AAM, Saboori H, Jadid S. Carbon-Constrained and Cost Optimal Hybrid Wind-Based System for Sustainable Water Desalination. IEEE Access 2021;9:84079–92. https://doi.org/10.1109/ACCESS.2021.3087540.

[28] Kariman H, Shafieian A, Khiadani M. Small scale desalination technologies: A comprehensive review. Desalination 2023;567:116985. https://doi.org/10.1016/j.desal.2023.116985.

[29] Ghazi ZM, Rizvi SWF, Shahid WM, Abdulhameed AM, Saleem H, Zaidi SJ. An overview of

water desalination systems integrated with renewable energy sources. Desalination 2022;542:116063. https://doi.org/10.1016/j.desal.2022.116063.

[30] Bundschuh J, Kaczmarczyk M, Ghaffour N, Tomaszewska B. State-of-the-art of renewable energy sources used in water desalination: Present and future prospects. Desalination 2021;508:115035. https://doi.org/10.1016/j.desal.2021.115035.

[31] Nurjanah I, Chang T-T, You S-J, Huang C-Y, Sean W-Y. Reverse osmosis integrated with renewable energy as sustainable technology: A review. Desalination 2024;581:117590. https://doi.org/10.1016/j.desal.2024.117590.

[32] Carta J, González J, Subiela V. The SDAWES project: an ambitious R&D prototype for wind-powered desalination. Desalination 2004;161:33–48. https://doi.org/10.1016/S0011-9164(04)90038-0.

[33] Subiela VJ, de la Fuente JA, Piernavieja G, Peñate B. Canary Islands Institute of Technology (ITC) experiences in desalination with renewable energies (1996–2008). Desalin Water Treat 2009;7:220–35. https://doi.org/10.5004/dwt.2009.733.

[34] Spyrou ID, Anagnostopoulos JS. Design study of a stand-alone desalination system powered by renewable energy sources and a pumped storage unit. Desalination 2010;257:137–49. https://doi.org/10.1016/j.desal.2010.02.033.

[35] Rosales-Asensio E, Rosales A-E, Colmenar-Santos A. Surrogate optimization of coupled energy sources in a desalination microgrid based on solar PV and wind energy. Desalination 2021;500:114882. https://doi.org/10.1016/j.desal.2020.114882.

[36] Mehrjerdi H. Modeling and optimization of an island water-energy nexus powered by a hybrid solar-wind renewable system. Energy 2020;197:117217. https://doi.org/10.1016/j.energy.2020.117217.

[37] Cabrera P, Carta JA, Matos C, Lund H. Lessons learned in wind-driven desalination systems in the Canary Islands: Useful knowledge for other world islands. Desalination 2024;583:117697. https://doi.org/10.1016/j.desal.2024.117697.

[38] Padrón I, Avila D, Marichal GN, Rodríguez JA. Assessment of Hybrid Renewable Energy Systems to supplied energy to Autonomous Desalination Systems in two islands of the Canary Archipelago. Renew Sustain Energy Rev 2019;101:221–30. https://doi.org/10.1016/j.rser.2018.11.009.

[39] Cabrera P, Carta JA, Lund H, Thellufsen JZ. Large-scale optimal integration of wind and solar photovoltaic power in water-energy systems on islands. Energy Convers Manag 2021;235:113982. https://doi.org/10.1016/j.enconman.2021.113982.

[40] Sanna A, Buchspies B, Ernst M, Kaltschmitt M. Decentralized brackish water reverse osmosis desalination plant based on PV and pumped storage - Technical analysis. Desalination 2021;516:115232. https://doi.org/10.1016/j.desal.2021.115232.

[41] Ajiwiguna TA, Lee G-R, Lim B-J, Cho S-H, Park C-D. Optimization of battery-less PV-RO system with seasonal water storage tank. Desalination 2021;503:114934. https://doi.org/10.1016/j.desal.2021.114934.

[42] Mentis D, Karalis G, Zervos A, Howells M, Taliotis C, Bazilian M, et al. Desalination using renewable energy sources on the arid islands of South Aegean Sea. Energy 2016;94:262–72. https://doi.org/10.1016/j.energy.2015.11.003.

[43] Liu Z, Zheng W, Yuan J, Zhang B, Lv B, Sun J. Optimal Configuration of Island Water-Energy Nexus Systems Considering Multistage Desalination. 2024 9th Asia Conf. Power Electr. Eng., IEEE; 2024, p. 278–83. https://doi.org/10.1109/ACPEE60788.2024.10532570.

[44] Clarke DP, Al-Abdeli YM, Kothapalli G. Multi-objective optimisation of renewable hybrid energy systems with desalination. Energy 2015;88:457–68. https://doi.org/10.1016/j.energy.2015.05.065.

[45] Smaoui M, Abdelkafi A, Krichen L. Optimal sizing of stand-alone photovoltaic/wind/hydrogen hybrid system supplying a desalination unit. Sol Energy 2015;120:263–76. https://doi.org/10.1016/j.solener.2015.07.032.

[46] Bilton AM, Kelley LC. Design of power systems for reverse osmosis desalination in remote communities. Desalin Water Treat 2015;55:2868–83. https://doi.org/10.1080/19443994.2014.940641.

[47] Ahmed FE, Hashaikeh R, Diabat A, Hilal N. Mathematical and optimization modelling in desalination: State-of-the-art and future direction. Desalination 2019;469:114092. https://doi.org/10.1016/j.desal.2019.114092.

[48] Okampo EJ, Nwulu N. Optimisation of renewable energy powered reverse osmosis desalination systems: A state-of-the-art review. Renew Sustain Energy Rev 2021;140:110712. https://doi.org/10.1016/j.rser.2021.110712.

[49] Ghenai C, Merabet A, Salameh T, Pigem EC. Grid-tied and stand-alone hybrid solar power system for desalination plant. Desalination 2018;435:172–80. https://doi.org/10.1016/j.desal.2017.10.044.

[50] Peng W, Maleki A, Rosen MA, Azarikhah P. Optimization of a hybrid system for solar-wind-based water desalination by reverse osmosis: Comparison of approaches. Desalination 2018;442:16–31. https://doi.org/10.1016/j.desal.2018.03.021.

[51] Meschede H. Increased utilisation of renewable energies through demand response in the water supply sector – A case study. Energy 2019;175:810–7. https://doi.org/10.1016/j.energy.2019.03.137.

[52] Mehrjerdi H. Modeling and integration of water desalination units in thermal unit commitment considering energy and water storage. Desalination 2020;483:114411. https://doi.org/10.1016/j.desal.2020.114411.

[53] Coelho L. Linearization of variable multiplication n.d. https://www.leandro-coelho.com/linearization-product-variables/.

[54] Wirtz M, Remmen P, Müller D. EHDO: A free and open-source webtool for designing and optimizing multi-energy systems based on MILP. Comput Appl Eng Educ 2021;29:983–93. https://doi.org/10.1002/cae.22352.

[55] Wirtz M. EHDO Tool - Github web page. Inst Energy Effic Build Indoor Clim RWTH Aachen Univ n.d. https://github.com/RWTH-EBC/EHDO/tree/master.

[56] Croatian Bureau of Statistics. Croatia 2021 Census. 2022.

[57] Croatian Meteorological and Hydrological Service. Weather data - Unije island n.d. https://meteo.hr/klima.php?section=klima_podaci&param=k1&Grad=mali_losinj.

[58] National Renewable Energy Laboratory. U.S. Solar Photovoltaic System and Energy Storage Cost Benchmarks, With Minimum Sustainable Price Analysis: Q1 2022. n.d.

[59] Wesley C, Akash K. Cost Projections for Utility Scale Battery Storage: 2023 Update. 2023.

PAPER 3

"Perfer et obdura"

("Endure and persist")

Publius Ovidius Naso

Energy Nexus 20 (2025) 100570

Contents lists available at ScienceDirect

Energy Nexus

journal homepage: www.elsevier.com/locate/nexus

Stochastic optimal design and operation of floating solar and hydropower system for integrated water-energy-food-ecosystem planning

Goran Stunjek *, Goran Krajačić

University of Zagreb, Faculty of Mechanical Engineering and Naval Architecture, Ivana Lucica 5, 10002 Zagreb, Croatia

ARTICLE INFO

Keywords:
Water-energy-food-ecosystem nexus
Renewable energy sources
Hydropower
Stochastic optimisation
Hybrid system operation

ABSTRACT

This study presents a high-resolution, two-stage stochastic optimisation framework for the configuration and operation of a hybrid floating photovoltaic (FPV) and pumped-storage hydropower (PSH) system. The model captures interdependencies among sectors through progressive optimisation perspectives, including energy-only (E), water-energy (WE), water-energy-food (WEF), and water-energy-food-ecosystem (WEFE), each expanding the system boundary and revealing cross-sectoral trade-offs. Methodological innovations include endogenising evaporation losses within the optimisation dynamically linked to FPV deployment, optimising agricultural area as decision variable, and embedding ecosystem values such as avoided CO_2 emissions, land-use savings, and biodiversity costs directly into the optimisation objective. Uncertainty is addressed through Monte Carlo-based hourly scenario generation, while a layered objective function systematically expands system integration. Results show that broader perspectives substantially shift optimal FPV capacity and hydropower dispatch, while enhancing the economic viability of hybrid configurations. In the WE case, evaporation savings drive larger FPV deployment and increase PSH output by over 11 % on average, while integration of irrigation constraints in the WEF case highlights seasonal trade-offs and optimal irrigation areas. Incorporating ecosystem values in the WEFE case leads to maximum FPV deployment across wide cost ranges, with hydropower ramp rate reduced by 16.4 %. CO_2-price sensitivity further confirms that higher carbon valuation widens the feasible deployment space, increasing FPV power by 15.84 % on average. The framework advances WEFE-integrated planning by linking high-resolution sectoral interactions with ecosystem valuation, offering practical insights for resource-efficient, low-carbon systems that balance competing demands under uncertainty and support long-term sustainability goals.

1. Introduction and literature review

Integrated management of Water-Energy-Food-Ecosystem (WEFE) sectors has become increasingly critical in addressing global sustainability challenges. A wide range of studies and review papers have emphasized the need for holistic system modelling that captures cross-sectoral trade-offs, resource interdependencies, and synergies.

A detailed review of integrated water-energy (WE) system modelling in [1] highlights the complexity of joint planning and the importance of incorporating uncertainty through parameterised stochastic perturbation sets. A broader survey of water-energy-food (WEF) nexus models in [2] emphasizes the diversity of existing approaches while identifying the persistent absence of stochastic treatment as a major gap in current research. The authors in [3] introduces a macro-scale methodology for assessing circular economy potential in the WEF, offering a framework to guide sustainable WEF strategies, though lacking system-level temporal dynamics and optimisation-based modelling. A modular, surrogate-based mixed-integer linear programming (MILP) formulation is introduced in [4] to capture high-resolution WEFE interactions, yet stochastic or robust methods are not applied, limiting the model's capacity to reflect system variability and risk.

1.1. Optimisation approaches and uncertainty modelling

A range of literature has examined optimisation strategies in more detail, particularly focusing on their formulation complexity, temporal resolution, and scope of application. A recent review of WEF optimisation studies [5] shows that most adopt multi-objective LP/MILP formulations is typically using ε-constraint or weighted-sum approaches. Uncertainty is mainly addressed through stochastic, robust, chance-constrained, or fuzzy methods, while true multi-level

* Corresponding author.
E-mail addresses: goran.stunjek@fsb.hr (G. Stunjek), goran.krajacic@fsb.hr (G. Krajačić).

https://doi.org/10.1016/j.nexus.2025.100570
Received 18 July 2025; Received in revised form 17 September 2025; Accepted 16 October 2025
Available online 17 October 2025

Nomenclature

Abbreviations

WEFE	Water-energy-food-ecosystem
FPV	Floating photovoltaic power plant
PSH	Pumped-storage hydropower plant
WE	Water-energy
WEF	Water-energy-food
MILP	Mixed-integer linear programming
LP	Linear programming
RES	Renewable energy sources
PV	Photovoltaic power plant
MC	Monte Carlo
EWP	Equivalent water price
FPVC	FPV investment cost
a.s.l.	Above sea level
NREL	U.S. National Renewable Energy Laboratory
ETS	Emission Trading System
LHS	Left-hand side
RHS	Right-hand side
LDC	Load duration curve

Model sets

$t \in T$	Time periods
$s \in S$	Scenarios
$fpvc \in FPVC$	FPV investment cost
$ewp \in EWP$	Equivalent water price
$x \in \{E, WE, WEF, WEFE\}$	Sector viewpoints

Model variables

FPV^p MW	FPV nominal power
$E^{FPV_P}_{s,\,t}$ MWh	Electricity flow – FPV to pump
$E^{P_g}_{s,t}$ MWh	Electricity flow – grid to pump
$E^{P}_{s,t}$ MWh	Electricity flow – total electricity to pump
$E^{T}_{s,t}$ MWh	Electricity flow – hydro electricity generation
$E^{FPV_g}_{s,t}$ MWh	Electricity flow – total FPV to grid
$W^{eva_{save}}_{s,t}$ m^3/h	Water flow – evaporation savings
$W^{spill}_{s,t}$ m^3/h	Water flow – total water spillage
$W^{dwn_{spill}}_{s,t}$ m^3/h	Water flow – lower storage water spillage
$W^{up_{spill}}_{s,t}$ m^3/h	Water flow – upper storage water spillage
$W^{ll}_{s,t}$ m^3/h	Water flow – lost load
$W^{agri}_{s,t}$ m^3/h	Water flow – total agriculture irrigation needs
$W^{up_{wl}}_{s,t}$ m^3	Upper storage hourly water level
$W^{P}_{s,t}$ m^3/h	Water flow through pump
$W^{T}_{s,t}$ m^3/h	Water flow through turbine
$W^{up_{eva}}_{s,t}$ m^3/h	Total upper storage evaporation
$W^{up_{spill}}_{s,t}$ m^3/h	Water flow – upper storage spillage
$X^{P}_{s,t}$ {1,0}	Binary variable for PSH pump activation
$X^{T}_{s,t}$ {1,0}	Binary variable for PSH turbine activation
$W^{dwn_{wl}}_{s,t}$ m^3	Lower storage hourly water level
$W^{dwn_{spill}}_{s,t}$ m^3/h	Water flow – upper storage spillage
$E^{FPV}_{s,t}$ MWh	Total upper storage FPV electricity generation
$A^{FPV_{tot}}$ m^2	Total upper storage FPV area
$A^{FPV_{eff}}$ m^2	Effective FPV area
A^{agri} m^2	Total agriculture irrigation area
$W^{up_{eva\_FPV}}_{s,t}$ m^3/h	Upper storage evaporation on FPV area
$W^{up_{eva\_b}}_{s,t}$ m^3/h	Upper storage base water evaporation on non FPV area
$Z^{E}_{s,\,t}$ EUR	Energy focused sum of revenues and costs
$Z^{WE}_{s,\,t}$ EUR	Water-Energy focused sum of revenues and costs
$Z^{WEF}_{s,\,t}$ EUR	Water-Energy-Food focused sum of revenues and costs
$Z^{WEFE}_{s,\,t}$ EUR	Water-Energy-Food-Ecosystem focused sum of revenues and costs

Model parameters

ΔkPa/°C	Saturation slope vapour pressure curve at T_{hr}
R_nMJ/m^2h	Net solar radiation
GMJ/m^2h	Soil/water body heat flux density
γkPa/°C	Psychrometric constant
T_{hr}°C	Mean hourly air temperature
u_2m/s	Average hourly wind speed at 2 m
$e^0[T_{hr}]$kPa	Saturation vapour pressure at T_{hr}
e_akPa	Average actual vapour pressure
ic^{FPV}EUR/MW	FPV investment cost
cr	Capital recovery factor
p_s %	Scenario s probability
isc %	Inverter share cost in total RES CAPEX cost
pvf_r	Present value factor for replacement r
lsr	Land sparing ratio (PV to FPV area ratio)
lusEUR/m^2	Land use savings
λ^{emp}_tEUR/MWh	Electricity market price
bb %	Electricity buy-back factor
hyd^{omc}EUR/MWh	Hydropower operation and maintenance cost
fpv^{omc}EUR/MWh	FPV operation and maintenance cost
λ^{ewp}EUR/m^3	Equivalent water price
λ^{spill}EUR/m^3	Water spillage cost
λ^{wll}EUR/m^3	Water lost load cost
λ^{eco}EUR/MWh	Ecological external cost on hydropower generation
sn	Small number cost value
co^{geq}_2tCO_2/MWh	Grid equivalent CO_2 emissions
co^{FPV}_2tCO_2/MWh	FPV CO_2 emissions
co^{hyd}_2tCO_2/MWh	Hydropower CO_2 emissions
$co^{c}_{2_{cp}}$EUR/tCO_2	CO_2 price
$w^{agri}_{s,t}$$m^3/m^2$	Agriculture irrigation needs per m^2
$w^{wdem}_{s,t}$$m^3/h$	Water demand for residential needs, industry and tourism
$w^{up_{inf}}_{s,t}$$m^3/h$	Upper storage river inflow
$w^{up_{pp}}_{s,t}$$m^3/h$	Upper storage precipitation
$w^{up_c}$$m^3$	Upper storage capacity
$w^{up_{wl}}_{t_0}$ %	Upper storage water level in the first time step in %
$w^{up_{cmax}}$ %	Maximum upper storage capacity in %
$w^{up_{cmin}}$ %	Minimum upper storage capacity in %
aei^PMWh/m^3	PSH pump average energy intensity
aei^TMWh/m^3	PSH turbine average energy intensity
p^CMW	PSH pump nominal power capacity
t^CMW	PSH turbine nominal power capacity
$w^{dwn_{inf}}_{s,t}$$m^3/h$	Lower storage river inflow
$w^{dwn_{pp}}_{s,t}$$m^3/h$	Lower storage precipitation
$w^{dwn_c}$$m^3$	Lower storage capacity
$w^{dwn_{wl}}_{t_0}$$m^3$	Lower storage water level in the first time step in %
$w^{dwn_{cmax}}$ %	Maximum lower storage capacity in %
$w^{dwn_{cmin}}$ %	Minimum lower storage capacity in %
$w^{dwn_{eva}}_{s,t}$$m^3/h$	Lower storage evaporation
fpv^sMW/m^2	FPV energy density per m^2
$fpv^{pot}_{s,t}$MWh/MW	FPV potential
fpv^{pf}	FPV packing factor
$et^{up}_{0_{s,t}}$ mm/h	Upper storage specific water evaporation

erf %	Evaporation reduction factor	ET_cmm/h	Crop evapotranspiration under standard conditions
$a^{up_{lake}}$m^2	Upper lake surface	K_c	Crop coefficient
$et_{0_{s,t}}^{dwn}$mm/h	Lower storage specific water evaporation	P_{eff}mm/h	Effective precipitation
$a^{dwn_{lake}}$m^2	Lower lake surface	P_{tot} mm/h	Total precipitation
ET_0mm/h	Reference evapotranspiration		

optimisation remains rare. The review also highlights the critical importance of temporal and spatial resolution, which is directly relevant to FPV-PSH-irrigation planning. In [6], a MILP-based model is developed to optimise the design and hourly scheduling of renewable (RES) and hydrogen hybrid system. While the model offers a techno-economic framework, it does not address uncertainty, and it omits pumped storage hydro (PSH) and agricultural sector integration. Similarly [7], propose a dual-optimisation structure, combining surrogate modelling for PSH sizing with MILP-based dispatch. The model focuses only on energy system performance and excludes cross-sectoral WEFE dimensions such as evaporation, irrigation, or food system interactions. The authors in [8] introduce a two-stage deterministic optimisation for shared energy storage integrated with FPV and hydropower. Their model accounts for stakeholder benefit distribution and carbon penalties but relies on a single 24-hour cycle extrapolated to annual values, omitting seasonal variability and excluding agricultural and water loss modelling. Authors in [9] present a combined MILP with ε-constraint for cost-water-land trade-offs in RES system design, demonstrated on Amarillo with PHS and compressed air storage integration.

Building on deterministic optimisation approaches, several studies introduce more structured treatments of risk and uncertainty, ranging from simulation sets to fully stochastic and robust formulations. The model in [10] applies a scenario-based approach to represent forecast uncertainties in wind and photovoltaic (PV) generation. The model performs hourly optimal dispatch over a 24-hour horizon and maximises expected profits, but it does not extend to longer-term uncertainty or include components like agriculture or PSH. In [11], a multi-objective optimisation framework is introduced for WEF nexus planning. However, the model is not temporally resolved and operates on aggregated scenarios rather than optimisation over time. A two-stage stochastic optimisation model combining interval parameters and fuzzy logic is introduced in [12] to support water allocation under complex uncertainty. The model effectively reflects uncertainty in a water management context but does not engage with energy or ecosystem sectors. In [13], a stochastic programming model is used to optimise hydropower dispatch under joint uncertainty in streamflows and electricity market prices. Uncertainty is captured through scenario trees, and the authors demonstrate that this formulation outperforms traditional stochastic dynamic programming and sampling-based methods. The authors in [14] extended this line of research into a coupled electricity and gas market, using a stochastic MILP model to optimise the operation of PSH under wind power uncertainty. While their approach advances real-time market coordination and profitability analysis, it remains confined to the energy sector without integration of water, agricultural, or environmental dynamics.

1.2. Hybrid hydropower and renewable energy sources operation

The integration of hydropower and variable RES has emerged as a strategic pathway toward enhancing flexibility and reliability in low-carbon energy systems. While these approaches offer valuable insights into coordinated dispatch, planning, and uncertainty management, they often remain confined to the energy domain and omit deeper connections with the broader WEFE nexus. In [15], a two-stage stochastic model is applied to explore climate adaptation strategies in a hydro-dominated power system. Although the model incorporates key uncertainties, it operates on an annual time step with fixed capacities, limiting operational insight. The authors emphasise the importance of a WEFE-oriented perspective for future system planning under climate risk. A robust day-ahead dispatch model for PV-hydro coordination is introduced in [16], where PV uncertainty is captured using non-parametric ambiguity sets. The model improves dispatch reliability but is confined to short-term scheduling and excludes water use beyond hydropower. A two-stage stochastic framework is proposed in [17] to evaluate wind-PV-hydropower configurations. Although effective in managing preference uncertainty, the model does not capture system dispatch or storage dynamics.

The integration of PSH with variable RES is increasingly seen as a cornerstone of flexible, resilient energy systems. Recent work has made important strides in developing modelling tools and optimisation strategies for hybrid configurations, but significant gaps remain, particularly in how these systems are treated under uncertainty, and how they connect to broader WEFE dimensions. Broad overviews of the field, such as [18] and [19], highlight the fragmented state of current modelling practice. While hybrid PSH-RES systems are gaining attention, many studies still rely on closed-source software and lack transparency in methodology. There is a notable shortage of models tailored to PSH configurations involving RES, and most existing research remains focused on short operational horizons. These reviews also point to a lack of real-world case studies and limited attention to uncertainty, despite its growing importance for system planning.

Several applied studies reflect these trends. In [20], a two-stage stochastic optimisation is used to determine water value in a diesel–wind–PSH hybrid system. However, the model runs over only a two-week period and omits water allocation or evaporative losses. Similarly, the long-term expansion planning model in [21] offers detailed integration of PSH with wind, PV, and thermal power, but focuses narrowly on electricity storage and does not account for broader WEFE dynamics. The authors in [22] propose a qualitative site selection framework for FPV-PSH integration based on multi-criteria decision-making, but without system dynamics or cross-sector modelling. Work provided in [23] examines a hybrid FPV-PSH system with hydrogen and thermal production, yet their model is deterministic and lacks optimisation or linkage to food and ecosystem components. The work in [24] presents a multi-objective stochastic scheduling model for cascade hydropower and PV, aiming to reduce output deviation and improve peak shaving. While successful in that regard, the model remains confined to energy metrics. Likewise, [25] addresses PSH integration under RES price uncertainty using robust MILP methods but limits the scope to short-term market operations. A more comprehensive approach appears in [26], which combines hydropower, PV, wind, and battery storage within a two-stage stochastic model. The study makes substantial progress in handling uncertainty through probabilistic sampling and scenario reduction. However, even at this level of detail, key WEFE components such as evaporation modelling or agricultural water demands are excluded.

1.3. Ecosystem integration modelling

What emerges across these works is a clear focus on energy-system coordination and uncertainty management, but with limited integration of water and land dynamics, and almost no direct modelling of food or ecosystem-related variables. Recent research has demonstrated a variety of modelling approaches aimed at capturing interactions within

the WEFE nexus, with particular attention to multi-sectoral water use, RES integration, and ecosystem constraints. An optimisation framework in [27], schedules hydropower generation while considering environmental flows and water demands. The study [28] introduces a hydro-economic model comparing priority-based and economically optimised water allocations but lacks hybrid RES integration and stochastic uncertainty management. A multi-objective optimisation presented in [29] generates hydropower withdrawal trade-offs, realistically integrating evaporation and flow constraints but excludes crop-specific demands and detailed temporal resolution. Operational scheduling for hybrid energy systems, especially FPV combined with PSH was examined in [30], optimising hourly operations for reduced costs and evaporation benefits, yet without addressing evaporation as a decision variable or agricultural needs. Reference [31] further analyses FPV-PSH systems, highlighting reservoir and cooling effects on energy performance but omitting infrastructure planning, explicit evaporation modelling, and food nexus integration, relying instead on scenario analysis for risk. Complementing, a study [32] evaluate FPV deployment on irrigation canals, quantifying substantial evaporation reductions and dual-purpose energy–water benefits, though their work remains deterministic and does not consider optimisation or agricultural linkages explicitly. At the sector level, authors in [33] formulate a large-scale WEF planning-and-scheduling model for greenhouses with hourly resolution and a superstructure MILP solved via ε-constraint/weighted-sum multi-objective strategies. Collectively, these studies enhance WEFE nexus integration but largely neglect detailed ecosystem services, food production, and robust uncertainty treatment.

In summary, existing studies either remain energy-centric, rely on short horizons or deterministic analyses, or omit explicit ecosystem and agricultural couplings. These limitations motivate the integrated, uncertainty-aware WEFE framework proposed in this study.

1.4. Proposed paper contribution

This study makes a significant contribution to the evolving body of literature on WEFE nexus optimisation by introducing a fully integrated, high-resolution modelling framework that jointly addresses energy generation, water use, food system demands, and ecosystem costs and benefits under uncertainty. While numerous previous works have explored partial dimensions of the nexus ([1–4]), the proposed approach stands out in its synthesis of detailed technical, financial, economic, and environmental factors through a unified, stochastic optimisation model.

Unlike prior partial or deterministic approaches ([5–9]), this study integrates technical, financial, economic, and environmental aspects through a unified two-stage stochastic model. Monte Carlo simulation is used for scenario generation of hourly inputs of uncertain parameters. These scenario-specific inputs are then passed into a deterministic-equivalent MILP formulation of the two-stage problem, which is solved once over all scenarios with assigned probabilities p_s. This captures resource variability and improves the robustness of system design beyond pure deterministic methods, short-horizon setups, and extends beyond energy-only setups that neglect WEFE integration [10–17,20–26]. This high-resolution, uncertainty-aware formulation represents a rare but necessary advancement in the modelling of complex WEFE systems.

A key methodological contribution of the study lies in the layered structuring of the objective function, which enables a progressive expansion of the system boundary from an energy-centric focus to fully integrated WE, WEF, and WEFE configurations. New parameters, constraints, and costs introduced at each stage allow systematic assessment of how additional nexus dimensions impact system design, operational strategies, and environmental co-benefits, such as emissions and land-use reductions [22–24,27–29]. Additionally, ecological external cost applied to hydropower generation, and a CO_2 price sensitivity is conducted to quantify how carbon valuation shifts optimal FPV deployment and hybrid FPV-PSH operation [8,15,16,18–21].

Evaporation is explicitly embedded within the optimisation using the FAO-56 Penman-Monteith equation and dynamically linked to FPV surface area. Unlike conventional models calculating evaporation post-optimisation or uniformly across scenarios, this approach directly integrates evaporation into decision-making, enabling valuation of water savings and their operational impacts with greater fidelity [24,30,31].

Agricultural water use is included by optimising irrigation area directly as a variable, explicitly representing the food component in the WEFE system. Irrigation demand is modelled as a dynamic function of crop area and time within reservoir balances and decision-making, contrasting with typical predefined or omitted agricultural demands. The model employs the FAO-56 Penman–Monteith method at hourly resolution, enhancing accuracy by aligning irrigation needs closely with climatic variability and operational strategies, strengthening the model's realism and integrative capacity [23,29,31–33].

By explicitly coupling PSH and FPV within a stochastic framework, the model addresses cross-sectoral linkages such as evaporative water loss, irrigation demands, and emissions and land-use savings. This facilitates comprehensive evaluation of hybrid system performance under various technical and environmental constraints, thus supporting resilience and climate adaptation strategies. Collectively, these methodological innovations represent an important step toward realistic, integrated WEFE nexus modelling, bridging critical gaps between theoretical exploration and practical infrastructure planning seen in the existing literature.

To the best of our knowledge, no prior study concurrently endogenises reservoir evaporation, optimises irrigation area, and couples FPV-PSH within a two-stage stochastic, hourly model spanning all four WEFE dimensions.

1.5. Paper organization

The remainder of the paper is structured as follows. Section 2 details the two-stage stochastic optimisation framework, covering sector-specific modelling of WEFE components. It includes evaporation modelling, agricultural irrigation calculations, uncertainty scenario generation, and the optimisation approach. Section 3 introduces the case study of the PSH Velebit system in Croatia. It outlines key input data and assumptions, including technical and spatial parameters for the FPV, hydrological and climatic conditions, irrigation modelling assumptions, financial and economic parameters, and quantification of ecosystem co-benefits. Section 4 presents results and discussion of the optimisation under four progressively complex viewpoints. Each viewpoint is analysed in terms of system configuration, operational trade-offs, and the impact of cross-sectoral integration under uncertainty. Finally, Section 5 concludes the study and outlines directions for future work, including planned model extensions and methodological improvements aimed at enhancing system adaptability and realism.

2. Methods

The proposed methodological framework, illustrated in Fig. 1, aims to identify optimal system configurations and dispatch strategies from the perspective of the WEFE nexus.

The framework begins with essential system-level inputs such as weather, geolocation, agricultural characteristics, hydropower infrastructure, and RES specifications, denoted by the blue-coloured blocks. A detailed description of the data types and specific input values is provided in Section 3. Water inflows, precipitation, evaporation, RES potentials, and sector-specific water demands as uncertain climate parameters are gathered into a set of climate uncertain data represented by dark blue block. Uncertain climatic drivers are fed into the climate scenario generation module, where a Monte Carlo (MC) simulation framework is applied to generate a finite set of plausible climate scenarios $s \in S$, which is further detailed in Section 2.3.

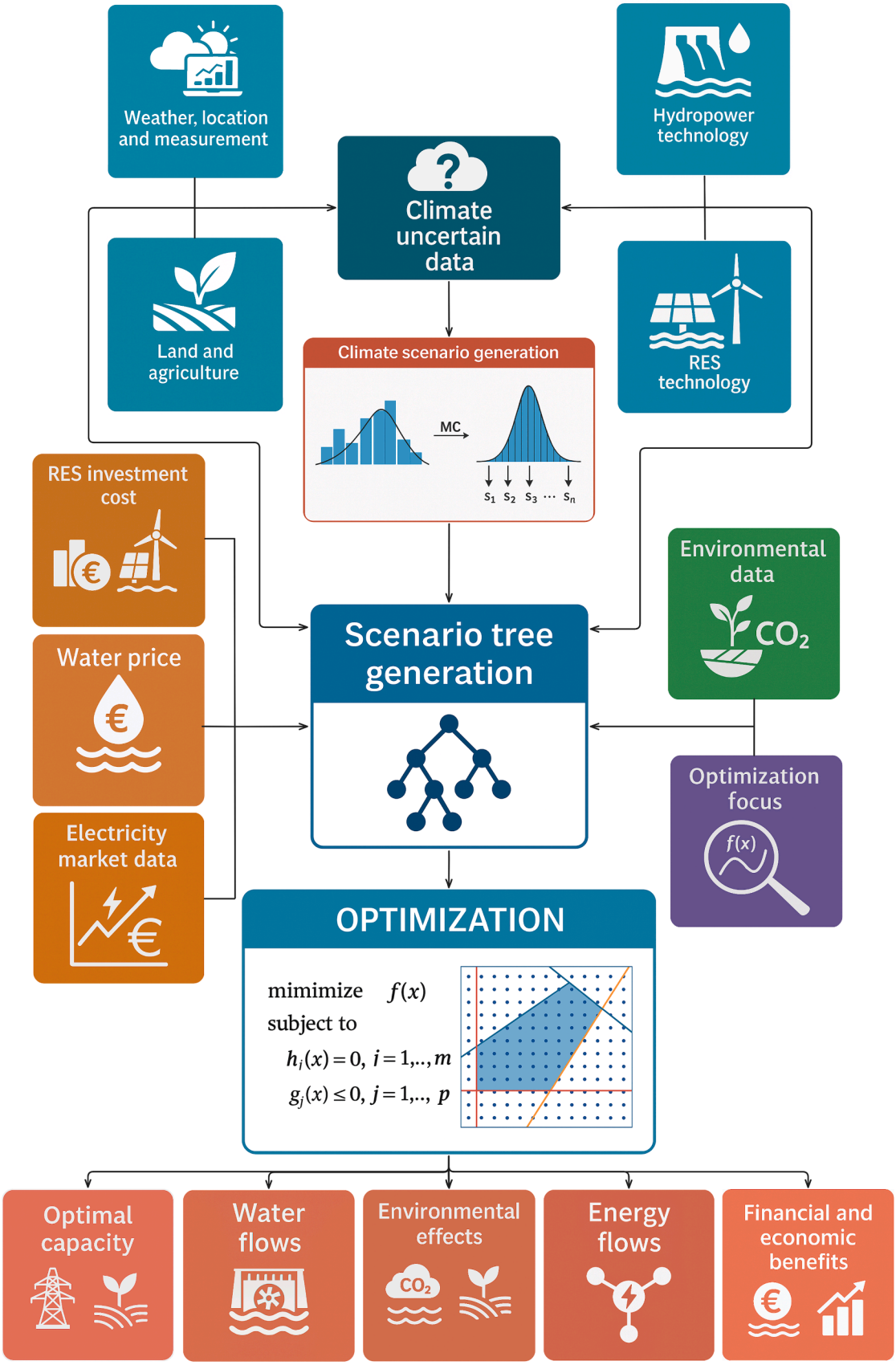

Fig. 1. Schematic of the modelling and optimisation approach.

Economic and financial parameters, represented by orange blocks, include RES investment costs, equivalent water pricing (EWP), and electricity market data. To reflect uncertainty and variability in market conditions, an hourly MC sampling approach was applied to model hourly representative electricity market price. The corresponding data sources and values are described in Section 3.4. The environmental parameters, represented by the green block, quantify ecological benefits including CO_2 emissions and land-use savings, as detailed in Section 3.5. The optimisation focus, illustrated by the purple block, outlines the sector-specific objective functions described further in Section 2.4, guiding the selection and integration of relevant sectors within the modelling approach.

All described inputs are synthesized within the scenario tree generation module, which structures parameters and scenarios for multiple optimisation runs, capturing diverse system responses. The optimisation employs a deterministic-equivalent formulation of the two-stage stochastic approach, where first-stage decisions define infrastructure sizing, and second-stage decisions manage operational dispatch under varying climate scenarios. The proposed optimisation approach evaluates integrated systems comprising PSH, FPV, agricultural irrigation systems, and assessment of ecosystem effects. It evaluates optimal configurations and operations through four distinct viewpoints defined by different objective functions. This structure highlights trade-offs and synergies among sectors, with detailed implementation provided in Section 2.4.

Optimisation results, represented in the lower part of Fig. 1, cover five main domains: optimal system capacities, including energy units and irrigated areas; hourly water flow allocations, reservoir operations, and spillage management; energy dispatch among hydropower, FPV, and the grid; ecological impacts of system operations; and associated financial and economic benefits. Subsequent subsections detail methodological aspects such as reservoir evaporation modelling, agricultural irrigation demand estimation, climate scenario generation, and the two-stage stochastic optimisation formulation.

2.1. Evaporation modelling

Estimating evaporation from open water bodies is crucial for water management, especially in arid regions. Common approaches include empirical methods, such as pan evaporation, which are simple but often overestimate evaporation and need local calibration [34,35]. Physically based methods, like energy-budget and mass-transfer models, improve accuracy but require extensive meteorological data, limiting practical use [34,36]. Combined approaches, such as Penman and Priestley–Taylor, integrate energy and aerodynamic factors. However, Priestley–Taylor performs less reliably in dry conditions [37], and Penman may overestimate evaporation in high-wind scenarios [36].

The FAO-56 Penman–Monteith method, originally designed for crop evapotranspiration has been successfully adapted for open water surfaces by setting surface resistance to zero. Studies demonstrate its evaporation estimates closely match observed data, typically within a 10 % margin, outperforming standard Penman and other modified models [38,39]. Due to its theoretical robustness, flexibility, and compatibility with widely available data, FAO-56 is considered highly reliable for open-water evaporation estimation. The subsequent section provides details on its formulation, assumptions, inputs, and typical applications in hydrological modelling.

2.1.1. FAO-56 – penman-monteith method

The calculation of reference evapotranspiration (ET_o) is essential for hydrological modelling and agricultural water management, reflecting atmospheric evaporative demand over a standardized surface. The FAO-56 Penman-Monteith method, internationally recognized for its accuracy and simplicity, estimates ET_o using net radiation, air temperature, wind speed, and vapor pressure deficit, calibrated for a hypothetical well-watered grass reference crop [40,41].

The formulation is valid across daily, and monthly time steps, but it has become increasingly recognized that hourly calculations enhance realism and responsiveness, especially important in regions with significant daily weather variability, such as Mediterranean or arid climates [40,42].

The FAO-56 Penman-Monteith equation for hourly ET_0 calculation is shown in (1).

$$ET_0 = \frac{0.408 \cdot \Delta \cdot (R_n - G) + \gamma \cdot \frac{37}{T_{hr} + 273} \cdot u_2 \cdot (e^0[T_{hr}] - e_a)}{\Delta + \gamma \cdot (1 + 0.34 \cdot u_2)} \quad (1)$$

This approach uses hourly inputs for net radiation, temperature, humidity, and wind speed, capturing sub-daily fluctuations often lost in daily averages [40]. Since most evapotranspiration happens during midday hours, daily aggregation can distort peak demand estimates [41,42]. The method has proven widely applicable in global studies and is integrated into tools like CROPWAT and AquaCrop. Recent updates highlight the benefits of gridded and hourly data, which better reflect spatial and temporal variability and enhance water management under extreme weather and climate change [41]. Further detailed description on FAO-56 ET_0 calculation steps can be found in [40].

2.2. Agriculture irrigation needs modelling

Following the ET_o calculation, crop evapotranspiration under standard conditions (ET_c) quantifies the water needed for optimal crop growth. In the FAO-56 framework [40], ETc is computed hourly as ET_o multiplied by a crop-specific coefficient (K_c), shown in Eq. (2).

$$ET_{c_{s,t}} = K_{c_{stage}} \cdot ET_{0_{s,t}} \ (\forall\, s \in S,\ \forall\, t \in T) \quad (2)$$

The single K_c value combines crop and soil effects and varies by crop type, climate, and growth stage. FAO-56 defines four stages, and three specific coefficients: Kc_{ini} (initial), $Kc_{\_mid}$ (mid-season), and Kc_{end} (end-season). Selecting accurate Kc values is crucial for precise ET_c estimation. More details are available in [40].

2.2.1. Effective precipitation

Calculating ET_c from Eq. (2) enables estimation of agricultural irrigation water needs ($w_{s,t}^{agri}$), determined as the difference between ET_c and effective precipitation (P_{eff}) shown in Eq. (3), since not all rainfall is available for crops [40].

$$w_{s,t}^{agri} = ET_{c_{s,t}} - P_{eff_{s,t}} \ (\forall\, s \in S,\ \forall\, t \in T) \quad (3)$$

Effective precipitation accounts for losses from runoff, deep percolation, or water held beyond root zones. P_{eff} can be estimated through methods ranging from simple empirical rules to detailed water balance models, with the CROPWAT method widely adopted and recommended for its accuracy, deviating <5 % from soil water balance measurements, especially in semi-arid regions [39,43]. CROPWAT calculates P_{eff} at daily resolution, aiding precise irrigation planning, and integrates seamlessly with climate databases and decision-support tools [44]. It is especially practical in irrigation planning because it integrates easily into scheduling tools and supports sub-monthly resolution [39,44].

P_{eff} is calculated following the CROPWAT approach in Eqs. (4) and (5), which is conventionally expressed in daily form. To ensure consistency with the hourly ET_c calculation, hourly precipitation data were first aggregated to daily totals for the application of Eqs. (4) and (5). Resulting P_{eff} is then scaled back to hourly resolution according to the known hourly precipitation distribution. This ensures that both ET_c and P_{eff} remain fully consistent at hourly resolution.

$$P_{eff_{s,t}} = P_{tot_{s,t}} \cdot \frac{125 - 0.2 \cdot P_{tot_{s,t}}}{125} \ for\ P_{tot_{s,t}} < 250\ mm\ (\forall\, s \in S, \forall\, t \in T) \quad (4)$$

$$P_{eff_{s,t}} = \left(125 + 0.1 \cdot P_{tot_{s,t}}\right) \ for\ P_{tot_{s,t}} > 250\ mm\ (\forall\, s \in S,\ \forall\, t \in T) \quad (5)$$

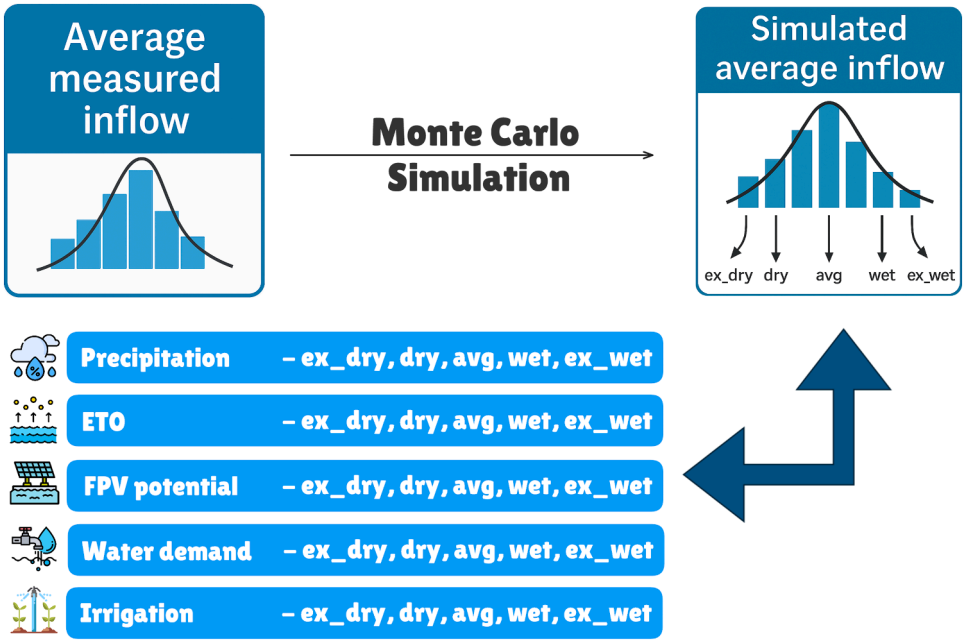

Fig. 2. Climate uncertain data scenario generation approach.

2.3. Climate uncertain data scenario generation

The climate uncertain data scenario generation for second-stage parameters in the two-stage stochastic optimisation is illustrated in Fig. 2. Key uncertain inputs include accumulation inflow, precipitation, evaporation (ET_o), FPV potential, and water demands across sectors like drinking, industry, tourism, and agriculture

We model uncertainty via five hydrologic year scenarios divided into extreme dry, dry, average, wet, and extreme wet. Using historical river flows from 2001 to 2022, we compute annual inflow totals and fit a normal distribution to annual inflows for each reservoir. Goodness-of-fit of the normal distribution was confirmed for both reservoirs. For the lower reservoir, the fitted distribution yielded a mean of 18.745 m^3/s and a standard deviation of 5.317 m^3/s. The Kolmogorov-Smirnov test (statistic = 0.0798, p-value = 0.988) and the Anderson-Darling statistic (0.157) both confirmed the adequacy of the normal fit. For the upper reservoir, the fitted distribution had a mean of 9.825 m^3/s and a standard deviation of 2.788 m^3/s, with a Kolmogorov-Smirnov statistic of 0.0766 (p-value = 0.992) and an Anderson-Darling statistic of 0.154, likewise confirming the appropriateness of the normal distribution. These results indicate that the normal distribution provides an excellent representation of the historical annual inflow series. Representative quantile values for each hydrologic-year scenario are reported in Table S2 in the Appendix A.

Monte Carlo sampling from the fitted normal is then used to characterize the annual inflow distribution. The five scenarios are selected as mid quantiles of the <5 %, 5–25 %, 25–75 %, 75–95 %, >95 % probability blocks with the assigned probabilities of 5 %, 20 %, 50 %, 20 %, and 5 %, respectively. For each scenario, an hourly inflow trace is obtained by scaling the closest historical hourly profile to match the scenario's annual total per the normal distribution. Other uncertain climate parameters, shown in Fig. 2, are co-selected consistently with the same hydrologic year as for the river inflow data. These five one year, hourly scenarios constitute the stochastic input set for the deterministic-equivalent formulation of the two-stage stochastic problem.

2.4. Two-stage stochastic optimisation model

This study employs a two-stage stochastic optimisation framework to determine optimal system design and dispatch under uncertainty. In the first stage, design choices like FPV capacity and irrigation area are set before uncertain conditions are realized, while the second stage optimises operations under various climate and market scenarios. For the clarity purposes, we solve the deterministic-equivalent MILP formulation of the two-stage stochastic problem once over all five scenarios with assigned probabilities p_s across a range of FPV investment costs ($fpvc \in FPVC$), and equivalent water prices ($ewp \in EWP$), allowing comprehensive parametric analysis. Though equations omit explicit indexing for clarity, these dependencies are maintained in the model.

Each optimisation run is formulated as a large-scale MILP with 963,618 constraints, 1051,204 continuous variables, and 87,600 binary variables. The problem is solved with an hourly time step over a one-year horizon. Variable limits are defined by the feasible ranges of installed FPV capacity, PSH operation, and water allocation constraints as described below. The same model size is used across all optimisation runs for the full range of FPVC-EWP pairs.

The optimisation considers four perspectives, each defined by distinct objective functions (6)-(9) aimed at maximizing system revenue, and expressed in monetary terms (EUR) ensuring a unified and comparable dimension:

- Energy-centric (E): captures electricity revenues minus investment and operational costs, as detailed in Eqs. (6) and (10).
- Water-Energy (WE): extends the E objective by including financial and economic gains from evaporation savings, and costs from spillage and lost water loads, described in Eqs. (7) and (11).
- Water-Energy-Food (WEF): adds constraints linked to irrigation water demands and constraints on water allocation, reflected in Eqs. (8) and (12). Further difference between the WE and WEF viewpoint can be seen in constraint (25) where agricultural irrigation water demand $W_{s,t}^{agri}$ is added. Notably, while irrigation water use is modelled, investment and operational costs for agricultural infrastructure are excluded, as the study focuses on implications of introducing irrigation water demand on the operation and configuration of the hybrid FPV-PSH system.
- Water-Energy-Food-Ecosystem (WEFE): builds on WEF by integrating revenues from avoided CO_2 emissions and costs from grid-

related CO_2 impacts, land-use savings, an ecological external cost applied to hydropower generation, as shown in Eqs. (9) and (13).

It is important to note that each of the four viewpoints is solved as a separate optimisation run, which enables progressively broader perspective. Each scenario-dependent revenue and cost component $Z^{x}_{s,\,t}$ for each optimisation perspective $x \in \{E, WE, WEF, WEFE\}$ is further defined in Eqs. (10) to (13), forming the core of the second-stage objective function. These equations capture revenues from FPV electricity sales, hydropower generation, water-related economic benefits, and ecosystem services, while subtracting operational and environmental costs. This layered structure ensures the model can capture sectoral interactions and trade-offs essential for WEFE nexus analysis under uncertainty.

$$\max \sum_{s} p_s \cdot Z^{E}_{s,t} - FPV^{p} \cdot ic^{FPV} \cdot cr - \sum_{r} FPV^{p} \cdot ic^{FPV} \cdot isc \cdot pvf_r \cdot cr, (\forall s \in S, \forall t \in T) \tag{6}$$

$$\max \sum_{s} p_s \cdot Z^{WE}_{s,t} - FPV^{p} \cdot ic^{FPV} \cdot cr - \sum_{r} FPV^{p} \cdot ic^{FPV} \cdot isc \cdot pvf_r \cdot cr, (\forall s \in S, \forall t \in T) \tag{7}$$

$$\max \sum_{s} p_s \cdot Z^{WEF}_{s,t} - FPV^{p} \cdot ic^{FPV} \cdot cr - \sum_{r} FPV^{p} \cdot ic^{FPV} \cdot isc \cdot pvf_r \cdot cr, (\forall s \in S, \forall t \in T) \tag{8}$$

$$\max \sum_{s} p_s \cdot Z^{WEFE}_{s,t} - FPV^{p} \cdot ic^{FPV} \cdot cr - \sum_{r} FPV^{p} \cdot ic^{FPV} \cdot isc \cdot pvf_r \cdot cr + A^{FPV_{tot}} \cdot lsr \cdot lus, (\forall s \in S, \forall t \in T) \tag{9}$$

$$Z^{E}_{s,t} = \sum_{t} \lambda^{emp}_{t} \cdot \left(E^{FPV_P}_{s,t} + bb \cdot E^{FPV_g}_{s,t} + E^{T}_{s,t} - E^{P_g}_{s,t} \right) - \sum_{t} hyd^{omc} \cdot E^{T}_{s,t} - \sum_{t} fpv^{omc} \cdot E^{FPV}_{s,t}, (\forall s \in S, \forall t \in T) \tag{10}$$

$$Z^{WE}_{s,t} = Z^{E}_{s,t} + \sum_{t} \lambda^{ewp} \cdot W^{eva_{save}}_{s,t} - \sum_{t} \lambda^{spill} \cdot W^{spill}_{s,t} - \sum_{t} \lambda^{wll} \cdot W^{ll}_{s,t}, (\forall s \in S, \forall t \in T) \tag{11}$$

$$Z^{WEF}_{s,t} = Z^{WE}_{s,t} + \sum_{t} sn \cdot W^{agri}_{s,t}, (\forall s \in S, \forall t \in T) \tag{12}$$

$$Z^{WEFE}_{s,t} = Z^{WEF}_{s,t} + \left(co^{geq}_{2} - co^{FPV}_{2} \right) \cdot E^{FPV}_{s,t} \cdot co^{c}_{2_{cp}} + \left(co^{geq}_{2} - co^{hyd}_{2} \right) \cdot E^{T}_{s,t} \cdot co^{c}_{2_{cp}} - co^{geq}_{2} \cdot E^{P_g}_{s,t} \cdot co^{c}_{2_{cp}} - \lambda^{eco} \cdot E^{T}_{s,t}, (\forall s \in S, \forall t \in T) \tag{13}$$

Eqs. (14)-(18) define constraints for upper reservoir storage. The water balance in Eq. (14) accounts for inflows from rivers, precipitation, and pumping, while outflows include turbine discharge, evaporation, and spillage. Constraints (15) and (16) fix initial and final water levels as percentages of total capacity, ensuring the final level is at least equal to the starting level. Eqs. (17) and (18) limit upper reservoir levels within minimum and maximum storage capacities, enabling dynamic operation and reflecting natural accumulation limits.

$$W^{up_{wl}}_{s,t} = W^{up_{wl}}_{s,t-1} + w^{up_{inf}}_{s,t} + w^{up_{pp}}_{s,t} + W^{P}_{s,t} - W^{T}_{s,t} - W^{up_{eva}}_{s,t} - W^{up_{spill}}_{s,t}, (\forall s \in S, \forall t \in [1, T]) \tag{14}$$

$$W^{up_{wl}}_{s,t} = w^{up_c} \cdot w^{up_{wl}}_{t_0}, (\forall s \in S, t = 0) \tag{15}$$

$$W^{up_{wl}}_{s,t} \geq w^{up_c} \cdot w^{up_{wl}}_{t_0}, (\forall s \in S, t = T) \tag{16}$$

$$W^{up_{wl}}_{s,t} \leq w^{up_c} \cdot w^{up_{cmax}}, (\forall s \in S, \forall t \in T) \tag{17}$$

$$W^{up_{wl}}_{s,t} \geq w^{up_c} \cdot w^{up_{cmin}} \mathrm{t}, (\forall s \in S, \forall t \in T) \tag{18}$$

Eqs. (19) to (24) govern PSH operation. Eq. (19) links pumped water volume to energy demand, while Eq. (20) splits energy between grid purchases and FPV self-consumption. Eq. (21) connects turbine discharge to hydropower generation. Constraints (22) and (23) limit pump and turbine operations to their maximum capacities, and Eq. (24) ensures mutual exclusivity, where only one mode can operate at any time step. Binary variables enforce this operational logic, resulting in a MILP formulation.

$$E^{P}_{s,t} = W^{P}_{s,t} \cdot aei^{P}, (\forall s \in S, \forall t \in T) \tag{19}$$

$$E^{P}_{s,t} = E^{P_g}_{s,t} + E^{FPV_p}_{s,t}, (\forall s \in S, \forall t \in T) \tag{20}$$

$$E^{T}_{s,t} = W^{T}_{s,t} \cdot aei^{T}, (\forall s \in S, \forall t \in T) \tag{21}$$

$$E^{P}_{s,t} \leq p^{C} \cdot X^{P}_{s,t} \cdot \Delta t, (\forall s \in S, \forall t \in T) \tag{22}$$

$$E^{T}_{s,t} \leq t^{C} \cdot X^{T}_{s,t} \cdot \Delta t, (\forall s \in S, \forall t \in T) \tag{23}$$

$$X^{P}_{s,t} + X^{T}_{s,t} \leq 1, (\forall s \in S, \forall t \in T) \tag{24}$$

Eqs. (25) to (30) model lower reservoir dynamics. The water balance in Eq. (25) includes inflows from rivers, precipitation, and turbine discharge, and outflows to pumping, evaporation, residential, industrial, tourism, and agricultural uses, plus spillage. To handle potential infeasibility under high demand, a water lost load variable with a high penalty cost is introduced. Eqs. (26) and (27) define initial and final lower reservoir levels as percentages of capacity, while Eqs. (28) and set upper and lower storage limits. Eq. (30) computes total irrigation water demand based on hourly crop water requirements $w^{agri}_{s,t}$ and optimised irrigated area A^{agri}.

$$W^{dwn_{wl}}_{s,t} = W^{dwn_{wl}}_{s,t-1} + w^{dwn_{inf}}_{s,t} + w^{dwn_{pp}}_{s,t} + W^{T}_{s,t} - W^{P}_{s,t} - w^{dwn_{eva}}_{s,t} - w^{wdem}_{s,t} - W^{agri}_{s,t} - W^{dwn_{spill}}_{s,t} + W^{wll}_{s,t}, (\forall s \in S, \forall t \in [1, T]) \tag{25}$$

$$W_{s,t}^{dwn_{wl}} = w^{dwn_c} \cdot w_{t_0}^{dwn_{wl}}, (\forall s \in S, t = 0) \quad (26)$$

$$W_{s,t}^{dwn_{wl}} \geq w^{dwn_c} \cdot w_{t_0}^{dwn_{wl}}, (\forall s \in S, t = T) \quad (27)$$

$$W_{s,t}^{dwn_{wl}} \leq w^{dwn_c} \cdot w^{dwn_{cmax}}, (\forall s \in S, \forall t \in T) \quad (28)$$

$$W_{s,t}^{dwn_{wl}} \geq w^{dwn_c} \cdot w^{dwn_{cmin}} t, (\forall s \in S, \forall t \in T) \quad (29)$$

$$W_{s,t}^{agri} = w_{s,t}^{agri} \cdot A^{agri}, (\forall s \in S, \forall t \in T) \quad (30)$$

Eqs. (31)-(35) describe FPV system modelling. FPV energy output in Eq. (31) is calculated using the EHDO tool [45], considering system characteristics, weather data, and technical parameters. Eq. (32) divides FPV output between grid sales and self-consumption for pump operation. Eq. (33) defines optimal FPV installed capacity, while Eq. (34) calculates total FPV area considering panel arrangement and packing factor. Eq. (35) limits FPV deployment to the available lake surface area. In this study, FPV is deployed exclusively on the upper reservoir due to space constraints and water level fluctuations in the lower reservoir.

$$E_{s,t}^{FPV} = A^{FPV_{eff}} \cdot fpv^s \cdot fpv_{s,t}^{pot}, (\forall s \in S, \forall t \in T) \quad (31)$$

$$E_{s,t}^{FPV} = E_{s,t}^{FPV_g} + E_{s,t}^{FPV_p}, (\forall s \in S, \forall t \in T) \quad (32)$$

$$FPV^P = A^{FPV_{eff}} \cdot fpv^s \quad (33)$$

$$A^{FPV_{tot}} = A^{FPV_{eff}} \cdot fpv^{pf} \quad (34)$$

$$A^{FPV_{tot}} \leq a^{up_{lake}} \quad (35)$$

Eqs. (36) to (41) describe evaporation and spillage modelling. The model determines the optimal FPV area and divides upper reservoir evaporation into two parts. Eq. (36) expresses total evaporation as the sum of evaporation over FPV-covered and uncovered areas. Evaporation over the FPV-covered surface is defined in Eq. (37) including a reduction factor from literature, while base evaporation over uncovered areas is described in Eq. (38). Total evaporation savings from FPV deployment are calculated in Eq. (39). Evaporation from the lower reservoir, without FPV coverage, is determined in Eq. (40).

$$W_{s,t}^{up_{eva}} = W_{s,t}^{up_{eva\_FPV}} + W_{s,t}^{up_{eva\_b}}, (\forall s \in S, \forall t \in T) \quad (36)$$

$$W_{s,t}^{up_{eva\_FPV}} = et_{0_{s,t}}^{up} \cdot A^{FPV_{tot}} \cdot (1 - erf) \cdot 10^{-3}, (\forall s \in S, \forall t \in T) \quad (37)$$

$$W_{s,t}^{up_{eva\_b}} = et_{0_{s,t}}^{up} \cdot \left(a^{up_{lake}} - A^{FPV_{tot}}\right) \cdot 10^{-3}, (\forall s \in S, \forall t \in T) \quad (38)$$

$$W_{s,t}^{eva_{save}} = et_{0_{s,t}}^{up} \cdot A^{FPV_{tot}} \cdot erf \cdot 10^{-3} t, (\forall s \in S, \forall t \in T) \quad (39)$$

$$W_{s,t}^{dwn_{eva}} = et_{0_{s,t}}^{dwn} \cdot a^{dwn_{lake}} \cdot 10^{-3}, (\forall s \in S, \forall t \in T) \quad (40)$$

$$W_{s,t}^{spill} = W_{s,t}^{dwn_{spill}} + W_{s,t}^{up_{spill}}, (\forall s \in S, \forall t \in T) \quad (41)$$

All optimisation runs were implemented in Python 3.7 using the GUROBI solver. The stopping criteria were set at a relative MIP optimality gap of 0.1 % and a feasibility tolerance of 1e-6. The average convergence time of an optimisation run is dependent on the FPVC/EWP values and other input parameters, but on average requires around 30 min on the workstation, which was equipped with two Intel Xeon Gold 6126 CPUs and 768 GB of RAM.

3. Case study – PSH Velebit - Croatia

PSH Velebit in Croatia was selected as appropriate case study due to available upper storage area for FPV implementation, high variable river inflow highly climate dependent and available area for agriculture development assessment. Its location in the Mediterranean region, expected to be significantly affected by climate change, further underscores its relevance for integrated WEFE system analysis.

Located in the southeast Lika region, PSH Velebit lies between the Gračac plateau and the Zrmanja River basin in Zadar County. The lower reservoir, Razovac, is at 9 m above sea level (a.s.l.), while the upper reservoir, Štikada, sits above 550 m a.s.l. [46]. The region's climate is transitional between inland mountains and the Adriatic coast, characterized as humid subtropical, with hot summers exceeding 30 °C, mild winters occasionally dropping below −5 °C, and annual precipitation between 1200 and 1700 mm, higher near the Velebit mountains. Climate variability poses increasing challenges for water quality, availability, and system management, affecting downstream ecosystems and settlements such as Obrovac and Zadar County [47].

The hourly river inflow data from 2001 to 2022 for lower and upper accumulations were obtained from Croatian Waters, enabling detailed analysis of inflow variability, seasonal shifts, and operational impacts [48]. Water demand for residential needs, industry and tourism equal to the amount of water distributed from lower Razovac accumulation was made available by the Water utility company for Zadar County [49]. The upper reservoir Štikada has a total volume of 13.6 million m³, with 9.6 million m³ usable for energy generation [46]. The average available surface area is 334 hectares [50]. Minimum upper storage is set at 30 % of total volume, with initial levels assumed at 50 %. Razovac reservoir holds up to 1.84 million m³ over 36 hectares [46]. Due to missing data, the minimum lower storage level is assumed at 20 % of total volume. These limits ensure a minimum natural outflow is always available.

PSH Velebit operates with two reversible Francis pump-turbine units, providing up to 280 MW in turbine mode with a flow of 60 m³/s, and 240 MW in pumping mode with a 40 m³/s flow [46]. Average specific energy consumption during pumping aei^P is 1.65 kWh/m³, while generation intensity from turbine operation aei^T is 1.3 kWh/m³, reflecting typical conversion and hydraulic losses in high-head systems. Variable operating and maintenance costs are estimated at 0.45 EUR/MWh [51].

3.1. Floating solar power plant assumptions

As outlined in Section 2.4, the approach of authors in [45] was adopted to calculate FPV potential in MWh/MW. The modelled system is based on a 580 W PV panel, each occupying an area of 2.174 m² [52]. The inclination angle is set at 0°, representing a flat, horizontal configuration that is often preferred for reducing wind loading and optimising layout density on reservoirs. A packing factor, fpv^{pf}, of 1.5 is adopted, accounting for the additional spacing and structural elements required for installation and maintenance access between floating panel rows.

The installation site is positioned at an elevation of 550 m above sea level, consistent with the altitude of the Štikada reservoir, which is the subject of the integration case with PSH Velebit. The investment cost for FPV systems is modelled within a realistic range of 1000 to 2000 EUR/kW, allowing flexibility in financial sensitivity analyses depending on technology choices, anchoring methods, and project-specific logistics.

Operating and maintenance costs reference NREL data, estimating variable expenses at 7.61 EUR/MWh, covering maintenance, monitoring, insurance, and performance reporting [53]. Inverter replacements are planned in the 10th and 20th year of operation, each costing 4 % of the total system investment [53].

3.2. Evaporation modelling assumptions

To evaluate reservoir evaporation in the hybrid FPV-PSH system, a detailed modelling approach was used, as described in prior methodology. The model was applied separately to the upper and lower reservoirs, accounting for their different elevations, surface areas, and microclimatic conditions. Meteorological inputs were obtained from the

ERA5-Land dataset [54], providing hourly data from 2001 to 2022. Parameters for the FAO-56 ET_0 calculation, representing evaporation, included air temperature, dew point, wind speed, and net surface radiation. This high-resolution data enabled realistic simulations capturing diurnal and seasonal evaporation patterns over two decades. An evaporation reduction factor of 87 % was applied to FPV-covered surfaces, based on literature reporting substantial mitigation of evaporation due to shading and wind shielding by FPV systems. This conservative factor assumes optimal FPV coverage under static conditions [36].

3.3. Agriculture irrigation needs assumptions

To calculate crop water needs using the single crop coefficient method described in Section 2.2, the model required crop-specific inputs for all four growth stages: initial, development, mid-season, and late season. Inputs included stage durations in days and Kc values for initial (Kc_{ini}), mid-season (Kc_{mid}), and end stages (Kc_{end}), along with each crop's planting start month to align water demand with the annual climate cycle.

Based on data from [55] and [56], the agricultural area is predominantly planted with vegetables, covering about 48.8 % of irrigated land. Olives follow at 18.1 %, cereals at 13.6 %, grapes at 7.8 %, and feed crops at 6.9 %, while other fruits represent around 4.9 %. Appendix A - Table S1 provides further detail on specific crops and input assumptions. This crop distribution reflects regional agricultural trends and is crucial for modelling irrigation demands.

3.4. Financial and economic assumptions

Several financial and economic assumptions support the hybrid FPV-PSH system, as introduced earlier, especially in Section 2.4 discussing investment and replacement costs. Beyond technology-specific investments, broader economic parameters are included for annualised cost analysis. The model uses a 6 % discount rate and a 25-year project lifetime, essential for the two-stage stochastic optimisation where annual total system cost is a key objective.

Hourly electricity prices were sourced from the Croatian Energy Exchange [57], with MC sampling used to generate representative hourly price scenarios and capture market uncertainty and variability.

Unlike typical shadow price methods applied in linear optimisation, the MILP structure here does not allow direct shadow price calculation. Instead, a parametric analysis was performed across predefined EWP values to examine how varying water valuations influence FPV adoption and system operations.

In this study, the EWP reflects the economic value of avoided evaporation rather than direct water usage, highlighting the benefits of water savings in regions facing seasonal scarcity. Values from 0 to 30 EUR/m^3 were analysed to identify conditions where FPV becomes economically beneficial. Although this approach does not fully replicate shadow pricing, it offers valuable insights into balancing energy production with water conservation.

3.5. Ecosystem assumptions

As part of the extended WEFE nexus analysis, this study incorporates environmental co-benefits and costs, specifically avoided CO_2 emissions, grid-related CO_2 costs, land-use savings, and an ecological external cost applied to PSH generation, as monetised values within the optimisation framework.

Carbon savings are calculated as the net difference between emissions from grid electricity and the zero-emission output of the hybrid FPV-PSH system. Both PSH and FPV are assumed emission-free, while grid electricity carries an emission factor of 131 gCO_2/kWh, based on national assessments for Croatia [58]. The economic value of avoided emissions is derived from the European Union Emission Trading System (ETS). Although the ETS still shows some sectoral gaps and price volatility [59], it has stabilized since late 2021, with prices ranging between 54.21 and 104.81 EUR/tCO_2. An average price of 79.51 EUR/tCO_2 is used in this study as the economic equivalent of avoided emissions. To assess sensitivity, additional optimisation runs were performed for the lower and upper bounds of the recent ETS price range.

Land-use savings are also quantified by comparing FPV deployment to conventional ground-mounted PV systems. Based on earlier FPV assumptions, including a panel area of 2.174 m^2, a packing factor of 1.5, and a land-sparing ratio of 2.7 [60]. The analysis estimates the land area avoided by installing PV on water rather than land. Monetisation uses NREL cost data, indicating 0.03 USD/W for land acquisition and site preparation in utility-scale PV projects [61], translating to a land-use savings value of approximately 2.96 EUR/m^2. This value is included as an ecosystem-related benefit in the model.

In addition to CO_2 and land-use impacts, the WEFE case internalizes an ecological external cost on PSH generation parameterized as a constant λ^{eco} value equal to 2.57 EUR/MWh. Following authors in [62], this represents an aggregated ecosystem losses term that monetises impacts from biodiversity loss, water-supply alteration, and soil-erosion.

4. Results and discussion

This section presents and discusses the results of the optimisation modelling carried out to determine the optimal configuration and operation of an integrated hybrid FPV-PSH system, incorporating progressively broader economic, environmental, and ecological considerations.

4.1. Energy-centric viewpoint

This section presents results for the energy-centric optimisation, focusing solely on electricity revenues and costs, as defined in Eq. (6). No water, environmental, or agricultural aspects are included, allowing isolated analysis of financial feasibility based on market conditions and system constraints.

The optimisation analysis reveals that the integration of the FPV system into the existing hydropower setup is financially justified only at the lowest considered investment cost of 1000 EUR/kW. At higher FPV costs, installation is not justified, as capital costs outweigh operational benefits. Under the optimal scenario at 1000 EUR/kW, the FPV system achieves a capacity of 340.04 MW, covering 1.911 km^2, leading to significant evaporation savings of 1.423 Mm^3 annually.

Annual FPV electricity production reaches 411.557 GWh, with 95.06 % (391.225 GWh) consumed for pump operation, indicating high self-consumption. Hydropower generation increases modestly from 897.414 GWh to 903.701 GWh, a 0.7 % gain, highlighting FPV's role in improving flexibility and slightly boosting hydropower output. It's important to note that grid electricity demand profiles are not explicitly modelled, as demand signals are embedded within market prices.

Financial analysis shows the hydropower-only scenario yields 37.744 million EUR in annual net operational revenues. The hybrid FPV-hydropower system generates higher operational revenues of 67.295 million EUR, but after deducting annualised FPV investment costs of 29.178 million EUR, the net annual financial benefit is 38.117 million EUR. This reflects an incremental advantage of approximately 372.67 thousand EUR per year, or around 1 % higher financial returns compared to hydropower alone.

Operational dynamics throughout the annual period are further illustrated by daily aggregated data presented in Fig. 3. For the sake of diagram representation clarity, hourly optimal dispatch is daily aggregated which provides clear visualization of system performance over a yearly cycle. The Fig. 3 illustrates daily aggregated optimal dispatch for the hybrid system. Positive values show PSH generation (blue) and FPV generation (yellow). Negative values represent pumping electricity consumption, divided into FPV-sourced power (green) and grid-sourced power (brown). The figure also depicts daily upper reservoir water level

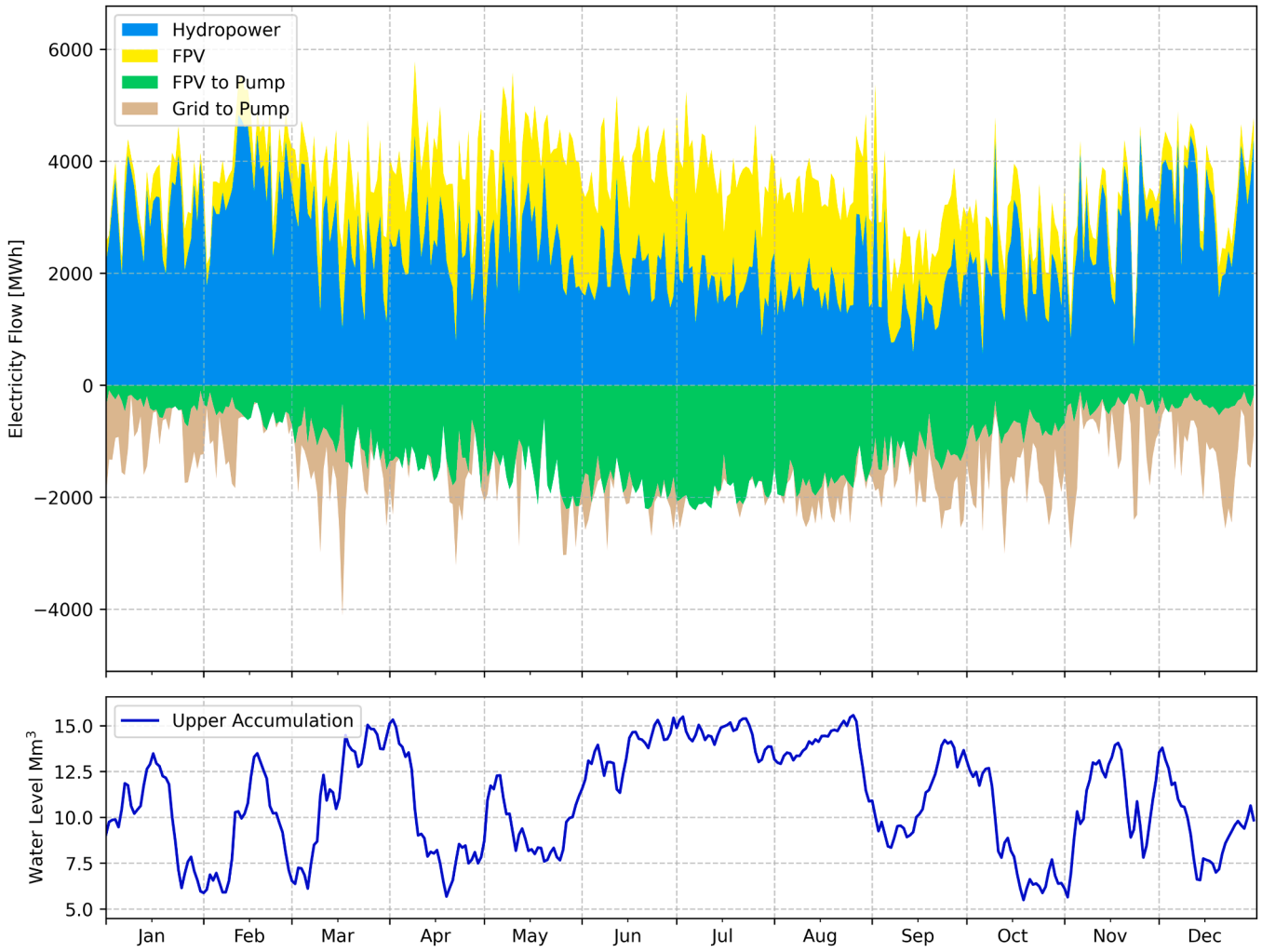

Fig. 3. Optimal system dispatch under energy-centric viewpoint – daily aggregated.

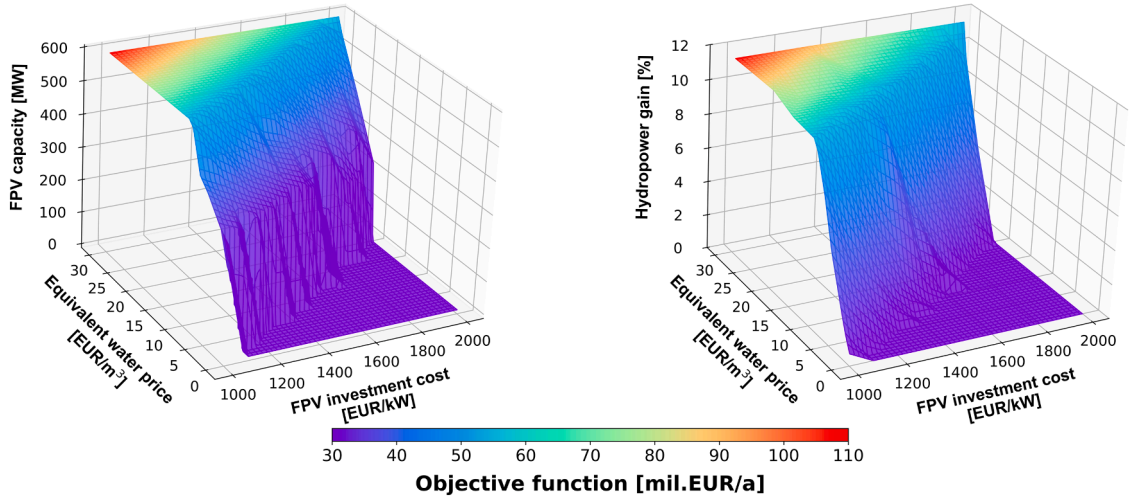

Fig. 4. Range of optimal water-energy viewpoint results; FPV capacity (left); Hydropower generation gain (right).

fluctuations, indicating operation within storage limits.

Although the increase in hydropower generation from integrating FPV is modest at around 0.7 %, significant differences appear in generation patterns between the hydro-only and hybrid FPV-PSH scenarios. The hybrid system delivers higher and steadier baseload hydropower with reduced variability, whereas the hydro-only system shows more frequent and pronounced peaks, indicating a more intermittent profile. This shift suggests that hybrid FPV-PSH operations can enable smoother hydropower dispatch and balance the inherent intermittencies of both technologies. Hydropower can help stabilise the hourly and seasonal

variability of FPV output, while FPV production, peaking in late spring and summer, supports hydropower by optimising water storage during periods of high demand and evaporation losses. Moreover, optimised dispatch with lower variability may reduce mechanical stress on turbines and other equipment, potentially enhancing operational reliability and extending the system's lifespan.

For clarity, the daily hydropower-only generation curve is not shown here, but the effects of FPV integration on hydropower dispatch and load duration patterns are analysed in the following Water-Energy section and illustrated in detail in Fig. 5.

4.2. Water-energy viewpoint

This section presents optimisation results for the Water-Energy (WE) perspective, expanding the analysis beyond electricity revenues to include economic benefits from evaporation savings. By incorporating the economic value of saved water, expressed through the EWP, the optimisation expands beyond the energy-centric scenario to explicitly reflect the interplay between energy production and water management.

Fig. 4 shows how optimal FPV capacity and hydropower generation gains vary with FPV investment cost (FPVC) and EWP. The left diagram depicts optimal FPV capacities, while the right shows percentage increases in hydropower generation compared to the hydro-only scenario.

The LHS diagram shows that at an EWP of 0 EUR/m^3, FPV deployment is only viable at the lowest investment cost of 1000 EUR/kW, achieving a capacity of 340.04 MW, consistent with the energy-centric analysis. The diagram also indicates an upper limit of 594.17 MW for FPV capacity, representing the maximum installable area. As FPV costs rise, higher EWP values are needed to justify investment. Notably, for FPV costs above 1600 EUR/kW, capacity increases by about 33.33 MW per EUR/m^3 of EWP, whereas below 1500 EUR/kW, the rate slows to roughly 25.61 MW per EUR/m^3, indicating less sensitivity to water valuation at lower capital costs.

The RHS diagram confirms that RES integration positively impacts hydropower generation, with gains closely matching optimal FPV capacities. This reflects a direct link between FPV deployment and hydropower efficiency. Reduced evaporation from FPV coverage conserves water, boosting hydropower output, with average gains of about 11.44 % across varying FPV costs and EWP values.

Further details on these operational effects and dispatch patterns from FPV integration are examined through load duration curves (LDC) shown in Fig. 5.

Table 1
Percentage of time that hydropower falls within the specific power ranges.

PSH power range [MW]	Hydro only	EWP = 0	EWP = 5	EWP = 10	EWP = 30	Δ
>= 250	52.12 %	45.34 %	45.26 %	45.62 %	43.75 %	−8.38 %
[200–250>	4.72 %	2.68 %	2.86 %	2.86 %	2.91 %	−1.81 %
[150–200>	9.47 %	9.27 %	9.19 %	9.20 %	9.91 %	0.44 %
[100–150>	10.30 %	12.32 %	11.96 %	11.58 %	11.96 %	1.66 %
[50–100>	11.47 %	15.97 %	16.34 %	16.23 %	16.45 %	4.98 %
<0–50>	11.91 %	14.42 %	14.39 %	14.51 %	15.01 %	3.11 %

The LDC shows consistent trends across different FPVC, with EWP changes having the strongest influence on curve shapes and magnitudes. Due to limited variability across FPVC values, LDC results are presented for an FPVC of 1000 EUR/kW, where FPV deployment remains economically optimal across all EWP levels for clarity and ease of interpretation.

Fig. 5 displays LDCs for hydropower generation under varying EWPs from 0 to 30 EUR/m^3. The legend indicates EWP values, corresponding optimal FPV capacities, and hydropower gains compared to the hydro-only case. As earlier noted in the Energy-centric section (Fig. 3), FPV integration reduces hydropower dispatch volatility. LDCs confirm this by showing additional hydropower generation shifting to lower, sustained power levels, visible as rightward shifts compared to the hydro-only baseline shown by the black dashed curve. This highlights how FPV and hydropower complement each other, jointly mitigating seasonal variability and enhancing baseload capacity.

For EWP values up to 7 EUR/m^3, FPV shifts hydropower production toward stable baseload rather than peak output. At EWPs of 10 EUR/m^3 and above, high-power generation durations are maintained or slightly increased, while longer low-power operation persists. LDCs for 20 EUR/m^3 and higher become nearly identical, indicating maximum FPV deployment and similar hydropower gains.

The frequency analysis of hourly hydropower generation further confirms the stabilizing effect of FPV-PSH hybrid operation. Table 1 shows the percentage of time that hydropower generation falls within specific power blocks as FPV implementation increases, with the increase in EWP.

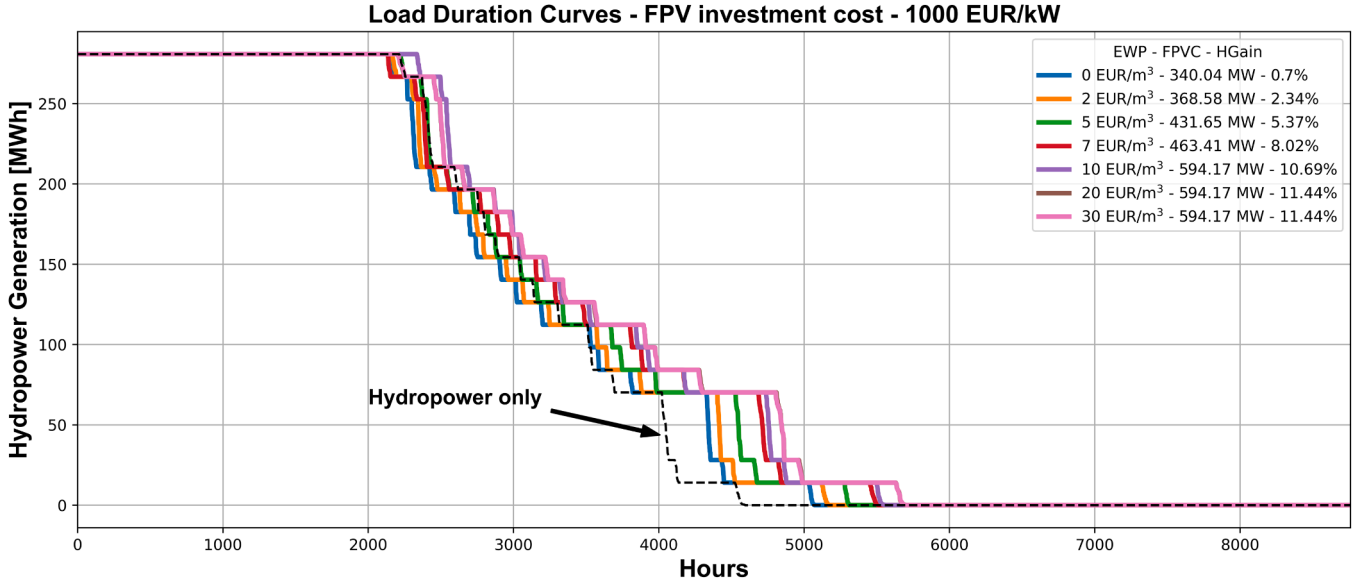

Fig. 5. Load duration curves for hydropower generation.

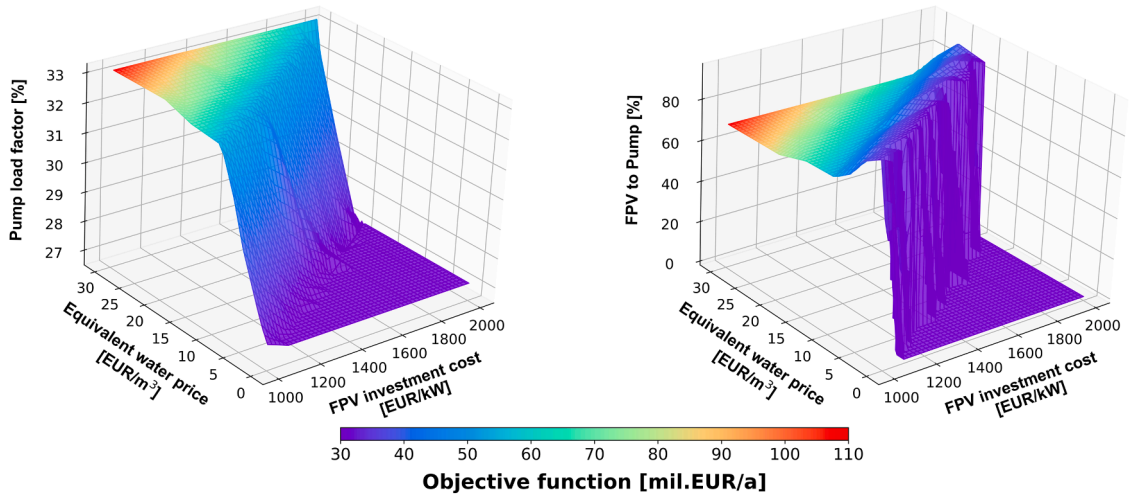

Fig. 6. Range of optimal pump specific water-energy viewpoint results; Pump load factor (left); RES self-consumption for pump operation (right).

The distribution confirms the stabilizing effect of FPV-PSH hybrid operation. Compared to the hydro-only case, the share of time with very high hydropower output (≥200 MW) decreases noticeably, with 8.38 % drop in the ≥250 MW block, and 1.81 % drop in the 200–250 MW block. These reductions are offset by systematic increases in the lower bands, with 4.98 % increase in the 50–100 MW block and 3.11 % increase in the 0–50 MW block, alongside smaller gains in the 100–150 MW range where 1.66 % increase is seen. This redistribution of hours demonstrates that hybrid operation reduces extreme peaks while extending periods of steady, mid-range generation, in line with the rightward shifts observed in Fig. 5. In addition, the average ramp up and down value for the hydropower generation decreases, with mean absolute falling from 128.46 MWh in the hydro-only case to 107.47 MWh under full FPV implementation, equivalent to a 16.4 % reduction. Together these results provide strong statistical evidence that FPV integration lowers volatility and enhances the baseload character of hydropower generation.

The analysis further examines operational dynamics of the integrated FPV-PSH system, focusing on pump operations. Fig. 6 shows how EWP and FPVC affect the pump load factor, the ratio of actual pump usage to its maximum possible usage, and the share of FPV-generated electricity used directly for pumping.

The left diagram reveals that the pump load factor improves from 27.08 % without FPV to a peak of 33.15 % as EWP rises and FPV capacity grows. This reflects FPV's role in boosting pump operation consistency and self-consumption, thanks to more available renewable energy. Sensitivity of the pump load factor to EWP changes becomes more pronounced at higher FPVC levels, mirroring trends in optimal FPV capacity adjustments. Initially, the FPV-to-pump ratio exceeds 90 %, indicating that new FPV capacity is predominantly used for pumping, reducing reliance on grid electricity. As EWP and FPV capacity increase further, this ratio gradually drops, stabilizing around 69.03 %. This decline signals a strategic shift: as the economic value of evaporation savings rises, operations prioritize broader evaporation reduction and enhanced hydropower generation over purely supplying pump energy. While direct FPV use for pumping decreases slightly, the overall economic and operational benefits improve due to gains in hydropower

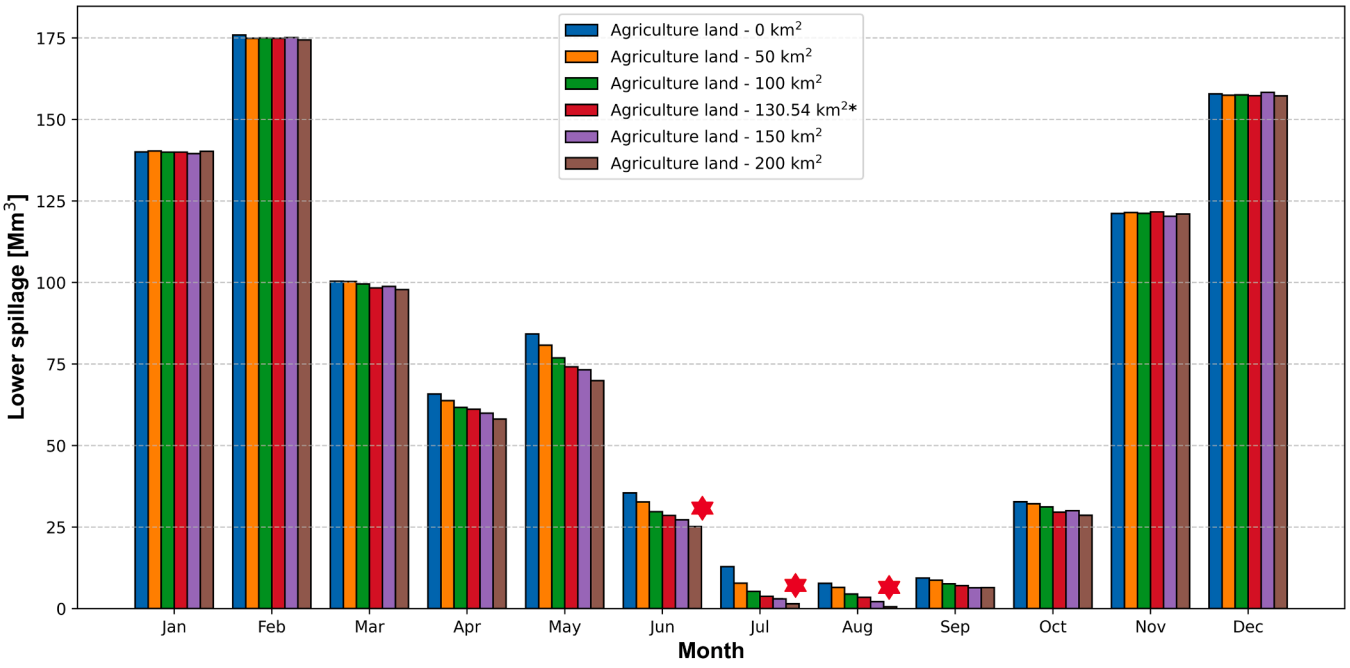

Fig. 7. Monthly lower accumulation spillage volumes for different agriculture irrigation areas.

efficiency and evaporation savings.

4.3. Water-energy-food viewpoint

This section builds on earlier analyses by adding the food dimension, incorporating agricultural irrigation demands into the optimisation. The WEF approach simultaneously optimises hydropower and FPV operations alongside the agricultural irrigation area. To maintain clarity, detailed graphics are omitted, focusing instead on key textual comparisons with the WE scenario.

Optimisation consistently identifies an optimal agricultural irrigation area averaging 130.54 km^2, with a low standard deviation of 0.522 km^2, showing stable results across the range of FPVC and EWP values.

Compared to the WE scenario (Fig. 4), the WEF results show similar trends in optimal FPV capacity, but with notable differences at lower EWP values. In the WEF case, higher irrigation demands reduce water availability for hydropower, diminishing the benefits of evaporation savings at lower EWP. Thus, lower FPV capacities are optimal initially. However, as EWP rises, evaporation savings become more valuable, bringing WEF results closer to those in the WE scenario. Only at the highest FPVC and EWP combination (2000 EUR/kW and 30 EUR/m^3) does the optimal FPV capacity remain slightly below the WE maximum, at 583.61 MW instead of 594.17 MW. Hydropower generation gains also plateau at about 10.71 % in the WEF scenario, lower than the 11.44 % in WE, due to added irrigation demands limiting available water for power generation.

Pump operations remain similar to the WE scenario, with minor differences. The WEF case sees a slightly lower maximum pump load factor of around 31.75 %, compared to 33.15 % in WE. The FPV-to-pump utilisation ratio remains slightly higher and declines more slowly across the EWP range, due to lower FPV capacities at low EWP levels. However, differences across the parameter space stay within 1 %, indicating only minor operational variations between WE and WEF.

The impact of agricultural water use is evident in monthly spillage data shown in Fig. 7, displayed for the FPVC/EWP pair of 1000 EUR/kW and 30 EUR/m^3, representing conditions allowing maximum FPV deployment. Analyses also examine fixed agricultural areas of 0, 50, 100, 150, and 200 km^2, alongside the optimal case of 130.54 km^2, to illustrate the effect of varying irrigation demands.

Monthly results highlight that summer is the primary constraint for hybrid FPV-hydropower operations. Higher irrigation needs overlap with peak electricity demand, low rainfall, and reduced river inflows, limiting system flexibility. FPV helps mitigate these constraints by generating power during late spring and summer, supporting water storage for hydropower. However, reservoir size still limits how much hydropower generation can be shifted outside summer. As reservoir expansion or additional accumulation capacity analysis was beyond the scope of this study, it is challenging to accurately define the maximum possible temporal shift of hydropower generation. Fig. 7 also shows that exceeding the optimal irrigation area leads to water shortages in June, July, and August, marked by red stars. This emphasizes the system's limits in handling excessive agricultural expansion.

Future research could examine alternative agricultural strategies, such as shifting crop types to avoid peak summer water demands or adopting technologies that enable year-round cultivation. However, these aspects were beyond this study's scope.

4.4. Water-energy-food-ecosystem viewpoint

This section extends previous analyses by incorporating ecosystem dimensions, monetising revenues from avoided CO_2 emissions and land-use savings, costs from grid-related CO_2, and an ecological external cost applied to PSH generation within the optimisation. The WEFE scenario delivers a holistic framework that evaluates environmental, water, energy, and agricultural factors.

Fig. 8 shows optimal FPV capacities and hydropower gains under varying FPVC and EWP values. Incorporating ecosystem benefits significantly increases optimal FPV deployment compared to the WE and WEF cases. For FPVC up to 1200 EUR/kW, the optimal FPV capacity consistently reaches the maximum allowable value of 594.17 MW. Unlike in the WE scenario, FPV capacity remains high even at moderate EWP levels, demonstrating how ecosystem valuation strongly incentivises RES integration. FPV deployment only drops out of the optimal solution at FPVC above 1900 EUR/kW combined with low EWP values below 2 EUR/m^3. Hydropower gains closely follow FPV deployment, showing rapid initial increases and then plateauing as FPV capacity maxes out. Under WEFE, this plateau averages a hydropower gain of around 17.74 %, relative to a hydro-only baseline of 808.01 GWh annual generation.

Additionally, incorporating ecosystem costs and benefits within the WEFE scenario significantly expands the overall range of objective function values, highlighting a more pronounced financial and economic incentive to adopt RES technologies and promote hybrid operation. Including ecosystem benefits expands the range of annual objective function values, now spanning 37 to 143 million EUR. In contrast, WE and WEF scenarios ranged from 37 to 105 million EUR. This broader range reflects the added financial and environmental value of considering ecosystem factors.

Fig. 9 explores pump operations under WEFE conditions. The pump load factor increases from 21.58 % in the hydro-only scenario to about

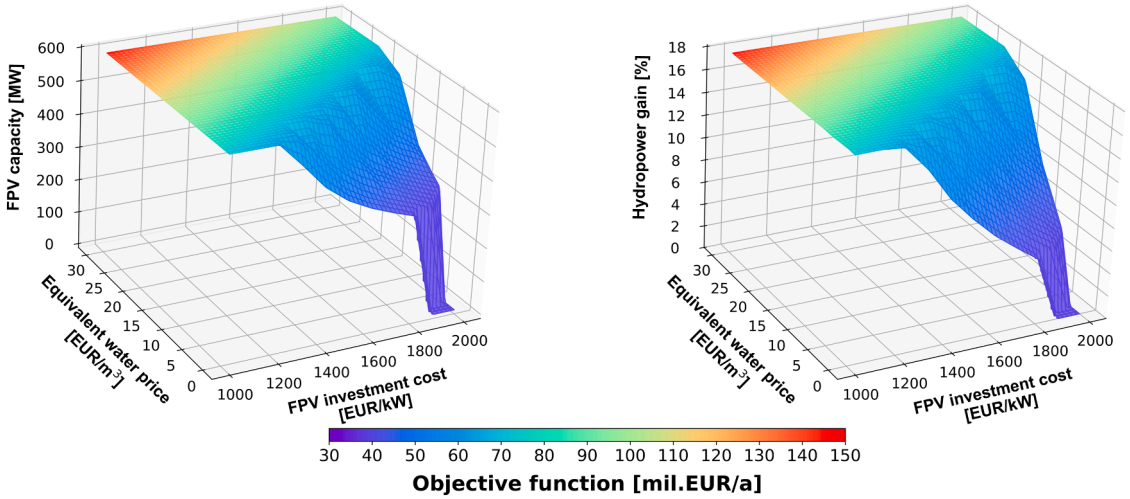

Fig. 8. Range of optimal water-energy-food-ecosystem viewpoint results; FPV capacity (left); Hydropower generation gain (right).

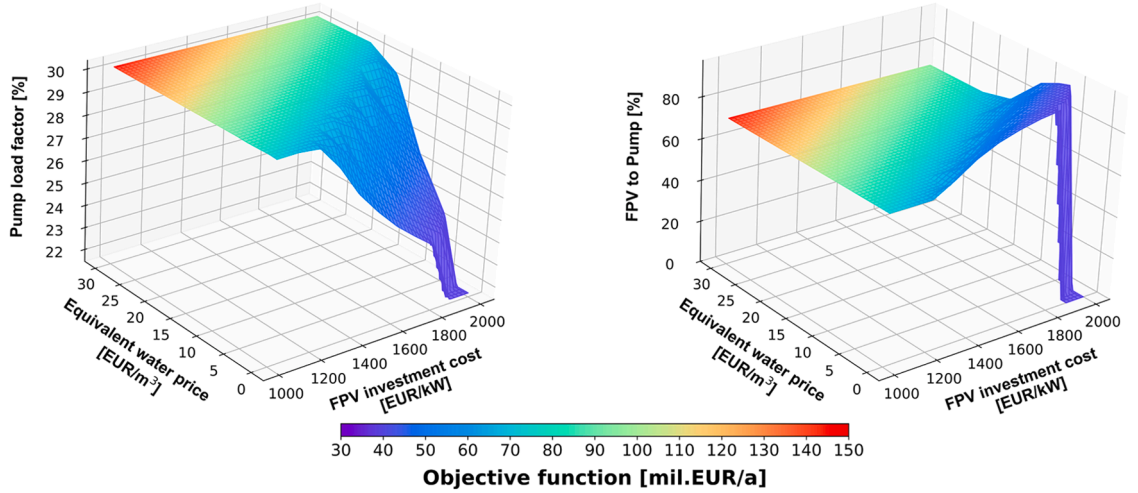

Fig. 9. Range of optimal pump specific water-energy-food-ecosystem viewpoint results; Pump load factor (left); RES self-consumption for pump operation (right).

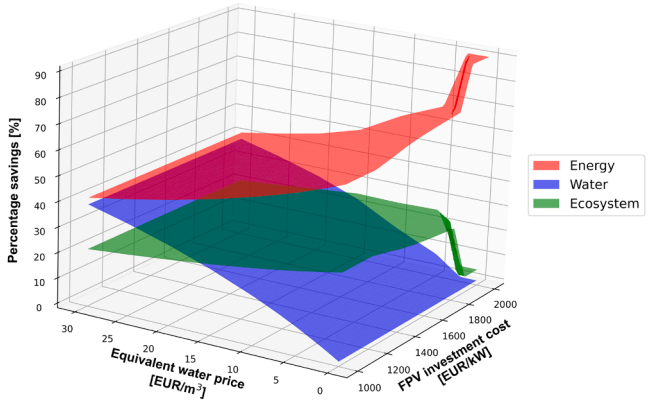

Fig. 10. Relative savings divided into categories Energy, Water and Ecosystem.

30.16 % at full FPV integration. Although this peak is slightly lower than in the WE scenario, the absolute gain of 8.58 % is larger when compared to WE. This result underscores how the incorporation of ecosystem costs and benefits significantly reshapes operational strategies, ultimately resulting in lower optimal hydropower dispatch in comparison to the WE scenario. Such findings highlight the critical importance of integrating ecosystem constraints into optimisation models to provide a more comprehensive view of optimal hybrid FPV-PSH configuration and dispatch patterns.

The RHS diagram on a Fig. 9 shows how the FPV-to-pump ratio remains high under WEFE. Initially averaging around 94.74 %, it indicates a strong preference for self-consumption of FPV electricity in pumping. As FPV capacity grows, this ratio gradually decreases to an average plateau of about 70.88 %. This consistently higher self-consumption ratio throughout the entire FPVC/EWP parameter space highlights that increased FPV self-consumption emerges as an economically and environmentally optimal operational strategy, distinctly surpassing values observed in the WE and WEF scenarios.

Continuing the WEFE analysis, Fig. 10 highlights the financial and economic aspects of the hybrid FPV-PSH system. Costs and savings are grouped into Energy, Water, and Ecosystem categories and shown as percentages, illustrating how these proportions shift with changes in FPVC and EWP.

Fig. 10 shows how Energy, Water, and Ecosystem costs and savings contribute across the full range of FPVC and EWP values in the WEFE optimisation. Energy savings include financial streams from hydropower and FPV, as described in Eq. (10). Water savings capture the economic value of reduced evaporation from FPV, linked to Eq. (11). Ecosystem savings reflect avoided CO_2 emissions, grid-related emissions costs, land-use savings due to FPV, and the PSH ecological external costs based on terms in Eq. (13). These percentages are relative and should be viewed alongside changes in the total objective function.

At high FPVC and low EWP values, energy savings dominate, reaching 90.44 %, reflecting scenarios without FPV deployment and minimal water or ecosystem savings. As FPV deployment grows, energy savings decline while water and ecosystem shares increase, highlighting trade-offs between pure energy gains and broader environmental benefits. Ecosystem savings remain stable at around 25.67 %, thanks to consistent CO_2 reductions and land-use benefits achieved when FPV operates at full capacity across much of the parameter space, as well as upper plateau values for additional hydropower generation gains. Water savings rise steadily with higher EWP values, reaching 38.03 % at the maximum EWP. This increase causes energy savings to drop to around 40.92 % on average. A notable balance occurs at an EWP of approximately 16.34 EUR/m^3, where water and ecosystem savings become equal, marking a point where water conservation and ecosystem benefits are equally valued. Notably, at an EWP of 0 EUR/m^3, growing FPV deployment shifts savings from energy to ecosystem benefits, reducing energy savings from 95.92 % to 66.32 % and raising ecosystem savings from 4.47 % to 33.67 %. This shift underscores how ecosystem benefits,

Table 2
Overall percentage change for key indicators across full FPVC/EWP range.

Indicator	$\bar{x}$ [%] Low to Avg.	σ [%] Low to Avg.	$\bar{x}$ [%] Avg. to High	σ [%] Avg. to High	$\bar{x}$ [%] Low to High	σ [%] Low to High
FPV power	8.14	2.12	7.68	2.14	15.84	4.93
Hydropower gain	4.17	2.23	4.39	2.27	8.44	3.42
Pump load factor	3.46	7.09	1.79	2.88	4.87	7.08
FPV to Pump	−2.94	1.71	−2.92	1.78	−5.93	3.02
Objective function	8.42	2.39	6.31	2.05	15.30	4.65

including land-use savings and CO_2 reductions, strongly influence optimal hydro-FPV system design and operations.

Sensitivity to the CO_2 price level further clarifies how ecosystem valuation drives RES deployment. While the results above are shown for the average CO_2 price, extending the analysis across low (54.21 EUR/tCO_2), average (79.51 EUR/tCO_2), and high (104.81 EUR/tCO_2) CO_2 price scenarios demonstrates systematic differences in optimal system configuration and dispatch. The overall percentage changes for key indicators across the full FPVC/EWP range are summarised in Table 2.

At low FPVC values (1000–1100 EUR/kW), FPV deployment reaches the maximum feasible capacity across all CO_2 price scenarios, as investment is profitable even without the additional benefit from avoided emissions. When FPVC increases and EWP is moderate, however, the effect of CO_2 price becomes clear, as no upper FPV power plateau is reached. At EWP of 2 EUR/m^3, for example, the FPVC of 1400 EUR/kW yields 472.06 MW in the low CO_2 scenario, rising to 522.01 MW in the average scenario, and 582.91 MW in the high scenario, corresponding to a 23.48 % increase from low to high CO_2 scenario. At FPVC value of 1600 EUR/kW, deployment grows from 370.45 MW to 396.32 MW and 425.52 MW across the three CO_2 scenarios, equal to a 14.87 % increase. A similar progression occurs at FPVC value of 1800 EUR/kW, where FPV power expands from 316.25 MW to 334.64 MW and 353.42 MW, amounting to an 11.76 % increase. These examples illustrate how the CO_2 value increment progressively unlocks additional FPV capacity when investment costs are high and water-related revenues alone do not support full deployment. Across all FPVC-EWP combinations where FPV is present in every scenario, the transition from the low to the high CO_2 price corresponds to an average increase in FPV power of 15.84 %, with a standard deviation (σ) of 4.93 %. The main conclusion is that higher CO_2 prices, by increasing the value of avoided emissions, accelerate RES integration by lowering the FPVC threshold at which FPV becomes viable. As a result, significant deployment can be achieved without requiring high water-saving incentives, since the CO_2 benefit alone is sufficient to support investment. This additional revenue stream therefore enables a faster trajectory for renewable expansion within the WEFE framework.

Beyond FPV capacity, changes in the CO_2 price also affect several key performance indicators of the hybrid FPV-PSH system across the full FPVC-EWP parameter space. Hydropower generation gains increase systematically with higher CO_2 values, averaging 8.44 % increase with a standard deviation of 3.42 %, reflecting the direct link between larger FPV implementation and hybrid system operation. Pump load factor follows a similar pattern, rising on average by 4.87 % ($\sigma = 7.08$ %) between the low and high CO_2 scenarios, with variability driven by cases where FPV deployment is absent under low CO_2 conditions but becomes optimal once carbon valuation improves. In parallel, the FPV-to-pump utilisation ratio decreases as higher CO_2 prices drive more rapid FPV expansion, showing an average decline of 5.93 % ($\sigma = 3.02$ %). These results are in line with the previously discussed FPV power outcomes, where faster capacity expansion leads to a relative shift in FPV electricity allocation away from pumping and toward broader system benefits. Finally, the total system objective value rises markedly with increasing CO_2 price, averaging a 15.3 % gain with a standard deviation of 4.65 %, underlining how avoided emissions act as a decisive revenue stream. Collectively, these results confirm that higher CO_2 prices not only accelerate FPV adoption but also reinforce the economic and operational benefits of hybridisation across a wide range of techno-economic conditions, highlighting the importance of including ecosystem valuation within the WEFE framework.

5. Conclusion and future work

This study presents a comprehensive optimisation framework for assessing hybrid FPV-PSH systems within an integrated WEFE nexus. The method developed builds on a two-stage stochastic optimisation model, incorporating sector-specific objectives, uncertainty in climatic and market conditions, and complex interactions among water use, energy generation, land use, and environmental valuation. By integrating technical performance, resource constraints, financial parameters, and environmental metrics into a unified decision-making process, the model captures both direct and indirect system-wide trade-offs and synergies.

Results show that FPV is only financially viable at the lowest investment cost (1000 EUR/kW) in purely energy-centric analysis. However, even under these narrow criteria, the system demonstrates favourable operational interactions, including high FPV self-consumption and improved hydropower flexibility. Integrating broader considerations, evaporation savings (WE), irrigation demands (WEF), and ecosystem benefits (WEFE), substantially shifts optimal configurations and financial outcomes. Each added dimension increases justification for FPV deployment and influences hydropower operation to align with broader sustainability goals.

In the WE scenario, the economic value of evaporation savings emerges as crucial, driving larger FPV capacities and boosting hydropower output by over 11 % on average. Load duration curves illustrate how FPV integration reduces hydropower variability, supporting steadier baseload operations. The frequency analysis shows that the share of hours with very high hydropower output above 250 MW decreases by 8.4 %, while generation in the 50–100 MW block increases by 5.0 %. This redistribution of output, together with a 16.4 % reduction in mean ramping, demonstrates that hybrid operation lowers volatility and strengthens the baseload character of hydropower. Pump load factors and FPV-to-pump ratios further confirm FPV's role in enhancing system flexibility. Adding agricultural irrigation constraints in the WEF scenario introduces more complexity. The model identifies a consistent optimal irrigation area of 130.54 km^2, but this affects water allocation, reservoir spillage, and hydropower output, particularly in summer. Agricultural water demands slightly reduce optimal FPV capacity at low water values and lower hydropower gains to about 10.7 %. Despite this, financial impacts remain minimal, indicating that integrated water and energy services can still function effectively under competing demands with holistic planning. Results show how exceeding the optimal agricultural area causes seasonal water shortages, especially in June, July, and August, underscoring the importance of integrated planning and demand management.

Under the WEFE scenario, incorporating ecosystem valuations for CO_2 savings and land-use benefits together with a biodiversity external cost on PSH generation, drives maximum FPV deployment across broad FPVC and EWP ranges. Hydropower gains reach their highest levels, and total objective function values increase significantly, underscoring how ecosystem services become powerful economic drivers. Savings shift from conventional energy revenues toward broader sustainability co-benefits as environmental values are integrated. Importantly, sensitivity analysis confirms that higher CO_2 prices increase the value of avoided emissions sufficiently to trigger FPV deployment even at higher FPVC and lower EWP values. Across all FPVC-EWP combinations, where FPV is present in every scenario, the increase from the low to the high CO_2 price corresponds to an average growth in FPV power of 15.84 %, with a standard deviation of 4.93 %. This widens the feasible deployment space of FPV-PSH systems, thereby accelerating RES integration within the WEFE framework.

Across all scenarios, the study confirms FPV's strong complementarity with PSH. FPV enhances peak energy supply, water conservation, and environmental benefits, while hydropower provides flexibility to manage solar variability. This synergy is particularly pronounced under WEFE conditions, where policy-driven environmental pricing supports significant RES investments even at higher capital costs. PV capacity under WEFE remains high even at moderate water price levels, with deployment only disappearing at FPVC above 1900 EUR/kW.

In the context of growing climate variability, increasing demand pressures, and the imperative for low-carbon transitions, the need for such comprehensive tools is becoming more urgent. This model provides

a flexible and extensible foundation for future research and policy analysis, capable of being tailored to specific geographies, technologies, and planning objectives. It offers a practical means for integrating resilience and efficiency into long-term resource planning, making it directly relevant to a wide range of stakeholders engaged in water, energy, food, and environmental governance.

Future work will explore multi-reservoir FPV deployment, real-time irrigation control, and expanded ecosystem valuation, including biodiversity and habitat metrics. Additional efforts will examine reservoir expansion impacts, improved evaporation modelling considering FPV's physical effects, and alternative agricultural strategies to enable flexible irrigation schedules and better align water use with seasonal availability.

CRediT authorship contribution statement

Goran Stunjek: Writing – review & editing, Writing – original draft, Visualization, Validation, Software, Resources, Methodology, Investigation, Formal analysis, Data curation, Conceptualization. **Goran Krajačić:** Writing – review & editing, Validation, Supervision, Project administration, Investigation, Funding acquisition, Conceptualization.

Declaration of competing interest

The authors declare that they have no known competing financial interests or personal relationships that could have appeared to influence the work reported in this paper.

Acknowledgements

The authors gratefully acknowledge the support of the Croatian Meteorological and Hydrological Service (DHMZ) for providing historical hourly river flow data, which formed the foundation for hydrological modelling in this study. We also thank the water utility company Zadar Vodovod d.o.o. for supplying historical records of water demand related to residential consumption, industrial activity, and tourism. Additionally, we extend our appreciation to the Croatian Power Exchange (CROPEX) for providing access to historical day-ahead electricity market prices, which were essential for modelling energy market dynamics. Furthermore, the contributions from European Union's Horizon Europe programme projects INITIATE, Grant agreement ID 101136775, as well as from the project EMERGE, Grant agreement ID 101118278 are greatly acknowledged.

Supplementary materials

Supplementary material associated with this article can be found, in the online version, at doi:10.1016/j.nexus.2025.100570.

Data availability

Data will be made available on request.

References

[1] G.C. de Oliveira, E. Bertone, R.A. Stewart, Optimisation modelling tools and solving techniques for integrated precinct-scale energy–water system planning, Appl. Energy 318 (2022) 119190, https://doi.org/10.1016/j.apenergy.2022.119190.
[2] D. Peña-Torres, M. Boix, L. Montastruc, Optimization approaches to design water-energy-food nexus: a litterature review, Comput. Chem. Eng. 167 (2022) 108025, https://doi.org/10.1016/j.compchemeng.2022.108025.
[3] E. Demir, E. Alp, A framework for assessing the circular economy potential in the water and agriculture sectors in Türkiye through the water-energy-food-ecosystem nexus, Sustain. Prod. Consum. 54 (2025) 335–347, https://doi.org/10.1016/j.spc.2025.01.009.
[4] M. Di Martino, P. Linke, E.N. Pistikopoulos, Overcoming modeling and computational complexity challenges in food–energy–water nexus optimization, Comput. Chem. Eng. 192 (2025) 108902, https://doi.org/10.1016/j.compchemeng.2024.108902.
[5] M. Di Martino, P. Linke, E.N. Pistikopoulos, A comprehensive classification of food–energy–water nexus optimization studies: state of the art, J. Clean. Prod. 420 (2023) 138293, https://doi.org/10.1016/j.jclepro.2023.138293.
[6] X.-J. Dong, G.-X. He, Z.-W. Zhou, J.-N. Shen, Y.-J. He, Simultaneous design and scheduling optimization of the photovoltaic-wind-hydropower-hydrogen hybrid system, Energy Convers. Manage 314 (2024) 118638, https://doi.org/10.1016/j.enconman.2024.118638.
[7] G.A.M. Castorino, E. Dahlquist, K. Kyprianidis, E. Losi, L. Manservigi, M. Pinelli, et al., Optimization of sizing and operation of pumped hydro storage plants under current and future economic scenarios, J. Energy Storage 119 (2025) 116130, https://doi.org/10.1016/j.est.2025.116130.
[8] Y.-C. Tsao, I.G.A. Banyupramesta, J.-C. Lu, Optimal operation and capacity sizing for a sustainable shared energy storage system with solar power and hydropower generator, J. Energy Storage 110 (2025) 115173, https://doi.org/10.1016/j.est.2024.115173.
[9] J. Cook, M. Di Martino, R.C. Allen, E.N. Pistikopoulos, S. Avraamidou, A decision-making framework for the optimal design of renewable energy systems under energy-water-land nexus considerations, Sci. Total. Environ. 827 (2022) 154185, https://doi.org/10.1016/j.scitotenv.2022.154185.
[10] L. Lu, W. Yuan, C. Su, P. Wang, C. Cheng, D. Yan, et al., Optimization model for the short-term joint operation of a grid-connected wind-photovoltaic-hydro hybrid energy system with cascade hydropower plants, Energy Convers. Manage 236 (2021) 114055, https://doi.org/10.1016/j.enconman.2021.114055.
[11] F. Mansour, M. Al-Hindi, M.A. Najm, A. Yassine, Multi-objective optimization for comprehensive water, energy, food nexus modeling, Sustain. Prod. Consum. 38 (2023) 295–311, https://doi.org/10.1016/j.spc.2023.04.013.
[12] T. Khosrojerdi, S.H. Moosavirad, S. Ariafar, M. Ghaeini-Hessaroeyeh, Optimal allocation of water resources using a two-stage stochastic programming method with interval and fuzzy parameters, Nat. Resour. Res. 28 (2019) 1107–1124, https://doi.org/10.1007/s11053-018-9440-1.
[13] B. Xu, P.-A. Zhong, B. Du, J. Chen, W. Liu, J. Li, et al., Analysis of a stochastic programming model for optimal hydropower system operation under a deregulated electricity market by considering forecasting uncertainty, Water. (Basel) 10 (2018) 885, https://doi.org/10.3390/w10070885.
[14] C.N. Dimitriadis, E.G. Tsimopoulos, M.C. Georgiadis, Optimization-based economic analysis of energy storage technologies in a coupled electricity and natural gas market, J. Energy Storage 58 (2023) 106332, https://doi.org/10.1016/j.est.2022.106332.
[15] O.J. Guerra, D.A. Tejada, G.V. Reklaitis, Climate change impacts and adaptation strategies for a hydro-dominated power system via stochastic optimization, Appl. Energy 233–234 (2019) 584–598, https://doi.org/10.1016/j.apenergy.2018.10.045.
[16] Z. Wang, F. Wu, Y. Li, J. Li, Y. Liu, W. Liu, Day-ahead dispatch approach for cascaded hydropower-photovoltaic complementary system based on two-stage robust optimization, Energy 265 (2023) 126145, https://doi.org/10.1016/j.energy.2022.126145.
[17] W. Liu, X. Guo, X. Xing, C. Jiang, J. Li, Q. Lu, et al., Two-stage stochastic multi-criteria group decision making for wind-photovoltaic-hydropower scheduling, Energy Rep. 12 (2024) 3732–3742, https://doi.org/10.1016/j.egyr.2024.09.068.
[18] R.J. Mahfoud, N.F. Alkayem, Y. Zhang, Y. Zheng, Y. Sun, H.H. Alhelou, Optimal operation of pumped hydro storage-based energy systems: a compendium of current challenges and future perspectives, Renew. Sustain. Energy Rev. 178 (2023) 113267, https://doi.org/10.1016/j.rser.2023.113267.
[19] P. Toufani, E.C. Karakoyun, E. Nadar, O.B. Fosso, A.S. Kocaman, Optimization of pumped hydro energy storage systems under uncertainty: a review, J. Energy Storage 73 (2023) 109306, https://doi.org/10.1016/j.est.2023.109306.
[20] D. Fernández-Muñoz, J.I. Pérez-Díaz, M. Chazarra, A two-stage stochastic optimisation model for the water value calculation in a hybrid diesel/wind/pumped-storage power system, IET Renew. Power Gener. 13 (2019) 2156–2165, https://doi.org/10.1049/iet-rpg.2018.6151.
[21] G. Micheli, M.T. Vespucci, M. Stabile, C. Puglisi, A. Ramos, A two-stage stochastic MILP model for generation and transmission expansion planning with high shares of renewables, Energy Syst. 14 (2023) 663–705, https://doi.org/10.1007/s12667-020-00404-w.
[22] F. Guo, J. Gao, H. Men, Y. Fan, H. Liu, Large-scale group decision-making framework for the site selection of integrated floating photovoltaic-pumped storage power system, J. Energy Storage 43 (2021) 103125, https://doi.org/10.1016/j.est.2021.103125.
[23] M. Temiz, I. Dincer, Design and analysis of a floating photovoltaic based energy system with underground energy storage options for remote communities, J. Energy Storage 55 (2022) 105733, https://doi.org/10.1016/j.est.2022.105733.
[24] Z. Wang, Y. Li, F. Wu, J. Wu, L. Shi, K. Lin, Multi-objective day-ahead scheduling of cascade hydropower-photovoltaic complementary system with pumping installation, Energy 290 (2024) 130258, https://doi.org/10.1016/j.energy.2024.130258.
[25] M.A. Nasab, M. Zand, S. Padmanaban, M.S. Bhaskar, J.M. Guerrero, An efficient, robust optimization model for the unit commitment considering renewable uncertainty and pumped-storage hydropower, Comput. Electr. Eng. 100 (2022) 107846, https://doi.org/10.1016/j.compeleceng.2022.107846.
[26] Y. Shi, H. Wang, C. Li, M. Negnevitsky, X. Wang, Stochastic optimization of system configurations and operation of hybrid cascade hydro-wind-photovoltaic with battery for uncertain medium- and long-term load growth, Appl. Energy 364 (2024) 123127, https://doi.org/10.1016/j.apenergy.2024.123127.

[27] P.D. Dabhade, D.G. Regulwar, Multi-reservoir optimization for maximization of releases for hydropower generation considering environmental flow, J. Water. Resour. Prot. 13 (2021) 931–944, https://doi.org/10.4236/jwarp.2021.1312050.
[28] W.D. Vichete, A.V. Méllo Júnior, GA dos S Soares, A water allocation model for multiple uses based on a proposed hydro-economic method, Water. (Basel) 15 (2023) 1170, https://doi.org/10.3390/w15061170.
[29] L.A. Mendes, M.T.L. de Barros, R.C. Zambon, W.W.-G. Yeh, Trade-off analysis among multiple water uses in a hydropower system: case of São Francisco River Basin, Brazil. J. Water Resour. Plan Manag. 141 (2015), https://doi.org/10.1061/(ASCE)WR.1943-5452.0000527.
[30] J. Li, Z. Zhao, P. Li, M. Apel Mahmud, Y. Liu, D. Chen, et al., Comprehensive benefit evaluations for integrating off-river pumped hydro storage and floating photovoltaic, Energy Convers. Manage 296 (2023) 117651, https://doi.org/10.1016/j.enconman.2023.117651.
[31] Y. Gao, L. Lei, M. Zhang, Z. Zhao, J. Li, M.A. Mahmud, et al., Boosting floating photovoltaics via cooling methods and reservoir characteristics: crafting optimal symbiosis with off-river pumped hydro storage, Energy 312 (2024) 133501, https://doi.org/10.1016/j.energy.2024.133501.
[32] A. Kaab, H. Ghasemi-Mobtaker, M. Sharifi, U. Jørgensen, Evaluating the viability of installing photovoltaic panels on irrigation canals for energy generation and water storage, Energy Nexus 18 (2025) 100455, https://doi.org/10.1016/j.nexus.2025.100455.
[33] M. Di Martino, S. Namany, F. Mahmood, T. Al-Ansari, P. Linke, E.N. Pistikopoulos, Food-energy-water nexus considerations in optimal greenhouse farming systems design and operation, Appl. Energy 379 (2025) 124900, https://doi.org/10.1016/j.apenergy.2024.124900.
[34] Finch, J. W., Hall,R. L. Estimation of open water evaporation. 2001.
[35] Finch J., Calver A. Methods for the quantification of evaporation from lakes. 2008.
[36] B. Gallego-Elvira, A. Baille, B. Martín-Gorriz, J.F. Maestre-Valero, V. Martínez-Alvarez, Evaluation of evaporation estimation methods for a covered reservoir in a semi-arid climate (south-eastern Spain), J. Hydrol. 458–459 (2012) 59–67, https://doi.org/10.1016/j.jhydrol.2012.06.035.
[37] A. Pérez, O. Lagos, M. Lillo-Saavedra, C. Souto, J. Paredes, J.L. Arumí, Mountain Lake evaporation: a comparative study between hourly estimations models and In situ measurements, Water. (Basel) 12 (2020) 2648, https://doi.org/10.3390/w12092648.
[38] I.P. Craig, Comparison of precise water depth measurements on agricultural storages with open water evaporation estimates, Agric. Water. Manage 85 (2006) 193–200, https://doi.org/10.1016/j.agwat.2006.04.010.
[39] M.O. FARUQ, S.A. TURASH, N. FATTAH, I.K NAHID, Estimation of crop water requirement for boro rice in Bandarban, Bangladesh based on cropwat 8.0 model, Asian J. Plant Soil Sci. 6 (2021) 31–38, https://doi.org/10.56557/ajopss/2021/v6i147.
[40] Allen, Richard G, Pereira, Luis S, Raes D., Smith M. Crop evapotranspiration-guidelines for computing crop water requirements-FAO Irrigation and drainage paper 56. 1998.
[41] L.S. Pereira, P. Paredes, D.J. Hunsaker, R. López-Urrea, N. Jovanovic, Updates and advances to the FAO56 crop water requirements method, Agric. Water. Manage 248 (2021) 106697, https://doi.org/10.1016/j.agwat.2020.106697.
[42] N. Katerji, G. Rana, FAO-56 methodology for determining water requirement of irrigated crops: critical examination of the concepts, alternative proposals and validation in Mediterranean region, Theor. Appl. Climatol. 116 (2014) 515–536, https://doi.org/10.1007/s00704-013-0972-3.
[43] A. Muratoglu, G.K. Bilgen, I. Angin, S. Kodal, Performance analyses of effective rainfall estimation methods for accurate quantification of agricultural water footprint, Water. Res. 238 (2023) 120011, https://doi.org/10.1016/j.watres.2023.120011.
[44] Land and Water Development Division of FAO., CropWat model. https://www.fao.org/land-water/databases-and-software/cropwat/en/.
[45] M. Wirtz, P. Remmen, D. Müller, EHDO: a free and open-source webtool for designing and optimizing multi-energy systems based on MILP, Comput. Appl. Eng. Educ. 29 (2021) 983–993, https://doi.org/10.1002/cae.22352.
[46] Elektroprojekt d.d. PSHP Velebit. 2014.
[47] d.o.o. Fidon, Elaborat Zaštite Okoliša Za Ocjenu o Potrebi Procjene Utjecaja Na Okoliš - Razvoj sustava Vodoopskrbe Vodovoda d.o.o, Zadar za sufinanciranje iz Fondova EU, 2021.
[48] Hrvatske Vode. Hrvatske Vode, 2025, https://www.voda.hr/hr.
[49] Zadar Vodovod d.o.o. Zadar Vodovod d.o.o., 2025, https://www.vodovod-zadar.hr/.
[50] Lov i ribolov na području općine Lovinac, 2025. https://www.lovinac.hr/page/lov-i-ribolov-na-podrucju-opcine-lovinac.
[51] Mongird K., Viswanathan V., Alam J., Vartanian C., Sprenkle V., Baxter R. 2020 Grid energy storage Technology Cost and Performance Assessment. N.d.
[52] Solvis, Solvis (2025). https://solvis.hr/.
[53] National Renewable Energy Laboratory, U.S. Solar Photovoltaic System and Energy Storage Cost Benchmarks, With Minimum Sustainable Price Analysis: Q1, 2022 n.d.
[54] Copernicus Climate Change Service. ERA-5- land database, 2025. https://cds.climate.copernicus.eu/datasets/reanalysis-era5-land?tab=download.
[55] Segarić D., Kovačić D., Erlić Š., Peričić S., Jurišić T., Brkljača M., et al. Program Ruralnog Razvoja Zadarske Županije. 2012.
[56] Romić D. Plan Navodnjavanja Za Područje Zadarske Županije. 2006.
[57] CROPEX, Croatian power exchange (2025). https://www.cropex.hr/en/.
[58] HEP. Croatian GHG emissions, 2025, https://www.hep.hr/odrzivost-i-okolis/zastita-zraka-i-klimatske-promjene/emisije-staklenickih-plinova/158.
[59] Trading Economics. ETS - EU carbon permits, 2025, https://tradingeconomics.com/commodity/carbon.
[60] S. Gadzanku, H. Mirletz, N. Lee, J. Daw, A. Warren, Benefits and critical knowledge gaps in determining the role of floating photovoltaics in the energy-water-food nexus, Sustainability. 13 (2021) 4317, https://doi.org/10.3390/su13084317.
[61] Ramasamy V., Feldman D., Desai J., Margolis R. U.S. Solar Photovoltaic system and energy storage cost benchmarks: Q1 2021. 2021.
[62] X. Liu, S. Xiao, H. Pan, X. Zheng, W. Han, C. Huang, et al., Optimizing hydropower plants based on carbon-water-energy-ecosystem nexus, Energy Convers. Manage 270 (2022) 116191, https://doi.org/10.1016/j.enconman.2022.116191.

PAPER 4

"Fascinating story. Any chance you're nearing the end?"

Geralt of Rivia

Review of the potentials for implementation of floating solar panels on lakes and water reservoirs

Article *in* Renewable and Sustainable Energy Reviews · April 2023

DOI: 10.1016/j.rser.2023.113237

CITATIONS
66

READS
185

5 authors, including:

Vladimir Vidović
University of Zagreb
2 PUBLICATIONS **68** CITATIONS
SEE PROFILE

Goran Krajacic
University of Zagreb
201 PUBLICATIONS **5,808** CITATIONS
SEE PROFILE

Nikola Matak
University of Zagreb
10 PUBLICATIONS **243** CITATIONS
SEE PROFILE

Goran Stunjek
University of Zagreb
11 PUBLICATIONS **132** CITATIONS
SEE PROFILE

Review of the potentials for implementation of floating solar panels on lakes and water reservoirs

Vladimir Vidović,
SDEWES Centre, Zagreb, Croatia.
vladimir@sdewes.org
Goran Krajačić (a), Nikola Matak (b), Goran Stunjek (c), Marko Mimica (d)
Faculty of Mechanical Engineering and Naval Architecture, University of Zagreb, Zagreb, Croatia.
Goran.krajacic@fsb.hr

ABSTRACT

Many places are dealing with the problem of water scarcity, especially in the summer months. This occurs mostly in the dry areas with hot climates that are exposed to intensive solar insolation which are the main driver for the evaporation of water. Some companies that are in charge of water service, and are operating open water reservoirs, have developed a solution to cover the water with floating balls to limit the solar insolation and to mitigate the evaporation of water. Another good approach is using floating solar panels for the same cause, which will provide an additional power source. It can enhance the productivity of hydropower plants with reservoirs. An additional benefit of the solution is the amount of the available water surfaces for placing the solar panels, instead of potentially useful areas for other purposes (agriculture, buildings…). This paper reviews the current development of the technology, potentials, and best practices. It shows that this technology is feasible and can compete with other power sources, considering the cheapest LCOE being 46 USD/MWh for a 50 MW power plant in Uttar Pradesh, India.

1. INTRODUCTION

Solar energy systems are developing faster than ever and are presenting a major potential for the production of clean electric energy [1]. Except for the energy side, many other fields can benefit from this technology, like shading for crops in agriculture, for water bodies to reduce evaporation, for car parking lots, and other uses [2]. Installing solar panels on water bodies has multiple benefits, like reducing water evaporation and reducing the water temperature on one side and improving the efficiency of the solar panel due to better cooling effect [3]. A detailed review of floating photovoltaic (FPV) technology was published in 2019. It speaks about the potential of efficient operation of photovoltaic (PV) panels and their utilization to reduce water evaporation [4]. Still, it doesn't cover the biggest plants and advancements in the last 3 years, with the stated specific cost of one plant at 1.71 USD/Wp, which has halved in the meantime. Assessment of FPV technology and global potentials is made, showing there is a potential to deploy between 3 and 7.6 TW of FPV around the world depending on the scenario [5]. A review describing typical FPV systems and their benefits was made, describing characteristics of canal mounted, offshore and floating plants [6]. Late assessment was made to deploy FPV plants on water bodies in mainland Spain [7]. There it is shown that 31% of electric demand in Spain could be met with covering only 10% of all water bodies. A case study for the western Iberian Peninsula is questioning the coupling of floating wind installations with floating solar installations due to their variations in energy production throughout the year [8]. It shows that their coupled operation would increase production stability, especially for the nearshore installations. An assessment was made to determine what percentage of the water surface should be covered for optimal reduction of evaporation. It shows that covering only 30% of the basin,

it is possible to achieve a 49% reduction of water evaporation [9]. A scientific review has been made on the sustainability of FPV, showing that FPV can be beneficial for the ecosystem, especially in terms of reducing evaporation, while downsides can be chemical changes in water, including nitrification and deoxygenation [10]. FPV has a significant potential for distant islands that are not connected to the electrical grid or water supply with the mainland. Case is showing utilization of FPV in Maldives, as a part of energy system aiming to be 100% renewable [11]. Digital numerical model simulation was made for the case of a water reservoir near Alicante, Spain [12]. The numerical model was compared with experimental structure installed together with CELEMIN ENERGY S.L. that covers 7% of the reservoir. It shows floating PV cover is economically feasible and safe for operation and can withstand changes in water level. Recently a detailed review of FPV technology has been made describing the current status, typical construction and design. Overall evaluation of the technology has been made, mentioning the main benefits - reducing water evaporation and more efficient operation of PV panels [13]. In this paper, analysis of the FPV technology is made, considering its feasibility and impact on problem of water scarcity. Interesting question of optimal water surface coverage is mentioned in the work. Also most notable examples across the continents are shown. This study aims to examine current situation and set the basis for future studies that would support development of FPV projects in technical but also legislative point of view, showing best practices of the industry. Additional research concerning natural preservation of aquatic life should be made in the future, and they are not included in this study.

2. METHODOLOGY AND MATERIALS

In this work, the existing scientific research on topic of FPV installations is reviewed. First, the feasibility of the technology is assessed, with latest updates in technology development, noting most feasible examples. Following the economy, the main beneficial utilization of FPV is described – first the topic of evaporation suppression and how can it help the arid areas with water scarcity. Another benefit that is described is hybridization of hydropower plants and FPV. Following the description, best practices in terms of size, feasibility and technology advancement are analysed, according to the regions of the world. The current status, barriers, feasibility and future potentials are discussed.

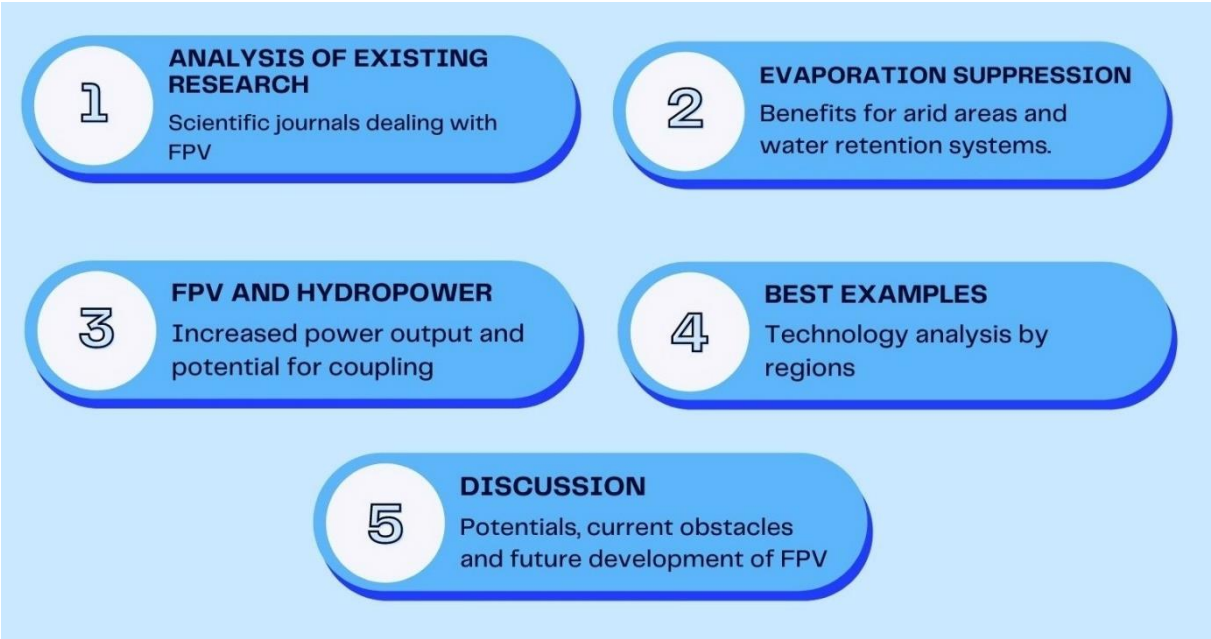

Figure 1. Methodology and parts of this review

Materials used for this review contain scientific work from journals what have analyzed floating solar technology, and other relevant fields that are dealing with suppression of water evaporation, PV efficiency, utilization of lakes and water surfaces etc. Many reports about FPV project plans and implementation are used as references, to give most up to date review on current status of FPV technology. This paper aims to further update the already conducted analysis of the existing status of the FPV. The work done in this paper is focused on the specific conditions for the development of the FPV in different regions. Furthermore, the paper tries to investigate are the FPV systems currently feasible for implementation in different regions and what conditions need to be fulfilled to facilitate their faster implementation considering legislative, technical, and economic conditions.

3. ECONOMY OF FLOATING SOLAR PLANTS

Floating solar photovoltaic (FPV) is a great solution for cases with growing electricity demand and problems with water scarcity that operate large reservoirs, either by covering the water reservoirs or coupling FPV plants with desalination plants in the coastal areas. Installing PV on water bodies is a great solution for areas with less available land like islands. Most important economic factor for energy plants is Levelized cost of energy (LCOE) that is being produced. LCOE considers both capital cost and running costs of the plant like fuel, operations and maintenance. Needless to say, FPV plants don't use fossil fuels, which makes them independent of volatile fuel costs. It is important to say that PV technology is becoming one of the most affordable and available sources of power with prices dropping continuously, being well below 50 USD/MWh today [14].

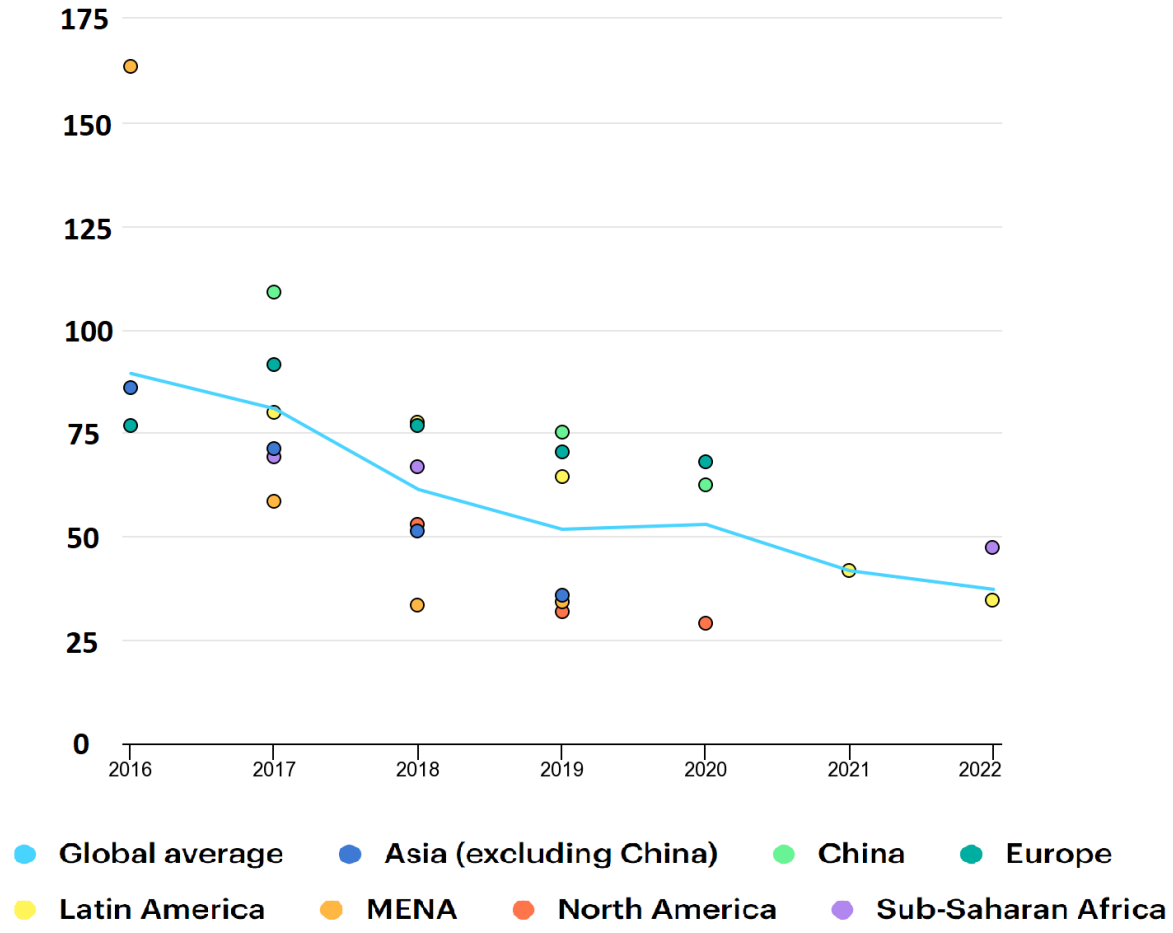

Figure 2. LCOE for PV panels [14]

It is important to consider costs for floating construction consisting of floaters, buoys, anchoring and mooring links which increase the overall cost. Anchoring can be made on the bottom of the lake, or dry sides of the lake. Inverters can be put on the dry ground by the water body, or on floaters which is often the case for larger installations. The problem can arise for the reservoirs with high variations in water level or in case the reservoir dries completely – the floating structure needs to stay functional after those events. An example of a lake that is drained during the winter is a man-made reservoir Lac des Toules in the Swiss Alps at 1810 m above sea level. FPV installation is located on the top of the reservoir, and is built in 2019. It needs to withstand cold weather and function after the reservoir is drained [15]. There are other examples of FPV that are operating in extremely cold conditions prone to snowing like Harbin Heilongjiang, China [16]. Also, there is an example of a robust FPV plant in Taiwan, built by Sungrow that survived drought and typhoon season without any damage reported [17]. It is interesting to see how PV modules act when submerged underwater. A study has shown that their efficiency is higher due to the cooling effect but will depend on depth. Also, the problem of cleaning the modules is solved [18].

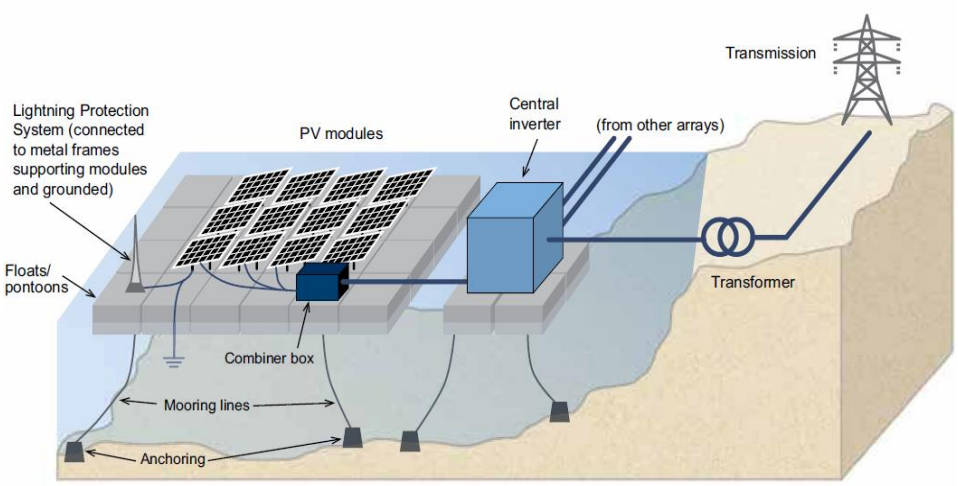

Figure 3. Scheme of a typical FPV [19]

Analysis from 2018 has shown that capital costs for the whole FPV systems are ranging from 0.8 to 1.2 USD/MWp [19]. Costs for the big FPV plants are decreasing with an example of the Tata Power Solar plant in the West Bengal region in India with the capital cost of 0.69 USD/MWp [20]. The lowest cost is set at 0.59 USD/Wp for a 100 MW plant in India [21]. In terms of capacity, Asian countries dominate the FPV market [22]. The biggest FPV plants are located in China with South Korea planning to build the biggest FPV with a total capacity of 2.1 GW [22]. The total capacity of FPV in the world in 2020 was 2.6 GW with expected yearly growth of more than 20% [23]. Prediction is made that FPV will continue to grow and that in 2025 there will be more than 100 GW of FPV installed around the globe [24]. The initiative is set by DNV GL to develop the first Recommended Practice for FPV plants that would involve industry leaders from the sector [25].

4. EVAPORATION SUPPRESSION

One of the problems FPV can help with is water evaporation. Analysis shows that every year more than 346 km^2 of water evaporates from artificial lakes and reservoirs in the world [26]. Examination of water evaporation losses from water storage in Australia was made in 2005 and shows that between 1 and 3.6 m of water height can be lost yearly, depending on weather conditions [27]. Significant case exists in Atacama Desert, Chile, which is known for arid climate and strong insulation. A simulation and experiment were made that has shown that evaporation in such conditions can be reduced by more than 90% with the deployment of floaters and PV cells on top of the pond, with power generation of 68 Wp/m^2 [28]. A laboratory study at ETH Zurich has shown that with floating covers it is possible to suppress evaporation by 70-80% [29]. There is also mentioned the most notable example in Los Angeles where a water reservoir with a surface of around 1 km^2 is covered with small black polyethylene spheres (shade balls). It is stated that the greatest potentials are for reducing water evaporation for smaller reservoirs (<0.1 km^2)[30]. This experiment concluded that water evaporation increases with solar radiation and wind, and it can be reduced by covering the water surface. For the experiment, they have used floating spheres and floating discs.

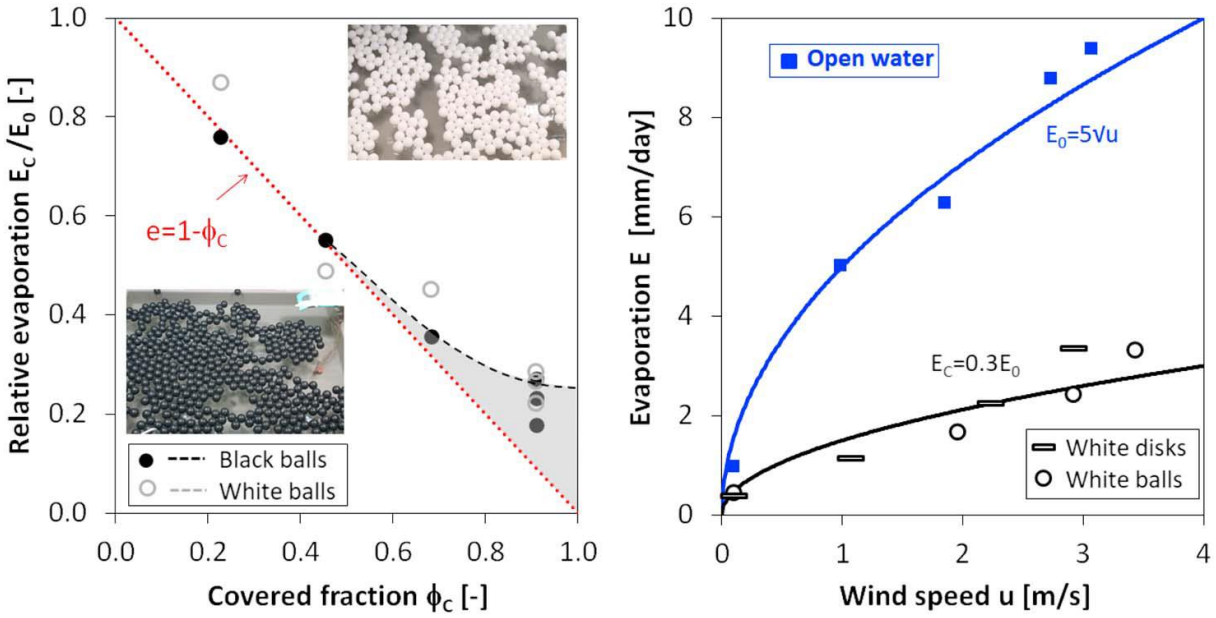

Figure 4. (left) Figure is showing the effect of a partial cover of water surface with spheres. Relative evaporation is a ratio between evaporation from the covered and uncovered water surface. The experiment shows that the efficiency of evaporation suppression is decreasing for high cover fractions. (right) Experiment shows a significant evaporation reduction for water surfaces covered with floating spheres or discs. [29]

The experiment showed that complete evaporation suppression cannot be achieved with the water surface completely covered (Figure 4). Also, this means that gaps uncovered by floating solar plants don't present large losses for evaporation suppression.

Artificial destratification on reservoirs in Brazil has been researched, showing it can reduce the temperature of the water surface by 1°C, and reduce the water evaporation by 10% [31]. In this work specific cost per cubic meter for retaining the water from evaporation is 1.2 USD/m^3 which is a competitive price in arid areas. Detailed analysis of artificial destratification of large water reservoirs in Cyprus has been made in 1999 [32]. It shows how covering the lake can reduce water evaporation and improve the water supply on the arid island in the Mediterranean.

5. HYBRIDIZATION WITH HYDROPOWER

Hydropower plants are one of the largest sources of electricity generation in the world. In 2019, 4329 TWh of electricity was generated from hydropower (22%) [33]. Although being the most represented source of renewable energy (45%), future development could face different barriers [34]. Main problem is that most of the forecasted projects in the future would be built on greenfield surfaces (Figure 5). Large hydropower plants are covering large surfaces that can be utilized differently. It is also important to consider GHG gasses, CH_4 and CO_2, that are being emitted from the water reservoirs of large hydro plants [35]. Similarly, the effect of the lower albedo of water reservoir than the surrounding soil has a negative impact on global warming [36]. Another significant question is their influence on society, especially for the transboundary plants [37]. Some hydropower plants present a political problem and can cause international conflicts [38]. Hydropower will play a major role in the decarbonization of electricity generation, but due to their limitations, we need to utilize the full potential of these plants.

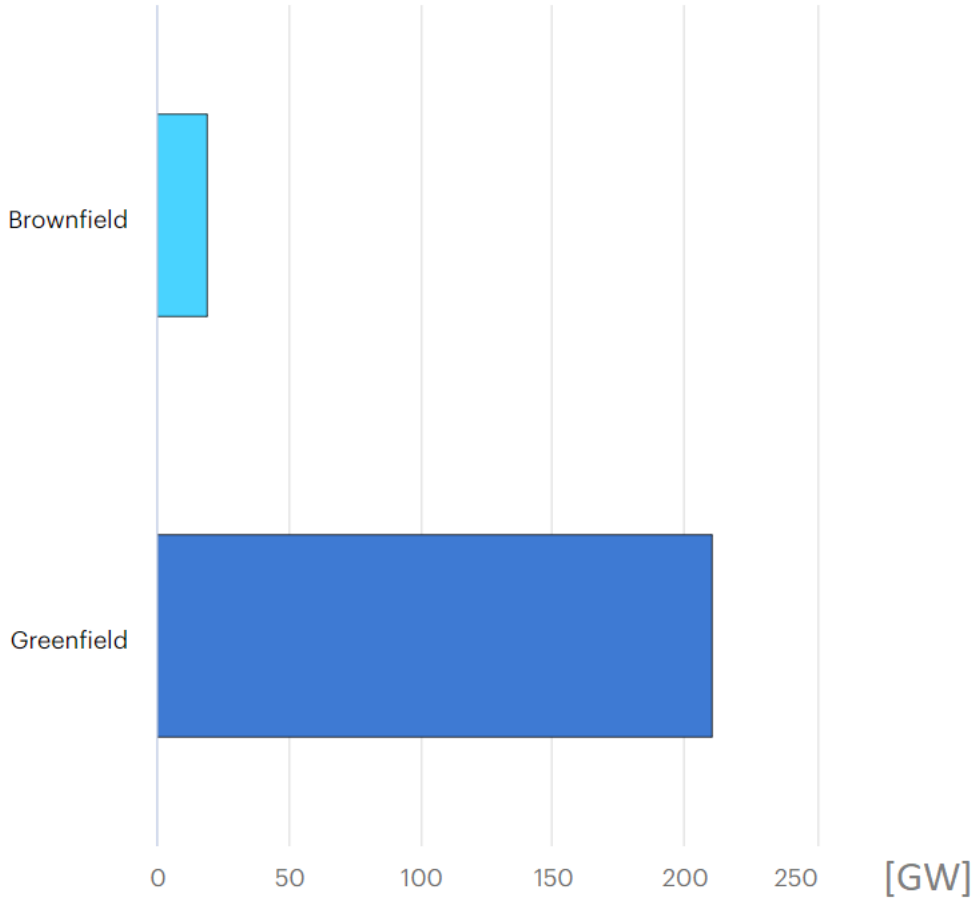

Figure 5. Greenfield (210.7 GW) vs. Brownfield (18.9 GW) forecasted world net capacity additions 2021-2030 [34]

The surface of water reservoirs in hydropower plants is a perfect solution for PV panels. This way PV panels wouldn't occupy valuable land and would increase the output of hydro plants. Another benefit is evaporation suppression, which is an additional benefit for the hydro plant. It is interesting to assess the influence of albedo difference for PV panels and water surfaces. The specific problem of Amazon dam underproduction can be reduced by utilizing the FPV [39]. It is mentioned how the combined operation can be beneficial, especially in the hours with peak demand.

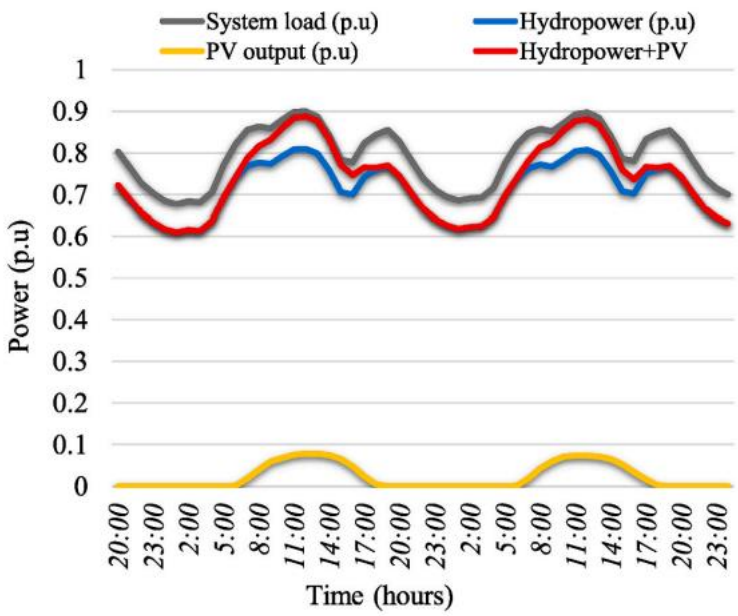

Figure 6. Estimated hybrid operation of the hydropower plant and FPV in Brazil [39].

One of the greatest advantages can be seen in combining FPV on reservoirs of pumped storage power systems. The evaluation was made for the Pumped storage with 1 GW capacity and a large FPV plant with 2 GW that would be deployed on top of the reservoir – results have shown there are different benefits, from reducing energy disbalance, higher electricity generation and reducing water evaporation by 19 million m^3 a year [40]. There are many side benefits like the existence of power lines for previously built plants and the possibility to store the excess energy from FPV. Late review was made on benefits of pairing hydropower plants and FPV, showing that covering less than 15% of water surface of reservoirs FPV would produce 50% of hydropower output [41]. Also covering 10% of reservoir area would save 1717.8 cubic meter of water annually. Another analysis shows the potential of integrating FPV and big hydropower plants with reservoirs, which states that if we covered 10% of reservoir surface for the 10 biggest hydropower plants in the world, their energy production would increase by 65% [42]. The Brazilian power sector depends on hydro plants which have significantly lower production in dry years. The case study was made for hydro plants built on the São Francisco river basin, which shows that energy gains from installing FPV would be 76% and the capacity factor of power plants would be increased by 17.3% on average [43]. Study for the complementing hydro plant in Pakistan with 200 MW FPV and optimizing the regime of the plant can result in 3.5% of additional power generation from Hydroelectric plant and possibility to cover peak demand in the midday [44]. A study made for a hydroelectric power plant with a reservoir in India shows the cost of installing FPV would be 35% higher in comparison with conventional PV systems but would also reduce water evaporation significantly. In the study, the FPV would cover 30% of the Vaigai reservoir and would have the capacity of 1.14 MW which would generate 1.9 GWh of electricity, but also save 42731 m^3 of water annually. This saved water would provide an additional 6 MWh of power from hydropower plant [45]. Research gives an interesting viewpoint that hydro plants can provide ancillary service as virtual batteries for FPV installed on their reservoirs and states if 25% of the reservoir's surface would be covered with FPV, generation from FPV would surpass generation from hydro significantly. Due to water retained in the reservoir because of the FPV, hydropower plant would produce 6.3% more energy in [46]. Assessment of FPV potential on existing hydropower plants in Africa shows promising results [47]. It states that the total potential is 2922 GW, and covering only 1% of those potentials would increase energy production by 58% and double installed capacity. In addition,

743 million m^3 of water could be saved every year because of reduced evaporation, which would result in 170.64 GWh more produced in hydropower plants. A specific problem for water reservoirs is the variability of water level and surface area of the lake. FPV plants should either cover only the area of the reservoir that never dries, or the construction needs to be adapted to get stranded onto the dry area. There are proven small FPV constructions that can just sit on the bed of an empty lake [15]. Installing PV panels within hydropower plants is cheaper due to existing infrastructure and connection to the grid.

6. SITUATION IN DIFFERENT CONTINENTS

ASIA

As mentioned before, Asia has the largest capacity of installed FPV with China recognized as a world leader in FPV installations. Data from 2018 are showing that more than 97% of FPV installations are in Asia [48].

In **China,** most of the FPV use Sungrow solutions. The biggest one of them is in Guqiao, Huainan City with a total capacity of 150 MW and is connected to the grid from 2018 [49]. The project was developed by the Sungrow company and is installed in the flooded coal mining subsidence area. The plant is covering 10% of the surface area of the water body and the average depth is 8 m. The Guqiao plant can produce 10 MWh of electricity yearly and save 150000 tons of CO_2 emissions. The second big FPV plant in Huainan City is Xinji Huainan, also using Sungrow equipment with the capacity of 102 MW which is covering 40% of the water body surface [16]. Other plants built in China by Sungrow are: the first big plant of this type in the Huainan is Panji Huainan with 40 MW, built in 2016. A plant in Yuanjiang Yiyang with 100 MW capacity is installed on the surface of Huaihe river in 2019 and is covering 70% of the water surface (Figure 7). Other big FPV plants in China are Huancheng Jining with 50MW and Weishan Jiing with 31 MW, built on coal subsidence area, Qintang Guigang with 20 MW, Yunxi Yueyang (20 MW), Qintang Guigang (20 MW) and Toncheng Anqing (22 MW) which was last built in 2020.

Figure 7. Plant in Yuanjiang Yiyang (100MW) on Huaihe river [16]

Another company developing FPV on large scale is state owned China Energy Conservation and Environmental Protection Group (CECEP) which developed a 70 MW power plant in Bengbu, Anhui in cooperation with French floating solar specialists Ciel & Terre [50]. The plant is located on the mine lake. Chinese Hangzhou Fengling developed a 320 MW project on a fishery in Cixi, Zhejiang [51]. The project is developed in 2 phases: the first was finished in

2017 with the capacity of 200 MW and the second phase in 2020 with the capacity of 120 MW. The cost of the second phase was 0.83 USD/Wp [52]. The biggest FPV in the world is developed by the China General Nuclear Power Group (CGN) in Dangtu, Anhui with a capacity of 260 MW on 400 ha. It is the first plant of this type operating without subsidy and is selling electricity at a price of 54 USD/MWh [53]. In addition, this project proves it is possible to integrate the development of fisheries and floating solar plants – to ensure water quality and conditions for aquatic life, monitoring sensors and controllers are installed on PV plants [54]. Another plant was developed by SPIC Jiangsu Electric Power on top of the fishery in Sihong with a capacity of 100 MW. Although it is not a floating installation but is built on fixed poles, shown in Figure 8 [55].

Figure 8. The Sihong 100 MW solar fishery plant [55]

Another 100 MW FPV plant is deployed in Changhe, Sihushan, Yiyang city by China Datang Corporation [56]. A list of mentioned plants in China is given in Table 1, with information on capacity, location, and name of the developer of the plant.

Table 1. List of all biggest FPV in China

Developer	Province	Plant (City)	MW
Sungrow	Anhui	Guqiao, Huainan	150
		Xinji Huainan	102
		Panji Huainan	40
		Toncheng Anqing	22
	Hunan	Yuanjiang Yiyang	100
		Yunxi Yueyang	20
	Shandong	Huancheng Jining	50
		Weishan Jining	31
	Guangxi	Qintang Guigang	20
CECEP	Anhui	Bengbu, Anhui	70
	Zhejiang	Cixi, Phase 1	200

Hangzhou Fengling		Cixi, Phase 2	120
CGN	Anhui	Dangtu, Anhui	260
SPIC Jiangsu	Jiangsu	Sihong	100
Datang Corporation	Hunan	Changhe, Sihushan, Yiyang	100
		Total	1385

Japan is one of the pioneers in FPV technology with a 2 MW plant on Reservoir in Kumagaya city built in 2014, and many smaller plants built even before [57]. Japan's large energy demand combined with lack of available land needed ingenuity which brought PV technology onto lakes. Today's largest FPV plant in Japan is developed by Kyocera TCL Solar on Yamakura Dam reservoir, Chiba Prefecture. The plant has a capacity of 13.7 MW and covers 180000 m^2 [58]. The second biggest plant in Japan is built on an irrigation reservoir in the prefecture of Saitama with the capacity of 7.5 MW developed by Ciel et Terre [59]. Another plant built by Ciel et Terre in Japan is Tsuga Ike in the prefecture of Mie with 2.5 MW [60]. There are many FPV plants in Japan with a capacity lower than 2 MW – by counting all of them Japan has more than 70 MW of FPV [57].

South Korea is one of the countries that have the biggest plans for deploying floating PV. The best proof is the plan of the government to build a 2100 MW FPV plant on Saemangeum estuarine tidal flat near. The South Korean Ministry of Trade, Industry and Energy announced that around 3.9 billion USD of private funds will be invested [61]. When built, it will be the biggest FPV plant in the world. The deal has been agreed to build the first 200 MW phase – it will be built by the South Korean SK Group [62]. Among already built plants, the biggest one in Korea is developed by SCOTRA on a water reservoir in Goheung-gun county, province of Jeonnam with 25 MW capacity [63]. SCOTRA also developed some projects with smaller capacity in Taiwan and Japan. 6 MW plant, built on two reservoirs: Otae and Jipyeong is built by LG CNS in Sangju, North Gyeongsang Province [64].

India has huge potential for FPV installations, and according to the assessment of The Energy and Resources Institute in India, it is possible to install 280 GW of FPV in the country [48]. There are not so many larger installations in India from before, but in the last years, many projects have been announced. The largest plant connected to the grid is a 5 MW plant in Murshidabad district, West Bengal; built on a raw water pond at the Sagardighi Thermal Power Project owned by The West Bengal Power Development Corp. Ltd (WBPDCL). It was commissioned by Bharat Heavy Electricals Limited (BHEL) [65]. 100 MW plant is currently being developed by the BHEL for the National power generator NTPC. It will be built in 40 arrays with 2.5 MW of capacity each. The arrays are installed on top of floaters made of high-density polyethylene and are produced by Prabh Dayal and Adtech from India [66]. Total investment should be 58.8 million USD, which presents a specific cost of 0.59 USD/Wp [21]. In Kerala state 92 MW FPV is being built for NTPC in 2 phases. The second phase of 70 MW is being built by TATA Power Solar at a cost of 0.69 USD/Wp [67]. Indian Shapoorji Pallonji Group is also developing FPV projects. In 2018 they agreed with Uttar Pradesh Power

Corporation Limited (UPPCL) on a tariff of 46 USD/MWh for the FPV plant with a capacity of 50 MW at Rihand dam [68]. On the same reservoir, an additional 100 MW is being built by ReNew Power [69]. Shapoorji Pallonji is also developing a project on the Middle Vaitarna Dam reservoir which signed a tariff to sell power for 65 USD/MWh to The Municipal Corporation of Greater Mumbai (MCGM) [70].

Project to build India's largest FPV plant is developed with a capacity of 600 MW, which would also be the largest plant of this type in the world. The plant would be built at Omkareshwar dam on Narmada River in Khandwa district, Madhya Pradesh, and the state power management company already signed an agreement to buy 400 MW power from the plant that should start operating in 2022 or 2023. The total cost of the project is estimated at 410 million USD, which sets specific costs at 0.68 USD/Wp [71]. It is interesting to note that national coal mining company Singareni Collieries Company Limited is building large floating solar plants – 300 MW is under construction in different phases on Manair Dam in the Karimnagar district, Telangana [72]. Following this project, the mining company is planning to build an additional 350 MW of FPV in the same region [73]. Additional FPV projects that are being built include a 25 MW plant in Andhra Pradesh, a 15 MW Koldam Hydroelectric power plant, 20 MW at Anta gas power station.

Smaller countries like **Singapore** have a high value of land and lack of space for building conventional ground-based PV solar farms. That's why they can benefit largely from installing PV systems on the water surface. Sembcorp is currently building a 60 MW FPV plant on Tengeh reservoir and has signed a power purchase agreement with the national water agency PUB [74]. Every component of the system is developed to fit the best climate conditions in Singapore and PV modules are placed on certified food-grade HDPE floaters that are UV resistant. Also, Singapore is testing and building offshore plants due to a lack of land.

EUROPE

Some of the first FPV plants have been built in Europe. In 2011 pilot plant was installed in Piolenc, France on a quarry lake with 15 kW [75]. The project was developed by French company Ciel et Terre that positioned themselves as the leaders of the floating PV market and initiated further development of technology. Up to today, Ciel et Terre has installed 520 MW of floating solar around the world. In 2020, Ciel et Terre installed 88 MW FPV on the sea in Taiwan, which is their first big offshore installation. In the place of the first pilot project in Piolenc, the largest French FPV plant has been installed by Bouygues Construction company together with French company Akuo that provided the floaters [76]. The modules have been supplied by Trina Solar. The plant has a capacity of 17 MW and the total cost was 17 million EUR, which means the specific cost is 1.22 USD/Wp [77]. Plant in Piolenc won't be the biggest in France for long. National utility company EDF Renewables is building its first FPV plant on a reservoir in the Lazer municipality with a capacity of 20 MW [78]. EDF Renewables is developing FPV projects outside of France as well. In Israel EDF commissioned 4 solar projects in 2022 with total of 54 MW of capacity [79]. Two of those projects are FPV plants and have been built with BELECTRIC [80]. First plant is The Lochamei HaGetaot built on set of fish ponds and has a capacity of 19 MW. Second one, smaller is The Holga FPV plant, built on top of irrigation pond. 4300 solar panels have capacity of 2 MW and they are covering 70% of the water surface [81]. The United Kingdom has developed significant capacity in FPV. The biggest and most famous is on a drinking water reservoir Queen Elizabeth II, with a capacity of 6.3 MW which is developed by Ciel et Terre [82]. *Fresher* project based in Europe deals

with FPV and mooring systems intending to demonstrate potential and reduce the costs of this technology [83]. In the Netherlands, there are smaller FPV plants built in the last few years. In 2020 largest plant was built with a capacity of 27.4 MW capacity near Zwolle by the BayWa r.e. company [84]. Portugal, through the national electric utilities company – EDP is aiming to support development of floating solar plants. They have installed and are currently operating FPV plant on Alqueva reservoir that has capacity of 5 MW [85]. EDP plans to build additional capacity, so the plant would have capacity of 70 MW of FPV, which would be part of hybrid farm having renewable capacity of 154 MW. Starkraft, a company that develops renewable energy sources for over a decade has started developing its solutions for FPV plants. They started building an FPV plant on top of the reservoir of the Banja hydropower plant operated also by Starkraft in Albania. The PV modules are installed on the circular floating membrane that is supplied by Ocean Sun. First 500 kW section has been built, with full capacity expected to be 2 MW [86]. Investment is expected to be around 2 million of EUR, which brings us to a specific cost of 1.22 USD/Wp.

Figure 9. Strarkraft's planned FPV plant in Banja reservoir, Albania [86]

NORTH AND SOUTH AMERICA

In 2008, wine producer Far Niente in Napa Valley, USA went live with one of the first FPV plants. The plant has a capacity of 400 kW which is more than the demand of the vineyard [87]. In Healdsburg, California is built 4.78 MW FPV plant on a wastewater pond and is operated by the White Pine company. It was developed together with FPV specialist Noria Energy [88]. Another FPV plant on wastewater storage is operating in Windsor, California with a capacity of 1.78MW. It was built by Ciel et Terre and Risen Energy has supplied the PV modules. It is interesting that the electricity is sold by the power purchase agreement and will save 5 million USD for the Town of Windsor in the next 25 years [89]. In Brazil, at the Batalha hydropower plant reservoir will be built 30 MW FPV plant by Tractebel, part of French group Engie [90].

7. DISCUSSION

The FPV technology is feasible, especially considering the raging prices of energy in Europe at the beginning of 2022. Besides economic feasibility, this technology can reduce water evaporation in arid areas and boost the operation of hydropower plants. From the review, it can be seen that China is the global leader in the deployment of FPV with more than half of the installed capacity. Also, many companies that develop FPV and equipment on the largest scale are coming from China. Except for China, big projects are being developed in other Asian countries, especially India and South Korea with their suppliers. The highest advancements in Europe are made in the United Kingdom. Considering the efforts, the EU is giving to reach carbon neutrality, it can be said that FPV is being neglected in some way and is stalling behind Asian countries. This can be considered as a paradox considering that some of the largest

equipment suppliers are based in the EU and the first pilot project of FPV have been developed and installed in the EU. Potentials of FPV are especially significant in the Mediterranean region that is poorly connected with gas pipelines and smaller islands and remote areas that don't have the best electric interconnections to the European mainland. Another problem in the Mediterranean is water scarcity and evaporation from lakes and reservoirs. Great benefits from FPV could be in Mediterranean islands like Cyprus and Canary Islands, which have big reservoirs for water supply coupled with desalination plants. Developing African countries are having problems with water scarcity, high evaporation losses due to hot climate and strong solar radiation, and very important growing electricity demand. FPV is a perfect technology to tackle these problems. It is proven water evaporation can be suppressed with floating covers, which is also an opportunity for the production of clean electricity using PV technology.

This technology has been proven feasible in India and China with costs between 0.59 USD/Wp to 0.9 USD/Wp for large plants. They are being built and operated without subsidies and often operate with tariffs guaranteeing them the agreed price. Examples show that those prices can be as low as 46 USD/MWh in India and China. Investment costs for plants in Europe are currently higher and are around 1.22 USD/Wp. Figure 10 shows difference in cost in India, China and EU. This difference can be also contributed to plants in India and China being much larger. Although being more expensive than larger plants in Asia this is a competitive cost considering average cost of energy in Europe, with the potential to decrease with further development and developing larger plants.

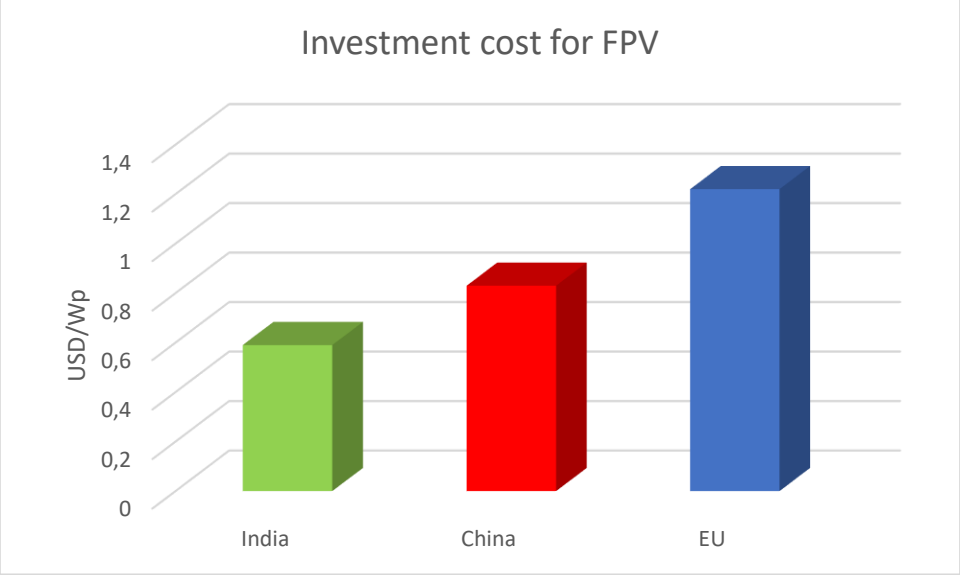

Figure 10. Comparison of investment costs for cheapest FPV plants in China, India and EU

Europe has many potentials for FPV, from islands in the Mediterranean with water scarcity problems to large hydropower plants. These areas would benefit from this technology and should include FPV in their energy strategies, especially with growing energy costs at the beginning of 2022. It should be questioned why EU and USA are stalling so much behind Asian countries, especially considering large effort in western countries to develop sustainable solutions in energetics and dependence on fuel imports. Problem could be in strict legislation in western countries that is neglecting FPV technology, which can be easier managed for large projects in Asian countries. EU is funding different research projects that are creating more sustainable future – more focus should be put on FPV due to its potentials. Important barrier could be impact on aquatic life and biodiversity.

8. CONCLUSIONS

Asian countries recognized the potential and benefits of developing FPV and are showing that this technology can be feasible without national subsidies. Among the most developed western countries, UK and Japan have significant capacity in FPV, but the USA and European Union are stalling. In EU the situation depends from country to country. It can be said that France and Portugal have made significant efforts through national electric utility companies to support development of FPV plants and can be an example to other countries. European countries should develop strategies for the development of FPV especially due to existing of equipment suppliers, public acceptance and desire for carbon neutrality, high prices of land and water scarcity in some areas. The continent with the greatest potential is Africa, but for many developing countries it's difficult to fund big projects by themselves. This is a great opportunity for humanitarian organizations, but also for investors that can help develop water resources and power generation with FPV. All that can be done in a feasible way both for investors and for the service recipients. This work presented overall analysis of the technology, showing that FPV is feasible and should be one of the answers to growing demand for clean electric energy, but also to demand for water in arid areas. This review has analysed most noticeable projects that have been developed in each continent, but also future projects that could be impactful to the society. Detailed analysis should be made about potentials of FPV in developing countries. That analysis should produce ideas how would FPV help the growing demand for electricity and help manage water resources in the best manner. Important question is how the FPV influences aquatic life is underneath the solar panels, and which percentage of the lake can be covered without having bad impact on it. Answer could be found in examples of fisheries in China being covered almost completely with FPV plants. In future work it should be examined:

- What are the influences of covering the lakes with FPV plants on aquatic life, on nitrification and deoxygenation? It would be useful to determine which coverage rate of water surface doesn't present a negative effect on aquatic life. This topic is out of the scope of mechanical and electrical engineering and should be examined in terms of chemistry and biology.
- Current legislation for installation of FPV in countries. In the EU, are there any initiatives to boost research and implementation of FPV technology? Even with EU initiatives, national legislations are the most important factor for the wider implementation of the technology.
- Modelling and experimental analysis of FPV panel cooling, to compare the efficiency and longevity with ground mounted PV.

INDEX OF ABBREVATIONS

BHEL	Bharat Heavy Electricals Limited
CECEP	China Energy Conservation and Environmental Protection Group
EDF	Électricité de France - French electric utilities company
EDP	Energias de Portugal - Portugese electric utilities company
ETH	Eidgenössische Technische Hochschule (Swiss Federal Institute of Technology in Zürich)
FPV	Floating photovoltaic
HDPE	High density polyethylene
LCOE	Levelized cost of energy
MCGM	The Municipal Corporation of Greater Mumbai
NTPC	National Thermal Power Corporation
PV	Photovoltaic
SDEWES	The International Centre for Sustainable Development of Energy, Water and Environment Systems
UPPCL	Uttar Pradesh Power Corporation Limited
USD	United States Dollar
WBPDCL	The West Bengal Power Development Corp. Ltd

REFERENCES

[1] C. L. Crago and E. Koegler, "Drivers of growth in commercial-scale solar PV capacity," *Energy Policy*, vol. 120, no. April, pp. 481–491, 2018, doi: 10.1016/j.enpol.2018.05.047.

[2] P. Santra *et al.*, "Agri-Voltaic System for Crop Production and Electricity Generation from a Single Land Unit," vol. 68, no. January, pp. 45–56, 2020, doi: 10.1007/978-981-15-2666-4_6.

[3] A. P. Sukarso and K. N. Kim, "Cooling E ff ect on the Floating Solar PV : Performance and Economic Analysis on the Case of West Java," 2020.

[4] P. Ranjbaran, H. Yousefi, G. B. Gharehpetian, and F. R. Astaraei, "A review on floating photovoltaic (FPV)power generation units," *Renewable and Sustainable Energy Reviews*. 2019, doi: 10.1016/j.rser.2019.05.015.

[5] N. Lee *et al.*, "Hybrid floating solar photovoltaics-hydropower systems: Benefits and global assessment of technical potential," *Renew. Energy*, vol. 162, pp. 1415–1427, 2020, doi: 10.1016/j.renene.2020.08.080.

[6] A. Sahu, N. Yadav, and K. Sudhakar, "Floating photovoltaic power plant: A review," *Renewable and Sustainable Energy Reviews*. 2016, doi: 10.1016/j.rser.2016.08.051.

[7] M. López, F. Soto, and Z. A. Hernández, "Assessment of the potential of floating solar photovoltaic panels in bodies of water in mainland Spain," *J. Clean. Prod.*, vol. 340, 2022, doi: 10.1016/j.jclepro.2022.130752.

[8] X. Costoya, M. deCastro, D. Carvalho, B. Arguilé-Pérez, and M. Gómez-Gesteira, "Combining offshore wind and solar photovoltaic energy to stabilize energy supply under climate change scenarios: A case study on the western Iberian Peninsula," *Renew. Sustain. Energy Rev.*, vol. 157, no. January, p. 112037, 2022, doi: 10.1016/j.rser.2021.112037.

[9] F. Bontempo Scavo, G. M. Tina, A. Gagliano, and S. Nižetić, "An assessment study of evaporation rate models on a water basin with floating photovoltaic plants," *Int. J. Energy Res.*, vol. 45, no. 1, pp. 167–188, 2021, doi: 10.1002/er.5170.

[10] G. Exley *et al.*, "Scientific and stakeholder evidence-based assessment: Ecosystem response to floating solar photovoltaics and implications for sustainability," *Renew. Sustain. Energy Rev.*, vol. 152, no. August, p. 111639, 2021, doi: 10.1016/j.rser.2021.111639.

[11] D. Keiner *et al.*, "Powering an island energy system by offshore floating technologies towards 100% renewables: A case for the Maldives," *Appl. Energy*, vol. 308, p. 118360, 2022, doi: 10.1016/j.apenergy.2021.118360.

[12] C. Ferrer-Gisbert, J. J. Ferrán-Gozálvez, M. Redón-Santafé, P. Ferrer-Gisbert, F. J. Sánchez-Romero, and J. B. Torregrosa-Soler, "A new photovoltaic floating cover system for water reservoirs," *Renew. Energy*, vol. 60, pp. 63–70, 2013, doi: 10.1016/j.renene.2013.04.007.

[13] M. Kumar, H. Mohammed Niyaz, and R. Gupta, "Challenges and opportunities towards the development of floating photovoltaic systems," *Sol. Energy Mater. Sol. Cells*, vol. 233, no. September, p. 111408, 2021, doi: 10.1016/j.solmat.2021.111408.

[14] IEA, "Average auction prices for solar PV by region and commissioning date, 2016-2022." https://www.iea.org/data-and-statistics/charts/average-auction-prices-for-solar-pv-by-region-and-commissioning-date-2016-2022.

[15] House of Switzerland, "World's first high-altitude floating solar farm – in the Swiss Alps," [Online]. Available: https://houseofswitzerland.org/swissstories/environment/worlds-first-high-altitude-floating-solar-farm-swiss-alps.

[16] Sungrow, "Project references of Sungrow Floating," [Online]. Available:

https://en.sungrowpower.com/SolutionsDetail/1088.

[17] pv-tech, “Sungrow highlights robust floating solar system after drought and typhoon season in Taiwan,” [Online]. Available: https://www.pv-tech.org/sungrow-highlights-robust-floating-solar-system-after-drought-and-typhoon-s/.

[18] M. Rosa-Clot, P. Rosa-Clot, G. M. Tina, and P. F. Scandura, “Submerged photovoltaic solar panel: SP2,” *Renew. Energy*, vol. 35, no. 8, pp. 1862–1865, 2010, doi: 10.1016/j.renene.2009.10.023.

[19] World Bank, ESMAP, and SERIS, “Where Sun Meets Water,” *Where Sun Meets Water*, 2019, doi: 10.1596/32804.

[20] CARBONCOPY, “INDIA ACHIEVES LOWEST COST OF FLOATING SOLAR POWER IN THE WORLD.” https://carboncopy.info/india-achieves-lowest-cost-of-floating-solar-power-in-the-world/.

[21] PV Magazine, “India’s largest floating solar power plant to go online by June.” https://www.pv-magazine-india.com/2021/03/12/indias-biggest-floating-solar-power-plant-to-go-online-by-june/ (accessed Jun. 10, 2021).

[22] Power Technology, “World’s biggest floating solar farms,” [Online]. Available: https://www.power-technology.com/features/worlds-biggest-floating-solar-farms/.

[23] PV Magazine, “Floating solar PV gains global momentum,” [Online]. Available: https://www.pv-magazine.com/2020/09/22/floating-solar-pv-gains-global-momentum/.

[24] R. Cazzaniga and M. Rosa-Clot, “The booming of floating PV,” *Sol. Energy*, vol. 219, no. September, pp. 3–10, 2021, doi: 10.1016/j.solener.2020.09.057.

[25] DNV, “DNV GL launches industry-wide collaboration to develop first ever Recommended Practice for floating solar power plants.” https://www.dnv.com/news/dnv-gl-launches-industry-wide-collaboration-to-develop-first-ever-recommended-practice-for-floating-solar-power-plants-177287.

[26] A. Kohli and K. Frenken, “Evaporation from Artificial Lakes and Reservoirs,” *FAO AQUASTAT Reports*, 2015.

[27] I. Craig, A. Green, M. Scobie, and E. Schmidt, “Controlling Evaporation Loss from Water Storages,” *Natl. Cent. Eng. Agric.*, no. 1000580/1, p. 207, 2005.

[28] M. E. Taboada, L. Cáceres, T. A. Graber, H. R. Galleguillos, L. F. Cabeza, and R. Rojas, “Solar water heating system and photovoltaic floating cover to reduce evaporation: Experimental results and modeling,” *Renew. Energy*, 2017, doi: 10.1016/j.renene.2016.12.094.

[29] P. Lehmann, M. Aminzadeh, and D. Or, “Evaporation Suppression From Water Bodies Using Floating Covers: Laboratory Studies of Cover Type, Wind, and Radiation Effects,” *Water Resour. Res.*, vol. 55, no. 6, pp. 4839–4853, 2019, doi: 10.1029/2018WR024489.

[30] National Geographic, “Why Did L.A. Drop 96 Million ‘Shade Balls’ Into Its Water?,” 2015. https://www.nationalgeographic.com/science/article/150812-shade-balls-los-angeles-California-drought-water-environment (accessed Jan. 29, 2022).

[31] I. E. L. Neto, “Impact of artificial destratification on water availabilof reservoirs in the Brazilian semiarid,” *An. Acad. Bras. Cienc.*, vol. 91, no. 3, pp. 1–12, 2019, doi: 10.1590/0001-3765201920171022.

[32] C. W. Cox, “Water Supply Enhancement in Cyprus through Evaporation Reduction,” *Civ. Environ. Eng.*, 1999.

[33] IEA, “Electricity production by source.” https://www.iea.org/fuels-and-technologies/electricity

(accessed Jan. 30, 2022).

[34] IEA, “Hydropower data explorer.” https://www.iea.org/articles/hydropower-data-explorer (accessed Jan. 30, 2022).

[35] L. Scherer and S. Pfister, “Hydropower’s biogenic carbon footprint,” *PLoS One*, vol. 11, no. 9, pp. 1–11, 2016, doi: 10.1371/journal.pone.0161947.

[36] G. Wohlfahrt, E. Tomelleri, and A. Hammerle, “The albedo–climate penalty of hydropower reservoirs,” *Nat. Energy*, vol. 6, no. 4, pp. 372–377, 2021, doi: 10.1038/s41560-021-00784-y.

[37] C. Llamosas and B. K. Sovacool, “The future of hydropower? A systematic review of the drivers, benefits and governance dynamics of transboundary dams,” *Renew. Sustain. Energy Rev.*, vol. 137, no. xxxx, p. 110495, 2021, doi: 10.1016/j.rser.2020.110495.

[38] M. K. Mahlakeng, “China and the Nile River Basin: The Changing Hydropolitical Status Quo,” *Insight on Africa*, vol. 10, no. 1, pp. 73–97, 2018, doi: 10.1177/0975087817741043.

[39] S. Sulaeman, E. Brown, R. Quispe-Abad, and N. Müller, “Floating PV system as an alternative pathway to the amazon dam underproduction,” *Renew. Sustain. Energy Rev.*, vol. 135, no. July 2020, p. 110082, 2021, doi: 10.1016/j.rser.2020.110082.

[40] L. Liu, Q. Sun, H. Li, H. Yin, X. Ren, and R. Wennersten, “Evaluating the benefits of Integrating Floating Photovoltaic and Pumped Storage Power System,” *Energy Convers. Manag.*, 2019, doi: 10.1016/j.enconman.2019.04.071.

[41] G. Kakoulaki *et al.*, “Benefits of pairing floating solar photovoltaics with hydropower reservoirs in Europe,” *Renew. Sustain. Energy Rev.*, vol. 171, no. November 2022, p. 112989, 2023, doi: 10.1016/j.rser.2022.112989.

[42] R. Cazzaniga, M. Rosa-Clot, P. Rosa-Clot, and G. M. Tina, “Integration of PV floating with hydroelectric power plants,” *Heliyon*. 2019, doi: 10.1016/j.heliyon.2019.e01918.

[43] N. M. Silvério, R. M. Barros, G. L. Tiago Filho, M. Redón-Santafé, I. F. S. dos Santos, and V. E. de M. Valério, “Use of floating PV plants for coordinated operation with hydropower plants: Case study of the hydroelectric plants of the São Francisco River basin,” *Energy Convers. Manag.*, 2018, doi: 10.1016/j.enconman.2018.05.095.

[44] H. Rauf, M. S. Gull, and N. Arshad, “Complementing hydroelectric power with floating solar PV for daytime peak electricity demand,” *Renew. Energy*, vol. 162, pp. 1227–1242, 2020, doi: 10.1016/j.renene.2020.08.017.

[45] R. Nagananthini and R. Nagavinothini, “Investigation on floating photovoltaic covering system in rural Indian reservoir to minimize evaporation loss,” *Int. J. Sustain. Energy*, 2021, doi: 10.1080/14786451.2020.1870975.

[46] J. Farfan and C. Breyer, “Combining floating solar photovoltaic power plants and hydropower reservoirs: A virtual battery of great global potential,” *Energy Procedia*, vol. 155, pp. 403–411, 2018, doi: 10.1016/j.egypro.2018.11.038.

[47] R. Gonzalez Sanchez, I. Kougias, M. Moner-Girona, F. Fahl, and A. Jäger-Waldau, “Assessment of floating solar photovoltaics potential in existing hydropower reservoirs in Africa,” *Renew. Energy*, vol. 169, pp. 687–699, 2021, doi: 10.1016/j.renene.2021.01.041.

[48] M. Acharya and S. Devraj, “Floating Solar Photovoltaic (FSPV): A Third Pillar to Solar PV Sector ?,” *TERI Discuss. Pap. ETC India Proj. (New Delhi Energy Resour. Institute)*, p. 68, 2019, [Online]. Available: www.teriin.org.

[49] DCTI, “GENERAL INFORMATION -SUNGROW Guqiao Floating Solar Plant,” 2018, [Online]. Available: http://www.dcti.de/fileadmin/img/pdf_projects/190411_ar_Fact Sheet - Global Leading RES Project - SUNGROW - Guqiao Hua.._.pdf.

[50] Ciel et Terre, “ANHUI CECEP: 70,005 KWP,” [Online]. Available: https://www.ciel-et-terre.net/project/anhui-cecep-70005-kwp/.

[51] PV Magazine, “Another 120 MW of solar aquaculture in China,” [Online]. Available: https://www.pv-magazine.com/2020/04/17/another-120-mw-of-solar-aquaculture-in-china/.

[52] KSTAR, “KSTAR 320MW Solar-water Power Plant,” [Online]. Available: https://www.kstar.com/newinformation/17387.jhtml.

[53] PV Magazine, “Chinese fishery hosting 260 MW of unsubsidized solar,” [Online]. Available: https://www.pv-magazine.com/2020/03/27/chinese-fishery-hosting-260-mw-of-unsubsidized-solar/.

[54] SAUR ENERGY, “260 MW Fishery PV Plant Is Largest in East China,” [Online]. Available: https://www.saurenergy.com/solar-energy-news/260-mw-fishery-pv-plant-is-largest-in-east-china.

[55] SAUR ENERGY, “100MW Solar-Fishery Plant Takes the Lead with Huawei 1500V Smart PV Solution,” [Online]. Available: https://www.saurenergy.com/solar-energy-news/solar-fishery-plant-huawei-1500v-smart-pv-solution.

[56] PVTIME, “China Datang Corporation Deploys 100MW of LONGi High Power Modules at Its First Floating Solar Plant in Hunan,” [Online]. Available: http://www.pvtime.org/china-datang-corporation-deploys-100mw-of-longi-high-power-modules-at-its-first-floating-solar-plant-in-hunan/.

[57] N. Dang and A. Thi, “The global evolution of floating solar PV THE EVOLUTION OF FLOATING SOLAR PHOTOVOLTAICS,” no. December, 2017, [Online]. Available: https://www.researchgate.net/publication/321461989.

[58] Kyocera, “KYOCERA TCL Solar begins operation of Japan’s largest 13.7MW Floating Solar Power Plant,” [Online]. Available: https://global.kyocera.com/news-archive/2018/0301_wvfh.html.

[59] Ciel et Terre, “UMENOKI: 7,550 KWP,” [Online]. Available: https://www.ciel-et-terre.net/project/umenoki-7550-kwp/.

[60] Ciel et Terre, “TSUGA IKE: 2,449 KWP,” [Online]. Available: https://www.ciel-et-terre.net/project/tsuga-ike-2449-kwp/.

[61] PV Magazine, “South Korean government announces 2.1 GW floating PV project,” [Online]. Available: https://www.pv-magazine.com/2019/07/19/south-korean-government-announces-2-1-gw-floating-pv-project/.

[62] PV Magazine, “Korean group to deploy 200 MW of floating PV at Saemangeum tidal flats,” [Online]. Available: https://www.pv-magazine.com/2020/09/21/korean-group-to-deploy-200-mw-of-floating-pv-at-saemangeum-tidal-flats/.

[63] SCOTRA, “Portfolio,” [Online]. Available: http://www.scotra.co.kr/en/sub/introduction/portfolio.asp?mode=view&idx=2216.

[64] The Korea Herald, “LG CNS builds mega floating solar power plants in Korea,” [Online]. Available: http://www.koreaherald.com/view.php?ud=20151015001073.

[65] PV Magazine, “BHEL commissions 5 MW floating solar plant in West Bengal,” [Online]. Available: https://www.pv-magazine-india.com/2021/06/10/bhel-commissions-5-mw-floating-solar-plant-in-west-bengal/.

[66] PV Magazine, “Module cleaning system sought for NTPC’s 100 MW floating solar,” [Online]. Available: https://www.pv-magazine-india.com/2021/06/02/module-cleaning-system-sought-for-ntpcs-100-mw-floating-solar/.

[67] MERCOM, “Tata Power Solar Bags 70 MW Floating Solar Project in Kerala from NTPC.” https://mercomindia.com/tata-power-floating-solar-kerala-ntpc/ (accessed Jun. 10, 2021).

[68] Power technology, “Shapoorji Pallonji wins India’s first large-scale floating solar project.” https://www.power-technology.com/comment/floating-solar-projects-in-india/.

[69] PV Magazine, “Uttar Pradesh cabinet clears 150 MW floating solar plant over Rihand Dam.” https://www.pv-magazine-india.com/2019/08/07/uttar-pradesh-cabinet-clears-150-mw-floating-solar-plant-over-rihand-dam/.

[70] MERCOM, “Mumbai to Buy Power from a 100 MW Floating Solar Hydro Hybrid Project at ₹4.75/kWh.” https://mercomindia.com/mumbai-100-mw-hybrid-project/.

[71] PinsetMasons, “600MW floating solar project to start operation by 2023.” https://www.pinsentmasons.com/out-law/news/600mw-floating-solar-project-to-start-operation-by-2023 (accessed Jun. 10, 2021).

[72] PV Magazine, “Coal miner Singareni Collieries mulling 300 MW floating solar.” https://www.pv-magazine-india.com/2021/01/27/coal-miner-singareni-collieries-mulling-300-mw-floating-solar/ (accessed Jun. 10, 2021).

[73] Telengana Today, “SCCL plans to set up 350 MW floating solar power plant on LMD.” https://telanganatoday.com/sccl-plans-to-set-up-350-mw-floating-solar-power-plant-on-lmd (accessed Jun. 10, 2021).

[74] sembcorp, “PUB and Sembcorp Commence Construction of 60 MWp Floating Solar Photovoltaic System on Tengeh Reservoir.” https://www.sembcorp.com/en/media/media-releases/energy/2020/august/pub-and-sembcorp-commence-construction-of-60-mwp-floating-solar-photovoltaic-system-on-tengeh-reservoir/.

[75] Ciel et Terre, “PIOLENC: FIRST FPV PILOT.” https://www.ciel-et-terre.net/project/piolenc-first-fpv-pilot/.

[76] “O’MEGA1: FIRST FLOATING SOLAR POWER PLANT IN FRANCE.” https://www.bouygues-es.com/energy/omega1-first-floating-solar-power-plant-france.

[77] “Floating solar: Europe’s largest power plant is French.” https://www.planet.veolia.com/en/floating-solar-power-plant-piolenc-france.

[78] “EDF Renewables Starts Construction of Its First Floating Solar Facility in France.” http://www.pvtime.org/edf-renewables-starts-construction-of-its-first-floating-solar-facility-in-france/.

[79] EDF, “EDF Renewables commissions four solar power plants, including two floating, in Israel.” https://www.edf-renouvelables.com/en/edf-renewables-commissions-four-solar-power-plants-including-two-floating-in-israel/.

[80] Power and Energy Solutions, “BELECTRIC builds one of the largest floating PV plants in Israel for EDF.” https://pes.eu.com/press-releases/belectric-builds-one-of-the-largest-floating-pv-plants-in-israel-for-edf/.

[81] Israel Science Info, “https://www.israelscienceinfo.com/en/environnement/edf-renouvelables-israel-met-en-service-4-centrales-solaires-dont-2-flottantes/.” https://www.israelscienceinfo.com/en/environnement/edf-renouvelables-israel-met-en-service-4-centrales-solaires-dont-2-flottantes/.

[82] Ciel et Terre, “QUEEN ELIZABETH II: 6,338 KWP.” https://www.ciel-et-terre.net/project/queen-elizabeth-ii-6-3-mwp/.

[83] “FreShER project.” https://fresher-project.eu/.

[84] BayWa r.e., “Making waves in solar energy.” https://www.baywa-re.com/en/cases/emea/making-waves-in-solar-energy.

[85] EDP, “EDP’s pioneer floating solar power plant in Portugal ready to start producing energy.” https://www.edpr.com/en/news/2022/07/15/edps-pioneer-floating-solar-power-plant-portugal-ready-start-producing-energy.

[86] Starkraft, “Banja floating solar plant.” https://www.statkraft.com/about-statkraft/where-we-operate/albania/banja-floating-solar-plant/.

[87] “Vineyard goes 100% solar and becomes first to use a floating solar array in its pond.” DNV GL launches industry-wide collaboration to develop first ever Recommended Practice for floating solar power plants.

[88] Noria Energy, “No Title.” https://noriaenergy.com/.

[89] “Town’s floating solar panel project up and running.” https://soconews.org/the_windsor_times/news/town-s-floating-solar-panel-project-up-and-running/article_1e1fb094-2926-11eb-965d-d3f244dbd93c.html.

[90] PV Magazine, “Brazilian hydropower dam to host 30 MW of floating solar.” https://www.pv-magazine.com/2020/02/14/brazilian-hydropower-dam-to-host-30-mw-of-floating-solar/.

“It’s gone.

It’s done.”

Frodo Baggins